Geochemical and microbiological characterization of effluent and pore water from low-sulfide content waste rock

by

Brenda Lee Bailey

A thesis
presented to the University of Waterloo
in fulfillment of the
thesis requirement for the degree of
Doctor of Philosophy
in
Earth Sciences

Waterloo, Ontario, Canada, 2013

AUTHOR'S DECLARATION

I hereby declare that I am the sole author of this thesis. This is a true copy of the thesis, including any required final revisions, as accepted by my examiners.

I understand that my thesis may be made electronically available to the public.

Abstract

Laboratory and field studies were completed to characterize the geochemistry and microbiology of drainage emanating from low-S content waste-rock test piles at the Diavik Diamond Mine (Diavik) from 2007 through 2010. The potential use of small-scale laboratory humidity-cell experiments to predict the water quality from larger-scale field-based experiments also was examined. Waste rock at Diavik is segregated into three categories according to sulfide content: Type I (target concentration: < 0.04 wt. % S), Type II (target concentration: 0.04 to 0.08 wt. % S) and Type III (target concentration: > 0.08 wt. % S). Four high-density polyethylene tanks, 2 m in diameter by 2 m in height, were filled with and surrounded by waste rock (active zone lysimeters; AZLs) at the Diavik site to study the upper 2 m of the active zone within a waste-rock pile and to evaluate the quality of effluent released from waste rock with differing S contents (Type I AZLs: 0.014 wt. % S and Type III AZLs: 0.035 wt. % S). In addition, three waste-rock test piles also were constructed at Diavik, two uncovered test piles (Type I test pile: 0.035 wt. % S and Type III test pile: 0.053 wt. % S) and a third pile was constructed based on the mine-closure plan which consists of waste rock (Type III: 0.082 wt. % S) capped with a 1.5 m layer of till and a 3 m layer of Type I material (Covered test pile). Each test pile is underlain by a high-density polyethylene geomembrane that captures and directs water to outflow drains.

Results show that the release and transport of blasting residuals could be used as a resident tracer, indicating the first flush of water through the AZLs and the test piles. Variations in concentrations of blasting residuals and the gradual rate of dissipation provide an indication of the heterogeneity of the distribution of blasting residuals and the relative contributions of

water and solutes from different flow paths. As temperatures within the test piles increase in response to ambient air temperature increases, larger proportions of the test pile contributed to the outflow, and increased concentrations of blasting residuals were observed in waste-rock test pile effluent.

Effluent from the Type I AZLs and test pile maintained near-neutral pH (ranged from 5.8 to 8) with concentrations of SO_4^{2-} < 500 mg L^{-1}. These results suggest that the near-neutral pH values were associated with the presence of carbonates in the waste rock and the lack of intense acid generation. As ambient air temperatures increased in spring and summer of each year, the measured pH in the Type III test-pile drainage decreased from near-neutral in May (pH 7.5) to acidic conditions by October (ranged from 5 to 4.5). As the pH in the Type III test pile decreased, concentrations of SO_4^{2-} and dissolved metals increased (e.g. SO_4^{2-} > 1500 mg L^{-1}) suggesting sulfide oxidation was occurring. Maximum concentrations of SO_4^{2-}, Al, Zn, Ni, Co, and Cu were observed in 2009 during the first flush of water through the Type III test pile. A sequence of acid-neutralization reactions was inferred based on the water chemistry of the effluent derived from the Type III AZLs and waste-rock test pile. This acid-neutralization sequence is similar to those observed at other AMD impacted sites. A series of mineral dissolution-precipitation reactions controlled pH and metal mobility; carbonate-mineral dissolution consumed H^+ generated from sulfide-mineral oxidation at near neutral pH and the dissolution of Al and Fe (oxy)hydroxides consumed H^+ at pH < 5.0.

The cover system on the Covered test pile dampened the effects of ambient air temperature on the internal temperatures within the core of the Covered test pile. As a result, the Covered test pile had a relatively steady change in flow rate, with decreased flow from June to August, which led to a slow but prolonged release of sulfide-mineral oxidation products,

such as SO_4^{2-} and dissolved metals, including Ni, Co, Zn, Cd, and Cu, compared to the uncovered Type III test pile. The pH decreased in 2008 and remained low for the duration of the study, whereas the pH in the uncovered test pile was near-neutral at the beginning of each field season in May and decreased to < 4.2 by the end of the field season in November.

The microbiological-community profiles observed in the AZLs and waste-rock test piles suggest typical AMD-related species were present in acidic effluent with elevated concentrations of metals, whereas typical soil microbes were present in effluent with a near-neutral pH and lower concentrations of SO_4^{2-} and dissolved metals. The Type III AZLs, Type III test pile, and Covered test pile maintained populations of acidophilic Fe-oxidizers, whereas, the Type I AZLs and Type I test pile maintained populations of neutrophilic S-oxidizers.

Laboratory humidity-cell (1 kg) results were scaled up to estimate the water quality from the Type III AZLs (6 t) using measured physical and chemical parameters. The results suggested over-prediction of SO_4^{2-} and metal concentrations when low mean annual precipitation occurred, limiting flushing of predicted oxidation products. In subsequent years with higher mean annual precipitation oxidation products from previous years were liberated and resulted in the under prediction of SO_4^{2-} and metal concentrations. Additionally, Fe and Al were over-predicted because Fe and Al concentrations in the AZL effluent may be controlled by the solubility and formation of secondary minerals, such as Fe oxyhydroxides, jarosite, and goethite, which were not included in the scaling procedure.

Acknowledgements

I would like to thank my supervisor, Dr. David Blowes, for his support and guidance over the course of my degree, and for challenging me with unique opportunities and experiences. I also thank Dr. Rich Amos, Dr. Leslie Smith, and Dr. Dave Sego for their collaborations and assistance; committee members, Dr. Doug Gould and Dr. Carol Ptacek, for their contributions, support, and engagement; Dr. Barrie Johnson and Barry Grail of Bangor University, Wales for their hospitality, collaboration and assistance; and, Dr. Marek Stastna for providing me with a math perspective to my research I would not otherwise have seen. Furthermore, I thank Dr. Jim Hendry for his thorough and helpful review of this dissertation that greatly improved its structure and flow.

As part of a multidisciplinary research project I worked with an incredible group of intelligent and skilled researchers, technicians, graduate students, and co-op students; without their help and support this research would not have been possible. I sincerely thank previous graduate students Lianna Smith, Mike Gupton, and Matt Neuner for their efforts to construct the test piles. I also thank my fellow graduate students on the Diavik project Nam Pham, Sheldon Chi, Mandy Moore, Ashley Stanton, Steve Momeyer, Nate Fretz, Stacey Hannam, and Sean Sinclair. Special thanks to Jeff Bain for his guidance, his ability to fix anything, and his dedication to our project. Thanks to Laura Groza, Joy Hu, Julia Jamieson-Hanes, and Corina McDonald for all their hard work in the laboratory. Also, thanks to Chris Hanton-Fong, Sue Fisher, Dr. Matt Lindsay, Dr. Blair Gibson, and Mike Moncur. This project benefited from the efforts of many co-op students that helped in the field and the laboratory,

including Adam, Brayden, Richard, Luke, Sadeed, Ellie, Meto, Jeff S., James, Manal, and Julia.

The support, encouragement, and friendship of Anita, Kristyn, Stacey, Nathan, Shannon, Jen, Mak, Lianna, Ash, Nadia, Nate, Blair, Krista, and Celia has been invaluable throughout this process; I thank you all. I also thank my fellow graduate students in the Department of Earth and Environmental Sciences for making my time at the University of Waterloo an amusing learning experience.

Above all, I am sincerely grateful to my family, Bob, Helen, Jen, Grant, Ebbie, and Mabel, for their unwavering patience, love, and support; your encouragement gave me the spirit to dream bigger than we all thought possible.

Dedication

To my family.

All things are possible if you don’t give up.

Table of Contents

List of Figures

List of Tables

Chapter 1:
Introduction

Mining generates the greatest volume of materials worldwide (ICOLD, 1996), including two types of waste: waste rock, which includes non-mineralized rock and mineralized rock that falls below economically viable grades, extracted to gain access to ore; and mine tailings, the residue from ore processing. Waste rock is typically stockpiled on the Earth's surface in large, unsaturated piles that can be greater than ten metres high and cover 100 000 m^2 in area (Ritchie, 1994). Explosives are commonly used at mine sites to fragment waste rock into workable-size fractions. Sulfide minerals, undetonated explosives, and blasting residue in waste-rock piles are exposed to atmospheric oxygen (O_2) and water immediately after blasting, during extraction and transport, and during storage in stockpiles. Sulfide minerals found in the waste-rock stockpiles can oxidize and potentially release acidic drainage with high concentrations of SO_4^{2-} and dissolved metals. Undetonated explosives, such as ammonium nitrate, which remain on or within waste rock, can dissolve on contact with water, liberating NH_4^+ and NO_3^-, and releasing these nutrients to nearby waterways. Accelerators, such as $NaClO_4$ and $KClO_4$, can release perchlorate, an anion toxic to fish and humans at low concentrations (Cox, 1994; NRC, 2005; Ting *et al*., 2006). Sulfide-mineral oxidation and the dissolution of undetonated explosives and blasting residuals from waste-rock stockpiles can potentially cause environmental problems for the mining industry and regulatory agencies. Poor-quality effluent from large unsaturated waste-rock piles is well documented (e.g., Lefebvre *et al*., 1993; Ritchie, 1994; Stromberg and Banwart, 1994;

MEND, 1995; Sracek *et al*., 2004; Stockwell *et al*., 2006); however, less is known about the (bio)geochemical processes and the rate of sulfide oxidation in the continuous-permafrost regions.

1.1 Purpose

The metal loadings in water affected by acid mine drainage (AMD) can cause environmental damage that can persist for decades (US EPA, 1994). With a growing mining industry in northern Canada, there is an increased demand for information about the long-term environmental impact on the Arctic, where unique climatic and physiographic conditions prevail. On a small scale, previous studies have attempted to investigate—with humidity cell and kinetic tests—water–rock interactions that control the release of metals from waste-rock piles (Murr *et al*., 1981; Stromberg and Banwart, 1999; Hollings *et al*., 2001; Benzaazoua *et al*., 2003; Garcia *et al.,* 2005; Sapsford *et al*., 2009; Plante *et al*., 2011). Predicting the quality of mine effluent is typically determined by using the results of these studies; however, it is unclear if these predictions adequately estimate the resulting water quality.

Larger-scale studies have also been completed (Lefebvre *et al*., 1993; Stromberg and Banwart, 1994; Ericksson *et al*., 1997; Tan and Ritchie, 1997); however, these waste-rock studies included sampling locations that were monitored after construction or included seepage water from tailings impoundments and infiltration from the surrounding catchment area. None of these studies monitored effluent emanating only from waste-rock stockpiles. To overcome these issues, this thesis focused on effluent emanating from three lined experimental waste-rock piles that were constructed and instrumented simultaneously.

One of the major questions about stockpiling low-sulfide content waste rock in northern climates is whether acidic drainage will be generated and, if so, what is the potential for and duration of the release of dissolved metals to the environment. Studies have shown bacteria are present at low temperatures and can be responsible for the oxidation of mine tailings in Arctic environments (Leduc *et al.*, 1993; Elberling *et al.*, 2000). Early data from the Ekati mine demonstrated low-pH values in waste-rock seepage (Morin, 2003). However, the processes resulting in AMD and acidity from diamond mine waste rock in northern regions are not well understood.

A comprehensive research programme was established at the Diavik Diamond Mine (Diavik) in the Northwest Territories, Canada, to characterize the physicochemical processes within waste-rock piles in the Arctic. In addition, the research programme aims to assess the potential to scale geochemical, microbiological, hydrological, thermal, and temporal data from laboratory humidity-cell experiments (Moore, in preparation) to: 2 m x 2 m-scale active zone field experiments (Chapter 3); to 15 m high, large-scale waste-rock piles (test piles); and to operational waste-rock stockpiles. Waste rock at the Diavik site contains a low abundance of sulfide minerals, but it also has a low acid-neutralization potential (Jambor, 1997; Smith *et al.*, in press), leading to uncertainty about the potential for the Diavik waste rock to generate acidic drainage. It is important to understand the migration of water through waste-rock piles in order to determine the quality of drainage at the base of the waste-rock piles. The physicochemical processes within waste-rock piles are influenced by many factors, such as porosity, permeability, S content, presence/absence of S-oxidizing bacteria, temperature, water content, and oxygen concentrations. Examining the construction methods and the physical and chemical properties of waste-rock stockpiles, can aid in a better

understanding of the physical and chemical processes that lead to AMD from waste-rock piles (MEND, 1995). This research programme is intended to examine the chemical processes within waste-rock stockpiles over time to aid in better predictions of the onset (lag time) and duration (longevity) of AMD generation, thereby quantifying the environmental impacts associated with waste-rock stockpiles.

1.2 Research Objectives

The primary objectives of this thesis were: 1) to investigate the geochemical and microbiological characteristics of effluent and pore water from waste-rock stockpiles in a continuous permafrost region; and 2) to determine an appropriate approach for a scale-up from laboratory studies to field investigations. The specific tasks of this research are outlined as follows:

- Determine the persistence of undetonated explosives and blasting residuals in the AZLs and waste-rock test piles;
- Characterize the quality of water emanating from the upper 2 m active zone of waste rock and large-scale waste-rock test piles with differing S content over time;
- Examine the microbial evolution of the waste-rock test piles in terms of type and abundance of different groups of S- and Fe-oxidizing bacteria, and investigate the succession of bacterial total diversity with the evolution of the water quality from waste-rock test piles over time;
- Determine the effects a thermal cover (Type I cover material) and a low-permeability layer (till layer) have on the geochemical conditions within a waste-rock test pile by using a comparison to an uncovered waste-rock test pile; and,
- Determine if results obtained from laboratory humidity-cell experiments can be used to predict the water quality of effluent from 2 m-by-2 m-scale AZLs.

1.3 Hypotheses

This research will address the following hypotheses:

- Blasting residuals will act conservatively and be flushed from the waste rock.
- The ambient air temperatures at the field site (Diavik) will affect the rate of sulfide-mineral oxidation.
- The finer-waste-rock fraction will be the most reactive fraction because of the larger amount of exposed surface area of sulfide minerals.
- The oxidation of sulfide minerals will release SO_4^{2-} and dissolved metals that will be mobilized in contact with water migrating through the waste-rock piles, thereby affecting water quality at the base of the waste-rock pile.
- The microbial community in the waste-rock effluent will evolve as the water chemistry changes over time with increased sulfide-mineral oxidation and depletion of acid-neutralization potential.
- Application of a cover, designed to limit the ambient temperature fluctuations within the waste-rock pile, will allow permafrost to migrate up through the waste-rock pile, thereby reducing the internal temperatures within the waste-rock pile and decreasing the rate of sulfide-mineral oxidation. In addition the cover will limit water infiltration and ingress of oxygen.
- Various, measured physiochemical characteristics of waste rock can be used to scale the release rates of SO_4^{2-}—from humidity-cell experiments up to large-scale experiments—in order to predict the water quality.

1.4 Background

1.4.1 Acid Mine Drainage

The oxidation of sulfide minerals, either through abiotic or biotic processes, can result in the generation and discharge of effluent with high concentrations of SO_4^{2-}, H^+, and dissolved

metals, such as Zn, Fe, Ni, Co, and Cu, known as AMD. Sulfide minerals, such as pyrite and pyrrhotite, in waste rock can be oxidized by oxygen and/or ferric iron. Oxygen is the dominant oxidant of pyrite (equation 1.1) and pyrrhotite (equation 1.2) at circum-neutral pH, which causes the release of Fe^{2+}, SO_4^{2-}, and H^+:

(1.1) $$FeS_2 + \tfrac{7}{2}O_2 + H_2O \rightarrow Fe^{2+} + 2SO_4^{2-} + 2H^+$$

(1.2) $$Fe_{1-x}S + \left(2 - \tfrac{1}{2}x\right)O_2 + xH_2O \rightarrow (1-x)Fe^{2+} + SO_4^{2-} + 2xH^+$$

The Fe^{2+} released may subsequently be oxidized to Fe^{3+}:

(1.3) $$Fe^{2+} + \tfrac{1}{4}O_2 + H^+ \leftrightarrow Fe^{3+} + H_2O$$

The Fe^{3+} generated by Fe^{2+} oxidation may contribute to the oxidation of Fe sulfides and becomes the predominant oxidant at pH < 4 when Fe^{3+} is more soluble (Nordstrom, 1982):

(1.4) $$FeS_2 + 14Fe^{3+} + 8H_2O \rightarrow 15Fe^{2+} + 2SO_4^{2-} + 16H^+$$

(1.5) $$Fe_{1-x}S + (8-2x)Fe^{3+} + 4H_2O \rightarrow (9-3x)Fe^{2+} + SO_4^{2-} + 8H^+$$

Alternatively, the hydrolysis of Fe^{3+} may occur and may precipitate as Fe (oxy) hydroxides, such as ferrihydrite [$Fe(OH)_3$ or nominally $5Fe_2O_3{\cdot}9H_2O$] and goethite [αFeOOH)]:

(1.6) $$Fe^{3+} + 3H_2O \leftrightarrow Fe(OH)_3 + 3H^+$$

The overall reaction for the oxidation of pyrite is acid producing, generating 4 moles of H^+ for each mole of pyrite oxidized:

(1.7) $$FeS_2 + \tfrac{7}{2} H_2O_{(aq)} + \tfrac{15}{4} O_{2(aq)} \rightarrow Fe(OH)_{3(s)} + 2SO_4^{2-} + 4H^+_{(aq)}$$

The rate law for pyrite oxidation with dissolved O_2 was described by Williamson and Rimstidt (1994) for a pH range of 2–10:

(1.8) $$R = 10^{-8.19(\pm 0.04)} \frac{\left(m_{DO}\right)^{0.5(\pm 0.04)}}{\left(m_{H^+}^{0.11}\right)^{(\pm 0.01)}}$$

where R is the rate of pyrite consumption in mol m^{-2} s^{-1}. The rate law for pyrite oxidation in the presence of O_2 was also described by Williamson and Rimstidt (1994) for a pH range of 0.2–3.0, when Fe^{3+} is the predominant oxidant:

(1.9) $$R = 10^{-6.07(\pm 0.57)} \frac{\left(m_{Fe^{3+}}^{0.93}\right)^{(\pm 0.07)}}{\left(m_{Fe^{2=}}^{0.40}\right)^{(\pm 0.06)}}$$

where R is the reaction rate in mol m^{-2} s^{-1} and is a function of the Fe concentrations. A rate expression for pyrrhotite oxidation with dissolved O_2 and Fe^{3+} was described by Brookfield *et al*. (2006), based on the shrinking core model with a calibrated effective rate coefficient:

(1.10) $$R = -\max\left[\left(\frac{r^p}{(r^p - r^r)r^r}\right)\left(10^{-9.62}\{O_2(aq)\} + 10^{-11.92}[Fe(III)]^{0.06}\right)\left[1 - \frac{IAP}{10^{-135.7}}\right], 0\right]$$

where R is the reaction rate, r^p is the radius of a particle (average grain size), r^r is the radius of the unreacted core of the mineral grain, and $\left[1 - \frac{IAP}{10^{-135.7}}\right]$ is the affinity term where IAP is the ion-activity product of the reaction, and $10^{-135.7}$ is the value of the equilibrium constant K at 25°C. Williamson and Rimstidt (1994) report on studies that present activation energies of pyrite ranging from 50–80 kJ mol^{-1}. Ahonen and Tuovinen (1992) determined the activation energy for pyrrhotite, based on a column-leaching experiment conducted at a range of temperatures from 4°C to 37°C, to be 25 kJ mol^{-1}, and suggested that the rate control is due to the diffusion of reactants or products. Activation energies are higher at near-neutral pH conditions (pH values ranging from 6–8) than under acidic conditions (pH 2–4; Blowes *et al*., 2003b).

Sulfide-oxidation rates are affected by temperature in a manner described by the Arrhenius equation (Ahonen and Tuovinen, 1992):

(1.11) $$\ln\frac{k_2}{k_1} = \frac{E_a}{R \times 2.3} \times \left(\frac{1}{T_1} - \frac{1}{T_2}\right)$$

where k_1 and k_2 are the rate constants at temperatures T_1 and T_2; E_a is the activation energy of the reaction; and R is the gas constant. Seasonal temperature fluctuations, therefore, may influence the rate of release of SO_4^{2-}.

Sulfide oxidation can be catalyzed by bacteria, including the *Thiobacillus* species and the *Acidithiobacillus* species, resulting in the accelerated generation of acidic drainage (Nordstrom and Southam, 1997). Microbial-mediated, sulfide-mineral oxidation occurs through contact or non-contact mechanisms. Both mechanisms result in the oxidation of Fe^{2+}, thereby generating an oxidizing agent (Fe^{3+}) that subsequently oxidizes S compounds (Rohwerder *et al*., 2003). The contact mechanism of bacterially mediated, sulfide-mineral oxidation involves the attachment of a cell or bacterium to the sulfide-mineral surface. The dissolution of the sulfide mineral occurs at the interface between the bacterial cell and the sulfide-mineral surface (Rohwerder *et al*., 2003). In non-contact mechanisms, the cell or bacterium does not directly interact with the sulfide mineral; rather, the bacterium oxidizes only dissolved Fe^{2+} (Rohwerder *et al*., 2003). Iron(3^+) can then come into contact with the sulfide-mineral surface, where it is reduced to Fe^{2+} (equation 1.12), thereby returning to the cycle (see equation 1.3).

(1.12) $$MeS + 2Fe^{3+} \rightarrow Me^{2+} + S^0 + 2Fe^{2+}$$

Under low-pH conditions, the oxidation of Fe^{2+} is the rate-limiting step in biotic pyrite oxidation (Singer and Stumm, 1970). *Acidithiobacillus ferrooxidans* and related species catalyze Fe^{2+} oxidation. Observations from field studies report microbially mediated sulfide-mineral oxidation to be orders-of-magnitude more rapid than abiotic laboratory rates (Kirby *et al.*, 1999). Microorganisms can contribute to the oxidation of mine tailings at low temperatures in Arctic environments (e.g., Leduc *et al*., 1993; Elberling *et al*., 2000). However, limited information exists on the importance of bacterially catalyzed oxidation of

sulfide minerals in waste-rock stockpiles and their role in the generation of AMD in Arctic conditions.

Acidity generated from the oxidation of sulfide minerals and the precipitation of Fe(III) oxyhydroxides can be neutralized by a series of mineral-dissolution reactions. A conceptual model of acid-neutralization was described by Jurjovec *et al*. (2002). The pH is buffered to a distinct series of acid-neutralization plateaus associated with the progressive depletion of primary and secondary minerals, including calcite (pH 6.5 - 7.5), siderite (4.8 - 6.3), $Al(OH)_3$ (4.0 - 4.3), and $Fe(OH)_3$ (2.5 < 3.5) (Blowes and Ptacek, 1994a; Jurjovec *et al*., 2002). In addition, aluminosilicate mineral dissolution consumes H^+ concurrently; however, it is not rapid enough to constrain the effluent to a specific pH.

1.4.2 Characteristics of Waste-Rock Stockpiles

Waste-rock stockpiles are typically constructed by push-dumping, end-dumping, free-dumping and contouring, or by disposal directly via a dragline/bucket excavator (Fala *et al*., 2003; Corazao, 2007). Waste rock deposited with end- and push-dumping tend to segregate fractions of coarser waste rock (cobbles and boulders) at the base, whereas the finer waste-rock fraction (gravel, sand, and fines) remains near the surface (MEND, 1995, 1999; Smith and Beckie, 2003; Wagner, 2004; Bay, 2009; Chi, 2010). Waste-rock piles are classified as rock-like or soil-like, depending on the size of the grain in the fraction. A soil-like pile has 20% of the material passing through a 2 mm grain-size sieve (e.g., sand) (Dawson and Morgenstern, 1995). Waste-rock stockpiles are heterogeneous, and the particle-size distribution and texture of the waste-rock pile affects water, air, and chemical transport pathways (Smith and Beckie, 2003).

Fluid flows through heterogeneous unconsolidated material in unsaturated waste-rock piles via pathways created by the matrix materials and the larger-void spaces (Smith and Beckie, 2003). Flow has three main mechanisms: 1) matrix flow, which is gravity driven flow within the fine-grained matrix; 2) macropore flow, which is gravity-driven flow through the larger-pore spaces and includes interaction with the surrounding matrix; and, 3) non-capillary flow, which is flow through the larger pore spaces, with little interaction with water retained in the fine-grained matrix (Nichol *et al*., 2005). Matrix flow tends to dominate in unconsolidated material classified as 'soil-like', and macropore flow dominates in 'rock-like' waste rock. Matrix flow is the dominate flow transport mechanism in coarse-grained waste-rock piles. During heavy rainfall, however, macropore flow may become the more dominate flow mechanism (Wagner *et al*., 2006; Neuner, 2009; Bay, 2009). The fine-grained matrix has a larger surface area compared to that of the larger-void spaces. It has also been shown that the fractions of finer rock are the most reactive, due to the increased surface area of exposed sulfide minerals (Stromberg and Banwart, 1999; Stockwell *et al*., 2006; Hollings *et al*., 2001).

Matrix flow is slow and results in more extensive water-rock interaction, producing outflow with higher solute concentrations and greater mass loadings (Stockwell *et al*., 2006). Wagner *et al*. (2006) show that the outflow volume from experimental waste-rock piles at the Cluff Lake mine in Saskatchewan, Canada, influenced drainage chemistry. During matrix flow, slow flow rates corresponded to concentrated outflow water as a result of increased contact time with greater surface area in the matrix material (Smith and Beckie, 2003; Wagner, 2004). In contrast, rapid flow through the macropores results in preferential flow through channels within the waste rock, resulting in less water–rock interaction and pathways

being continuously flushed—leading to lower solute concentrations and less mass loading in the outflow water. Wagner *et al*. (2006) observed that a rapid increase in flow rates from infiltration events resulted in fresher outflow water as the water migrated through the macropores. At the Mine Doyon in Quebec, Canada, maximum concentrations were observed during dry periods in unsaturated waste-rock piles, and decreased concentrations were observed during recharge periods (Sracek *et al*., 2004). The shorter residence time of water, results in lower concentrations of solutes and less mass loading.

The O_2 present in waste-rock piles may be consumed in sulfide-mineral oxidation reactions. The transport of oxygen through diffusion and advection can replenish oxygen consumed in these reactions (Ritchie, 1994; Amos *et al*., 2009a). Gas-transport mechanisms and the rate of oxygen transport are influenced by the water content, porosity, and permeability of the waste-rock material. In some waste rock piles, oxygen transport is the predominant factor limiting the rate of sulfide-mineral oxidation reactions (Hollings *et al*., 2001; Amos *et al*., 2009 and references therein). In coarse waste rock, oxygen transport is often replenished through advection or convection. In fractions of finer waste rock, oxygen depletion can be rapid, whereas oxygen replenishment is controlled by diffusion, which can be slow and affected by the moisture content (Lefebvre *et al*., 2001). Oxygen consumption rates are the highest between 12 % and 25 % saturation (Hollings *et al*., 2001). In addition, Amos *et al*. (2009) suggest wind-induced airflow through waste rock has the potential to be a significant mechanism of oxygen transport.

Lefebvre *et al*. (2001) described the depletion of O_2 with depth within a permeable, highly reactive waste-rock pile at the Mine Doyon in Quebec, Canada, where high internal

temperatures (over 65°C) resulted in temperature-driven air convection as the main as transport mechanism. Higher O_2 concentrations were observed near the top of the pile, where a less reactive diorite layer was placed (Lefebvre *et al*., 2001). Heat-driven gas transport due to exothermic sulfide-mineral oxidation reactions also was observed at the Nordhalde mine in Germany (Lefebvre *et al*., 2001). Hollings *et al*. (2001) suggest grain size was the principal factor that affected the oxygen-consumption rates of low-sulfide (< 0.55 wt. % S) content gneissic waste rock in laboratory studies. The water content, temperature, and biological activity, however, only moderately influenced the oxygen-consumption rates. But oxygen-consumption and sulfate-release rates determined from laboratory-based tests are often orders-of-magnitude higher than those in the field (Ritchie, 1994). It is, therefore, important to understand the mechanisms influencing sulfide-oxidation processes and the release of oxidation products from field studies to better estimate the potential, intensity, and duration of AMD for waste-rock planning and management purposes.

The fraction of finer rock has the greatest surface area (Stockwell *et al*., 2006), and it tends to be segregated at the upper portions of a waste rock-stockpile (Chi, 2010). This fraction is the most reactive, due to the increased surface area of exposed minerals (Stromberg and Banwart, 1999; Hollings *et al*., 2001), and, therefore, the top of the waste-rock pile is considered to be the most reactive. However, weathering rates measured in an experimental waste-rock pile deconstruction study at the Key Lake mine in Saskatchewan show no discernible correlation with grain-size distribution after six years of weathering (Stockwell *et al*., 2006). It was suggested that the time frame may have been too short for weathering patterns and fluid flow paths to fully develop (Stockwell *et al*., 2006). Further investigation of pore water concentrations in waste-rock piles is needed.

Temperature also affects the rate of sulfide-mineral oxidation in a manner that can be described by the Arrhenius equation (section 1.4.1). In northern climates, average maximum air temperatures can fluctuate between -31°C in the winter and 18°C in the summer (Smith *et al*., 2012) affecting sulfide-mineral oxidation rates over the course of one year. However, the exothermic reaction of sulfide-mineral oxidation can increase internal waste-rock piles well above ambient air temperatures. Internal temperatures observed in the waste-rock pile at Mine Doyon in Quebec, Canada were as high as 60°C at depth, greater than 10 times the ambient air temperature (5°C; Sracek, *et al*., 2004 and references therein). Increased temperatures, compared to ambient temperatures, were observed at the Aitik mine in Sweden. At this site, the ambient air temperature is 0°C, with average summer temperatures of 15°C and winter temperatures of -15°C. Surface temperature ranged from -5°C to 12°C, the base maintained temperatures of 0°C to 3°C, and internal temperatures were 1°C to 4°C, suggesting that exothermic sulfide-mineral oxidation affected temperatures (Stromberg and Banwart, 1994). At the Nordhalde mine in Germany, surface temperatures of waste rock measured 9°C, while internal temperatures increased to 15°C to 20°C (Lefebvre *et al*., 2001).

Laboratory-based experiments, such as static and kinetic tests, are used to estimate the lag time and longevity of AMD from waste-rock piles and tailings impoundments (Sapsford *et al*., 2009 and references therein). To date, there is no standardized method for scaling laboratory studies to full-scale, operational waste-rock piles (Sapsford *et al*., 2009). Scaling these small-scale experiments to field experiments has resulted in sulfate oxidation rates that differ by orders of magnitude (e.g., Benzaazoua *et al*., 2003; Garcia *et al.*, 2005; Sapsford *et al*., 2009; Plante *et al*., 2011). Laboratory experiments are designed for controlled conditions, such as moisture content and temperature. The difficulties associated with scaling these

controlled experiments to field experiments have been overcome, with some success, by the application of site-specific correction factors. Malmstrom *et al*. (2000) were able to predict weathering rates within two orders of magnitude for the Aitik site in Northern Sweden by using bulk-averaged physiochemical characteristics to scale laboratory experiments. However, few large-scale waste-rock studies have been completed that included sampling locations monitored immediately after construction of a waste-rock pile with sampling locations isolated from other seepage waters, such as those from tailings impoundments and infiltration from the surrounding catchment area.

At the end of mining operations, waste-storage facilities (tailings impoundments and waste-rock stockpiles) at mine sites are reclaimed in an appropriate manner as part of a closure or reclamation strategy (MEND, 2012). Generally, this includes a cover system that restores the surface to a stable, natural condition to minimize the degradation of the surrounding receiving environment (MEND, 2012). Specifically, the application of a cover system can be used to control the oxidation of sulfide-bearing minerals in waste-rock piles. Cover systems are used to limit the infiltration of atmospheric water, the ingress of atmospheric oxygen; to control erosion of waste materials, and upward movement of process-water constituents and oxidation products; and to provide a medium for revegetation (MEND, 2012). Johnson and Hallberg (2005) describe methods used to prevent acid generation, including: flooding/sealing of underground mines; underwater storage of mine tailings (water covers); land-based storage in sealed waste heaps; blending of mineral wastes; total solidification of tailings; and application of anionic surfactants and microencapsulation (coatings). Typical cover systems consist of a single layer or multiple layers of one or more of the following materials: native soils, overburden, non-reactive tailings, non-reactive waste

rock, geosynthetic materials, water, and oxygen-consuming materials (MEND 2004). The application of cover systems to the surface of waste-rock piles has been previously studied in modelling studies and laboratory experiments, and in few field-based applications (e.g., Yanful *et al*., 1993; Yanful *et al*., 2000; Shurniak and Barbour, 2002; Bussiere *et al*., 2003; Aachib *et al*., 2004; Miller *et al*., 2006; Wagner *et al*., 2006; Taylor *et al*., 2009; Song, 2010; Demers *et al*., 2011; MEND, 2012).

1.4.3 Blasting Practices

Mining practices require the use of explosives, such as ammonium-nitrate fuel oil (ANFO), to extract ore and waste rock. The chemical compounds used in ANFO are released to the environment, potentially causing detrimental effects to water quality. Furthermore, perchlorate can be derived from accelerants, typically $NaClO_4$ and $KClO_4$, used in blasting materials and can release Cl^-, and Na, or K, during detonation. The flushing rates of undetonated explosives and blasting residuals have not been well documented.

The dissociation of ammonium nitrate in water releases nitrate (NO_3^-) and ammonium (NH_4^+). Ammonium can dissociate to NH_3 in alkaline conditions (Clark, 1981). Ammonia is oxidized to the unstable intermediate N species, NO_2^-, by the *Nitrobacter* group of nitrifying bacteria under aerobic conditions (Koren *et al*., 2000). The *Nitrosomonas* group of nitrifying bacteria further oxidize NO_2^- to NO_3^- (Sawyer and McCarty, 1967). Under anaerobic conditions denitrifying bacteria, such as *Thiobacillus denitrificans*, reduce NO_3^- to N_2 gas. Nitrate can be removed from industrial waters by denitrification; however, reducing conditions and a sufficient supply of soluble organic C are required to promote this reaction

by a number of bacterial genera (*Pseudomonas, Paracoccus, Flavobacterium, Alceligenes* and *Bacillus* spp.; Koren *et al*., 2000).

Perchlorate has been found in surface water and groundwater surrounding explosives-processing plants, military testing sites, mine sites, and sites where fireworks have been detonated (Susarla *et al*., 1999; Motzer, 2001; ITRC, 2005; Jackson *et al*., 2005; Parette *et al*., 2005; Sanchez *et al*., 2005; Schaefer *et al*., 2007; Wilkin *et al*., 2007). The range of ClO_4^- concentrations observed in mine wastewaters is similar to concentrations observed in municipal water supplies affected by ClO_4^- from explosives-processing plants, military testing sites, and sites where fireworks have been detonated (Susarla *et al*., 1999; Motzer, 2001; ITRC, 2005; Jackson *et al*., 2005; Parette *et al*., 2005; Sanchez *et al*., 2005; Schaefer *et al*., 2007; Tikkanen, 2006, Wilkin *et al*., 2007).

1.5 Field Site Description and Current Results

Diavik is an open pit and underground diamond mining operation, and is located 300 km northwest of Yellowknife, Northwest Territories, Canada, on a 20 km^2 island in Lac de Gras (64°29' N; 110°18' W; elevation 440 m). Diavik is in the Slave Geologic Province, and the economic ore body is diamondiferous kimberlite hosted in granite (75 %) and granite pegmatite (14 %) containing irregular xenoliths of biotite schist (10 %). These host rocks are cut by diabase dikes (< 1 %). The granites contain only trace sulfides and consist mainly of potassium feldspar [$KAlSi_3O_8$], albite [$NaAlSi_3O_8$], and quartz [SiO_2], with < 5 % each of biotite [$KMg_3AlSi_3O_{10}(OH)_2$] and muscovite [$KAl_2AlSi_3O_{10}(OH)_2$] (Jambor, 1997). The biotite schist (< 0.42 wt. % S) contains locally disseminated pyrrhotite with lesser amounts of pyrite, sphalerite, and chalcopyrite (Smith *et al*., in press). The biotite schist aluminosilicate

mineral assemblage consists mainly of quartz (20 to 50 %), albite (35 to 55 %), and biotite (10 to 25 %; Jambor, 1997). Diavik segregates waste rock into three types based on sulfide content— Type I (< 0.04 wt. % S), Type II (0.04 wt. % S to 0.08 wt. % S), and Type III (> 0.08 wt. % S) —and will generate a waste-rock stockpile up to 120 Mt at closure (Smith *et al*., 2012).

The Diavik mine site is located in a continuous permafrost region. Air temperatures range from a maximum of 27 °C in July to a minimum of -44 °C in January/February, with a mean annual air temperature of -9.0 °C from March 1998 through March 2007 (Environment Canada, 2010). The mean annual precipitation from March 1998 through March 2007 was 280 mm, of which 65 % occurs as snow (Environment Canada, 2010). A regional study of the local climate over 50 years suggests the mean annual precipitation for the region was 351 mm, of which 53 % occurred as snow (187 mm) and 47% occurred as rain (164 mm), and the mean annual air temperature was -10.1°C (Golder Associates, 2008). Over a five-year period, 2007 through 2011, the mean annual rainfall measured at the test piles was 113 mm and the mean annual air temperature was -8.8°C.

1.5.1 Research Facilities

Four high-density polyethylene (HDPE) tanks were filled with and surrounded by waste rock in 2006 (Figure 1.1 and Table 1.1; Smith *et al*., 2012). Two AZLs were filled with Type I waste rock (Type I East AZL and Type I West AZL; Figure 1.2), and have a collection diameter of 2.2 m and a zero-tension drain at a depth of 1.45 m to collect water migrating downward through the waste rock under the influence of gravity (Neuner *et al*., 2012). Two AZLs were filled with Type III waste rock (Type III East and Type III West AZL), and had a

collection diameter of 1.6 m and a zero-tension drain at a depth of 1.7 m (Neuner *et al*., 2012). The AZLs were constructed with a drainage system at the base of the tank.

Drainage from the AZLs flowed to a series of acrylic flow-through cells located in an adjacent heated instrumentation trailer (Figure 1.3). The flow-through cells were instrumented to provide continuous measurements of pH, electrical conductivity (EC), temperature, and flow rate. Three tensiometers to measure pressure head and three soil moisture sensors (ECH_2O probes, Decagon Devices, USA) to monitor moisture content were installed next to the AZL, at the same elevation and in similar waste rock, at depths of 30, 60, and 90 cm.

Three large-scale test piles were also constructed at the Diavik Waste Rock Research Facility: two uncovered test piles and one covered test pile (Table 1.2). Two large-scale test piles (15 m in height and 60 m by 50 m at the base) were constructed with differing S content by using push- and end-dumping methods: one Type I test pile (average of 0.035 wt. % S in the < 55-mm fraction; approximately 68,000 t of waste rock) and one Type III test pile (average of 0.053 wt. % S in the < 55-mm fraction; approximately 70,000 t of waste rock).

Both Type I and Type III test piles were constructed on low-permeability, high-density polyethylene (HDPE) liners placed on graded bases. Infiltrating water collected at the base of the test piles was directed through mineral-insulated, heat-traced drains at the base of the test piles. Effluent from the Type I test pile was collected by a single drainage conduit that discharged to an instrumentation hut at the base of the Type I test pile. The effluent from the Type III test pile was collected in two outflow drains (north and south) and directed to two

instrumentation huts (Figure 1.2), where water was collected in a flow-through cell system as previously described.

Basal lysimeters were constructed at the base of each test pile to capture water infiltrating limited portions of the test piles. Each cluster of lysimeters included two 4 m by 4 m basal lysimeters and two 2 m by 2 m basal lysimeters. Three clusters were installed in each test pile with one cluster below the centre of the test pile and two clusters located below the batters. These cells were lined with HDPE, and drainage was directed to instrumentation huts where water was collected in a flow-through cell system as previously described.

The Covered test pile (base of 80 m by 125 m based on contoured 18º (3H:1V) slopes and a 24 m wide crest; Figure 1.2) was constructed using Type III waste rock with an average S content of 0.082 wt. % S ($n = 183$, $\sigma = 0.053$; Smith *et al*., in press). This test pile was re-sloped and capped with a 1.5 m layer of lower-permeability till and a 3 m layer of Type I waste-rock cover (Smith *et al*., 2012). The Type III core had approximately 70, 000 t of waste rock; the till layer had approximately 25,000 t of till; and the Type I layer had approximately 75,000 t of waste rock. The Covered test pile was constructed on a high-density polyethylene (HDPE) liner placed on a graded base that directs infiltrating water through mineral-insulated, heat-traced drainage lines to an instrumentation hut at the base of the Covered test pile where water was collected in a flow-through cell system as previously described.

The Covered test pile had a cluster of four 4 m by 4 m basal lysimeters and four 2 m by 2 m basal lysimeters under the crest of the test pile, and two 4 m by 4 m basal lysimeters and two 2 m by 2 m basal lysimeters under the sloped edges (batters) of the test pile. A self-

regulating heating cable, rated at 2.4 W m^{-1}, was installed in each basal lysimeter to ensure that any water arriving at the lysimeter base would flow to the drain. The Type III test pile and Covered test pile were each instrumented with four tensiometers at depths of 60 cm and 120 cm to monitor moisture content.

1.5.2 Oxygen Transport

Waste rock at Diavik has a porosity of 0.25 (Neuner *et al*., 2012), and the permeability ranged from 2×10^{-10} m^2 to 3×10^{-9} m^2 and averaged 1.4×10^{-9} m^2 (Amos *et al*., 2009a). Concentrations of O_2 and CO_2 equivalent to atmospheric levels were observed throughout the Type I and Type III test piles over the duration of the study (Amos *et al*., 2009b). The high permeability of the waste rock permits the ingress of O_2 into the uncovered waste rock in the Type I and III test piles. Oxygen depleted during sulfide-oxidation reactions probably was rapidly replenished due to high rates of advective gas transport (Amos *et al*., 2009a). Although thermally driven convective gas transport, due to exothermic sulfide-mineral oxidation, has been observed within waste-rock piles at several mine sites (Ritchie and Bennett, 2003), the temperature gradients measured at Diavik do not indicate the potential for convection resulting from exothermic sulfide oxidation (Pham *et al*., 2012). Temperature fluctuations due to seasonal changes in the ambient air temperature do occur and may result in thermally driven convective gas transport. Pore-gas concentrations were not made in the AZLs.

In most locations in the Covered test pile, gas concentrations remain near atmospheric levels (Amos *et al*., 2009a). Oxygen depletion was observed in Covered test piles in 2007 and 2008 in isolated sampling locations, and O_2 concentrations showed a progressive

depletion over the summer months followed by an increase in CO_2 concentrations in the autumn (Amos *et al*., 2009a). This depletion of O_2 provides estimates of sulfide-oxidation rates within the test pile ranging from 1.7×10^{-11} to 4.1×10^{-11} kg O_2 m^{-3} s^{-1} (Amos *et al*., 2009a). Measurements in 2009 and 2010 were difficult to obtain, due to frozen gas-measurement lines; however, those collected show concentrations of O_2 and CO_2 equivalent to atmospheric levels. The wetting up of the till layer in the Covered test pile should further enhance the function of the till layer as an oxygen transport barrier; however, oxygen concentrations at atmospheric levels are currently observed in the Covered test pile.

1.5.3 Temperature

Type I and III waste-rock AZLs and test piles were affected by seasonal temperature cycles (Pham *et al*., 2012); as the ambient air temperature in the region increased in the spring, the temperature within the waste-rock test piles also increased. Temperatures within the AZLs at a depth of 0.9 m reached a maximum of 18 °C in the summer and decreased to a minimum of -23 °C in the winter (Figure 1.4; Fretz, in preparation).

The internal temperature in the Type III test pile (innermost thermistor string on north side 31N5; Face 1) reached a maximum of 11 °C at a depth of 1 m in July 2007 and 5°C at the base (12 m) in August 2007 (Pham, in preparation). The minimum temperature was -15 °C at 1 m below the surface and -11 °C at the base of the Type III test pile in April 2008 (Pham *et al*., 2012). Temperature increases were accompanied by an increase in the flow rate at the base of the test piles from May through September. The flow rate decreased as ambient air temperatures decreased in the fall and the internal test pile temperatures decreased. Flow

ceased after the temperatures within the central portion of the test piles fell below freezing (~0°C).

A detailed description of the thermal conditions within the Type III pile is presented by Pham *et al.* (2011; 2012). Seasonal temperature cycles were observed in the Type III test pile. As the air temperature in the region increased in the spring, the temperature within the Type III test pile also increased, reaching a maximum of 15 °C at a depth of 1 m and 4°C at 12 m in August each year, and a minimum temperatures of -15 °C to -20 °C in April (Pham *et al*., 2012). The rate and extent of the temperature changes were more rapid than could be sustained by thermal conduction alone, suggesting that the thermal regime is affected both by conductive heat flow and advective heat flow driven by winds external to the Type III test pile (Pham *et al*., 2012).

Thermistors in the Type I layer of the Covered test pile showed temperature fluctuations similar to the Type III test pile; increasing and decreasing with ambient air temperatures and driven by thermal conduction and wind-driven advection gas transport (Pham, *et al*., 2011). The temperature in the Type I layer increased to above 0°C in the period from June through October of each year (Pham *et al*., 2012). The till layer is intended to provide a frozen, low-permeability layer, which limits seasonal temperature fluctuations in the core of the test pile, preventing warm air from being driven into the test pile during the summer months. Temperature measurements indicated that the upper portion of the till layer remained between 0 °C and -12.2 °C, and the base of the till layer remained between 0 °C to -8.2 °C in areas not affected by the heat trace placed at the base on the test pile (Pham *et al*., 2012). As a consequence of the cover design, the Type III core in the Covered test pile experienced

lower amplitude changes in temperature, primarily driven by conductive heat flow, than the Type I layer in the Covered test pile and the Type III test pile, where thermal conditions were affected by conductive heat flow and advective gas transport (Pham *et al*., 2012). Although the cover design implemented on the Covered test pile was intended to sustain frozen conditions throughout the Type III core, the basal lysimeters and the basal drains were heated to allow sample collection and to prevent freezing and rupturing of the drainage conduits at the base of the test pile. The heat trace lines provided a heat source within the Covered test pile which reached up to 8 °C. The till directly above the basal lysimeters (Face 1 and Face 2) was influenced by the heat trace allowing the till layer in this area to remain above 0°C, thereby allowing water to migrate downward. As a consequence, temperatures in much of the Type III core of the Covered test pile remained above freezing (Pham, in preparation). The heat trace to the basal lysimeters was turned off in June 2011. Since that time, only the heat trace in the basal drain has operated.

1.5.4 Hydrology

A detailed description of the Diavik site hydrology for 2007 is provided by Neuner *et al*. (2012), and the hydrology from 2007 through 2011 is provided by Fretz (in preparation). The annual rainfall at the Diavik research site was 93 mm in 2007, 152 mm in 2008, 73 mm in 2009, and 95 mm in 2010, all below the maximum regional average of 164 mm, although 2008 was close to an average precipitation year (Fretz *et al*., 2012). Wetting fronts in the adjacent waste-rock test piles migrated during periods of thaw at rates of 0.2 to 0.4 m day^{-1} in response to common rainfall events and up to 5 m day^{-1} in response to intense rainfall (Neuner *et al*., 2012). The downward pore-water flux was estimated to be < 10^{-2} to 3 x 10^{-2} m

day^{-1} in response to common rainfall and up to 0.7 m day^{-1} in response to intense rainfall (Neuner *et al*., 2012). Infiltration rates from 2007 to 2010 ranged from 8 to 57% (Fretz, in preparation).

1.5.4.1 AZLs

During 2007, flow occurred in the Type III AZLs between August and November (Table 1.3). In 2008, flow commenced in late June in the Type III AZLs and in one Type I AZL (Type I West). By mid-August 2008, flow also was recorded in the fourth AZL (Type I East). In 2009 and 2010, flow was observed between June and the end of October in all AZLs.

In 2007, limited flow reached the base of the Type III AZLs (Figure 1.5 and Table 1.3). Five artificial rainfall events (total volume: 183 L) were applied to the Type III AZLs in 2007 to bring the moisture content up to field capacity. A total of 35 L reported to the base of the Type III East AZL and 33 L to the Type III West AZL from late August through November 2007. In 2008, an artificial rainfall event (21.3 L) and a tracer test (29.9 L) were applied to the Type III AZLs. In addition, a 1-in-100-year natural rainfall event occurred in August 2008. A total of 201 L reported to the base of the Type III East AZL and 202 L to the Type III West AZL during the period from late June through November 2008. In 2009, flow returned to volumes of 21 L in the Type III East AZL and 34 L in the Type III West AZL, similar to the volumes measured in 2007 (Figure 1.5). The flow volume increased in 2010, to 55 L in the Type III East AZL and 63 L in the Type III West AZL.

The Type I AZLs reached field capacity through natural rainfall. Flow was delayed compared to the Type III AZLs, and commenced in 2008 with 194 L measured in the Type I East AZL and 297 L in the Type I West AZL. The apparent delay in flow in the Type I AZLs

relative to the Type III AZLs observed in 2007 can be attributed, in part, to the artificial rainfall events applied to the Type III AZLs. In addition, differences in flow volumes between the Type I and Type III AZLs probably were due to one or all of the following: 1) delay in the wetting of the matrix material in the AZLs; 2) the Type I East AZL was damaged and repaired during construction, leading to uncertainty in the flow measurements; or, 3) a lower proportion of matrix material contained in the Type I East AZL than was estimated (Chapter 3; Bailey *et al*., 2012). In 2009, 22 L reported to the base of the Type I East AZL and 65 L to the base of the Type I West AZL (Figure 1.5). Flow in 2010 totalled 93 L in the Type I East AZL and 100 L in the Type I West AZL.

1.5.4.2 Type I and Type III Test Piles

A simulated 5- to 10-year return-period (16.5 mm) rainfall event with a deuterium tracer was applied to the Type III test pile on August 17, 2007 (Neuner, 2009). A Cl and Br tracer test, which added 29 mm of simulated precipitation, was applied to the Type III test pile on September 13, 2007 (Neuner, 2009). These two events added 60 mm of precipitation to the Type III test pile above the natural precipitation in 2007, and the rainfall in subsequent years was derived entirely from natural events. The Type I test pile was not irrigated and reached field capacity based on natural rainfall events.

Flow first reported to the Type III north and south basal drains in May 2007, and flow ceased in November, when the internal test pile temperature decreased below freezing (Figure 1.6). Flow in 2008, 2009, and 2010 began in May and ceased late October. Limited flow reported to the Type I basal drain flow-through cells in 2007, and few data were collected from this location as a result of damage to the drain lines or because there was no

flow to the base of the pile (Figure 1.6). The Type I test pile drain was repaired in April 2008, and flow began in early May and ceased in October. Similarly, in 2009 flow commenced in May and ceased in October. In 2010, however, technical problems with the heat trace prevented the drain from thawing, and water did not reach the instrumentation hut in May or June. After the heat trace was repaired, flow recommenced in July and ceased in October. Detailed hydrology from both test piles in 2007 through 2008 is described by Neuner *et al*. (2009, 2012).

In 2007, limited flow reached the base of the Type III test pile as the pore space filled to field capacity. Flow commenced in the Type III test pile in May 2007 and a total of 110 m^3 reported to the Type III north and south drains combined, over the period from late May through November. In 2008, the total outflow volume from the Type III basal drains was 150 m^3 and 117 m^3 in 2009. In 2010, the outflow increased to 213 m^3. Flow in the Type I test pile was delayed compared to the Type III test pile, and commenced in 2008 with a total of 51 m^3 of outflow. In 2009, 10.5 m^3 reported to the base of the Type I test pile, and 44 m^3 reported to the base of the Type I test pile in 2010.

1.5.4.3 Covered Test Pile

Construction of the Covered test pile began in 2006 and was completed in early 2007. Rainfall on the Covered test pile was derived entirely from natural events. In September 2007, sporadic flow commenced and continued through January 2008, releasing a total of 0.5 m^3 (Figure 1.7). Flow resumed in September 2008, and complications with the tipping-bucket flow gauge resulted in the loss of flow measurements between September and November 2008; flow continued until June 2009. The measured flow was 55 m^3, and the

interpolated volume of lost flow was 120 m^3, for a total of 175 m^3. After a short, dry period, flow started in August 2009 and continued through the end of May 2010 (30 m^3). Flow recommenced in July 2010 and continued through to July 2011 (Figure 1.7), and a total of 100 m^3 reported to the drain between July 2010 and January 1, 2011.

Unlike observations for the Type III test pile, the basal effluent flow rates from the Covered test pile did not correlate to external temperatures. In the Covered test pile, the rate of basal outflow was limited by the rate of infiltration through the till layer. The maximum discharge rates were observed in the winter months. Measurements on the Type I layer in the Covered test pile indicated that the permeability and porosity of this layer were similar to that of the rock within the Type III test pile. Measurements indicated that the permeability of the Covered test pile till layer was lower 1.5×10^{-10} m^2, and lessened the rate of infiltration into the underlying Type III core of the Covered test pile. However, the total volume of water that reported to the base of the Covered test pile was greater than that of the uncovered Type I pile for the same time period, indicating water may have migrated through the till layer. The till directly above the basal lysimeters (Face 1 and Face 2) was influenced by the heat trace, causing temperatures within the till layer to remain above 0°C, allowing water to migrate downward. The first flush of water through the matrix material is determined by the dissipation of resident tracers within the waste rock, such as the blasting residuals NO_3^- and Cl^- (Chapter 2; Bailey *et al*., 2012). The Covered test pile experienced consistent concentrations of blasting residuals with a gradual decrease over time (Chapter 2; Bailey *et al*., 2012).

1.6 Thesis Organization

This thesis is presented as a series of chapters related to the objectives outlined in the previous sections. Each chapter (excluding the introduction and overall conclusion) is prepared in the form of a journal article, which will be submitted for publication in a peer-reviewed journal; therefore, some repetition in chapters was unavoidable. The first chapter (Chapter 1) provides a global introduction and introduces the research objectives, hypothesis, background and justification; the results of the research are presented in six chapters, Chapters 2 through 7; and the thesis research is summarized in Chapter 8.

The first research paper (Chapter 2) describes the persistence of blasting residuals emanating from waste rock at different scales. This chapter has been published in *Applied Geochemistry* (Bailey *et al*., 2012). The next chapter (Chapter 3) describes the geochemical and microbiological evolution in the upper 2 m active zone of waste-rock material through the study the AZLs. Chapter 4 characterizes the geochemistry and microbiology of effluent and pore water from the two large-scale, waste-rock test piles: one with Type I waste rock (0.035 wt. % S) and the other with Type III waste rock (0.053 wt. % S). Chapter 5 presents a comparison between the large-scale Type III test pile (described in Chapter 4) and an additional Type III test pile with a dry cover reclamation system applied to the surface (Covered test pile). Chapter 6 discusses the spatial and temporal analysis of the microbial communities in the AZLs and the Type I, Type III, and Covered test piles with evolving geochemistry. Chapter 7 evaluates the potential use of laboratory humidity-cell experiments to predict the water quality the AZLs. The final chapter, Chapter 8, presents a general summary of the findings from the research papers and suggestions for future study.

Table 1.1 Known characteristics of the Type I and Type III AZLs (from Neuner, 2009).

	Units	Type III	Type I
Volume of AZL	m^3	5.947	4.87
Volume of rock	m^3	3.866	3.166
Mass of rock	t	10.24	8.389

Table 1.2 Waste-rock test pile construction properties (from Neuner, 2009).

Test pile properties		Type I test pile	Type III test pile	Covered test pile			
				Core	Type I	Till	Total
Volume of pile	1000 m^3	39	44	40	44	14	99
Volume of rock	1000 m^3	25	28	26	28	9	64
Mass of rock	1000 t	68	70	70	75	25	170
Sulfur content	wt. %	0.037	0.053	0.080	0.037	0.03	
Mass of sulfur	t S	25	74	56	28	7	91

Table 1.3 Annual flow volumes (L) from the Type I and Type III AZLs (2007 to 2010; from Fretz, in preparation).

AZL	Flow (L)				
	2007	2008	2009	2010	Total
Type III West	33	202	34	63	332
Type III East	35	201	21	55	312
Type I West	--	297	65	100	462
Type I East	--	194	22	93	309

a) b)

Figure 1.1 Construction series of AZL: a) HDPE tanks with drain lines installed; b) completed AZLs (photographs from Neuner *et al.*, 2012).

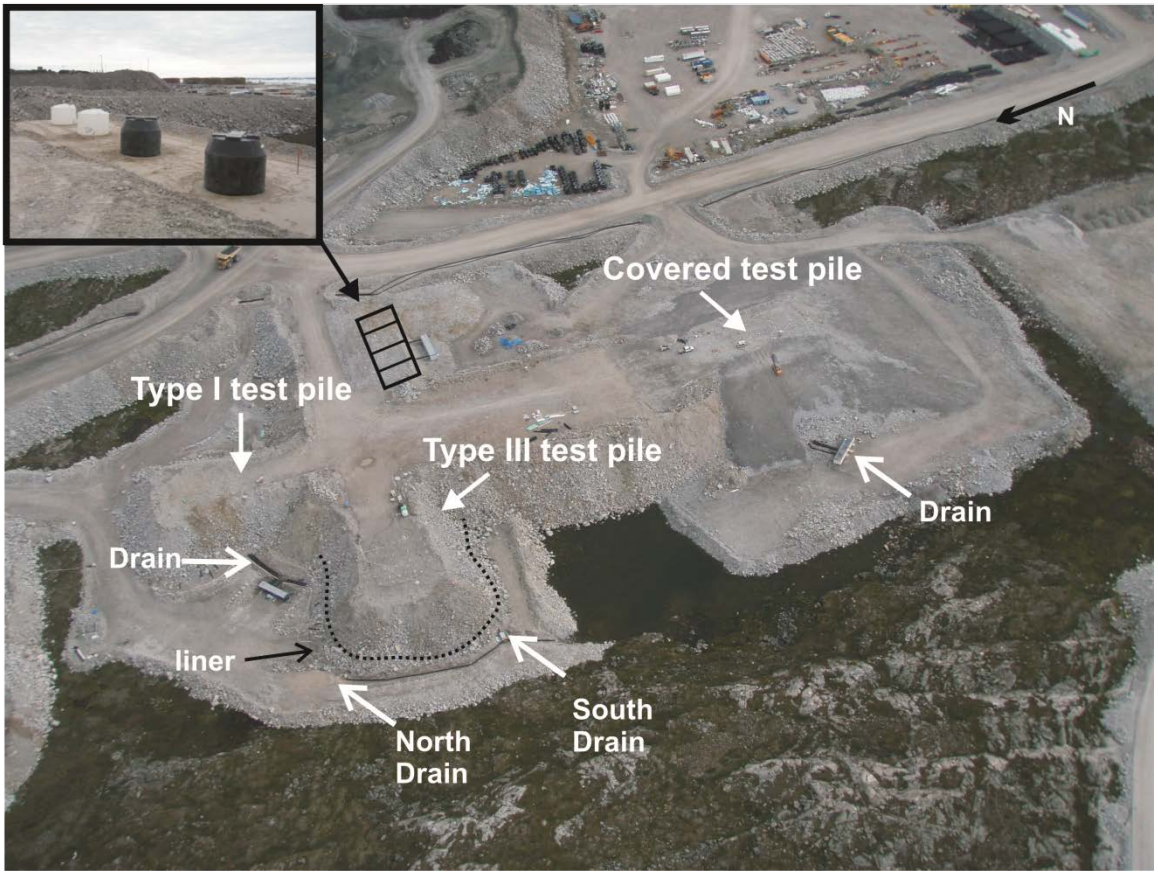

Figure 1.2 Aerial view of the Diavik Waste Rock Research Facilities showing locations of the Type I test pile, Type III test pile, Covered test pile, and AZLs. Dashed line represents the HDPE liner. Insert shows the HDPE barrels used in the construction of the AZLs before rock placement.

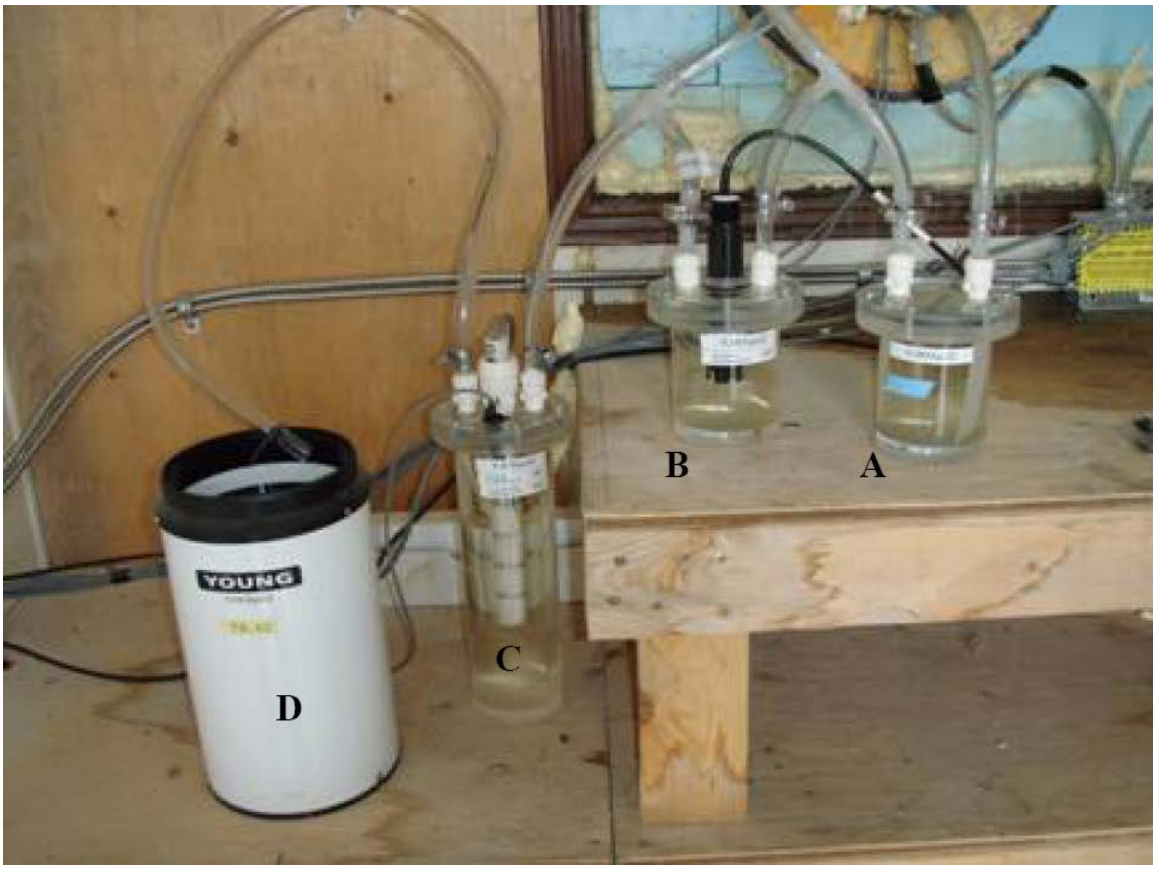

Figure 1.3 Flow-through cell set-up: a) water sampling cell; b) pH measurements; c) electrical conductivity measurements; d) flow measurements

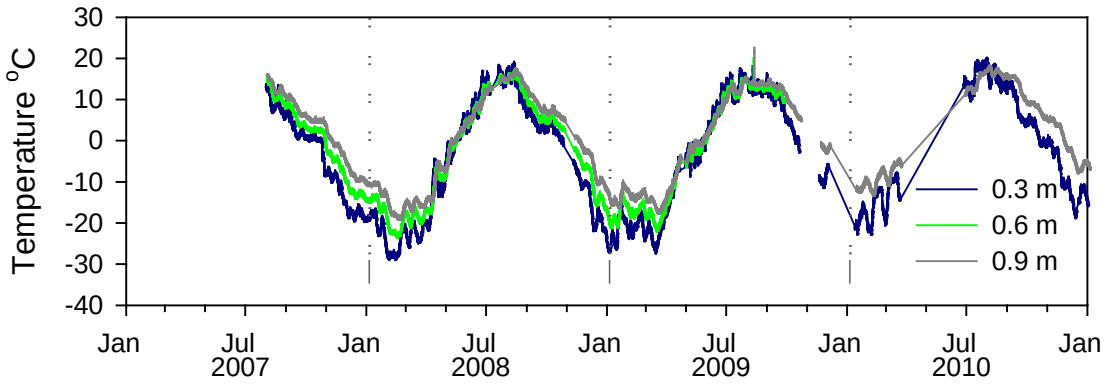

Figure 1.4 Temperatures in the AZLs at 0.3, 0.6, and 0.9 m depths from 2007 through 2010 (Fretz, in preparation).

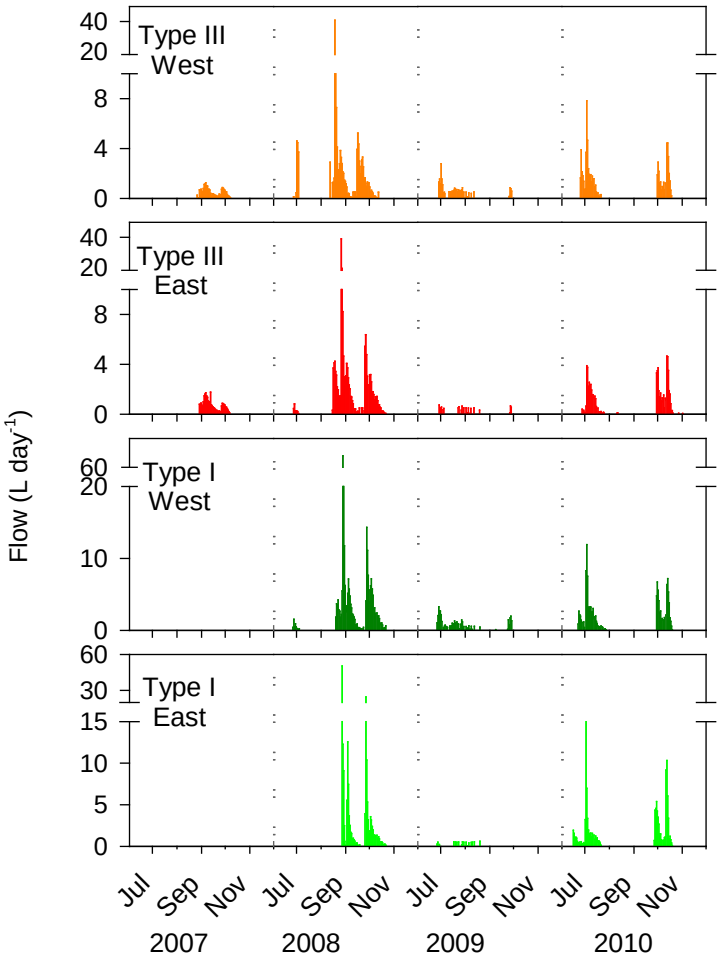

Figure 1.5 Flow (L day^{-1}) for each location from 2007 through 2010. The dashed line represents a break in time during dry periods over the frozen months (Fretz, in preparation).

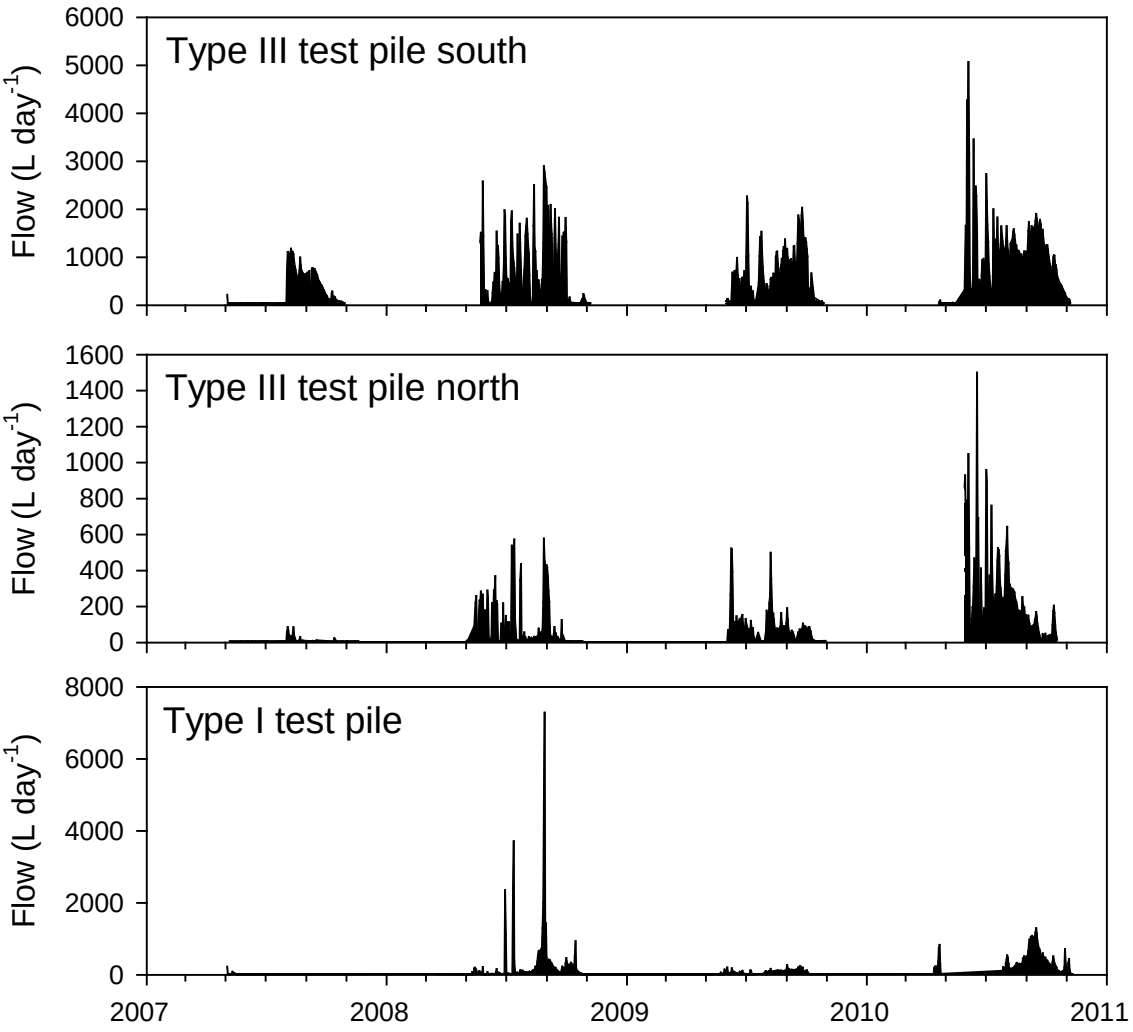

Figure 1.6 Flow (L day^{-1}) for each location from 2007 through 2010 (Fretz, in preparation).

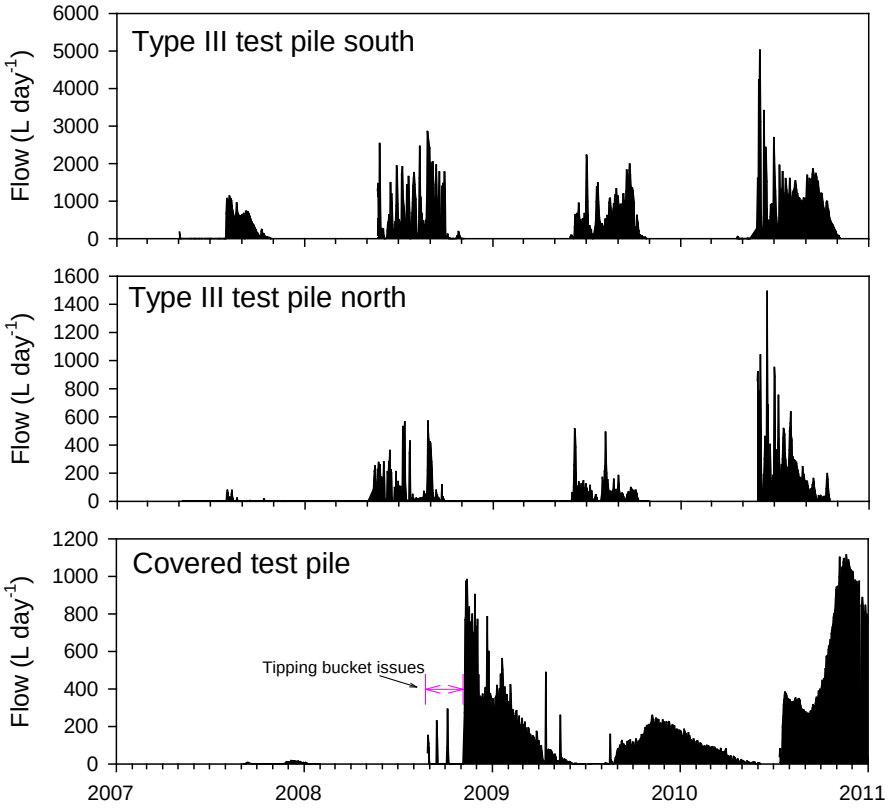

Figure 1.7 Flow (L day^{-1}) for each location from 2007 through 2010 (Fretz, in preparation).

Chapter 2:

Persistence of contaminants from blasting agents in waste-rock effluent

Bailey, B.L., Smith, L.J.D., Blowes, D.W., Ptacek, C.J., Smith, L., Sego, D. 2012. Diavik Waste Rock Project: Persistence of contaminants from blasting agents in waste rock effluent. Appl. Geochem. DOI 10.1016/j.apgeochem.2012.04.008. Editorial and formatting changes have been made to accommodate reproduction in this thesis.

2.1 Executive Summary

During mining operations, explosives are used to fragment rock into workable size fractions. Mine-water chemistry can be affected by blasting agent residuals, including NH_3, NO_2^-, NO_3^-, Cl^-, and ClO_4^-. At the Diavik diamond mine, Northwest Territories, Canada, waste rock generated from open-pit and underground mining is stockpiled on site. Three large-scale test piles measuring 60 by 50 m at the base and 15 m in height, along with four 2 × 2 m lysimeters each 2 m in height, were constructed at Diavik as part of a comprehensive research program to evaluate the quality of water emanating from waste-rock stockpiles. On-going monitoring of the water chemistry since 2007 shows that blasting residuals comprise a large proportion of the dissolved constituents in the initial pore water and effluent. Leach tests conducted on freshly blasted rock from Diavik indicate the mass of N released corresponds to a 5.4 % N loss from the blasting explosives; this mass is in the range for N loss reported for blasting operations at Diavik during the period when the test piles were constructed. The total mass of N released from the lysimeters was also within this range. The three large-scale test piles have only released a small fraction of the N estimated to be contained within them. Blasting of waste rock contributes SO_4^{2-} to effluent through the oxidation of sulfide minerals in the rock during the blast. During the initial flush of water, the test pile that contained waste rock with the higher S content was observed to release higher concentrations of SO_4^{2-} than the test pile with lower S content waste rock. Mass-balance calculations based on the ratios of SO_4^{2-} to total N can be used to estimate the relative contributions of sulfide oxidation within the test piles and SO_4^{2-} released when S in the host rock is oxidized during blasting. These calculations provide an estimate of S mass released during the first flush of the test piles.

2.2 Introduction

2.2.1 Background

Mining generates and moves the greatest volume of materials in the world (ICOLD, 1996). At mine sites around the globe, explosives are used to fragment rock into workable size fractions. In 2009, mining consumed 87 % of explosives used in the United States, excluding military use (USGS, 2009). Ammonium nitrate mixed with fuel oil (ANFO) is the primary blasting agent used in the mining industry (80 %) versus alternatives such as 2,4,6-trinitrotoluene (TNT), nitroglycerine, and perchlorate salts. Although relatively inexpensive and safe to transport, store, and use, ammonium nitrate is hygroscopic. Increases in moisture content can cause the explosive to lose efficacy, potentially resulting in detonation failures (Pommen, 1983) and the eventual release of undetonated explosives to the environment. Emulsion explosives are similar in composition to ANFO, but include an aqueous solution supersaturated with respect to ammonium nitrate prill surrounded by an immiscible fuel oil. This formulation decreases the dissolution of ammonium nitrate in water (Egly and Neckar, 1964). Emulsions contain 20 to 30 % total N (N_{Total}) and are usually blended with ANFO for applications in wet blast holes (Pommen, 1983). Ore and waste rock are blasted using ANFO emulsion explosives at the Diavik diamond mine (Diavik), Canada. Explosives are detonated with a boosting agent that contains ClO_4^-, which can release Cl^- during detonation (Aziz, 2006).

Nitrate has low toxicity to aquatic life (Pommen, 1983) and is an important nutrient source for aquatic plants; however, elevated concentrations of NO_3^- can lead to eutrophication if other requirements such as light and P are abundant (Stumm and Morgan, 1996). Nitrite and

NH_3 are toxic to fish at low concentrations (CWQG, 1987). In addition to blasting, sources of NO_3^- and NH_3 to the environment include agricultural activity, wastewater disposal, and landfills.

Perchlorate can have harmful effects to human health at concentrations in the low $\mu g\ L^{-1}$ range (Cox, 1994; NRC, 2005; Ting *et al*., 2006). Perchlorate has been found in surface water and groundwater surrounding explosive processing plants, military testing sites, mine sites, and sites where fireworks have been detonated (Susarla *et al*., 1999; Motzer, 2001; ITRC, 2005; Jackson *et al*., 2005; Parette *et al*., 2005; Sanchez *et al*., 2005; Schaefer *et al*., 2007; Wilkin *et al*., 2007).

Ammonium nitrate is highly soluble in water, rapidly dissociating into NO_3^- and ammonium (NH_4^+). Ammonium can further dissociate to NH_3 in alkaline conditions (Clark, 1981):

(*2.1*) $$NH_4NO_3 + H_2O \rightarrow NO_3^- + NH_4OH + H^+$$

(*2.2*) $$NH_4^+ + OH^- \rightarrow NH_3 + H_2O$$

Under aerobic conditions, NH_3 is oxidized to the unstable intermediate N species NO_2^- by the *Nitrobacter* group of nitrifying bacteria (Koren *et al*., 2000):

(*2.3*) $$2NH_4^+ + 3O_{2(g)} \rightarrow 2NO_2^- + 2H_2O + 4H^+$$

Nitrite is further oxidized to NO_3^- by the *Nitrosomonas* group of nitrifying bacteria (Sawyer and McCarty, 1967):

$$2NO_2^- + O_{2(g)} \rightarrow 2NO_3^- \quad (2.4)$$

Under aerobic conditions, NO_3^- persists in solution and is not readily adsorbed by soils or aquifer materials (Baalsrud and Baalsrud, 1954). Reducing conditions and sufficient soluble organic C are required for denitrification by heterotrophic bacteria including *Pseudomonas, Paracoccus, Flavobacterium, Alceligenes,* and *Bacillus* spp. (Koren *et al*., 2000). Denitrification by autotrophic bacteria, such as *Thiobacillus denitrifican*, reduces NO_3^- to $N_{2(g)}$ coupled with the oxidation of sulfide or organic C at neutral pH (Schedel and Truper, 1980; Sanmugasunderam *et al*., 1987; Kuenen *et al*., 1992).

Remediation systems have been developed to remove N species from waste water disposal sites and landfills (Blowes *et al*., 1994b; Diamadopoulos *et al*., 1997; Robertson *et al*., 2000, 2009), but few studies have addressed the removal of N species from mill and mine effluents. Koren *et al*. (2000) demonstrated microbial treatment methods for the removal of NH_3 and NO_3^- from simulated mill and mine effluent with low nutrient content. Zaitsev *et al*. (2008) demonstrated the removal of NH_3 and NO_3^- from two underground mine water samples using fixed-bed biofilm reactors at low temperatures. However, these studies do not discuss the release of N species from waste-rock piles.

Waste rock is commonly stockpiled on the ground surface, where both undetonated explosives and blasting residuals within the waste rock can be flushed by rain water,

snowmelt, or groundwater. At locations where waste rock or ore contain sulfide minerals, such as pyrite [FeS_2] and pyrrhotite [$Fe_{1-x}S$], these minerals may be oxidized during blasting, potentially releasing SO_4^{2-} to the environment (Briggs and Kelso, 2001). Nitrate and NH_3 released from the use of explosives are usually attributed to ammonium nitrate spillage or incomplete detonation and subsequent dissolution (Cameron *et al.*, 2007). These sources result in releases of NO_3^- and NH_3 in mine effluent. The objectives of this study are to determine the concentrations of blasting agents, their residuals, and S oxidation products resulting from blasting in drainage water derived from waste-rock test piles located at the Diavik diamond mine.

2.2.2 Site Description

Diavik is located 300 km north of Yellowknife, Northwest Territories (64°29' N; 110°18' W; elevation 440 m), on a 20 km^2 island in the oligotrophic Arctic lake Lac de Gras. The study area is in the continuous permafrost region with a mean annual air temperature of -9.0 °C within a range of 27 °C in July to -44 °C in January/February (1998 to 2007 data; Environment Canada, 2010). This study area is located in a semi-arid climate, receiving an average mean annual precipitation of 280 mm from March 1998 to March 2007 of which 65 % occurred as snow (Environment Canada, 2010).

At Diavik, an open pit and underground diamond mine, the economic ore body is diamondiferous kimberlite. The host rock consists of granite and granite pegmatite, both containing irregular xenoliths of biotite schist. These host rocks are cut by diabase dikes. The granites contain only trace sulfides, and are considered non-acid generating with little neutralization potential. The granite consists mainly of K-feldspar [$KAlSi_3O_8$], albite

[$NaAlSi_3O_8$], and quartz [SiO_2], with < 5 % each of biotite [$KMg_3AlSi_3O_{10}(OH)_2$] and muscovite [$KAl_2AlSi_3O_{10}(OH)_2$] (Jambor, 1997). The biotite schist (< 0.42 wt. % S) contains locally disseminated pyrrhotite with lesser amounts of pyrite, sphalerite, and chalcopyrite and has little neutralization potential; therefore, it is considered potentially acid generating (Smith *et al*., in press). The biotite schist aluminosilicate mineral assemblage consists mainly of quartz (20 to 50 %), albite (35 to 55 %), and biotite (10 to 25 %). Waste rock at the mine site is classified and segregated according to S content: Type I (< 0.04 wt. % S), Type II (0.04 wt. % S to 0.08 wt. % S), and Type III (> 0.08 wt. % S). The mine is expected to generate a 120 Mt waste-rock stockpile over the course of production. Although the S content of the Diavik waste rock is low, the carbonate mineral content is also very low, providing little neutralizing capacity (Jambor, 1997; Smith *et al*., in press).

2.2.3 Test Pile Instrumentation

Three large-scale test piles were constructed at Diavik to assess the hydrology, temperature, and (bio)geochemical reactions in waste-rock piles in permafrost terrains (Smith *et al*., 2012, in press; Figure 2.1). Two of the test piles, measuring 60 by 50 m at the base and 15 m in height, are constructed of run of mine waste rock resting at the angle of repose. The Type I test pile contains 0.035 wt. % S and the Type III test pile contains 0.053 wt. % S (lower than the operational S target of > 0.08 wt. % S; Smith *et al*., in press). A third test pile (the Covered test pile) was constructed based on a reclamation concept for the Type III waste rock at Diavik. The configuration consists of 13 m of Type III waste rock (average of 0.082 wt. % S) covered with 1.5 m of glacial till and then 3 m of Type I waste rock. The test piles are underlain by an impermeable high-density polyethylene (HDPE) liner, which

collects effluent at their respective bases. This water is directed to instrumentation huts by gravity flow through polyvinyl chloride (PVC) drain lines with mineral insulated (MI) heating cable set to maintain temperatures between 5 and 10°C to facilitate the collection of water samples. Water in the instrumentation huts flows through a series of flow through cells, where water samples are collected and continuous measurements of pH, electrical conductivity (EC), and flow rates are obtained.

Four lysimeters were constructed in the upper 2 m of waste rock (referred to as active zone lysimeters; AZLs) at a site adjacent to the test piles to provide detailed information on the hydrology and geochemistry within the thermally active layer near the pile surface (Figure 2.1). These lysimeters were constructed using 2 m diameter × 2 m high HDPE tanks; two are filled with sub-samples of Type I waste rock from the same haul truck load with an average of 0.017 ± 0.0095 wt. % S (n = 2; Type I East and West lysimeters) and two with Type III waste rock from the same haul truck load with an average of 0.035 ± 0.015 wt. % S (n = 2; Type III East and West lysimeters). Drainage from the AZLs is directed to an instrumentation trailer through gravity flow where the effluent pH, EC, temperature, and flow rate are continuously monitored. Full details on the design, construction and instrumentation of the test piles and AZLs are provided by Smith *et al*. (2012). Pham *et al*. (2012) provides a discussion of the thermal regime within the test piles, and Neuner *et al*. (2012) and Fretz *et al*. (2011) provide discussions of hydrologic processes controlling infiltration through the test piles and the AZLs.

2.3 Methods of Investigation

2.3.1 Laboratory Leach Test Methods

Eight laboratory leach tests were completed using recently blasted (within 3 months) Type I waste rock collected from the open pit at the Diavik site in September 2009. The samples were from the same blast pattern at the mine site. Leach tests (LT1 through LT8) consisted of 100 g of run-of-mine un-crushed waste rock sieved to < 20 mm. Waste rock was mixed with 1 L of Milli-Q-grade water in a pre-washed HDPE bottle placed on a bench top orbital shaker (Model 3520, Lab-Line Instruments, USA) at 40 rpm for 48 h and were completed in triplicate. Mean values were calculated and were labelled according to the sample (e.g., LT1 through LT8). Water samples were collected using a sterile 30 mL polyethylene (PE) syringe placed in the leach test bottle. Water was then passed through 0.45 μm cellulose-acetate membrane filters into pre-washed and sample triple-rinsed HDPE bottles. The samples were refrigerated at 4 °C until analysis at the University of Waterloo. Concentrations of SO_4^{2-}, NO_3^-, NO_2^-, and Cl^- were determined using ion chromatography (IC; DX600, Dionex, USA). All concentrations of NO_3^- and NO_2^- are expressed as mg L^{-1} NO_3^--N and mg L^{-1} NO_2^--N, respectively. Concentrations of NH_3 (NH_3-N; salicylate method) were determined using a Hach spectrophotometer DR/8400 (SMEWW, 2005).

2.3.2 Field Characterization Methods

At each sampling location, pH, EC, temperature, and alkalinity were determined for water collected from the sampling-cell system. Water samples were collected from flow-through cells using 0.64 cm PE tubing attached to a sterile 60 mL PE syringe. The water was passed through 0.45 μm cellulose-acetate membrane filters into pre-washed HDPE sample bottles

that had been triple-rinsed with sample water prior to filling. This water passed through the basal drains prior to entering the sampling system and thus was exposed to $O_{2(g)}$. Pore-gas concentrations within the lysimeters were not measured; however, testing in the large-scale waste-rock piles indicated that $O_{2(g)}$ and $CO_{2(g)}$ concentrations throughout the test piles were at atmospheric levels (Amos *et al*., 2009a). The pH measurements were made using a combination electrode (Orion ROSS Ultra® 8156, Thermo Scientific, USA) calibrated using pH 7, 4, and 10 or 1.68 standard buffer solutions. E_h measurements were made with a Pt redox electrode (Orion 96-78; Thermo Scientific, USA) checked against ZoBell's (Nordstrom, 1977) and Light's solutions (Light, 1972). Alkalinity measurements were made using a Hach digital titrator with bromcresol green/methyl red indicator and 0.16 N H_2SO_4. Field measurements were completed using a Hach spectrophotometer DR/8400 for the determination of NH_3 (NH_3-N; salicylate method) concentrations for selected samples (SMEWW, 2005). Additional non-acidified, filtered samples were refrigerated at 4 °C until analysis at the University of Waterloo for inorganic anion concentrations (SO_4^{2-}, NO_3^-, NO_2^-, and Cl^-) by ion chromatography (IC; DX600, Dionex, USA) within 3 weeks of the sampling date. All concentrations of NO_3^- and NO_2^- are expressed as mg L^{-1} NO_3^--N and mg L^{-1} NO_2^--N, respectively. Quality control and quality assurance were assessed by evaluating several standards covering the range of measured concentrations, and incorporating both field replicates and blanks into the protocol.

2.3.3 Perchlorate Analysis

Water samples were collected from flow-through cells and filtered as described above, then frozen at -20 °C until analysis at the University of Waterloo. The analytical method for

perchlorate followed the procedure described by Snyder *et al*. (2005), with an additional step involving the addition of ^{18}O-labelled ClO_4^- to all standards and samples to assess matrix interferences. Each water sample was prepared by elution through an OnGuard II barium cartridge and an OnGuard II hydronium cartridge (Dionex, USA) to remove high concentrations of SO_4^{2-} and polyvalent cations, such as Ca and transition metals, from sample matrices. The cartridge extracts were analyzed using high performance liquid chromatography (HPLC; Agilent 1100, Agilent Technologies, Mississauga, Canada) with electrospray tandem mass spectrometry (LC/MS/MS; 4000 Q Trap, Applied Biosystems, Foster City, USA) operated in electrospray ionization (ESI) negative mode. The following conditions were found to provide the optimum signal: curtain gas -10 arbitrary units (a.u.), turboionspray voltage -4500 V, temperature 750 °C, nebulizer gas 55 a.u., auxiliary gas (turbo) 60 a.u., and collision gas 8 a.u. Four multiple reaction monitoring transitions were determined: m/z 99 to 83 and m/z 101 to 85 for native ClO_4^-, and m/z 107 to 89 and m/z 109 to 91 for enriched ClO_4^-.

Perchlorate was quantified using the internal standard technique. Instrument calibration was performed using a 10-point linear regression with $1/x^2$ weighting. Measured responses were corrected for the recovery of internal standards added to both standards and unknown samples. Method blanks were analyzed and calibration checks conducted every 10 samples. Perchlorate was not detected in the method blank samples and instrument calibration blank samples. The analytical precision was checked by analyzing duplicate samples following the entire preparation procedure. The relative standard deviation of duplicates was less than 5 % and the error less than 0.2 %. The instrument and practical detection limits were 0.02 and 0.05 $\mu g\ L^{-1}$, respectively.

2.4 Results and Discussion

2.4.1 Laboratory Leach Tests

The concentrations of NO_3^--N and NO_2^--N followed similar trends in all of the leach tests; however, higher concentrations of both species were observed in leach test LT1 and lower concentrations in LT7 and LT8 (Table 2.1). The NH_3-N was below detection (< 0.02 mg L^{-1}) for all leach test samples. For the eight laboratory leach tests conducted on the freshly blasted waste rock, N_{Total} concentrations averaged 0.46 mg L^{-1} (4.6 mg N kg^{-1} waste rock), with lower concentrations observed in two samples (LT7 and LT8; Table 1). All leach tests had similar SO_4^{2-} concentrations with the exception of higher levels in LT1 and LT8. Chloride concentrations were similar for all leach tests with the exception of higher concentrations in LT1.

Six leach tests (LT1 through LT6) had similar ratios of N_{Total} to Cl^-, SO_4^{2-} to N_{Total} and SO_4^{2-} to Cl^-; whereas, values for leach tests LT7 and LT8 were lower (Table 2). Leach test LT1 had the highest concentrations of Cl^-, N_{Total}, and SO_4^{2-}, resulting in a higher than average ratio of N_{Total} to Cl^-, and a lower than average ratio of SO_4^{2-} to Cl^-. The ratio of SO_4^{2-} to N_{Total} was consistent with average ratios (Table 2). Leach test LT7 had the lowest N_{Total} concentration, and leach test LT8 had the second lowest N_{Total} concentration (after LT7) and second highest SO_4^{2-} concentration (after LT1; Table 1). The differences in the observed N_{Total} released likely reflect variations in leachable blasting residuals in the waste-rock samples attributable to differences in the blasting activity, with samples derived from locations in the vicinity of blast holes having higher concentrations of blasting residuals than those located further away. Similarly, the variation in SO_4^{2-} released during the leach tests

was likely due to differences in the mass of S exposed to the explosion during blasting. These differences could be a result of variations in the proximity of the sample to the blast hole or the original S content of the rock, with higher SO_4^{2-} concentrations expected for samples with a higher original S mass. Humidity cell leaching experiments completed on Type I and Type III waste rock show that SO_4^{2-} to N_{Total} ratios are greater for samples with a greater S content relative to samples with a lower S content (unpublished data).

2.4.2 Diavik Field Site

2.4.2.1 Blasting Residuals in the Active Zone Lysimeters

Drainage commenced in the Type I AZLs in the spring of 2008. Both the Type I East and West AZLs maintained near neutral conditions for the duration of the study (Figure 2.2). The blasting residuals attained maximum concentrations of NO_3^--N, NO_2^--N, NH_3-N, and ClO_4^-, in the Type I West and East AZLs in early 2008 (Figure 2.2 and Table 2.3), with the exception of NO_2^--N and ClO_4^- in the Type I East which had maximums in 2010. The maximum ClO_4^- concentration may have occurred in samples not analyzed from 2008 with high concentrations of other blasting residuals. Concentrations of Cl^-, SO_4^{2-}, and NO_3^--N decreased sharply at the end of August and beginning of September 2008, indicating flushing of the blasting residuals initially present in the Type I AZLs. The concentrations of these components remained low for the remainder of 2008. Although the concentrations of dissolved NH_3-N and NO_2^--N also decreased sharply in September 2008, low concentrations persisted in the effluent. Concentrations of dissolved SO_4^{2-} increased early in 2009 and 2010. The absence of Cl^- during these years suggests that most of the SO_4^{2-} was derived from *in situ* sulfide-mineral oxidation within the AZLs.

A sharp decline in Cl^- concentrations occurred after approximately 153 L of flow through the Type I West AZL. The volume of flow prior to the decline in Cl^- concentrations was lower (77 L) in the Type I East AZL. However, the record of flow measurements was less comprehensive for the Type I East AZL. In addition, the Type I East AZL was damaged during placement of waste rock in the lysimeter, requiring a repair, but leading to greater uncertainty in the Type I East AZL flow measurements.

The sharp declines in Cl^- concentrations that occurred after 77 L in the Type I East AZL and 155 L in the Type I West AZL probably represent the first flush of recharge water. The total volume of the Type I AZLs is 5.7 m^3. Neuner *et al*. (2012) estimated the total porosity of the Diavik waste rock to be 0.25, and that 18 % of this porosity is associated with the matrix, corresponding to a bulk matrix porosity of 0.05 computed for the volume of the AZL. Using these values, the calculated matrix volume of the Type I lysimeters is 0.256 m^3 (256 L). The volume of water that passed through the Type I West AZL prior to the sharp decline in the concentrations of blasting residuals observed in September 2008 represents approximately 59 % of the matrix porosity volume. Flow in the Type I East AZL prior to the sharp decline in Cl^- concentrations corresponds to 30 % of the matrix porosity volume, suggesting that all of the flow through the Type I East AZL may not have been recorded. Alternatively, it may reflect differences between hydrologic properties of the Type I waste rock placed in these two lysimeters, and the subsequent influence of surface infiltration and flushing

Five artificial rainfall events were applied to the Type III AZLs in 2007, increasing the rainfall to 115 % of the annual mean rainfall (Neuner *et al*., 2012). A 53 mm artificial rainfall

event was applied on August 12, 2008; this event included the addition of a LiCl tracer. As a consequence of the artificial rainfall events, flow through the Type III AZL was greater than observed for the Type I AZLs. The addition of the LiCl tracer to the Type III AZLs precludes the use of Cl^- to identify the first flush of water from these lysimeters.

The Type III East AZL maintained near neutral (pH ~6) conditions in 2007, but the pH decreased to < 4.5 in 2008 and remained low for the remainder of the study. The pH in the Type III West AZL decreased through 2007 to pH 4 and remained low (pH < 4.5) through 2010 (Figure 2.3). From 2007 to 2010, the NH_3-N, NO_3^--N, and ClO_4^- concentrations in effluent from the Type III AZLs followed trends similar to those observed in the Type I AZLs: high concentrations in 2007, maximum concentrations during the mid-summer of 2008, a sharp decrease in concentrations at the end of August through the beginning of September 2008; and subsequently lower concentrations through 2009 and 2010 (Figure 2.3). Maximum concentrations of ClO_4^- and NO_3^--N were observed in 2007 in the Type III West, whereas NO_2^--N and NH_3-N were at their maximum in 2008. Concentrations of Cl^- and SO_4^{2-} reached maximum concentrations in 2010 (Table 3). The Type III East AZL effluent contained maximum concentrations of NO_3^--N, NH_3-N, ClO_4^-, and Cl^- in 2008 and maximum concentrations of NO_2^--N and SO_4^{2-} in 2010.

The tracer test initiated on the Type III AZLs in 2008 makes it difficult to distinguish the decrease in Cl^- concentrations associated with the first flush through these AZLs. However, the sharp decline in the concentrations of other blasting-derived constituents, including NO_3^--N, NH_3-N, and ClO_4^-, at the end of August probably represents the conclusion of the first flush of water through the finer grained matrix in these lysimeters. This decline corresponds

to a flow volume of 155 L in both AZLs. The Type III AZLs have an internal volume of 3.4 m^3. Based on the parameters estimated by Neuner *et al*. (2012), the bulk matrix porosity of these lysimeters is estimated at 0.17 m^3 (170 L). The volume of water that passed through the lysimeters prior to the sharp decline in the concentrations of blasting residuals observed in September 2008 represents approximately 91 % of the matrix porosity volume. The concentration of Cl^- sharply increased and decreased after the first flush, at the beginning of September. Chloride concentrations after this time were influenced by both Cl^- from the tracer test and blasting residuals.

The maximum concentrations of Cl^- and SO_4^{2-} increased in 2009 and 2010 in the Type III East AZL and in the Type III West AZL (Figure 2.3). Because Cl-containing minerals are very soluble and the potential for adsorption of Cl^- is low, transport of Cl^- through the AZLs is expected to be conservative. The N_{Total} to Cl^- ratios remained relatively constant in 2007 but declined in 2008, 2009, and 2010, possibly due to the addition of Cl^- during the tracer test. These observations suggest that although transformations may have occurred between N species, the overall transport of N_{Total} was conservative. The transport of ClO_4^- and N_{Total} initially resident in the AZLs suggests that the period of release of constituents present on the rock ended in August 2008. The subsequent increase in SO_4^{2-} concentrations and ratios of SO_4^{2-} to N_{Total} in the Type III AZLs in 2009 was probably due to *in situ* sulfide-mineral oxidation.

2.4.2.2 Blasting Residuals in the Experimental Test Piles

Intermittent flow was observed in the test pile basal drains over the study period (2007 to 2010). Because of the cold winter temperatures at the Diavik site, the entire thickness of both

the Type I and Type III test piles fell below freezing each winter. Each spring, as the temperatures in the test piles rose, flow commenced in the basal drains and increased throughout the summer before decreasing in September (Fretz *et al*., 2011). As the test piles warmed from the margins inward, increased regions of the test piles contributed water to the drains. The initial drainage was probably derived from the shorter flow paths originating on the sides (batters) of the test piles, with longer flow paths associated with the central portion of the test piles reporting later in the year. Furthermore, the Type III test pile received additional recharge through three artificial rainfall experiments in each of 2006 and 2007, including two tracer tests conducted in 2007 (Neuner *et al*., 2012). The artificial rainfall was applied only to the tops of the test piles and not to the test pile batters. Consequently, flow to the Type III test pile basal drains was substantially greater than flow to the Type I test pile basal drain.

2.4.2.3 Blasting Residuals in the Type I Test Pile Basal Drain

Significant water flow began to report to the Type I test pile basal drain in 2008. In 2009 and 2010, concentrations of blasting residuals increased gradually from May until October when they increased sharply as the volume of flow decreased. The maximum concentrations of blasting residuals in the effluent occurred in November 2010 (Figure 2.4; Table 4).

2.4.2.4 Blasting Residuals in the Type III Test Pile Basal Drains

The Type III test pile has two outflow drains (north and south). Flow to the Type III test pile basal drains commenced in 2007, with increased flow in subsequent years varying in response to changes in annual precipitation and temperature fluctuations. As the Type III test pile warmed during each field season, the pH decreased and concentrations of the blasting

residuals NO_3^--N, NH_3-N, SO_4^{2-}, Cl^-, and ClO_4^- increased (Figure 2.5). Concentrations of blasting residuals reached a maximum in August 2008 (Table 4) in the Type III north basal drain, and subsequently decreased and remained low throughout 2009. The concentrations of blasting residuals in the effluent from the Type III south basal drain peaked in October 2009 and remained elevated until the end of the field season. In 2010, Cl^-, N_{Total}, and SO_4^{2-} concentrations followed similar trends but at lower levels. Elevated concentrations at the end of the sampling session indicate contributions derived from longer flow paths and sources of blasting residuals not previously contributing to the pile drainage.

2.4.2.5 Blasting Residuals in the Covered Test Pile Basal Drain

The Covered test pile had limited outflow in 2007, but concentrations of blasting residuals increased from September to January 2008 when flow declined and then ceased (Figure 2.6). Flow resumed in September 2008 with the maximum concentrations of Cl^- and elevated concentrations of NO_3^--N and SO_4^{2-}. Flow continued until June 2009. Flow recommenced in August 2009 through the end of May 2010 when the maximum concentrations of N_{Total} and SO_4^{2-} were recorded (Table 5). Flow recommenced in July 2010 and continued for the remainder of the study.

2.4.3 Nitrogen Species

Nitrogen is present in the ANFO emulsion explosives used at Diavik as NH_4^+ and NO_3^-. The results of the leach test conducted on samples of recently blasted rock indicate the presence of NO_3^--N and NO_2^--N (Table 1); concentrations of NH_3-N were below detection. In the summers, when temperatures within the test piles rise to a maximum of 15 °C, the presence of detectable concentrations of NO_2^--N indicates the nitrification of NH_3 to NO_2^-. Elevated

concentrations of NO_3^--N were observed concurrent with maximum concentrations of NH_3-N and NO_2^--N, suggesting oxidation of NO_2^- to NO_3^-. As the first flush of water advanced through the test piles, un-detonated blasting residuals, principally NH_3 and NO_3^- with trace amounts of NO_2^-, as well as SO_4^{2-}, ClO_4^-, and Cl^-, were transported through the unsaturated waste rock. Nitrate can be removed by denitrification; however, reducing conditions and a sufficient supply of a labile electron donor are required. Denitrification by heterotrophic bacteria, e.g., *Pseudomonas, Paracoccus, Flavobacterium, Alceligenes,* and *Bacillus* spp., requires a labile source of organic C (Koren *et al*., 2000). The organic C content of the Diavik waste-rock piles is low. In addition, bacteria such as *Thiobacillus denitrificans* reduce NO_3^- to $N_{2(g)}$ coupled with the oxidation of sulfide or organic C at neutral pH, however, this reaction does not seem to have resulted in extensive denitrification within the AZLs or test piles. The presence of elevated concentrations of NO_3^--N were consistent with the high concentrations of $O_{2(g)}$ present (Amos *et al*., 2009a) and absence of labile organic C.

2.4.3.1 Ammonia

Concentrations of NH_3-N were only determined once in water collected from the Type III AZLs in 2007. The 2007 NH_3-N concentration was 2.6 mg L^{-1} in the Type III West AZL and 2.9 mg L^{-1} in the Type III East AZL. Ammonia reached maximum concentrations of 8.7 mg L^{-1} in the Type III East AZL in late July and 3.5 mg L^{-1} in the Type III West AZL in early August of 2008. In 2009, the NH_3-N concentration in the Type III West AZL effluent reached a maximum of 2.6 mg L^{-1} in 2009 and 3.5 mg L^{-1} in 2010. The Type III East AZL effluent NH_3-N concentration reached 6.6 mg L^{-1} in 2009 and 9.0 mg L^{-1} in 2010. Ammonia concentrations in the Type I East and West AZLs reached maximum values of 0.8 and

1.7 mg L^{-1}, respectively, in 2008. In 2009 and 2010, NH_3-N concentrations remained low (< 0.5 mg L^{-1}) in both the Type I East and West AZLs.

Concentrations of NH_3-N in the Type III south drain were low in early 2007 and increased to a maximum of 23 mg L^{-1} in July 2007. The Type III north drain reached maximum NH3-N concentrations in August 2007 at 34 mg L^{-1}. The NH_3-N concentrations progressively decreased through to the end of November 2007 when flow ceased due to low temperatures.

In 2008, the NH_3-N concentrations attained maximum values of 31 mg L^{-1} in the Type III north drain in July and 15 mg L^{-1} at the Type III south drain in August. The NH_3-N concentrations remained low through 2009 with the exception of the Type III south drain, which increased in October to its maximum and remained elevated until the end of the field season. Throughout 2010 NH_3-N concentrations in the Type III north drain were < 6 mg L^{-1}. The NH_3-N concentrations in the Type III south drain in 2010 followed a similar trend as in 2009, with low NH_3-N concentrations followed by much higher concentrations (54 mg L^{-1}) in October. These higher concentrations were attributed to an increase in the volume of waste rock affected by water flow, and, therefore, an increase in sources of blasting residuals. Elevated NH_3-N concentrations corresponded to increases in NO_3^--N, NO_2^--N, Cl^-, and SO_4^{2-}. Overall, effluent from the test pile basal drains had higher NH_3-N concentrations than effluent from the AZLs.

Flow in the Type I test pile began in May 2008. The maximum NH_3-N concentration (36 mg L^{-1}) was observed in September 2008 followed by a decrease (to 5.7 mg L^{-1}) for the remainder of the year. In 2009, NH_3-N concentrations in the Type I basal drain remained

< 5.0 mg L^{-1} with the exception of one sample (at 10 mg L^{-1}). In 2010, concentrations increased through the field season and reached a new maximum of 410 mg L^{-1} in November.

The Covered test pile had a low volume of flow from September 2007 to January 2008. Flow recommenced in September 2008 and continued through to the end of 2009. Ammonia concentrations increased over time to a maximum of 10 mg L^{-1} in April 2009 before decreasing for the remainder of the year. In 2010, concentrations reached a minimum of 1.0 mg L^{-1} in July and increased to 6.6 mg L^{-1} by the end of November.

2.4.3.2 Nitrite

Nitrite was not detected (< 0.05 mg L^{-1}) in any of the Type III AZLs in 2007. In 2008, concentrations were below detection in the Type III East and West AZLs prior to late September, and then increased to reach concentrations of 7.3 and 22 mg L^{-1}, respectively. In 2009 and 2010 the concentration of NO_2^--N were below detection with the exception of spikes in concentrations (6-10 mg L^{-1}) in August 2009 and July 2010. The NO_2^--N concentration in the Type I West AZL reached a maximum of 7.7 mg L^{-1} in July 2008. Concentrations of NO_2^--N in the Type I East AZL reached a maximum of 3.0 mg L^{-1} in late September 2008 and end of July 2010. Increases in NO_2^--N coincide with increases in NH_3-N and NO_3^--N.

Maximum NO_2^--N concentrations in the Type III test pile north drain were 1.8 mg L^{-1} in 2007 and 0.65 mg L^{-1} in 2008, whereas NO_2^--N concentrations in the Type III test pile south drain reached 3.7 mg L^{-1} in 2007 and 2.8 mg L^{-1} in 2008. The concentration of NO_2^--N was below detection in both the Type III north and south basal drains for most of 2009, with the exception of September when a maximum concentration of 1.6 mg L^{-1} was detected in the

south drain. In 2010, concentrations were also below detection in both drains, with the exception of July when low concentrations of ~1 mg L^{-1} were measured in both the north and south drains.

The NO_2^--N concentration in the Type I test pile reached a maximum value of 6.5 mg L^{-1} in late August 2008. Concentrations in 2009 were low when flow resumed in May, and remained below detection until October when the concentration increased to 6.5 mg L^{-1}. In 2010, NO_2^--N concentrations were elevated in comparison to previous years. The maximum concentration of 7.9 mg L^{-1} was detected in October when the peaks of other blasting residuals were observed at this location.

Effluent from the Covered test pile had low (< 2 mg L^{-1}) to undetectable concentrations of NO_2^--N in 2007. The peak NO_2^--N concentration of 13 mg L^{-1} occurred in September 2008 before decreasing to below detection. Concentrations were detectable in late 2009, but remained low (< 1 mg L^{-1}) and returned to below detection through 2010.

The measurement of low NO_2^--N concentrations in the leach tests, combined with the consistent observation of low initial NO_2^--N concentrations and subsequent increases to concentrations exceeding 1 mg L^{-1} in the field studies, suggests that NO_2^--N was derived from the nitrification of NH_3. This reaction is catalyzed by chemoautotrophic nitrifying bacteria (e.g., *Nitrobacter sp.*), and the delayed appearance of NO_2^--N in the effluent from the AZLs and the test pile basal drains may represent the time required to establish a viable population of nitrifying species.

2.4.3.3 Nitrate

Nitrate concentrations reached a maximum of 600 mg L^{-1} in the Type III West AZL and 340 mg L^{-1} in the Type III East AZL in 2007 (Figure 2.3). In 2008, water was collected in all four AZLs. The maximum NO_3^--N concentrations were similar in the two Type III AZLs (560 mg L^{-1} in the Type III West AZL and 640 mg L^{-1} in the Type III East AZL) and in the Type I East AZL (480 mg L^{-1}); however, high NO_3^--N concentrations of 2400 mg L^{-1} were observed in the Type I West AZL. As greater volumes of the AZLs began to contribute to flow, portions containing higher concentrations of blasting residuals were likely encountered, thereby releasing the higher concentrations observed. Nitrate concentrations in all four AZLs remained lower (< 300 mg L^{-1}) for the remainder of 2008, all of 2009 and 2010.

In 2007, the concentrations of NO_3^--N in the Type III test pile north and south basal drain effluent increased from May through August (maximum of 365 mg L^{-1} in the north drain and 170 mg L^{-1} in the south drain), followed by a decrease through to the end of October when flow ceased (Figure 2.5). These high concentrations probably represent contributions from the batters of the Type III test pile. In 2008, the concentrations were much lower with a maximum of 30 mg L^{-1} in the Type III test pile north drain and 66 mg L^{-1} in the Type III south drain. Concentrations remained low through 2009, with the exception of the Type III south drain that increased in October to the maximum reported concentration (720 mg L^{-1}) and remained elevated until the end of the field season. Similar trends were observed in 2010, with the maximum of 660 mg L^{-1} occurring in October. This increase in NO_3^--N late in the season is likely attributable to the increasingly large contributions to flow from the central portions of the test pile, which had not previously contributed to the flow to the basal drains. In all years following 2007, the concentrations of N species increased during the late

fall when larger portions of the test piles were flushed with water, and during periods of higher flow rates.

Discharge from the Type I test pile had elevated NO_3^--N concentrations in 2008 (up to 210 mg L^{-1}). Similar to the Type III test pile, the high NO_3^--N concentrations in the initial flow reporting to the Type I test pile basal drain probably were derived from the batters of the Type I test pile. Nitrate concentrations were lower at the beginning of 2009, but increased in September to a maximum of 430 mg L^{-1} at the end of the field season. In July 2010, NO_3^--N concentrations were lower, at < 50 mg L^{-1}, but steadily increased through the field season to the highest concentrations observed at this location (2000 mg L^{-1}).

Only a limited number of water samples were collected from the Covered test pile from August 2007 to January 2008 due to low flow volumes. The samples that were collected had NO_3^--N concentrations ranging from 250 to 380 mg L^{-1} (Figure 2.6). In 2008, NO_3^--N concentrations in the Covered test pile effluent increased from 103 to 340 mg L^{-1} within the first month of flow, then decreased and remained stable between 250 and 320 mg L^{-1} through 2010.

2.4.4 Nitrogen Mass Loading

Nitrogen is released from undetonated explosives left residual on rock in the area surrounding a blast hole. In mining operations, the mass of explosives required to break a quantity of rock is referred to as the powder factor. Powder factors vary depending on the lithology, hardness and competence of the rock. The mass of N used to blast a mass of rock (N_{used}) can be estimated based on the powder factor used in the blast. Measurements of the total mass of undetonated N in effluent can be used to estimate the loss of N during blasting,

referred to as nitrogen loss (N_{loss}). Data from two surface mines indicate the mass of undetonated N associated with blasting typically ranges from 0.1 to 6 % N_{loss}/N_{used} (Pommen, 1983). The average N_{loss} at Diavik during the construction of the experimental waste-rock piles was also within this range (DDMI, 2006). The average concentration of N_{loss} (0.59 mg L^{-1}) in the leach tests corresponds to a 5.4 % N loss from the blasting explosives (Table 5), which is in the range for N loss observed at Diavik over the period between 2003 and 2005 (DDMI, 2006), before N loss mitigation measures were initiated.

The concentrations of blasting residuals decreased over time to very low concentrations in the AZLs. Assuming that the majority of available blasting residuals were flushed from the AZLs, the mass loading can be used to determine the amount of un-detonated explosive remaining in the waste rock after blasting. The total mass of N released was 0.040 kg N in the Type III West AZL and 0.022 kg N in the Type III East AZL (Table 5). Combining an average powder factor (*total explosives (kg) per total tonnage (t)*) estimate of 0.32, for the AZL construction period, with the mass of rock in each AZL, indicates that the explosives used to blast the rock in the Type I AZLs contained 1.1 kg of N and 0.93 kg N was contained in the explosives used to blast the rock in the Type III AZLs. Comparing the mass of N contained in the explosives to the mass of N present in blasting residuals flushed from the AZLs indicates that un-detonated explosive was 3.7 % of the original mass in the Type III West AZL and 2.0 % of the original mass in the Type III East AZL. The total mass of N released from the Type I West AZL was 0.11 kg N, and the mass of N released from the Type I East AZL was 0.042 kg N (Table 5). These masses correspond to 12 % of un-detonated explosives in the Type I West AZL and 4.6 % in the Type I East AZL. The increased mass of N present at the Type I East AZL may be attributed to a larger mass of un-

detonated explosives associated with the rock in this lysimeter prior to construction, suggesting that the distribution of un-detonated explosives in waste-rock piles may be heterogeneous.

The total mass of N released from the Type III test pile (sum of the Type III north and south drains) was 35.2 kg N (Table 5). The Type I test pile released a total mass of 31.9 kg N. These values correspond to a release of 0.45 % of the residual N contained in the Type III test pile and 0.43 % of the residual N contained in the Type I test pile. A total mass of 43.5 kg N was released from the Covered test pile, which corresponds to 0.23 % of the residual N. The low release of N_{Total} from the waste-rock test piles indicates that a significant mass of explosive residuals remains within the test piles, probably because at the time of this publication flow has yet to report from large portions thereof. The N_{Total} mass released from the test piles is anticipated to initially increase as reaction products from previously un-flushed waste rock are released and report to the basal drainage system, before declining as the initial N is flushed from the waste rock.

2.4.5 Perchlorate

Perchlorate can be derived from accelerants, typically $NaClO_4$ and $KClO_4$, used in blasting materials. The range of ClO_4^- concentrations observed in mine wastewaters is similar to concentrations observed in municipal water supplies affected by anthropogenic ClO_4^- (Tikkanen, 2006). Perchlorate concentrations in the test piles followed a similar trend to other blasting residuals at all sampling locations. Perchlorate concentrations reached a maximum of 16 μg L^{-1} in effluent from the Type III East AZL and 23 μg L^{-1} from the Type III West AZL in 2007 (Figure 2.3). In 2008, ClO_4^- concentrations reached maximum values in July in

the Type III East (38 μg L^{-1}) and West (18 μg L^{-1}) AZLs and decreased to < 8 μg L^{-1} for the remainder of 2008, 2009, and 2010. In 2008, ClO_4^- concentrations reached a maximum of 3.7 μg L^{-1} in effluent from the Type I East AZL, but were much higher, at 130 μg L^{-1} in the Type I West AZL (Figure 2.2). Perchlorate concentrations decreased and remained low (< 10 μg L^{-1}) through 2008 and for all of 2009 and 2010.

Perchlorate concentrations in the Type III test pile exhibited temporal trends similar to other blasting residuals (Figure 2.5). In 2007, the ClO_4^- concentrations reached a maximum of 12 μg L^{-1} in the Type III north drain and 10 μg L^{-1} in the Type III south drain (Figure 2.5). Concentrations draining from the Type III test pile remained low through 2008 and 2009, except for an increase in ClO_4^- concentrations in the south drain, similar to other blasting residuals at the end of October 2009 and 2010.

The ClO_4^- concentrations in the Type I test pile effluent increased throughout 2008, reaching a maximum of 14 μg L^{-1} in October (Figure 2.4). In 2009 and 2010, ClO_4^- concentrations increased at the end of the field season, similar to Cl^-, NO_3^--N and SO_4^{2-}. The maximum ClO_4^- concentration in 2009 was 21 μg L^{-1}. The ClO_4^- concentration increased though 2010 to 340 μg L^{-1}, the maximum concentration observed at this location. Perchlorate concentrations ranged between 6 to 25 μg L^{-1} in the Covered test pile for the duration of the study, following similar trends to other blasting residuals (Figure 2.6).

Overall, the maximum ClO_4^- concentrations in all piles corresponded with the highest NO_3^--N and Cl^- concentrations, further demonstrating the coincidence of the maximum concentrations of blasting agents in the effluent.

2.4.6 Chloride

Chloride is present in the rock deposited in the waste-rock pile and from blasting residuals. Release and transport of Cl^- can be used to indicate the first flush of water through the AZL and test piles, where irregular concentrations represent flushing along different flow paths.

The maximum concentrations of Cl^- in the Type I AZLs occurred at the onset of flow in the spring of 2008 with 140 mg L^{-1} in the Type I East AZL and 370 mg L^{-1} in the Type I West AZL. The Cl^- concentration remained low for the remainder of the study. The Cl^- concentrations in the Type III AZLs followed a similar trend to NO_3^--N and SO_4^{2-} in 2007 and early 2008. Chloride concentrations after August 2008 were variable as a result of additional Cl^- applied to the Type III AZLs from the LiCl tracer test. The maximum concentration of Cl^- prior to the breakthrough of the tracer test was 230 mg L^{-1} in the East AZL and 130 mg L^{-1} in the West AZL.

In 2007, Cl^- concentrations exhibited trends similar to those for NO_3^--N, with a maximum concentration of 110 mg L^{-1} in the Type III north drain and 25 mg L^{-1} in the Type III south drain. In September 2007, Cl^- was released within a suite of tracers applied to the Type III test pile, which obscured trends in Cl^- concentrations in 2008. During 2008, Cl^- concentrations remained low in the Type III test pile reaching a maximum of 9.9 mg L^{-1} in the north drain and 32 mg L^{-1} in the south drain; although low, these concentrations may have been affected by the Cl^- tracer applied in September 2007. Concentrations remained low through early 2009 and 2010, with the exception of the water collected from the south drain that increased to 227 mg L^{-1} in October 2009 and 200 mg L^{-1} in October 2010, similar to other blasting residuals.

Chloride concentrations in water collected from the Type I test pile in 2008 were similar to concentrations observed for the Type III test pile in 2007, with a maximum concentration of 140 mg L^{-1}. Chloride concentrations were low (< 10 mg L^{-1}) through 2009, but in late 2009 elevated concentrations to a maximum of 540 mg L^{-1} were observed, similar to trends in other blasting residuals. In 2010, concentrations increased as temperatures in the test pile increased and reached a maximum of 2800 mg L^{-1}.

Chloride concentrations from the Covered test pile reached peaks of 130 mg L^{-1} in January 2008 and 240 mg L^{-1} at the beginning of the 2008 field season. The Cl^- concentration in the Covered test pile effluent decreased to approximately 90 mg L^{-1} through 2009 and decreased slightly through 2010 to ~50 mg L^{-1}.

2.4.7 Sulfate Predictions

Ratios of N_{Total} to Cl- for the Type III test pile for 2007 to 2008 were constant, and show a slight excess of Cl- in 2009-2010, possibly due to the tracer test initiated in 2007. The ratios of N_{Total} to Cl- in 2007-2008 were consistent and highly correlated, suggesting N species and Cl- were derived from blasting residuals flushed through the test pile (Figure 2.7). Ratios of SO_4^{2-} to N_{Total} in the effluent from the Type III test pile were relatively uniform in 2007 and averaged 6.3 ± 0.89 in the north drain effluent and 7.2 ± 1.23 in the south drain effluent (Figure 2.7). Sulfate concentrations increased as temperatures in the test piles increased and corresponded to increases in N_{Total} mass. In 2008, the SO_4^{2-} to N_{Total} ratio increased and averaged 25 ± 6.7 in effluent from the north drain and 20 ± 7.0 from the south drain. Sulfate concentrations in 2008 were not correlated as strongly to the N_{Total} mass. In 2009, the ratios became more erratic, suggesting the potential impact of SO_4^{2-} sources in addition to blasting

residues. However, at the end of October 2009 the increase in SO_4^{2-} concentrations in the south drain effluent reflected the increase in other blasting residuals.

The coincident rise of SO_4^{2-} with other blasting agents suggests the initial release of SO_4^{2-} in 2007 was mainly derived from sulfide oxidation during the blasting of rock (Figure 2.8 and Figure 2.9). During a blast, a small amount of sulfide in the rock is oxidized, and the product is subsequently mobilized when exposed to water. Thus, the SO_4^{2-} to N_{Total} ratios from 2007 can be used to estimate the concentration of SO_4^{2-} attributable to blasting in subsequent years when concentrations are more erratic, and to determine the proportion released due to *in situ* sulfide oxidation. The ratio of SO_4^{2-} to N_{Total} observed in 2007 in the Type III test pile was compared to the N_{Total} concentrations from 2008 and 2010 to estimate the mass of SO_4^{2-} derived from blasting, thereby differentiating the sulfide oxidation during blasting from subsequent *in situ* sulfide oxidation. This comparison suggests that the SO_4^{2-} in the Type III test pile effluent through 2008 and most of 2009 was largely derived from *in situ* sulfide oxidation. The SO_4^{2-} concentration peak in October 2009 in the Type III south drain effluent corresponded to the increase in other blasting residuals. The majority of this SO_4^{2-} probably originated in areas of the test pile remote from the basal drains, and migrated along longer flow paths. The predicted SO_4^{2-} concentrations (Figure 2.8 and Figure 2.9) at this time show a deficit, potentially due to the loss of SO_4^{2-} to the formation of secondary minerals, principally jarosite, which remove SO_4^{2-}. At these high SO_4^{2-} concentrations, geochemical speciation calculations suggest equilibrium of the effluent with respect to jarosite.

Ratios of SO_4^{2-} to N_{Total} from the Type III AZL during the initial flush in 2008 were 6.7 ± 0.65 in the West and 7.25 ± 0.48 in the East (Figure 2.10). These ratios were similar to

the Type III test pile basal drains in 2007. As more water arrived at the base of the Type III AZLs, the SO_4^{2-} to N_{Total} ratio became more erratic; this is similar to the pattern observed in the Type III test pile, suggesting that the SO_4^{2-} contribution from *in situ* sulfide-mineral oxidation exceeded the contribution from blasting residuals.

Ratios of SO_4^{2-} to N_{Total} from the Type I waste rock were much lower than those from the Type III test pile and Type III AZL effluent (Figure 2.10). The Type I test pile contains a lower mass of S and the volume of water that reported to the drain was significantly less than in the Type III test pile. The overall average ratio of SO_4^{2-} to N_{Total} (3.3 ± 1.6) suggests that much of the SO_4^{2-} reporting to the Type I test pile basal drain was released during blasting. The overall average SO_4^{2-} to N_{Total} ratios observed for the Type I AZLs were 2.2 ± 1.6 in the West and 2.0 ± 0.93 in the East. The Type I AZL effluent is similar to that observed for the Type I test pile effluent, suggesting that blasting is the principal source of SO_4^{2-} for this location as well.

In 2007, the SO_4^{2-} to N_{Total} ratio in the effluent from the Covered test pile was similar to the SO_4^{2-} to N_{Total} ratio measured in the effluent from the Type III test pile basal drains (Figure 2.11). Flow ceased in January 2008 and resumed in August 2008. The Covered test pile effluent had consistent concentrations of blasting residuals versus SO_4^{2-} over time, with a slight increase in the SO_4^{2-} to N_{Total} ratio in the fall of 2008. The SO_4^{2-} to N_{Total} ratio steadily increased from 4 to 11 from 2007 to 2009. The total volume of water reporting to the base of the Covered test pile from 2007 to 2009 was similar to the volume draining from the Type III test pile in 2007. The SO_4^{2-} to N_{Total} ratio in the effluent from the Covered test pile is

anticipated to increase as more water migrates to the drain and the initial mass of blasting residuals is flushed from the pile.

The Type III AZLs and Type III test pile basal drains had similar SO_4^{2-} to N_{Total} during the initial flush of water through each experiment. As *in situ* sulfide-mineral oxidation increased, the ratios became more erratic. The Type I AZL and Type I test pile basal drains had lower S content than the Type III sample locations and thus had lower and more consistent SO_4^{2-} to N_{Total} ratios.

2.5 Conclusions

Substantial concentrations of N species, ClO_4^-, and Cl^- have been derived from the release of undetonated explosives and blasting residuals from waste rock at Diavik. The concentrations of these blasting residuals were used as a resident tracer to indicate the first flush of water through experimental waste-rock piles. The breakthrough of these components indicated volumes that were similar to estimates of the matrix porosity within the AZLs. Irregular concentrations and gradual dissipation of blasting residuals provided an indication of the test pile heterogeneity and the relative contributions of portions of the test piles along different flow paths. As the temperature within the test piles increased and larger portions of the test pile contributed to flow, increased concentrations of blasting residuals were observed. The initial release of SO_4^{2-} was a result of the oxidation of sulfide minerals during blasting and was highly correlated to blasting residuals. After the dissipation of the blasting residuals, additional SO_4^{2-} was derived from the *in situ* oxidation of sulfide minerals. The release of SO_4^{2-} during blasting was dependant on the mass of sulfide present within the rock. In this experiment, Type III waste rock released higher ratios of SO_4^{2-} to N_{Total} than Type I waste

rock. The mass of sulfide released during blasting was estimated using the ratio of SO_4^{2-} to N_{Total}, thus providing a novel approach for estimating the mass of S released during the first flush of the piles.

Table 2.1 Leach test concentrations of Cl^-, NO_2^--N, NO_3^--N, sum of N species (NO_3^--N^- and NO_2^--N), and SO_4^{2-}. NH_3-N was below detection in all leach test samples (< 0.02 mg L^{-1}).

Leach Test	Cl^- (mg L^{-1})		NO_2^--N (mg L^{-1})		NO_3^--N (mg L^{-1})		N_{Total} (mg L^{-1})		SO_4^{2-} (mg L^{-1})	
	Average	st. dev.	Average	st. dev.	Average	st. dev.	Average	st. dev.	Average	st. dev.
LT1	1.49	0.14	0.054	0.006	1.27	0.11	1.32	0.06	7.19	0.69
LT2	0.67	0.04	0.003	0.0003	0.33	0.03	0.33	0.03	1.80	0.14
LT3	0.53	0.12	0.006	0.001	0.59	0.13	0.60	0.13	2.88	0.72
LT4	0.22	0.04	0.002	0.0004	0.37	0.08	0.37	0.08	2.53	0.07
LT5	0.22	0.07	0.002	0.0005	0.35	0.11	0.35	0.11	1.76	0.71
LT6	0.36	0.12	0.003	0.0003	0.45	0.14	0.45	0.14	2.45	0.77
LT7	0.13	0.02	0.001	0.0001	0.10	0.01	0.10	0.01	2.76	0.47
LT8	0.28	0.04	0.002	0.0001	0.13	0.02	0.13	0.02	5.73	0.89
Average	0.49	0.44	0.009	0.017	0.45	0.37	0.46	0.38	3.39	1.98

Table 2.2 Leach test ratios of N_{Total} to Cl^-, SO_4^{2-} to N_{Total}, and SO_4^{2-} to Cl^-.

Leach test	N_{Total}:Cl^-		SO_4^{2-}:N_{Total}		SO_4^{2-}:Cl^-	
	Average	st. dev.	Average	st. dev.	Average	st. dev.
LT1	3.8	0.24	5.1	0.22	4.5	0.13
LT2	2.2	0.06	5.4	0.03	2.7	0.08
LT3	1.1	0.04	4.8	0.22	5.5	0.15
LT4	1.7	0.10	6.8	1.40	11.6	1.74
LT5	1.6	0.03	5.0	0.59	8.0	0.90
LT6	1.3	0.03	5.4	0.04	6.8	0.18
Average (LT1 through LT6; n = 18)	1.2	0.91	5.5	0.42	6.55	3.01
LT7 (n = 3)	0.8	0.03	27	2.5	21	2.6
LT8 (n = 3)	0.5	0.003	42	0.88	20	0.28

Table 2.3 Maximum concentrations of SO_4^{2-}, Cl^-, NH_3-N, NO_2^--N, and NO_3^--N in the AZLs.

AZL	SO_4^{2-} (mg L^{-1})	Cl^- (mg L^{-1})	NH_3-N (mg L^{-1})	NO_2^--N (mg L^{-1})	NO_3^--N (mg L^{-1})
Type I East	780	140	0.8	3.4	480
Type I West	950	370	1.7	7.7	2400
Type III East	8580	660	9.0	9.0	640
Type III West	13300	870	4.3	28	600

Table 2.4 Maximum concentrations of SO_4^{2-}, Cl^-, NH_3-N, NO_2^--N, and NO_3^--N in the basal drains of the Type I, Type III and Covered test piles.

Basal drain	SO_4^{2-} (mg L^{-1})	Cl^- (mg L^{-1})	NH_3-N (mg L^{-1})	NO_2^--N (mg L^{-1})	NO_3^--N (mg L^{-1})
Type I	1200	2800	410	7.9	2000
Type III south	2950	230	54	3.7	720
Covered	3530	245	10	13	380

Table 2.5 Summary of mass loadings and undetonated explosives released from laboratory leach tests, 2 m by 2 m AZLs, and basal drains from large-scale test piles.

Location	Estimated Mass of explosives used (kg)	Mass of N from explosives (kg) N_{used}	Mass loading of N released (kg) $(NH_4^+ + NO_3^- + NO_2^-)$ N_{loss}	% of estimated residual N released from 2007 to 2010
Leach Test	31 mg	11 mg	0.59 mg	5.4
AZLs				
Type III West	3.2	1.1	0.040	3.7
Type III East	3.2	1.1	0.022	2.0
Type I West	2.7	0.93	0.11	12
Type I East	2.7	0.93	0.042	4.6
Basal drains				
Type III	22,000	7,800	35.2	0.45
Type I	21,000	7,500	31.9	0.43
Covered	54,000	19,000	43.5	0.23

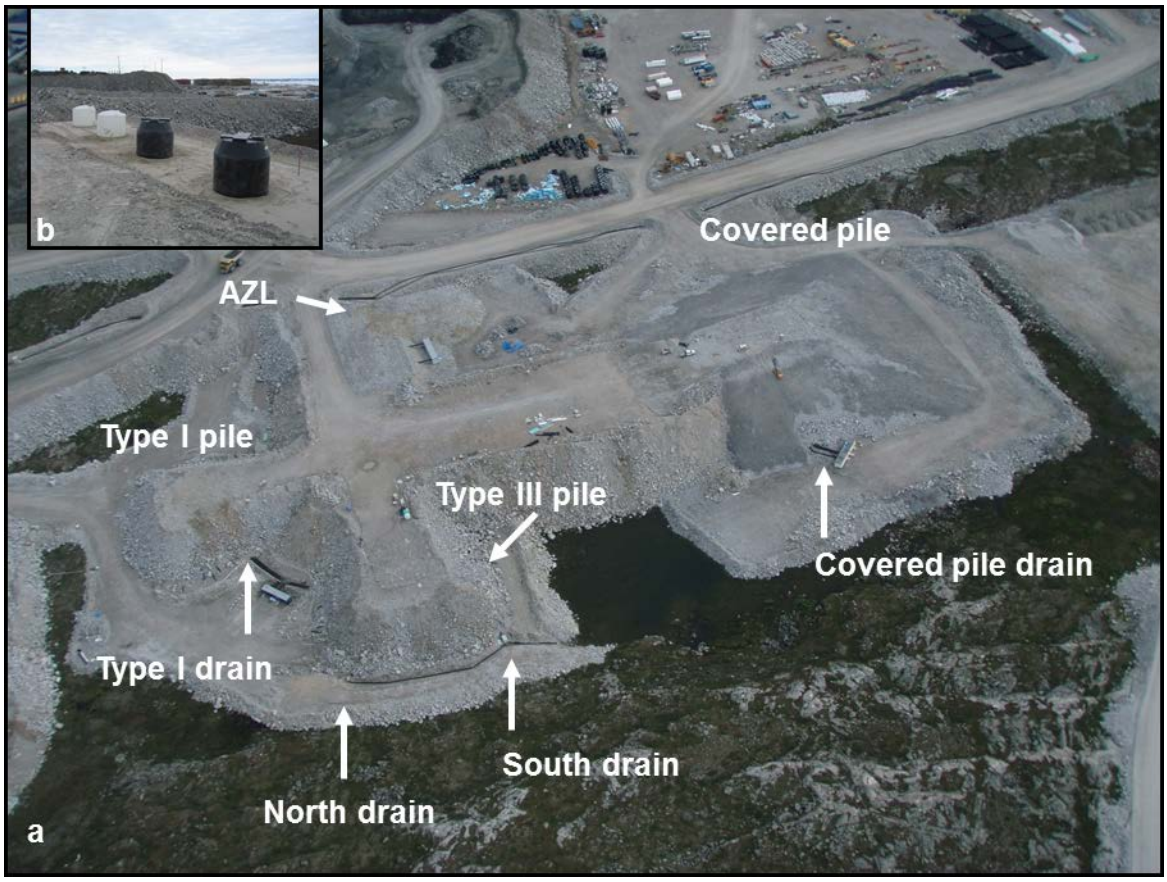

Figure 2.1 Aerial view of the Diavik Waste Rock Research Facility: a) locations of the Type I test pile, Type III test pile, Covered test pile, and AZLs; b) high-density polyethylene barrels used in the construction of the AZLs before rock placement.

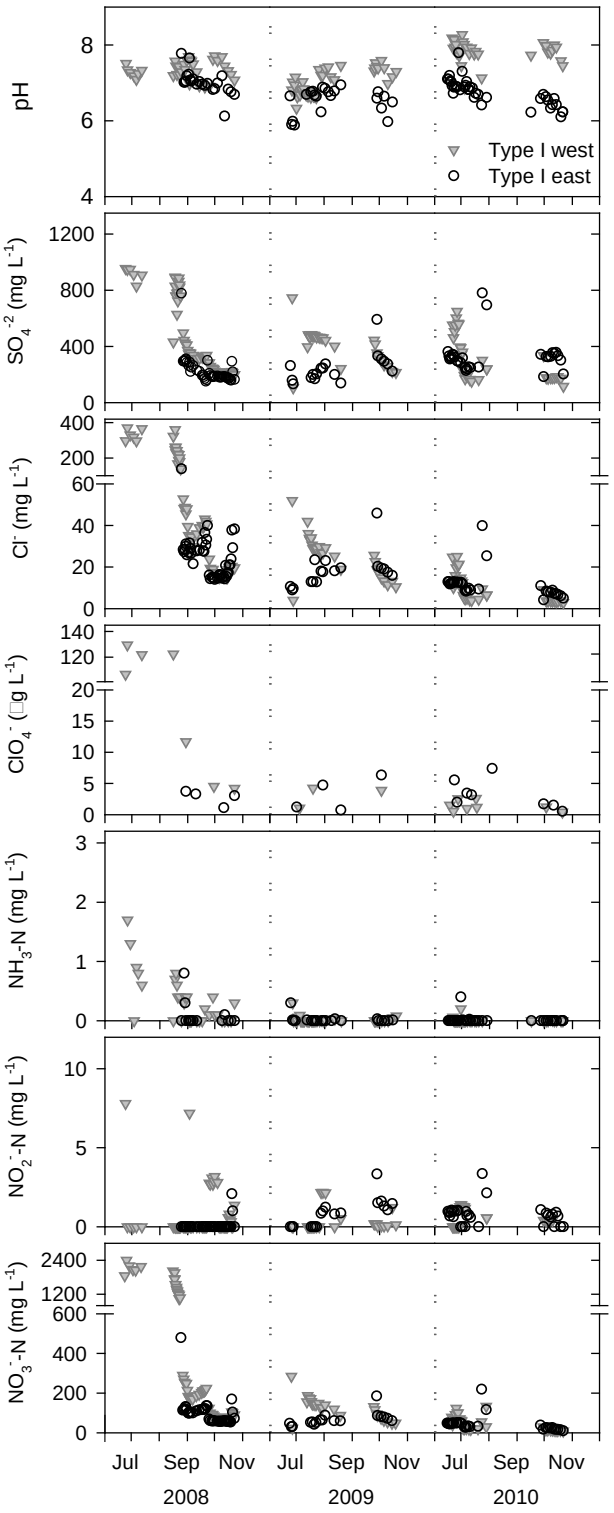

Figure 2.2 Blasting residual concentrations for the Type I West and East active zone lysimeters.

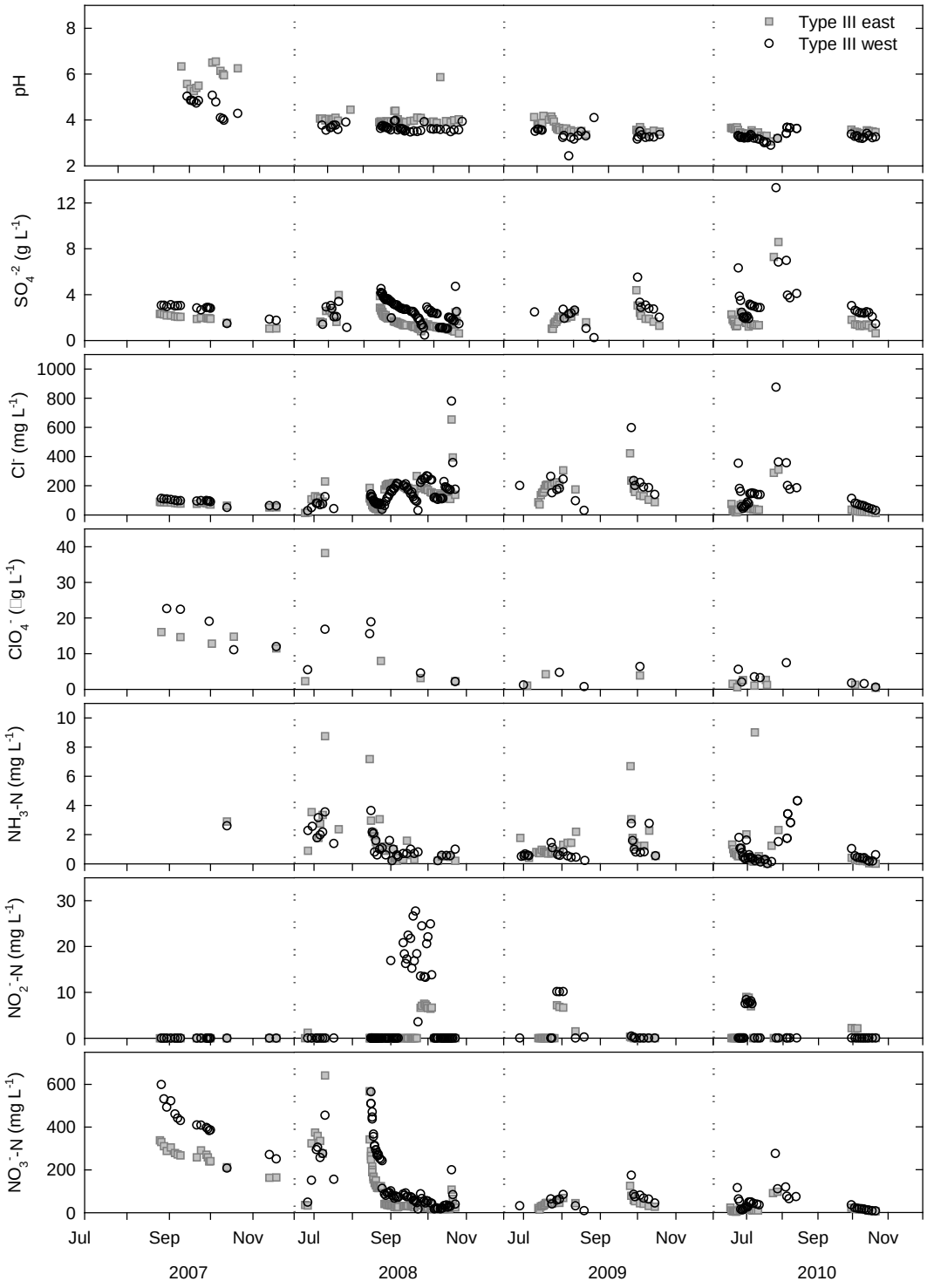

Figure 2.3 Blasting residual concentrations for the Type III West and East active zone lysimeters.

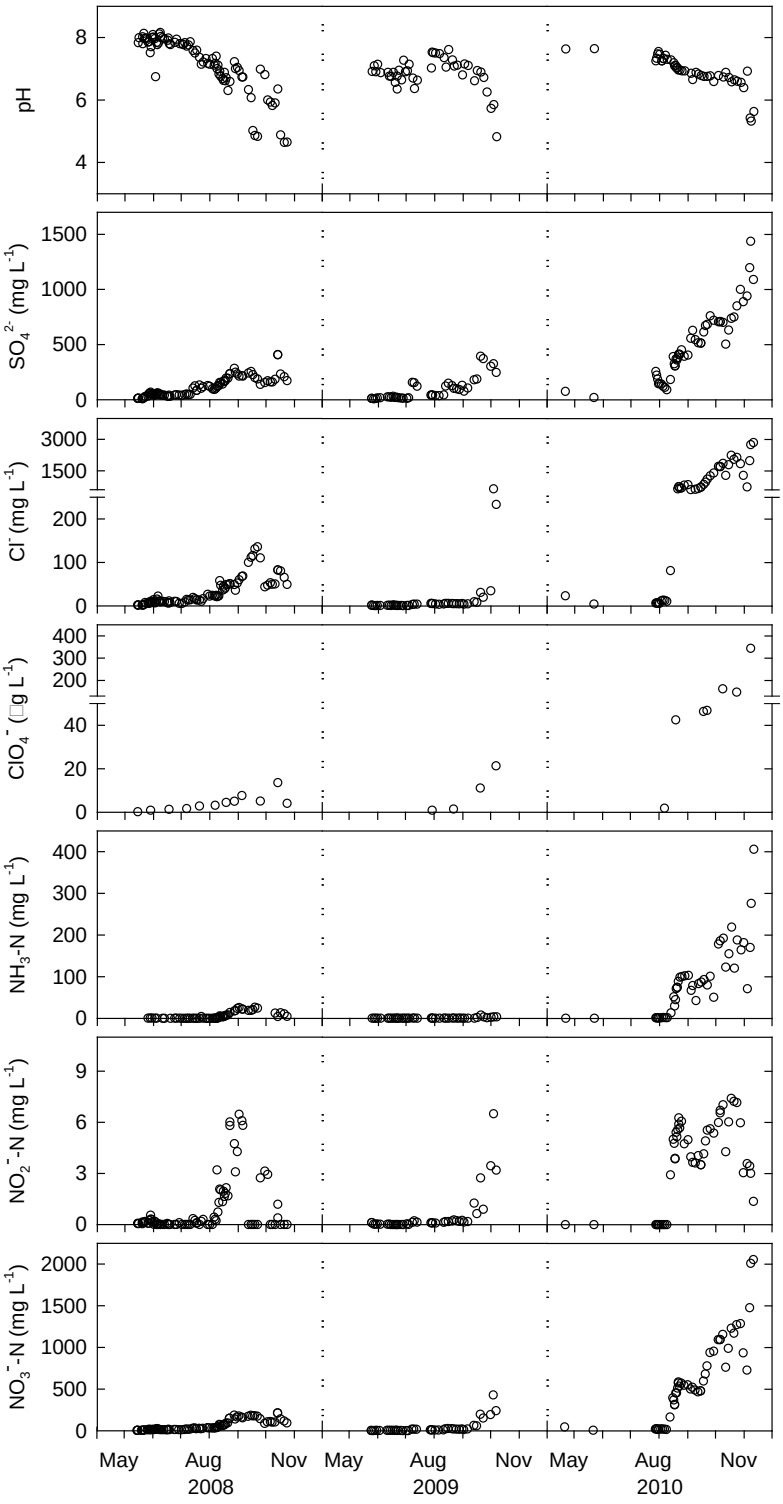

Figure 2.4 Blasting residual concentrations for the Type I test pile drain.

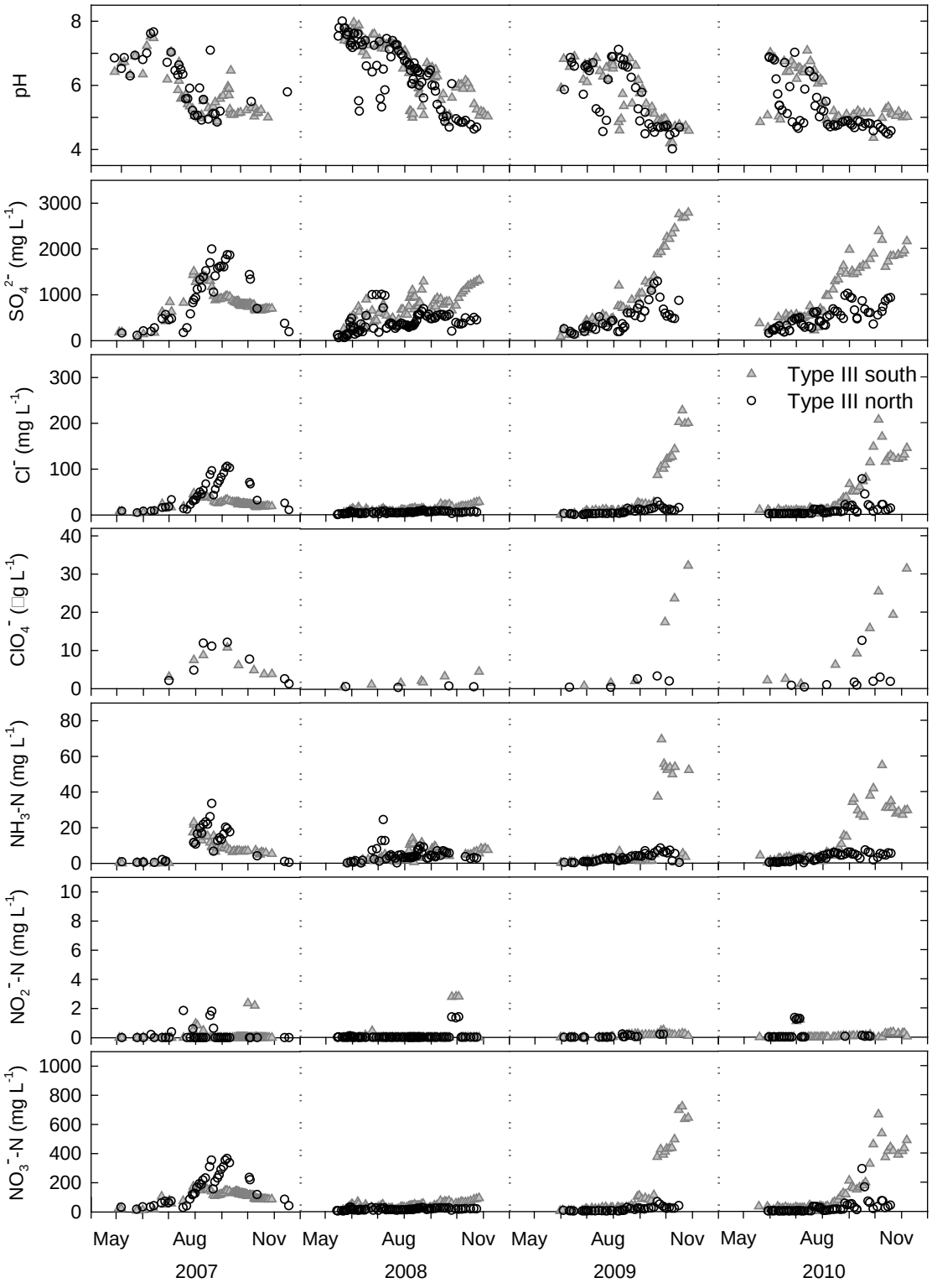

Figure 2.5 Blasting residual concentrations for the Type III north basal drain and Type III south basal drain.

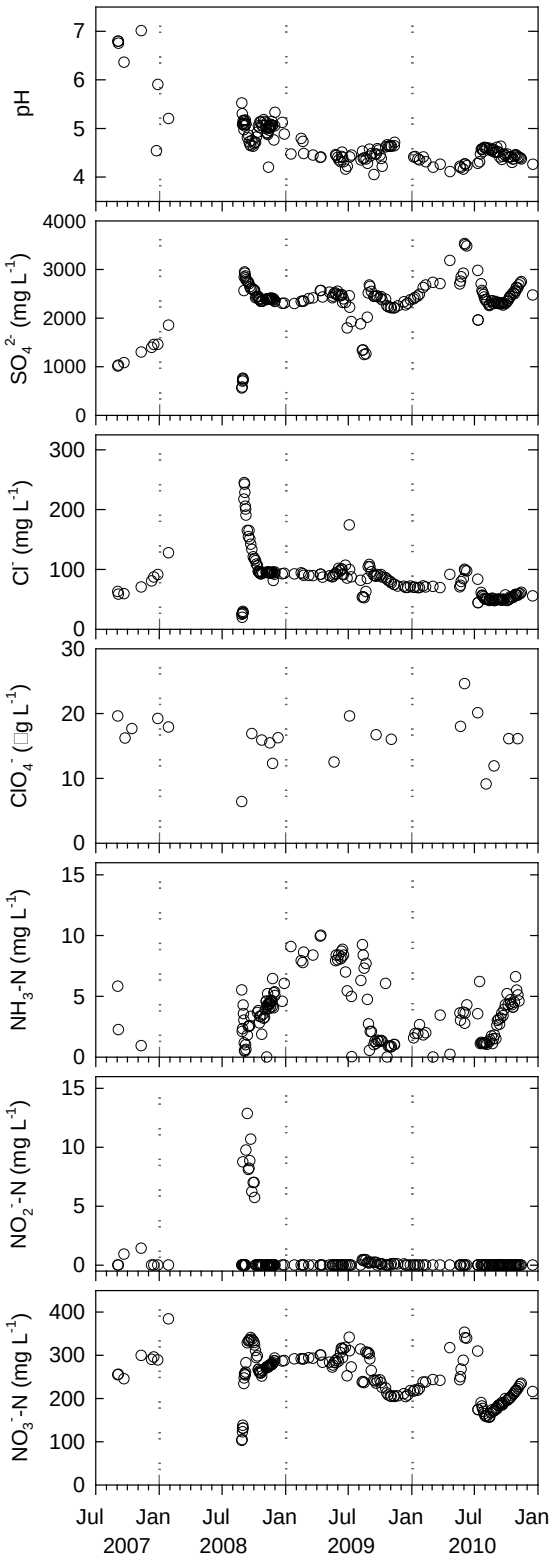

Figure 2.6 Blasting residual concentrations for the Covered test pile basal drain.

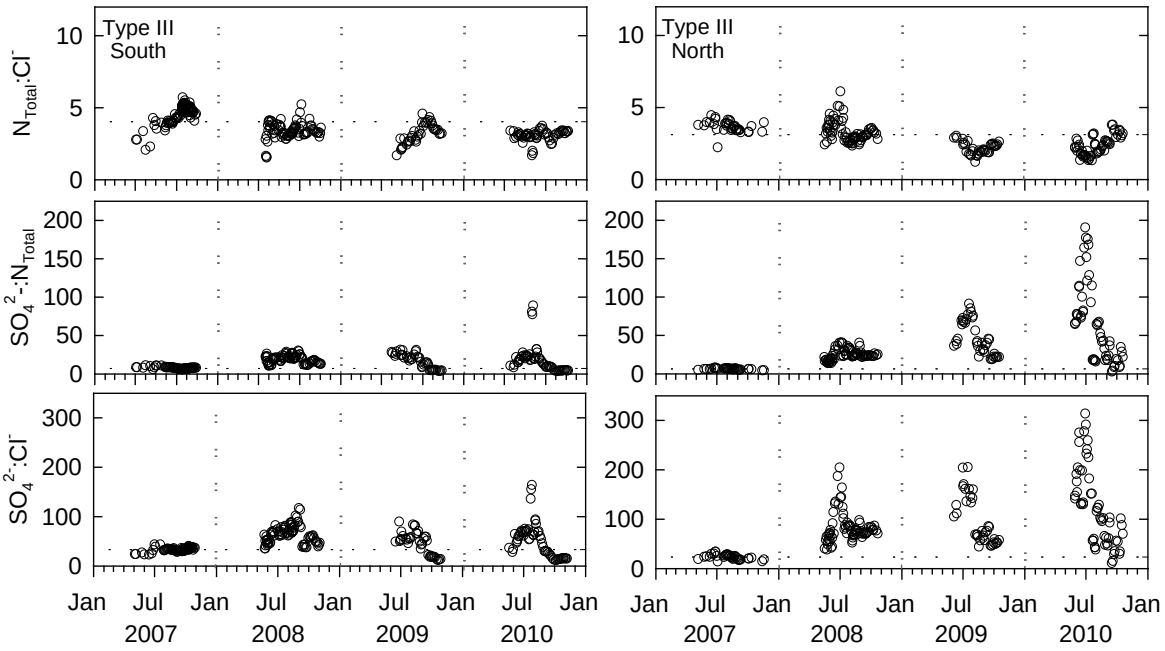

Figure 2.7 Type III south (left) and north basal drain (right) ratios of N_{Total} to Cl^-, SO_4^{2-} to N_{Total}, and SO_4^{2-} to Cl^-. The horizontal dashed line represents the 2007 average ratios.

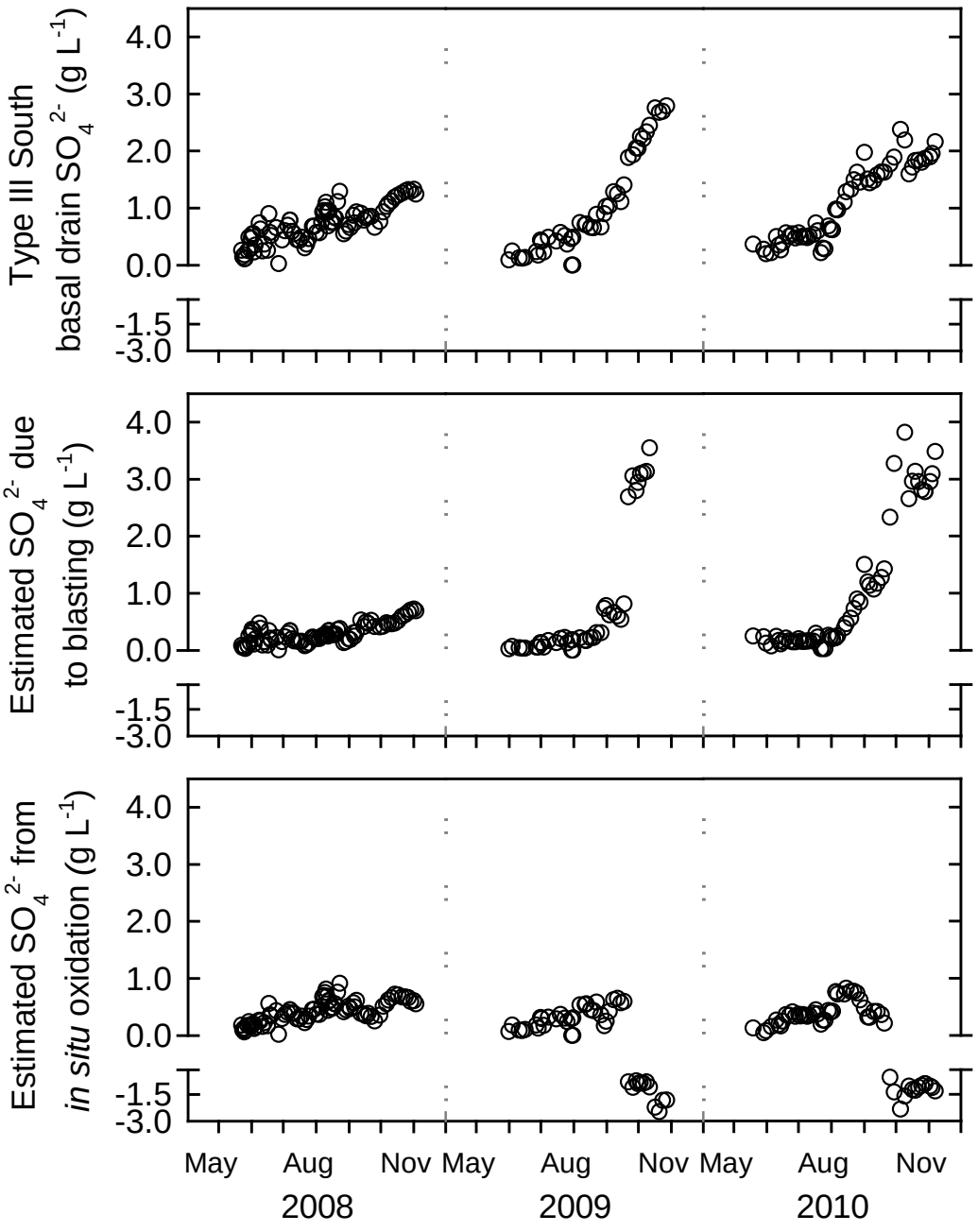

Figure 2.8 Type III south basal drain predictions of SO_4^{2-} from *in situ* oxidation versus oxidation during blasting.

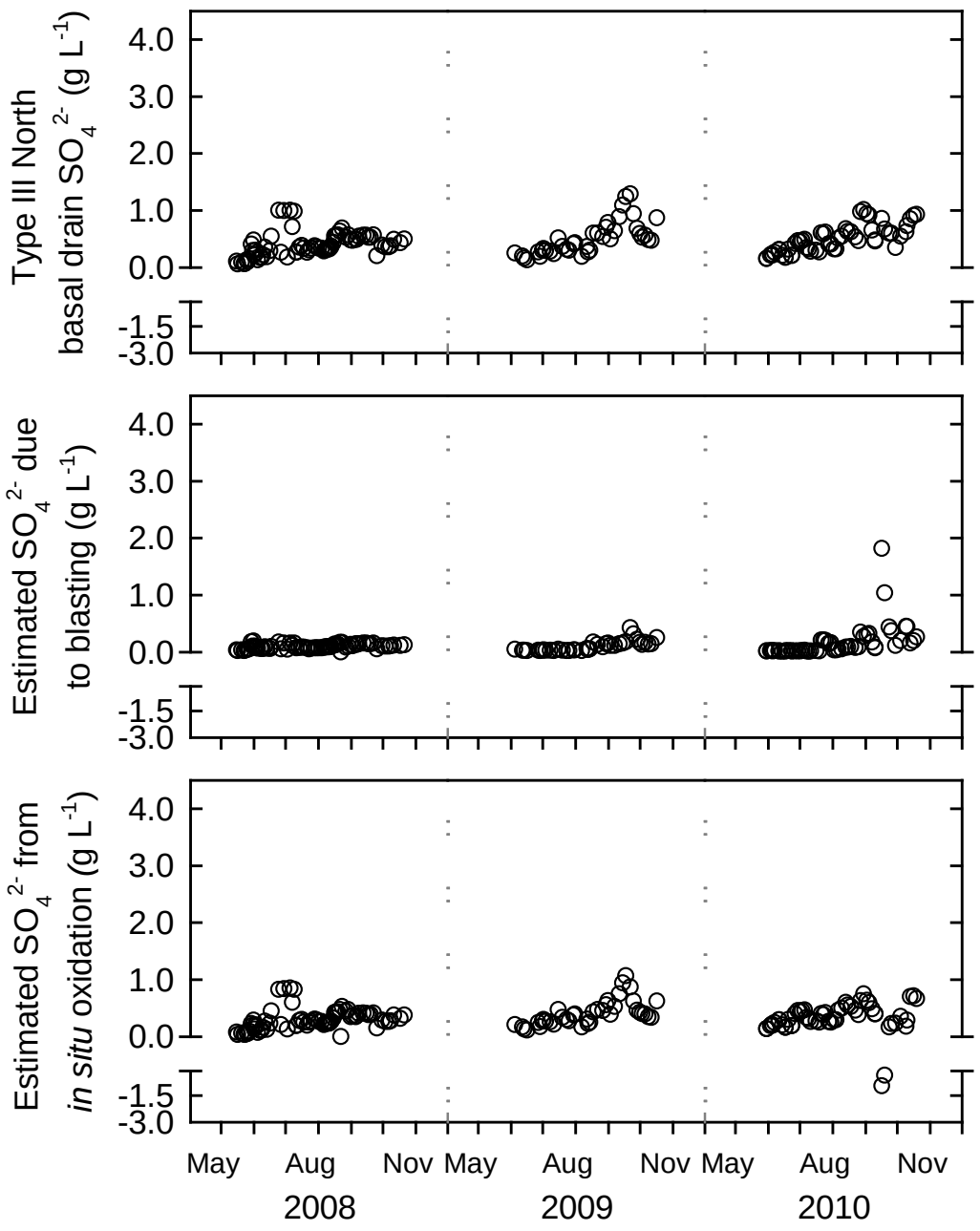

Figure 2.9 Type III north basal drain predictions of SO_4^{2-} from *in situ* oxidation versus oxidation during blasting.

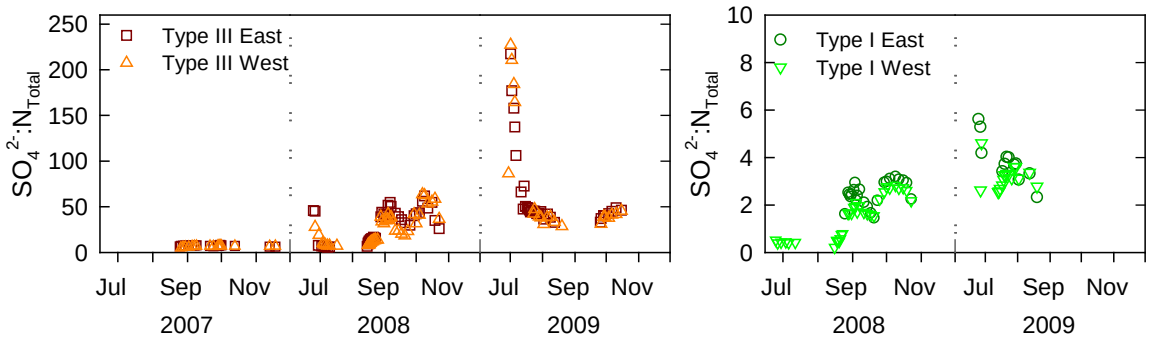

Figure 2.10 Ratios of SO_4^{2-} to N_{Total} for Type III East and West AZLs (left) and Type I East and West AZLs (right).

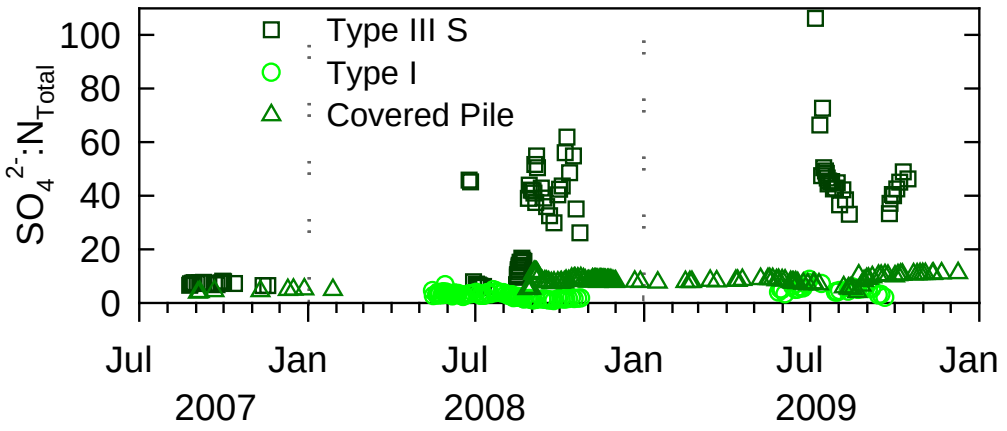

Figure 2.11 Ratios of SO_4^{2-} to N_{Total} for Type I, Type III south, and Covered test pile basal drains.

Chapter 3:

Geochemical and microbiological characterization of drainage from low-sulfide content waste rock: active zone field experiments

3.1 Executive Summary

A field experiment was conducted at the Diavik diamond mine to evaluate the potential for acid generation and metal release from the active layer of unsaturated waste-rock piles in the Arctic. Four active zone lysimeters (AZLs) were constructed in 2006 using high-density polyethylene tanks filled with, and surrounded by, waste rock to evaluate the geochemical and biogeochemical characteristics in the upper 2 m of waste-rock stockpiles. Two AZLs were filled with waste rock containing an average of 0.014 wt. % S (Type I AZLs) and two AZLs were filled with waste rock containing an average of 0.035 wt. % S (Type III AZLs). The geochemistry and microbiology of the effluent from the AZLs was monitored for 4 years. The effluent from the Type III AZLs was characterized by low pH (pH < 3.5) with high concentrations of SO_4^{2-} and dissolved metals. An increase in SO_4^{2-}, Fe, and most dissolved metals coincided to the decrease in pH to 3.0 and the depletion of alkalinity. Maximum concentrations of SO_4^{2-}, Al, Zn, Ni, Co, and Cu were observed in 2010, the final year of the dataset analyzed here. The effluent from the Type I AZLs maintained neutral pH (7.5) and lower concentrations of SO_4^{2-} (< 2000 mg L^{-1}), Fe (< 1.4 mg L^{-1}), and other dissolved metals. Populations of Fe- and S-oxidizing bacteria in the AZLs were determined by MPN methods. Enumerations for the Type III AZL indicated an abundance of acidophilic S-oxidizing microorganisms, whereas neutrophilic S-oxidizing microorganisms were most abundant in the Type I AZLs. Iron-oxidizing microorganisms were generally less abundant than S-oxidizing microorganisms, but were detected in low-pH effluent with high dissolved metals in one of the Type III AZLs.

3.2 Introduction

The oxidation and weathering of exposed sulfide minerals in mine tailings, waste rock, and mine workings have the potential to generate acid mine drainage (AMD). The concentrations of reactive minerals within waste-rock piles, and the availability of water and oxygen, are important factors controlling the rate and extent of AMD generation. Although the release of AMD from unsaturated waste-rock piles is well documented (Ritchie, 1994; MEND, 1995; Sracek *et al*., 2004; Stockwell *et al*., 2006), information on the (bio)geochemical evolution of waste rock and the rate of sulfide oxidation in regions of continuous permafrost is limited. Therefore, the effects of the cold and semi-arid Arctic environment on the kinetics of AMD generation also are not well documented (MEND, 1999).

Sulfide-mineral oxidation and the generation of AMD have been extensively reviewed (Lowson, 1982; Nordstrom, 1982; Bierens de Haan, 1991; Alpers and Blowes, 1994; Evangelou and Zhang, 1995; Salomons, 1995; Banks *et al*. 1997; Belzile *et al*., 1997; Nordstrom and Alpers, 1999; Keith and Vaughan, 2000; Rimstidt and Vaughan, 2003; Blowes *et al*., 2003b). Sulfide minerals, such as pyrite and pyrrhotite, oxidize and release oxidation products including SO_4^{2-}, Fe and other dissolved metals through a complex series of elementary reactions. Despite decades of research, advances in understanding the chemical and electrochemical processes involved in sulfide-mineral oxidation have only recently been made (Rimstidt and Vaughan, 2003; Rohwerder *et al*., 2003; Chandra and Gerson, 2010, 2011).

Acid-neutralization reactions between acidic mine waters and non-sulfide minerals present within waste rock and tailings can lessen the impact of AMD generation. These reactions

result in the neutralization of pH and the attenuation of some dissolved metals. Acid-neutralization reactions observed within mine-waste disposal areas include the dissolution of carbonate minerals, Al hydroxide and Fe(III) (oxy)hydroxide minerals, and aluminosilicate minerals. The depletion of acid-consuming minerals from mine wastes can be accompanied by the dissolution of primary metal-bearing minerals, dissolution of secondary minerals, and desorption of metals from secondary mineral surfaces, which can exacerbate and prolong AMD generation (Alpers *et al*., 1994; Blowes and Ptacek, 1994; Blowes *et al*., 2003b).

The objectives of this field-based research were to evaluate the (bio)geochemical evolution of low-S content waste rock from four active zone lysimeters (AZLs; 2 m by 2 m by 2 m in scale) installed at the Diavik mine site. Effluent was collected from 2007 to 2010 to evaluate metal release rates, the acidity of the drainage water, and microbial activity.

3.3 Methods of Investigation

3.3.1 Waste Rock Characterization

Waste-rock samples were collected from each haul truck load used to construct the Type I (n = 3) and Type III (n = 2) AZLs. Subsamples of the < 4-mm fraction were collected for measurements of the S and C content, whole-rock analysis, and the particle-size distribution of the matrix material. Particle-size samples were riffle split and sieved using a metric sieve set (4, 2, 1, 0.6, 0.25, 0.125 and 0.063 mm and a pan for smaller size fractions). Each fraction was pulverized using a four-position Fritsch Pulverisette Analysette planetary ball mill. Samples were further split for S and C analysis, and whole-rock analysis. Sulfur and C content was measured using a resistance furnace (CS-2000; Eltra, Germany). Sulfur standards were analyzed prior to sample analysis with six standards analyzed; the two most

similar results were used for calibration. The wt. % S and wt. % C were reported as particle-size weighted values. Whole-rock analysis was completed using 10 g of Type III (n = 2) and Type I (n = 2) samples analyzed as powders firmly compressed in cups with a polyester X-ray film using an energy dispersive X-ray fluorescence spectrometer (EDXRF; Minipal4; Panalytical, The Netherlands). The instrument was calibrated using in-house laboratory standards and granite, granodiorite and granite gneiss certified reference materials.

3.3.2 Sample Collection and Analysis

3.3.2.1 Water Chemistry

Water samples for chemical analysis were collected from the Type I East and West AZLs from 2008 through 2010, and the Type III East and West AZLs from 2007 through 2010. Effluent was collected in a series of flow-through cells that ultimately directed water to a calibrated tipping-bucket flow gauge to measure the flow rate and volume. At each sampling location, the pH, redox potential relative to the standard hydrogen electrode (E_h), EC, temperature, and alkalinity were determined for water collected from the flow-through cell system. Water samples were passed through 0.45 μm cellulose-acetate membrane filters prior to measurement of field parameters. Measurements of pH were made using a combination electrode (Orion ROSS Ultra® 8156, Thermo Scientific, USA) calibrated using pH 7, 4, and 10 or 1.68 standard buffer solutions. E_h measurements were made with a platinum redox electrode (Orion 96-78; Thermo Scientific, USA). The performance of the E_h electrode was confirmed using ZoBell's (Nordstrom, 1977) and Light's solutions (Light, 1972). Alkalinity measurements were made using a Hach Company (Loveland CO, USA) digital titrator, with 0.16 N H_2SO_4 and bromocresol green/methyl red as the end-point indicator.

Field measurements using a spectrophotometer (Hach DR/8400; Hach Company, Loveland CO, USA) were made to determine the concentrations of orthophosphate (o-PO_4; Ascorbic Acid method), Fe(II) (Phenanthroline method), H_2S (Methylene Blue method), and NH_3 (Salicylate method) on select samples (SMEWW, 2005).

Water samples were collected from flow-through cells using 0.64 cm inner-diameter polyethylene (PE) tubing attached to a sterile 60 mL PE syringe. Water was passed through 0.45 μm cellulose-acetate membrane filters into pre-washed and sample triple-rinsed high-density polyethylene (HDPE) bottles. Inorganic anion concentrations (SO_4^{2-}, NO_3^-, NO_2^-, and Cl^-) were determined on non-acidified, filtered samples by ion chromatography (IC; DX600, Dionex, USA). Analysis was completed within three weeks of sampling. All concentrations of NO_3^- and NO_2^- were expressed as mg L^{-1} NO_3^--N and mg L^{-1} NO_2^--N, respectively. Total (non-filtered) and dissolved (filtered) cation concentrations were determined from samples acidified with trace-metal grade HNO_3 to a pH < 2. All samples were refrigerated until analysis was completed at the University of Waterloo.

Concentrations of the major cations (Ca, K, Mg, and Na) were measured by inductively coupled plasma-optical emission spectrometry (ICP-OES; iCAP 6000, Thermo Scientific, USA). Minor and trace cation (Al, As, B, Ba, Be, Cd, Co, Cr, Cu, Fe, Mn, Mo, Ni, Pb, Si, Sr, V and Zn) concentrations were determined by inductively coupled plasma-mass spectrometry (ICP-MS; XSeries 2, Thermo Scientific, USA). Quality control and quality assurance were assessed by evaluating several standards covering the range of measured concentrations, and incorporating both field replicates and laboratory blanks into the protocol (Appendix A).

3.3.2.2 Microbial Enumerations

Effluent samples were collected for microbiological study. These samples were stored and shipped in ice-packed coolers and were delivered to the University of Waterloo for analysis. Microbiological enumerations were conducted for three physiological groups of bacteria using the most probable number (MPN) technique (Cochran, 1950). Techniques and media for the enumeration of neutrophilic S-oxidizers (*T. thioparus* and related species), acidophilic S-oxidizers (*At. thiooxidans*), and acidophilic Fe-oxidizers (*At. ferrooxidans*) are described by Hulshof *et al*. (2006).

3.3.3 Data Interpretation

Saturation indices (SI) for discrete mineral phases were calculated to assist in the interpretation of aqueous geochemistry. These thermodynamic calculations were performed using the equilibrium/mass-transfer model MINTEQA2 (Allison *et al*., 1990). The MINTEQA2 database was modified for consistency with the WATEQ4F (Ball and Nordstrom, 1991) database. Speciation calculations were determined on samples collected from the Type III East, Type III West, Type I East, and Type I West AZLs, using field analyses and laboratory cation and anion analyses.

3.4 Results and Discussion

3.4.1 Sulfur Content and Acid-Base Accounting Calculations

Waste-rock samples were collected from most haul truck loads used to construct two waste-rock test piles (Type I and Type III test piles; Table 3.1) located adjacent to the AZLs over the period of AZL construction (Smith *et al*., in press). Due to the heterogeneity of S and C content in the waste rock, samples of waste rock (n = 5 from both Type I and Type III waste

rock) used to construct the large-scale test piles for a month period around the construction of the AZLs were used to compare the average S and C content to samples collected for the construction of the Type I (n = 3) and Type III (n = 2) AZLs.

The average S content of the < 1 mm (0.018 wt. % S; n = 3, σ = 0.012) and < 4 mm (014 wt. % S; n = 3, σ = 0.009) fractions of waste rock fall within one standard deviation of the average S content of the < 5-mm fraction of the waste rock used to construct the Type I test pile over a month period during the construction of the AZL (Table 3.2). Grab samples of the < 50-mm fraction from the same period suggest a higher S content in the Type I waste rock; however, the results were within one standard deviation of the < 5-mm fraction.

The Type III AZL had an average S content of 0.039 wt. % S (n = 2, σ = 0.012) in the < 1-mm fraction and 0.035 wt. % S (n = 2, σ = 0.015) in the < 4-mm fraction. The < 5-mm fraction of waste rock used to construct the Type III test pile for the one month period of construction of the AZLs was similar to the < 50-mm fraction of waste rock in grab samples from the Type III test pile for the same period (Table 3.2). However, both the < 5-mm fraction and the < 50-mm fractions have a higher S content than the < 1-mm and < 4-mm fractions (Table 3.2). The difference in the median values between the average S contents was not great enough to exclude the possibility that the difference was due to random sampling variability, the results were within one standard deviation. These results are consistent with Smith *et al*. (in press) that indicate there is a general trend of increasing S content, with decreasing particle size, for particle sizes ≤ 1.25 mm for Type I (n = 242) and Type III (n = 270) waste rock used to construct large-scale test piles. Smith *et al*. (in press) also suggest the finer fraction may be more reactive because the size of individual sulfide

grains measure < 0.2 μm (Jambor, 1997). The estimated mass of S, calculated using weighted values based on particle size, was 1.17 kg in each of the Type I AZLs and 3.59 kg in each of the Type III AZLs.

The average carbon content of the < 1-mm fraction of Type I waste rock was determined to be 0.044 ± 0.007 wt. % C (n = 3) and the < 4-mm fraction was 0.039 ± 0.005 wt. % C (n = 3; Table 3.2). The average carbon content for the < 5-mm fraction of waste rock used to construct the Type I test pile for a one month period around the AZL construction was 0.027 ± 0.007 wt. % C; n = 5 (Table 3.2). This was lower than the < 4-mm fraction of Type I AZL waste rock, but within two standard deviations (66.6%).

The Type III waste rock in the AZL had an average carbon content of 0.034 ± 0.003 wt. % C (n = 2) in the < 1-mm fraction and 0.029 ± 0.003 wt. % C (n = 2) in the < 4-mm fraction (Table 3.2). Similarly, the < 5-mm fraction of Type III waste rock used to construct the Type III test pile, over a one month period of AZL construction was (0.029 ± 0.005 wt. % C; n = 10; Table 3.2). Smith *et al* (in press) determined there is a decrease in carbon content with increasing particle size; this trend was not observed in the samples obtained from the AZLs. The estimated mass of carbon, calculated using weighted values based on particle size, was 3.31 kg in each of the Type I AZLs and 2.97 kg in each of the Type III AZLs

Acid-base accounting calculations were conducted using the total S and total C contents of the AZLs, assuming that carbonate minerals are the only significant acid-consuming phases. The acid-producing potential (AP) was determined using the S content of the waste rock, assuming that the S was present as pyrite or pyrrhotite, based on standard methods (MEND,

2009). These calculations assume that each mole of S generates two moles of H^+. The neutralization potential (NP) was determined assuming that the analytically-determined wt. % C consisted entirely of $CaCO_3$ (Smith *et al*., in press). The ratio of NP to AP is used to evaluate the acid generating potential; a NP:AP ratio of < 1 is considered to be potentially acid generating, > 3 is considered to be non-acid generating, and > 1 and < 3 remains uncertain (Smith *et al*., in press).

The average calculated AP value for the < 4 mm size fractions were lower for the Type I waste rock (0.43 ± 0.29 kg t^{-1} $CaCO_3$; n = 3) than the Type III waste rock (1.10 ± 0.48 kg t^{-1} $CaCO_3$; n = 2), whereas the average calculated NP for the Type I waste rock (3.30 ± 0.41 kg t^{-1} $CaCO_3$; n = 3) was higher than the Type III waste rock (2.40 ± 0.23 kg t^{-1} $CaCO_3$; n = 2; Figure 3.1). The ratio of NP:AP for the < 4-mm fraction was 10.50 ± 7.17 for Type I waste rock and 3.50 ± 1.65 for Type III waste rock, both considered non-acid generating. The < 1 mm size fraction had a higher NP than the < 4-mm fraction for the Type I waste rock (3.60 ± 0.55 kg t^{-1} $CaCO_3$; n = 3) and slightly higher AP (0.54 ± 0.40 kg t^{-1} $CaCO_3$; n = 3; Figure 3.1). The NP for < 1 mm size fraction of Type III waste rock (2.80 ± 0.36 kg t^{-1} $CaCO_3$; n = 2) was slightly higher than the < 4-mm fraction, and the AP was higher (1.20 ± 0.36 kg t^{-1} $CaCO_3$; n = 2). The NP:AP ratio for the < 1 mm size fraction was higher in the Type I waste rock (10.70 ± 6.5), but lower in the Type III waste rock (2.62 ± 0.38), suggesting the finer fraction holds greater acid-generating potential.

The samples of waste rock collected during a month period around the construction of the AZLs were used to estimate the variability in the acid generating potential of the Type I and Type III waste rock. The average calculated NP:AP ratio for the < 5-mm fraction of Type III

waste rock used to construct the test pile for a month period around the construction of the AZLs was 1.73 ± 1.2, suggesting the waste rock had an uncertain acid generating potential. This NP:AP ratio was lower than the samples collected from the AZL construction. The NP:AP ratio for the Type I waste rock used in construction of the Type I test pile was 12.01 ± 9.5 which falls in the non-acid generating classification. This result was slightly higher than the average NP:AP ratio determined for the Type I waste rock present in the Type I AZLs.

3.4.1.1 Net Neutralization Potential

The effluent pH from the Type I AZLs remained near neutral, with alkalinity values of 60 mg L^{-1} as $CaCO_3$ in Type I West AZL and 10 mg L^{-1} as $CaCO_3$ in Type I East AZL for the duration of the study. These observations are consistent with the NP:AP ratios measured on the Type I waste rock used to construct the AZLs. The effluent pH from the Type III AZLs decreased below 4.5 in the first year. Alkalinity declined with decreasing pH in 2007 to below detection and remained undetectable for the duration of the study. The NP:AP ratios measured on the < 4 mm size fraction of the Type III waste rock indicate little potential for acid generation, whereas measurements conducted on the finer fraction (< 1 mm) suggested an uncertain net-neutralization potential which is more consistent with the observed water geochemistry. This observation is consistent with results presented by Smith *et al*. (in press) and suggests the fine-grained matrix fraction strongly affects the effluent geochemistry.

3.4.2 Whole-Rock Analysis

Whole-rock analysis of the waste rock used to fill the Type I and III AZLs indicates the material is dominated by SiO_2 and Al_2O_3, followed by K_2O, Ba, Na_2O and S (Table 3.3). The

sulfide minerals present in the Type III waste rock include pyrrhotite, sphalerite, chalcopyrite and pyrite. The Type III waste rock had 2.41 wt. % Fe_2O_3 and lesser amounts of Zn (32 ppm), Ni (27 ppm), Cu (5 ppm), and Co (5 ppm). The Type I AZL waste rock had a similar composition, with the exception of lower wt. % S and higher wt. % Sr and Cr. The Type I waste rock had 1.97 wt. % Fe_2O_3 and lesser amounts of Zn (27 ppm), Ni (31 ppm), Cu (2.7 ppm), and Co (4 ppm). The elemental composition of these waste-rock samples are consistent with the observation that both the Type I and Type III rock types were dominated by granite and granite pegmatite lithologies (Jambor, 1997).

3.4.3 Sulfide-Mineral Oxidation

Sulfate concentrations in the Type III AZL effluent were elevated during the initial sampling in August 2007 (3500 mg L^{-1} in the Type III West and 2200 mg L^{-1} in the Type III East) and decreased through the remainder of 2007 (Figure 3.2). In 2007, sulfate concentrations were highly correlated to the concentrations of constituents derived from blasting residuals, including NO_3^- and Cl^- (NO_3^-:SO_4^{2-} R^2 = 0.92; Cl^-:SO_4^{2-} R^2 = 0.87), suggesting much of the SO_4^{2-} was derived from sulfide oxidation during blasting (Bailey *et al*., 2012). The proportion of sulfate derived from *in situ* oxidation increased in 2008 (Bailey *et al*., 2012) and the combined SO_4^{2-} concentration reached 4500 mg L^{-1} in the West AZL and 4000 mg L^{-1} in the East AZL (Figure 3.2). After the depletion of the blasting-related SO_4^{2-} in October 2008, concentrations became more variable; suggesting the majority of SO_4^{2-} was derived from *in situ* sulfide-mineral oxidation (Bailey *et al*., 2012). In 2009 and 2010, SO_4^{2-} concentrations increased and decreased in response to ambient air temperature fluctuations and the volume of water flowing through the AZLs. The maximum SO_4^{2-} concentrations were 8600 mg L^{-1}in

the Type III East AZL and 13300 mg L^{-1} in the Type III West AZL at the end of July 2010. During this period, the pH was at the minimum value of 3.0 and concentrations of dissolved metals were at their maximum. The total mass of SO_4^{2-} released from the Type III East AZL was 576 g, which is half the amount released from the Type III West AZL (1023 g). This discrepancy may have been due to a greater proportion of matrix material in the Type III West AZL than the Type III East AZL. Similar concentrations were observed by Wagner (2006) in lysimeter experiments (2 m by 2 m) at Cluff Lake in Saskatchewan. These cells contained low-S content waste rock (0.44 to 0.76% S) and had median SO_4^{2-} concentrations of 10000 mg L^{-1}.

The effluent derived from Type I AZLs contained concentrations of SO_4^{2-} of up to 950 mg L^{-1} in 2008 when the first flush of water migrated through the waste rock. Much of this SO_4^{2-} was derived from blasting (Figure 3.2). Concentrations quickly decreased and remained lower through 2009 (105 mg L^{-1} to 780 mg L^{-1}), with variations that were associated with changes in ambient temperature. The total mass of SO_4^{2-} released from the Type I East AZL was 108 g and a slightly higher mass was released from the Type I West AZL at 176 g, with an average of 142 g. This value is much lower than the average mass of SO_4^{2-} released from the Type III AZLs (800 g).

The release rate of S was higher in the Type III AZLs (0.011 mol kg S^{-1} $week^{-1}$) compared to the Type I AZLs (0.0081 mol kg S^{-1} $week^{-1}$). These release rates were similar to those estimated based on the humidity-cell experiments for both Type I (0.0088 mol kg S^{-1} $week^{-1}$) and Type III (0.015 mol kg S^{-1} $week^{-1}$) waste rock for a mean annual temperature of 4°C (Moore, in preparation).

Measurements of pore gas concentrations were not made in the AZLs, measurement of O_2 and carbon dioxide (CO_2) concentrations within adjacent 15 m by 60 m waste-rock test piles indicate concentrations remained at atmospheric levels throughout the year (Amos, personal communication, 2011). Based on the porosity and permeability of the waste rock used in this experiment, it is assumed the atmospheric conditions in the AZL experiments were similar to the waste-rock test piles.

Schoonen *et al* (2000), show the rate of abiotic pyrite oxidation increases with increasing pH. Based on equation 3.8, the rate of pyrite oxidation by O_2 at pH 7 is 2.4 times higher than at pH 3.5, with dissolved oxygen concentrations of 5 ppm. This observation suggests that the difference in sulfate release rates may be due to more rapid, bacterially-mediated sulfide oxidation under the low pH conditions that prevail in the Type III AZLs, rather than abiotic oxidation.

3.4.4 Microbial Populations

Three groups of Fe- and S-oxidizing bacteria (*Acidithiobacillus ferrooxidans* and related species, *Acidithiobacillus thiooxidans* and related species, and *Thiobacillus thioparus* and related species) were monitored in effluent from the AZLs and enumerated. Neutrophilic S-oxidizing bacteria were observed in both Type III AZLs in 2008 and decreased in number in 2009 and through 2010 (Figure 3.3). Populations of neutrophilic bacteria were higher in the Type I AZLs with an increased population in the Type I West AZL from 2008 to 2009, followed by decreased numbers in 2010. Samples were not collected in the Type I East AZLs in 2008 due to limited outflow. Populations in 2009 and 2010 were similar for both the Type

I East and West AZLs (Figure 3.3). The pH (pH ~ 7) in the Type I AZL effluent was well suited for neutrophilic S-oxidizing bacteria.

Acidophilic S-oxidizing bacteria were present in the Type III AZLs in 2008. Populations increased in the Type III East AZL in 2009, but were not detected in the West AZL. In 2010, populations slightly increased in both Type III AZLs, whereas very low populations were detected in the Type I AZLs. No Fe-oxidizing bacteria were observed in the Type I AZLs and Type III East AZL. Iron oxidizing bacteria were detected in November 2010 in the Type III AZLs, after the minimum pH (3.0) and maximum dissolved metal concentrations were observed.

In a field investigation at an active tailings impoundment, Blowes *et al*. (1995) observed low populations of acidophilic Fe- and S-oxidizing bacteria in locations where sulfide-mineral oxidation was limited by low O_2 concentrations. Higher population numbers were observed at locations where low pH conditions prevailed, and higher numbers of neutrophilic S-oxidizing bacteria were observed in areas where the pore-water pH was near neutral. Benner *et al*. (2000) also observed higher populations of acidophilic S-oxidizing bacteria and Fe-oxidizing bacteria at low pH. The results from this study are consistent with previous studies (Benner *et al*., 2000; Blowes *et al*., 1995) that show a bacterial succession that is consistent with the observed pH conditions.

3.4.5 Water Chemistry

The effluent from the Type III AZLs was acidic and contained high concentrations of SO_4^{2-}, and dissolved metals over the four consecutive years of the study. The increase in SO_4^{2-}, and most dissolved metals coincides with the decrease in pH to 3.0. The mean annual

concentrations of Al (66 mg L^{-1}), Ni (30 mg L^{-1}), Co (6.4 mg L^{-1}), Zn (20 mg L^{-1}), Cd (0.081 mg L^{-1}), and Cu (3.9 mg L^{-1}) in the Type III West AZL were the highest in 2010 (Table 3.4). Similarly to the Type III West, the mean annual concentrations of Al (30 mg L^{-1}), Ni (17 mg L^{-1}), Co (3.7 mg L^{-1}), Zn (11 mg L^{-1}), Cd (0.053 mg L^{-1}), and Cu (1.9 mg L^{-1}) in the Type III East AZL were the highest in 2010 (Table 3.4). Alkalinity was only detected in 2007 and decreased along with decreasing pH (Figure 3.2).

The effluent from the Type I AZLs maintained a near-neutral pH (7.5) with lower concentrations of SO_4^{2-}, and dissolved metals (Figure 3.2). The maximum SO_4^{2-} concentration was observed in 2008 at 950 mg L^{-1} in the Type I West AZL and 780 mg L^{-1} in the Type I East AZL and concentrations were highly correlated to blasting residuals (Bailey *et al*., 2012). The mean annual concentrations in the Type I AZLs were lower than in the Type III AZLs. The maximum mean annual concentrations in the Type I West AZL occurred in 2008 for Cd (0.002 mg L^{-1}), in 2009 for Al (0.29 mg L^{-1}), Cu (0.17 mg L^{-1}), and Zn (0.80 mg L^{-1}), and in 2010 for Co (0.030 mg L^{-1}; Table 3.4). The maximum mean annual concentrations in the Type I East AZL occurred in 2009 for Al (0.21 mg L^{-1}), Cu (0.17 mg L^{-1}), and Zn (0.80 mg L^{-1}), and in 2010 for Co (0.044 mg L^{-1}) and Cd (0.022 mg L^{-1}; Table 3.4). Alkalinity was present in the effluent at both the Type I West and East AZL for the duration of this study.

An important aspect of understanding the geochemistry of waste-rock stockpiles is to assess the quality of effluent from the first flush of water. The first flush in the AZLs can be determined by measuring the dissipation of blasting residuals initially present within the unsaturated waste rock (Chapter 2; Bailey *et al*., 2012). Subsequent flushes can be estimated

based on the first flush volume. These initial conditions provide a benchmark for the geochemical evolution in waste-rock stockpiles. In a study completed by Nichol *et al*. (2005), macropore flow was a significant portion of the outflow only during high intensity rainfall events, and represented 5 % of the total flow through a constructed experimental waste-rock pile. Neuner *et al*. (2012) has shown that at the 2 m by 2 m scale, in the AZLs, flow is likely to be dominated by the matrix flow component and flow through macropores is limited. Metal concentrations were highest during periods of high-intensity outflow events. This observation is consistent with an absence of preferential flow paths (Neuner *et al*., 2012).

3.4.6 pH, Alkalinity, and Acid Neutralization

A conceptual acid-neutralization model describing the sequence of mechanisms of H^+ consumption in mine tailings impoundments was described by Jurjovec *et al*. (2002). The pH is buffered by the dissolution of a sequence of minerals to a distinct series of acid-neutralization plateaus associated with the progressive depletion of primary and secondary minerals including; calcite (pH 6.5 - 7.5), siderite (4.8 - 6.3), $Al(OH)_3$ (4.0 - 4.3), and $Fe(OH)_3$ (2.5 < 3.5) (Blowes and Ptacek, 1994a; Jurjovec *et al*., 2002). Aluminosilicate mineral dissolution occurs concurrently with the dissolution of other minerals consuming H^+, however, it is not rapid enough to constrain the effluent to a specific pH.

The pH of the effluent from both Type I AZLs remained circum-neutral (pH ~ 7) for the duration of this study. The effluent of Type I West AZL contained alkalinity at 40 to 60 mg L^{-1} (as $CaCO_3$) and the Type I East AZL effluent contained ~ 20 mg L^{-1} (as $CaCO_3$). Geochemical equilibrium modeling suggests the Type I West effluent was supersaturated with respect to calcite and dolomite at the beginning of 2008 and was slightly undersaturated

with respect to calcite from late 2008 through 2010. Calculations suggest effluent from the Type I East AZL was undersaturated with respect to both calcite and dolomite for the duration of the study (Figure 3.4); however, the continued presence of alkalinity in the effluent suggests that the initial mass of carbonate minerals has not yet been completely depleted. The initial sulfide content of the Type I waste rock was very low, resulting in limited acid-generating potential. Equilibrium calculations suggested the effluent from both Type I AZLs remained undersaturated with respect to siderite, indicating precipitation of secondary siderite was not favoured. Throughout the sampling period, equilibrium calculations suggested the Type I AZL effluent remained supersaturated with respect to goethite, gibbsite, and all other Al-bearing secondary minerals considered, suggesting a potential for the precipitation of these minerals.

The initial pH of Type III West AZL effluent was 5.7, and the pH of the effluent from the Type III East AZL was 6.5. In both Type III AZLs the pH decreased to a relatively constant value of approximately 4.0 from 2007 through 2008, and further decreased to approximately 3.0 through 2009. The initial alkalinity in the Type III AZLs was 20 mg L^{-1} (as $CaCO_3$) and declined with decreasing pH. Geochemical equilibrium modeling suggests the effluent was undersaturated with respect to all carbonate minerals (Figure 3.4). The trends in pH suggest that the initial mass of carbonate minerals within the Type III AZLs was depleted rapidly as H^+ was released by sulfide-mineral oxidation.

The decrease in pH (to values ranging from 3.5 to 4.2) observed in 2008 through 2009 (Figure 3.4) was accompanied by an increase in dissolved Al concentrations from < 10 mg L^{-1} to 60 mg L^{-1}, and an increase in the concentrations of Ca, Mg, K, Na, and H_4SiO_4 (Figure

3.5). The biotite schist aluminosilicate mineral assemblage in the Type III waste rock consists mainly of quartz [SiO_2] (20 to 50%), albite [$NaAlSi_3O_8$] (35 to 55%), and biotite [$KMg_3AlSi_3O_{10}(OH)_2$] (10 to 25%). The granite consists mainly of potassium feldspar [$KAlSi_3O_8$], albite, and quartz, with < 5% each of biotite and muscovite [$KAl_2AlSi_3O_{10}(OH)_2$] (Jambor, 1997). The increased concentrations of Ca, Mg, K, Na, Sr, and H_4SiO_4 probably were derived from the dissolution of aluminosilicate minerals, principally biotite and plagioclase, present in the biotite schist, and K-feldspar and albite present in the granite component of the Type III rock. During this period, the effluent was undersaturated with respect to gibbsite and boehmite, and near equilibrium with Fe hydroxides (Figure 3.4). Subsequently the pH declined further to pH < 3.5, favouring the dissolution of secondary Fe(III) (oxy)hydroxides and subsequently resulting in increases in the concentrations of Fe and SO_4^{2-}.

Cravotta *et al*. (1999) show a distribution of mine drainage from the eastern U.S. coal province to have a bimodal distribution with few samples between pH 4 and 6. The pH of drainage from the Type I and Type III AZLs from 2007 through 2010 had a similar bimodal distribution (Figure 3.6). This suggests drainage from the Type I and Type III AZLs was either distinctly acidic or near neutral, with few samples in the range of pH 4.5 to 6. Bigham and Nordstom (2000) note that acidic drainage occurs when acid generation exceeds the buffering capacity of the materials present that neutralize acidity. Carbonates are known to buffer pH between pH 6.5 - 7.5 and the next distinct pH buffering zone is from buffering by Al and Fe (III) (oxy)hydroxides between pH 2.5 and 4.3 (Blowes and Ptacek, 1994a; Jurjovec *et al*., 2002). The frequency distribution observed in the Type I and Type III AZLs

suggest the pH from the Type I AZLs was buffered by the dissolution of carbonate minerals, whereas Al and Fe(III) oxyhydroxides dissolution buffered the pH in the Type III AZLs.

3.4.7 Major Ions

The maximum concentrations of dissolved Ca in the Type III AZLs (400 mg L^{-1} to 600 mg L^{-1} in the West AZL and 310 mg L^{-1} to 500 mg L^{-1} in the East AZL) were observed during the initial sampling in 2007 when alkalinity was present (Figure 3.5). In subsequent years Ca concentrations showed a consistent pattern, with increasing Ca concentrations in the spring, followed by declining concentrations through to the summer and fall. In 2008, Ca concentrations increased in July to 480 mg L^{-1} in the West AZL and 380 mg L^{-1} in the East AZL; but decreased through to the end of the field season. The lowest Ca concentrations were reported at the end of 2010 (< 35 mg L^{-1}). At times, geochemical modeling suggests the Type III AZLs effluent was at saturation with respect to gypsum; therefore, Ca concentrations may have been limited by gypsum precipitation.

The Type I West AZL first had flow report to the drain in 2008. The Ca concentration in the Type I West AZL effluent was the highest reported for all sampling locations with an initial concentration of 2000 mg L^{-1}. Equilibrium modeling suggests effluent initially was supersaturated with respect to calcite and dolomite. Concentrations decreased through August and remained low (< 200 mg L^{-1}) for the remainder of 2008. A similar trend was observed in 2009 and 2010. In 2010, concentrations at the end of the field season were the lowest observed to date. A 2:1 ratio of Ca to Mg was observed for the Type I West AZL for the duration of the study.

Dissolved Ca concentrations in the effluent of the Type I East AZL were lower than the Type I West AZL, with the maximum occurring in early 2008 at 310 mg L^{-1} decreasing to 47 mg L^{-1} by the end of the season. Concentrations in 2009 ranged from 40 to 180 mg L^{-1}, with the maximum occurring at peak flow rates. Calcium concentrations further decreased in 2010 to 18 mg L^{-1}. The effluent from the Type I East AZL remained undersaturated with respect to all carbonate minerals throughout the study. The total mass of Ca released was highest in the Type I West AZL, followed by the Type III AZLs and the Type I East AZL having the least (Table 3.5).

The maximum Sr concentration in the Type III West AZL was 5.6 mg L^{-1} and 3.7 mg L^{-1} in the Type III East AZL in 2007 (Figure 3.7). In 2008, Sr concentrations in the Type III AZLs reached similar concentrations, and were < 4.0 mg L^{-1} for the duration of the study (Figure 3.7). In the Type I AZLs the Sr concentration followed a similar trend to Ca with a decreasing trend though 2007 (Figure 3.7). Maximum concentrations of Sr in the Type I West AZL were observed in early 2008 at the initiation of flow and decreased through the remainder of 2008 (Figure 3.7). Concentrations of Sr in the Type I East AZL were lower than in the Type I West AZL with a maximum of 3.1 mg L^{-1} in early 2008, and concentrations < 2.0 mg L^{-1} for the remainder of the study (Figure 3.7). Strontium followed a similar trend as Ca, and probably is released from biotite and lesser amounts from the granite and pegmatite granites (Jambor, 1997). Weathering of calcite present in trace amounts in granitic bedrock may be an important source of Ca (Clow, *et al*., 1997), and calcite can contain a relatively high concentration of Sr (Taylor, *et al*., 2000). Studies have found that the bicarbonate and Sr fluxes in some granitic catchments are dominated by trace calcite dissolution (Blum *et al*.,

1998; Clow *et al*., 1997). Mineralogical data has shown carbonate mineral assemblages present in the fractures found in the granite host rocks at Diavik (unpublished data).

Trends similar to those observed for Ca concentrations were observed for Mg, K, and Na (Figure 3.5). The maximum Mg concentrations occurred in 2010, 1040 mg L^{-1} in the Type III East AZL and 900 mg L^{-1} in the Type III West AZL. The Mg concentrations decreased through October to the lowest reported Mg concentrations at the end of 2010. Concentrations of Mg in the Type I West AZL were elevated at the beginning of 2008 (910 mg L^{-1}), similar to trends in Ca concentrations, and was at saturation with respect to dolomite. Concentrations decreased by September 2008 and the effluent was undersaturated with respect to all carbonate minerals. The concentrations of Mg decreased to < 43 mg L^{-1} by the end of the 2008 season and remained < 230 mg L^{-1} for the remainder of the study. The Type I East AZL effluent contained low Mg concentrations (< 180 mg L^{-1}) for the duration of the study and was undersaturated with respect to all carbonate minerals. The principal source of Mg probably was the dissolution of biotite and spinel. Spinel has been observed in minute amounts in the granite with the formula $(Fe_{0.58}Mg_{0.46}Mn_{0.01})_{\Sigma 1.05}(Al_{1.95}Ti_{0.01})_{\Sigma\ 1.96}O_9$ (Jambor, 1997). The greatest mass of Mg was released from the Type III West AZL. The Type III East and Type I East AZLs released a similar mass of Mg, while the Type I West AZL released the lowest mass loading (Table 3.5).

The dissolution of biotite, which is probably the primary source of dissolved K, is favoured at low pH (Acker and Bricker, 1992). The chlorination of biotite releases K that can be used to form secondary mineral precipitates, such as jarosite and alunite. The pH of the Type III AZLs remains < 4.5 after the first year. The maximum concentrations of K in the Type III

AZLs were observed at the end of July 2010 at 900 mg L^{-1} in the Type III West AZL and 980 mg L^{-1} in the Type III East AZL (Figure 3.5). Concentrations of K decreased by the end of the season in 2010 to the lowest measured concentrations (130 mg L^{-1} in the Type III West AZL and 65 mg L^{-1} in the Type III East AZL). Geochemical calculations indicate that the effluent from the Type III AZLs was at saturation with respect to jarosite in 2007. The effluent from both of the Type III AZLs was supersaturated with respect to alunite, suggesting concentrations of K were limited by precipitation of jarosite or possibly alunite. The presence of jarosite in column studies of the biotite schist was confirmed by Debye-Scherrer X-ray patterns (Blowes and Logsdon, 1998). Alunite has not been observed in samples from Diavik waste rock, but alunite has been found in secondary SO_4^{2-} rims of pyrrhotite grains in a tailings impoundment (Moncur *et al*., 2005).

Potassium can also be released from the oxidation of perchlorate salts used in blasting at Diavik (Chapter 3). The concentration of K released from blasting can be estimated based on the maximum concentration of ClO_4^- in the first flush of water through the waste rock. It is assumed that blasting was 99% efficient and the maximum observed concentration of ClO_4^- (130 μg L^{-1} in the Type I West AZL in 2008) would correspond to 1% of the total mass of $KClO_4$ used in blasting. Assuming all K remains within the waste rock and is mobilized during flushing, a maximum K concentration of 5.1 mg L^{-1} would be due to blasting. The maximum concentration of K in 2008 was 370 mg L^{-1}; therefore, the contribution of K from blasting is considered negligible.

The pH in the Type I AZLs remained near neutral and the concentrations of K in the Type I West AZL reached a maximum in July 2008 (370 mg L^{-1}) and decreased to < 100 mg L^{-1} by

the end of the 2008 field season. A similar trend was observed each year; however, the maximum concentrations were lower each year. The first sample in 2009 was 200 mg L^{-1}, concentrations decreased to < 100 mg L^{-1} for the remainder of 2009. In 2010, the maximum concentration was 160 mg $L^{-1}$and at the end of the season K concentrations were < 100 mg L^{-1}, the lowest concentrations observed to date. The effluent from the Type I East AZL followed a similar trend to the Type I West AZL effluent, but in general concentrations were lower with the maximum in 2008 of 200 mg L^{-1} and all samples < 90 mg L^{-1} for the remainder of the study. Equilibrium calculations suggest that effluent from the Type I East AZLs was consistently undersaturated with respect to jarosite and supersaturated with respect to alunite, suggesting concentrations of K may have been limited by precipitation of alunite. Additional mineralogical study is required to determine whether alunite, or another K-bearing secondary mineral, limits the K concentrations in the Type I and III AZLs.

The maximum Na concentrations for the Type III West AZL was 580 mg L^{-1} in July 2008 and the maximum in the Type III East AZL was 420 mg L^{-1} in late August 2008; Na concentrations decreased through the remainder of 2008 (Figure 3.5). The Type I West AZL had similar Na concentrations to the Type III AZLs in 2008, with a maximum of 610 mg L^{-1} in July, decreasing to < 180 mg L^{-1} for the remainder of the study. The concentration of Na in the Type I East AZL was < 120 mg L^{-1} for the duration of the study. Geochemical modeling results suggest that there are no secondary mineral controls on Na concentrations.

The concentration of Mn in the Type III AZL effluent followed a similar trend to Mg. The maximum Mn concentrations were 130 mg L^{-1} in the Type III West AZL and 77 mg L^{-1} in the Type III East AZL in 2010. The Mn concentrations from the Type I AZLs in 2008 decreased

from 2.5 mg L^{-1} in the East AZL and 4.5 mg L^{-1} in the West AZL to < 1.5 mg L^{-1} for the remainder of the study. Manganese can substitute in biotite and plagioclase feldspar, and can be released during the dissolution of these minerals. The total mass released from the Type III West AZL was 7.7 g and 4.3 g from the East AZL, whereas the total mass released from Type I West AZL was 0.36 g and 0.35 g from the East AZL.

In 2007, the Al concentrations were below 10 mg L^{-1} in both Type III AZLs. In 2008, the pH decreased from near neutral to 3.7 in the Type III West AZL and the concentrations of Al increased to 44 mg L^{-1}. The Type III East AZL had a slightly higher pH in 2008 (pH ~ 4) and the maximum Al concentration was 13 mg L^{-1}. In 2009, the pH in both locations further decreased and Al concentrations increased to 100 mg L^{-1} in the Type III West AZL and 50 mg L^{-1} in the Type III East AZL. The maximum Al concentrations increased further in 2010 to 140 mg L^{-1} in the Type III West AZL and 130 mg L^{-1} in the Type III East AZL. The total mass of Al released from the Type III AZL was 12 g in the Type III West and 4.5 g in the Type III East (Table 3.5). Aluminium was probably released from the dissolution of aluminosilicates, principally biotite. Geochemical modeling of the Type III AZL effluent suggests supersaturation with respect to the Al-secondary minerals alunite, gibbsite, diaspore, and basaluminite in early 2007, and subsequently the water became undersaturated with respect to gibbsite, diaspore, and basaluminite as the Al concentrations increased and pH decreased (Figure 3.8).

The Type I AZLs maintained near-neutral pH conditions and dissolved Al remained low, with maximum concentrations of 1.3 mg L^{-1} in the West and 0.84 mg L^{-1} in the East in 2009. The Type I AZLs had much lower total mass loadings than the Type III AZLs with 0.033 g

of Al in the West and 0.026 g of Al in the East (Table 3.5). Geochemical calculations indicated supersaturation with respect to amorphous Al-hydroxide, alunite, and basaluminite in 2008 and 2009, and undersaturation in 2010. The effluent water was supersaturated with respect to gibbsite and diaspore for the duration of the study.

3.4.8 Metals

As the temperature within the AZLs increased with the ambient air temperatures, increased concentrations of metals were observed in the effluent. The concentrations of dissolved metals in the effluent from the Type III AZLs were consistent in 2007 and increased from July to September 2008, then decreased until the end of November (Figure 3.7). In 2009, concentrations were initially low, but increased as internal temperatures increased until the end of August, and followed a decreasing trend through the remainder of 2009 as the internal temperature decreased. A similar trend was observed in 2010 and maximum concentrations occurred in August 2010.

The effluent from the Type I AZLs contained lower concentrations of all metals, but followed the same seasonal trends observed in the Type III AZLs (Figure 3.7). A relatively small fraction of metals was released from each AZL over the 4 year study period. The < 50-mm fraction of rock, which constitutes approximately 40% of the total Type III test pile volume, is the most reactive fraction (Smith *et al*., in press). The mass of individual metals released from each AZL by 2010 was less than 0.06 % of the mass of each metal initially contained within the < 50-mm fraction.

The maximum concentration of dissolved Fe in the effluent from the Type III East AZL was 2.4 mg L^{-1} and the Type III West AZL effluent was 14 mg L^{-1}. Lower Fe concentrations

were observed in the Type I AZLs with a maximum of 0.25 mg L^{-1} in the East AZL and 1.4 mg L^{-1} in the West AZL. This Fe was released from the oxidation of sulfide minerals, principally pyrrhotite with small amounts of chalcopyrite, sphalerite and pyrite. Geochemical modeling suggests that initially the effluent from all of the AZLs was supersaturated with respect to goethite and lepidocrocite, suggesting that the accumulation of these secondary minerals may have limited Fe concentrations (Figure 3.8). As the pH decreased in 2008, Fe concentrations slightly increased and SI values indicate undersaturation with respect to both goethite and lepidocrocite. Concentrations of Fe were probably controlled by the rate of sulfide oxidation, and by the accumulation and solubility of secondary minerals, such as Fe(III) oxyhydroxides and Fe(III) hydroxysulfates. Fe-oxyhydroxides have been observed in AMD impacted sites (Blowes and Jambor, 1990; Blowes *et al*., 1991, 1992; Moncur *et al*., 2005; Gunsinger *et al*., 2006b; Stockwell *et al*., 2006), however, further mineralogical work is required to determine if secondary Fe minerals exists, and if, metal concentrations are controlled by adsorption or coprecipitation reactions. The total mass loadings of Fe from the Type III AZLs were 0.83 g from the West AZL and 0.093 g from the East AZL (Table 3.5; Figure 3.9). Approximately $2.1x10^{-3}$ % of the total available Fe in the Type III West AZL was released after four years and $2.4x10^{-4}$ % in the East AZL (Table 3.6).

The mass of Fe released from the Type I AZLs was much lower, with total mass loadings of Fe with 0.045 g released from the Type I West AZL and 0.033 g from the Type I East AZL (Table 3.5; Figure 3.9). Approximately, $2.3x10^{-4}$ % of the total available Fe in the East AZL and $1.9x10^{-4}$ % in the West AZLs (Table 3.6) was released after four years.

The maximum observed Ni concentrations were 150 mg L^{-1} in the effluent from the Type III West AZL and 86 mg L^{-1} from the Type III East AZL, both in 2010. The Type I AZLs

released lower Ni concentrations (< 600 μg L^{-1}), this was consistent with the low concentrations of sulfide minerals in Type I waste rock. The highest Co concentrations were observed in the effluent from the Type III West AZL in 2008 (30 mg L^{-1}) and Type III East (19 mg L^{-1}) in 2010 (Figure 3.7). The effluent from the Type I AZLs contained low Co concentrations, with a maximum of 0.079 mg L^{-1} derived from the West AZL and 0.78 mg L^{-1} from the East AZL.

Electron-microprobe analysis of Diavik waste rock indicates that the composition of pyrrhotite is $(Fe_{0.852}Ni_{0.004}Co_{0.001})_{\sum 0.857}S_{1.000}$ (Jambor, 1997), suggesting the oxidation of pyrrhotite was the main source of dissolved Ni and Co. Geochemical equilibrium modeling suggests the all AZL effluent was undersaturated with respect to all secondary Ni and Co minerals included in the WATEQ4F database, including amorphous Ni hydroxide [$Ni(OH)_2$] (Figure 3.8). The total mass loading of Ni from the Type III West AZL was 6.8 g, 0.06 % of the estimated available mass of Ni initially present in the lysimeter (Table 3.3 and Table 3.4; Figure 3.9). The Type III East AZL total mass loading was 3.5 g or 0.03 % of the total available Ni in the lysimeter (Table 3.3 and Table 3.4; Figure 3.9). The Type I AZLs released lower total masses of Ni with 0.040 g derived from the Type I West AZL and 0.045 g derived from the Type I East AZL (Table 3.5; Figure 3.9). A total mass of Co released from the Type III West and East AZL (Table 3.5; Figure 3.9) were proportionate to masses of Ni released from the Type III AZLs. The total mass of Co released from the Type I AZLs was much lower (Table 3.5 and 3.6; Figure 3.9).

Whole-rock analysis of Type III waste rock used to construct the large-scale test piles indicates 89% of the S in the waste rock is present as pyrrhotite (Chapter 4), therefore the relative mobility of S to Ni, Co, and Fe can be determined by estimating the average ratio of

S to Ni, Co, and Fe in the effluent from each sampling location (Table 3.7). The ratio of S to Fe in the Type I AZLs (5800 in the West and 7200 in the East) and Type III AZLs (2100 in the West and 4900 in the East) indicates that Fe concentrations were lower in the effluent than would be estimated on the basis of the pyrrhotite stoichiometry, and the Fe concentrations were more affected by secondary mineral formation than SO_4^{2-} concentrations. The ratios of S:Fe in the effluent from the Type I AZLs were much higher than those in the Type III AZL effluent because of the differences in chemical composition of the waste rock in the Type I and Type III AZLs (Table 3.7); the Type I AZLs had less Fe due to the low concentrations of sulfide minerals.

Based on the observed pyrrhotite composition the expected ratio of S:Ni was 250, and the expected ratio of S:Co was 1000. In the Type I AZLs effluent the ratios of S to Ni (6900 in the West and 2100 in the East) and S to Co (43000 in the West and 14000 in the East) were higher than inferred from the stoichiometry of pyrrhotite (Table 3.7), suggesting retention of Ni and Co relative to SO_4^{2-}. The Type III West AZL effluent ratios of S:Ni of 74 and S:Co of 320, and the Type III East AZL effluent S:Ni ratio of 110 and S:Co ratio of 610, suggest retention of S relative to both Ni and Co under the low pH conditions prevalent in the Type III AZLs. Precipitation of gypsum and jarosite may limit the maximum SO_4^{2-} concentrations. No secondary mineral controls on Ni and Co concentrations were suggested from the geochemical modeling results (Figure 3.8).

The ratio of Ni to Co in pyrrhotite was determined to be 4:1 using microprobe analysis (Jambor, 1997). Similar ratios were observed in the effluent from the Type III AZLs; the Type III West AZL effluent had an average Ni to Co ratio of 4.4 and the Type III East AZL

effluent a ratio of 4.6 (Table 3.7). The Ni:Co ratios for the Type I East AZL (6.9) and the Type I West AZL (6.2) suggest preferential retention of Co over Ni or that another source of Ni may be present in the granite. The ratios of Ni to Co observed in the effluent suggest there were no adsorption/complexation reactions controlling Ni and Co concentrations in the Type III AZLs below pH 5, but may have influenced Ni and Co concentrations in the Type I AZLs at near neutral pH (Figure 3.10).

The maximum Zn concentration in the Type III West AZL effluent was 87 mg L^{-1} and the maximum Zn concentration in the Type III East AZL effluent was 20 mg L^{-1} in 2010 (Figure 3.7). Zinc in the effluent probably was derived from the oxidation of sphalerite. The total mass loading of Zn from the Type III West AZL was 4.3 g and 2.3 g from the Type III East AZL (Table 3.5). These masses correspond to a total of 0.03 % released from the available Zn in the Type III West AZL and 0.01 % released from the available Zn in the Type III East AZL. The Type I AZL effluent contained much lower Zn concentrations with a maximum of 4.9 mg L^{-1} in the West AZL and 0.79 mg L^{-1} in the East AZL in 2008. The Type I AZLs released much lower total masses of Zn (0.015 g in the West and 0.0081 g in the East; Table 3.5) and very modest fraction of the total available mass of Zn in the AZLs ($1.6x10^{-4}$ % in the West and $2.7x10^{-4}$ % in the East; Table 3.6). The Type I AZL effluent was undersaturated with respect to discrete Zn minerals and no secondary Zn-bearing minerals are expected to form (Figure 3.8).

The maximum concentration of Cd was 0.38 mg L^{-1} in the effluent from the Type III West AZL and 0.26 mg L^{-1} in the Type III East AZL, and the total mass loading of Cd was 0.005 g from the East AZL and 0.006 g from the West AZL (Table 3.5). Dissolved Cd concentrations

were below detection in the Type I AZLs. The Type I and Type III AZL effluent was undersaturated with respect to Cd minerals and no secondary Cd-bearing minerals are expected to form. The main source of Cd associated with acid mine drainage tends to be released from sphalerite as Cd can replace Zn in the lattice structure (Jambor *et al*., 2005). Zn and Cd were highly correlated (R^2 = 84%) in the effluent from the Type III AZLs for the duration of the study suggesting sphalerite oxidation was the main source of Cd in the effluent.

Concentrations of Cu in the Type III West AZL increased from July through August 2008 and subsequently decreased through the end of the field season (Figure 3.7). In 2009 and 2010 similar trends were observed, with the maximum concentrations of 12 mg L^{-1} in the Type III West AZL effluent and 7.9 mg L^{-1} in the effluent from the Type III East AZL in 2010. Concentrations of Cu in the Type III East AZL exhibited similar trends to the Type III West AZL from 2007 through 2010; however, Cu concentrations were lower than in the effluent of the Type III West AZL. The total mass of Cu released from the Type III West AZL was 0.71 g and from the Type III East AZL was 0.38 g (Figure 3.9). The total mass released corresponded to 0.017 % of the total available Cu in the West AZL and 0.007 % from the East AZL (Table 3.6).

The Type I AZLs effluent had lower Cu concentrations than the Type III AZLs. Maximum Cu concentrations of 0.92 mg L^{-1} and 0.78 mg L^{-1} were observed in the Type I West and Type I East AZLs, respectively, in 2008. The effluent from the Type I AZLs had low concentrations ranging from 0.92 mg L^{-1} to below detection. In addition, low mass loadings reported to the base of the Type I AZLs compared to the Type III AZLs over the four year

period was observed in the Type I AZLs due to a lower proportion of sulfide minerals than in the Type III AZLs (Table 3.3 and Table 3.4; Figure 3.9).

At near neutral pH, concentrations of dissolved metals, such as Ni, Zn, Cd, and Cu, can be controlled by adsorption onto or coprecipitation with Fe(III)-oxyhydroxide minerals (Dzombak and Morel, 1990; Ribet *et al*., 1995; Webster *et al*., 1998; Carlsson *et al*., 2002; McGregor and Blowes, 2002; Galan *et al*., 2003; Lee *et al*., 2005; Moncur *et al*., 2005; Gunsinger *et al*., 2006; Heikkinen *et al*., 2009). Although geochemical equilibrium modeling suggests the potential for formation of Fe(III)-oxyhydroxide minerals (SI > 0) at times, further mineralogical work is required to determine if metal concentrations in the AZLs were controlled by coprecipitation. However, dissolved metals concentrations increased with decreasing pH below 5 (Figure 3.10). Adsorption/complexation reactions may have influenced concentrations in the Type III AZLs above pH of 5, similar to those observed in mine tailings at the Bersbo mine in Sweden (Karlsson *et al*., 1987). However, the pH in the Type III ALZs decreased below 5 in 2008 and has remained low, suggesting adsorption/complexation no longer control the metal concentrations. The pH in the Type I AZLs remained near neutral for the duration of the study and adsorption/complexation reactions may have had greater impact on dissolved metal concentrations.

3.4.9 Summary

The S content and C content of waste rock at Diavik is considered to be low (< 0.08 wt. % S and < 0.03 wt. % C) compared with other northern mine sites, such as in Saskatchewan (Cluff Lake 0.44 to 0.76 wt. % S; Wagner *et al*., 2006), and Sweden (Aitik mine; 0.7–1.7% S; Stromberg and Banwart, 1999). Poor quality effluent has been documented from waste rock

at Cluff Lake, with median SO_4^{2-} concentrations of 10,000 mg/L in test pads (Wagner *et al*., 2006) and at the Aitik site, with 1310 mg/L SO_4^{2-} in a drainage ditch (Stromberg and Banwart, 1999). These SO_4^{2-} concentrations are similar to those observed in the effluent from the Type III AZLs (maximum SO_4^{2-} = 13,300 mg/L). The results from this study indicate that even very modest sulfide masses can result in the generation of acidic conditions when flow is matrix dominated in a semi-arid climate. This observation is consistent with regulator guidance documents that suggest there is no lower limit of % S in predicting the generation of acidic conditions (Price, 2009).

The annual air temperature fluctuations observed at Diavik influenced the sulfide-oxidation rates; pH values and concentrations of dissolved SO_4^{2-} indicate that lower rates of sulfide oxidation prevailed during the winter. Although the rate of sulfide-mineral oxidation increased during the summer months, the resulting SO_4^{2-} concentrations were lower than those observed in waste-rock piles with a higher S content and with more temperate climates *e.g.,* Ritchie(2003) and Taylor *et al*.(2003). Furthermore, the semi-arid conditions at Diavik resulted in limited infiltration compared to other locations, such as the Antamina mine site in Peru which has a mean annual precipitation of 1200 to 1300 mm; approximately 10 times higher than at Diavik (Bay, 2009). The slow oxidation rates of the sulfide minerals and limited precipitation infiltrating the AZLs at Diavik resulted in high concentrations of sulfide-mineral oxidation products that migrated downwards through matrix dominated flow. The total load at the end of each flow year was modest compared to the total sulfide-mineral content in the rock, suggesting a long-lived source of low quality effluent.

Although the AZLs (either Type I or Type III) were assumed to have the same waste rock composition, the physical and geochemical heterogeneity of the waste rock, at this scale, resulted in differing effluent chemistry from each AZL. This suggests more than two tests of each target S content should be completed to better predict the evolution of the water chemistry or, alternatively, the test size was less than the representative elementary volume.

3.5 Conclusions

Waste rock from the Diavik diamond mine consists of granite and pegmatite granite, and biotite schist, which occurs as irregular laths within the host granite. Pyrrhotite, the principal sulfide mineral, is disseminated within the biotite schist with lesser amounts of pyrite, sphalerite and chalcopyrite. The low volume of water that migrated through the Type III AZLs was characterized by low-pH with high concentrations of SO_4^{2-}, Fe and other metals, suggesting sulfide minerals were oxidized and any primary neutralization potential from carbonates was depleted. The Type I AZLs maintained neutral pH and lower concentrations of SO_4^{2-}, Fe, and other dissolved metals, suggesting any acid generated from sulfide-mineral oxidation was consumed by reaction with the available carbonate minerals. The Type III AZLs, with an NP:AP ratio of 3.50 ± 1.65 was acid generating, whereas the Type I AZLs with an NP:AP ratio of 10.50 ± 7.17 maintained neutral pH over 4 years of testing. Sulfide-mineral oxidation rates were affected by temperature, and the presence of neutrophilic and acidophilic S-oxidizing bacteria, and Fe-oxidizing bacteria present in the AZL effluent. The microbial population evolved with the effluent geochemistry. The observed bacterial succession was consistent with the observed pH conditions.

Table 3.1 Characteristics of the Type I and Type III AZLs.

	Units	Type III	Type I
Volume of AZL	m^3	5.947	4.87
Volume of rock	m^3	3.866	3.166
Mass of rock	t	10.24	8.389
Sulfur content	wt. % S	0.035 ± 0.015	0.014 ± 0.009
Mass of S	t S	0.39	0.12
Carbon Content	wt. % C	0.029 ± 0.003	0.039 ± 0.005
Mass of Carbon	t C	0.30	0.33

Table 3.2 Characteristics of the Type I and Type III AZLs.

		S content (wt. % S)	
AZLs	**n**	**< 1 mm**	**< 4 mm**
Type I	3	0.018 (σ = 0.012)	0.014 (σ = 0.009)
Type III	2	0.039 (σ = 0.012)	0.035 (σ = 0.015)

Test Piles	**n**	**< 5 mm**
Type I	5	0.006 (σ = 0.004).
Type III	10	0.045 (σ = 0.024).

	n	**< 50 mm**
Type I	111	0.020 (σ = 0.017)
Type III	77	0.049 (σ = 0.024)

		C content (wt. % C)	
AZLs	**n**	**< 1 mm**	**< 4 mm**
Type I	3	0.044 (σ = 0.007)	0.039 (σ = 0.005)
Type III	2	0.034 (σ = 0.003)	0.029 (σ = 0.003)

Test Piles	**n**	**< 5 mm**
Type I	5	0.027 (σ = 0.007)
Type III	10	0.029 (σ = 0.005)

Table 3.3 Average elemental composition of Type I (n = 3) and Type III (n = 2) waste rock used to fill the AZLs determined by XRF.

%	Type III (σ)	Type I (σ)
SiO_2	70.5 (0.92)	72 (0.11)
Al_2O_3	16.5 (0.48)	15.8 (0.13)
Fe_2O_3	2.41 (0.27)	1.97 (0.44)
TiO_2	0.24 (0.029)	0.18 (0.064)
MnO	0.03 (0.0018)	0.023 (0.0041)
MgO	0.65 (0.15)	0.69 (0.01)
CaO	0.91 (0.083)	0.94 (0.029)
Na_2O	3.2 (0.024)	3.2 (0.033)
K_2O	5.5 (0.12)	5.1 (0.27)
ppm		
Ba	411 (17)	399 (20)
Rb	103 (5)	89 (3)
Sr	122 (6)	131 (1)
Pb	30 (1)	29 (1)
Cr	110 (10)	114 (3)
Cu	5.0 (1.4)	2.7 (2.3)
Zn	32 (2)	27 (6)
As	< 0.2	< 0.2
V	19 (2)	14 (6)
Ni	27 (5)	31 (3)
Co	5.0 (0.4)	4.0 (1)

Table 3.4 Mean annual concentrations of select metals in the Type I and Type III AZLs

AZL	Year	Al (mg L^{-1})	Fe (mg L^{-1})	Co (mg L^{-1})	Ni (mg L^{-1})	Cu (mg L^{-1})	Zn (mg L^{-1})	Cd (mg L^{-1})
Type I East	2008	0.10	0.10	0.019	0.12	0.10	0.044	0.001
	2009	0.21	0.093	0.007	0.050	0.15	0.076	0.002
	2010	0.043	0.05	0.044	0.17	0.027	0.042	0.022
Type I West	2008	0.11	0.18	0.026	0.13	0.12	0.076	0.002
	2009	0.29	0.41	0.006	0.033	0.17	0.80	0.001
	2010	0.070	0.013	0.027	0.13	0.027	0.076	0.001
Type III East	2007	1.1	0.24	1.6	8.0	0.18	2.3	0.029
	2008	9.1	0.60	2.5	12	1.2	6.9	0.048
	2009	24	0.32	3.4	15	1.7	11	0.061
	2010	30	0.61	3.7	17	1.9	11	0.053
Type III West	2007	6.2	0.84	4.9	22	0.66	8.0	0.073
	2008	31	3.1	5.5	24	2.4	15	0.084
	2009	38	1.6	4.4	25	2.6	14	0.072
	2010	66	2.6	6.4	30	3.9	20	0.081

Table 3.5 Calculated mass loadings for parameters of interest from the Type I and Type III AZLs (2007 to 2010).

AZL	Year	Mass (g)										
		Ca	Mg	K	Na	Al	Fe	Ni	Co	Zn	Cu	SO_4^{2-}
Type III East	2007	10	7.5	4.3	5.3	0.022	0.007	0.16	0.042	0.04	0.004	61
	2008	48	36	32	20	1.9	0.051	1.9	0.49	1.3	0.21	340
	2009	4.7	4.4	3.5	1.9	0.67	0.013	0.45	0.11	0.32	0.06	67
	2010	10	10	8.4	3.4	1.9	0.022	0.94	0.22	0.65	0.11	110
	Total	73	58	48	30	4.5	0.093	3.5	0.79	2.3	0.38	578
Type III West	2007	16	16	8.7	10	0.19	0.021	0.72	0.17	0.26	0.022	100
	2008	70	66	49	31	7.3	0.58	4.32	1.1	2.8	0.49	690
	2009	5.3	5.6	4.0	2.1	0.85	0.015	0.26	0.058	0.18	0.054	56
	2010	15	17	12	5.6	3.5	0.21	1.5	0.31	1.0	0.19	170
	Total	106	105	74	49	12	0.83	6.8	1.5	4.3	0.71	1016
Type I East	2008	31	21	10	19	0.023	0.027	0.028	0.0046	0.0059	0.021	75
	2009	1.5	1.1	0.7	1.0	0.0028	0.0008	0.0006	0.0001	0.0003	0.0019	5.8
	2010	6.4	4.3	2.6	3.6	0.0006	0.0040	0.016	0.0024	0.0019	0.0002	27
	Total	39	26	13	24	0.026	0.032	0.045	0.0071	0.0081	0.023	108
Type I West	2008	124	37	58	47	0.022	0.035	0.037	0.0065	0.010	0.023	130
	2009	7.7	3.6	3.8	3.6	0.0098	0.0087	0.0013	0.0002	0.0049	0.008	22
	2010	7.5	3.8	4.1	3.5	0.0009	0.0010	0.0020	0.0003	0.0002	0.0003	26
	Total	139	44	66	54	0.033	0.045	0.040	0.007	0.015	0.031	178

Table 3.6 Percent of Fe, Ni, Co, Zn, Cu, and SO_4^{2-} released from the AZLs after 4 years.

	% Released					
AZL	**Fe**	**Ni**	**Co**	**Zn**	**Cu**	**SO_4^{2-}**
Type III East	$9.4x10^{-5}$	$1.2x10^{-2}$	$1.3x10^{-2}$	$5.5x10^{-3}$	$3.7x10^{-3}$	$4.8x10^{-2}$
Type III West	$8.2x10^{-4}$	$2.4x10^{-2}$	$2.4x10^{-2}$	$1.0x10^{-2}$	$6.9x10^{-3}$	$8.4x10^{-2}$
Type I East	$9.2x10^{-5}$	$4.2x10^{-4}$	$5.6x10^{-4}$	$8.3x10^{-5}$	$7.3x10^{-4}$	$4.3x10^{-2}$
Type I West	$7.6x10^{-5}$	$3.1x10^{-4}$	$3.0x10^{-4}$	$6.5x10^{-5}$	$7.0x10^{-4}$	$7.0x10^{-2}$

Table 3.7 Ratios of S to Ni, Co, and Fe and ratios of Ni to Co in pyrrhotite minerals in effluent from all AZLs.

AZL	Pyrrhotite (Jambor, 1997)	Type I East	Type I West	Type III East	Type III West
S:Ni	250	2100	6900	110	74
S:Co	1000	14000	43000	610	320
S:Fe	1.2	7200	5800	4900	2100
Ni:Co	4	6.9	6.2	4.6	4.4

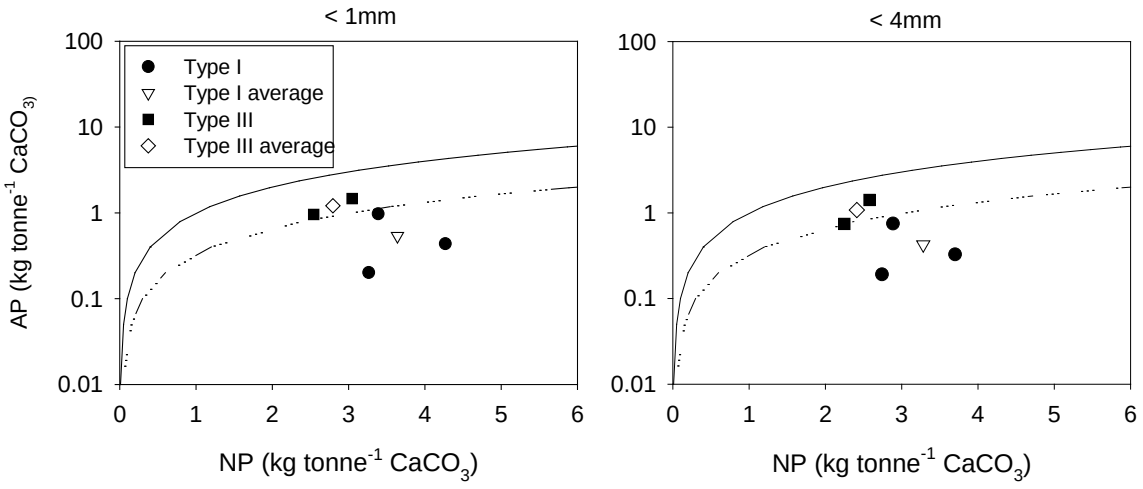

Figure 3.1 Acid generating potential (kg tonne^{-1} $CaCO_3$) and neutralization potential (kg tonne^{-1} $CaCO_3$) for Type I and Type III waste rock used in the construction of the AZLs.

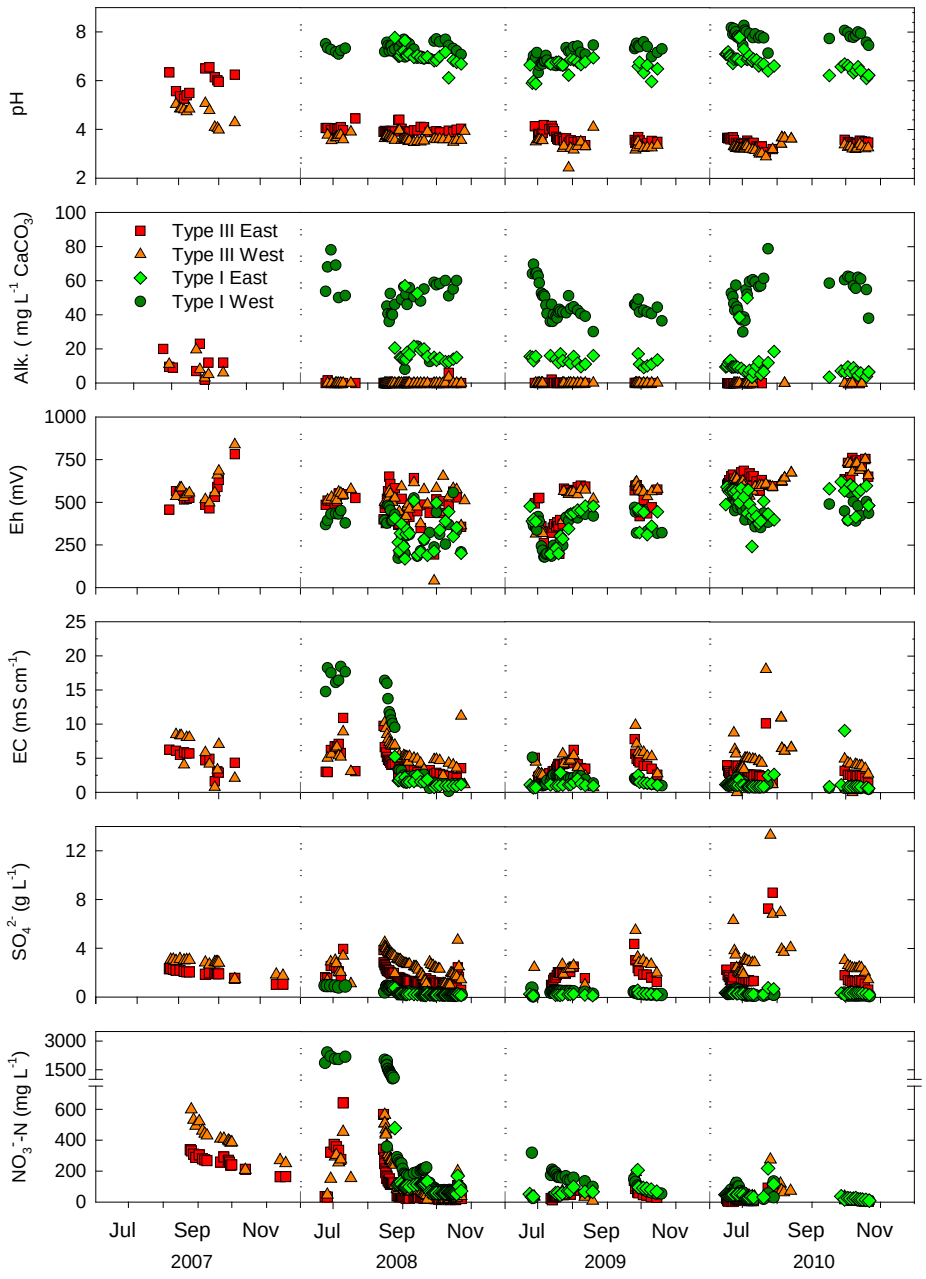

Figure 3.2 Time series plots presenting the pH, alkalinity (mg L^{-1} as $CaCO_3$), Eh (mV), conductivity (mS cm^{-1}), SO_4^{2-}, and NO_3^--N for each sample location. The dashed line represents a break in time during dry periods over the frozen months.

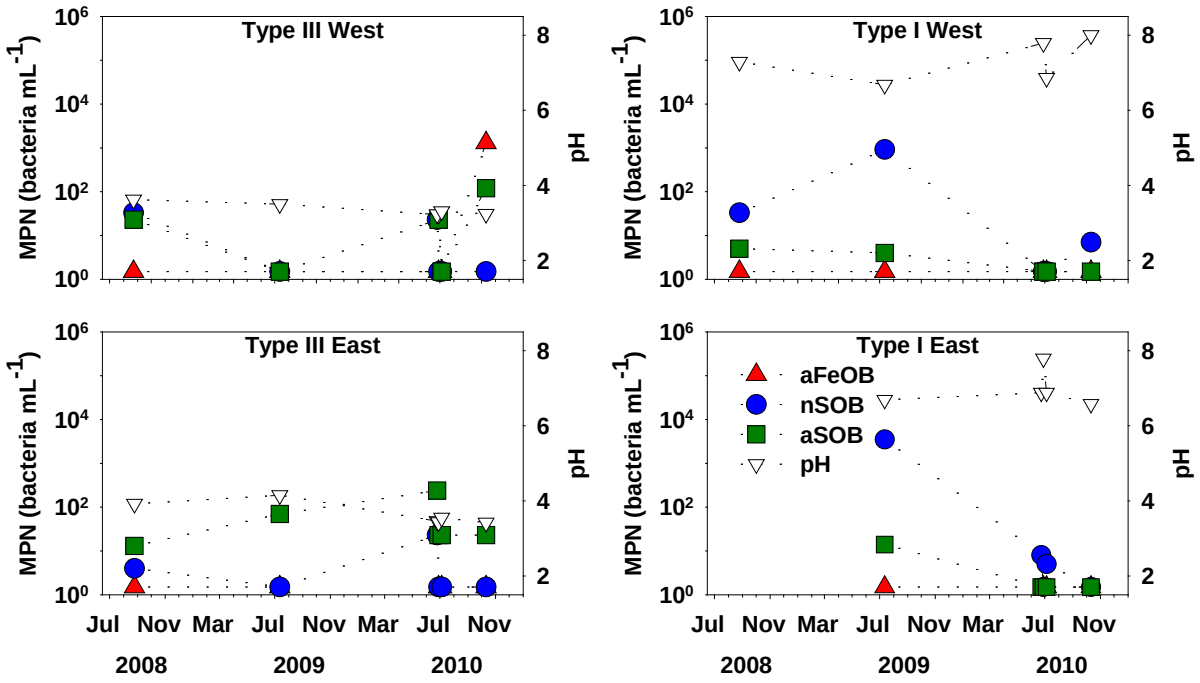

Figure 3.3 Most probable number (MPN) populations of Fe-oxidizing bacteria (aFeOB), neutrophilic S-oxidizing bacteria (nSOB), and acidophilic S-oxidizing bacteria (aSOB) for each AZL.

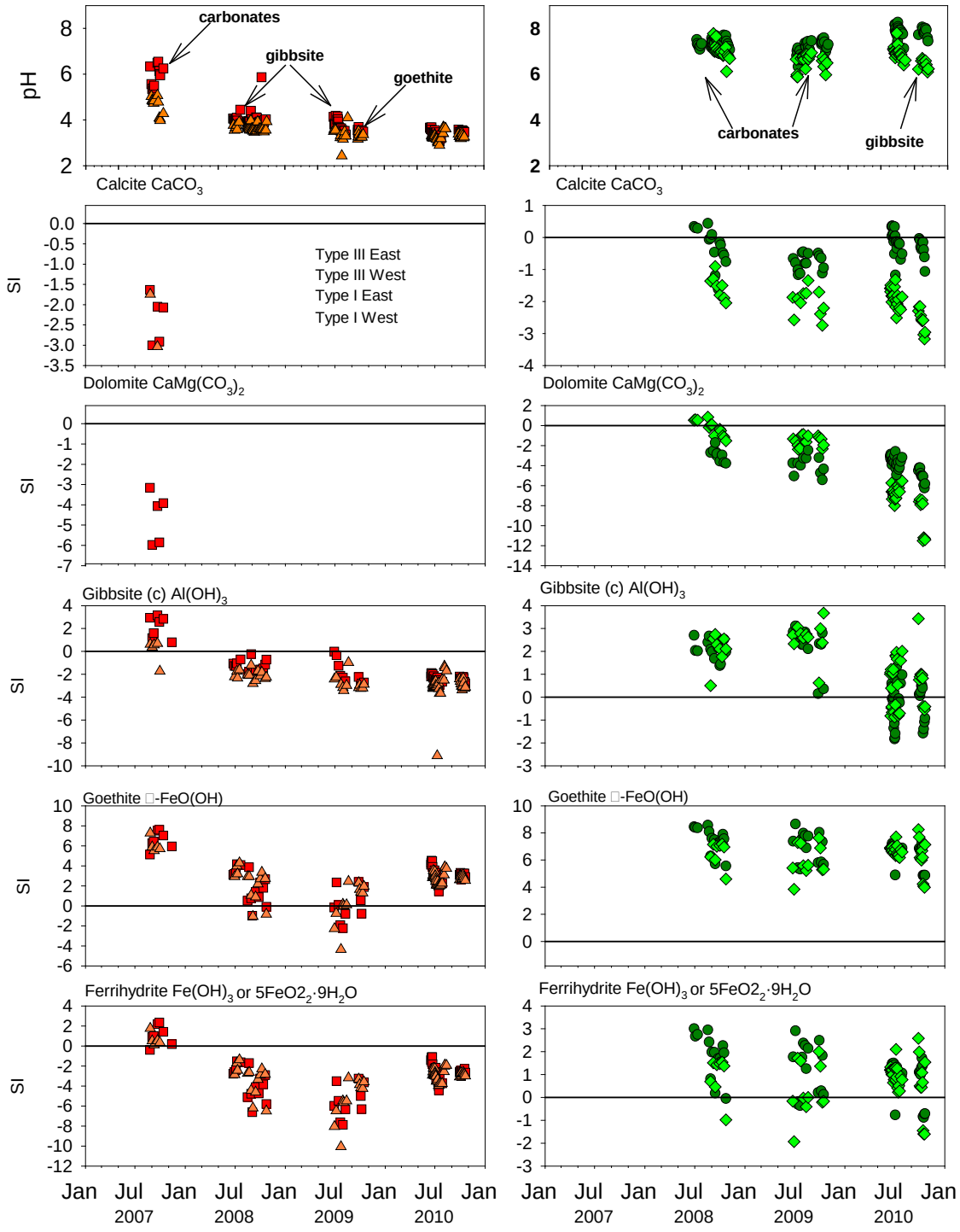

Figure 3.4 Calculated saturation indices (SI), using MINTEQA2, over time representing the pH-buffering sequence for the Type I and Type III AZLs. The solid line at 0 represents equilibrium.

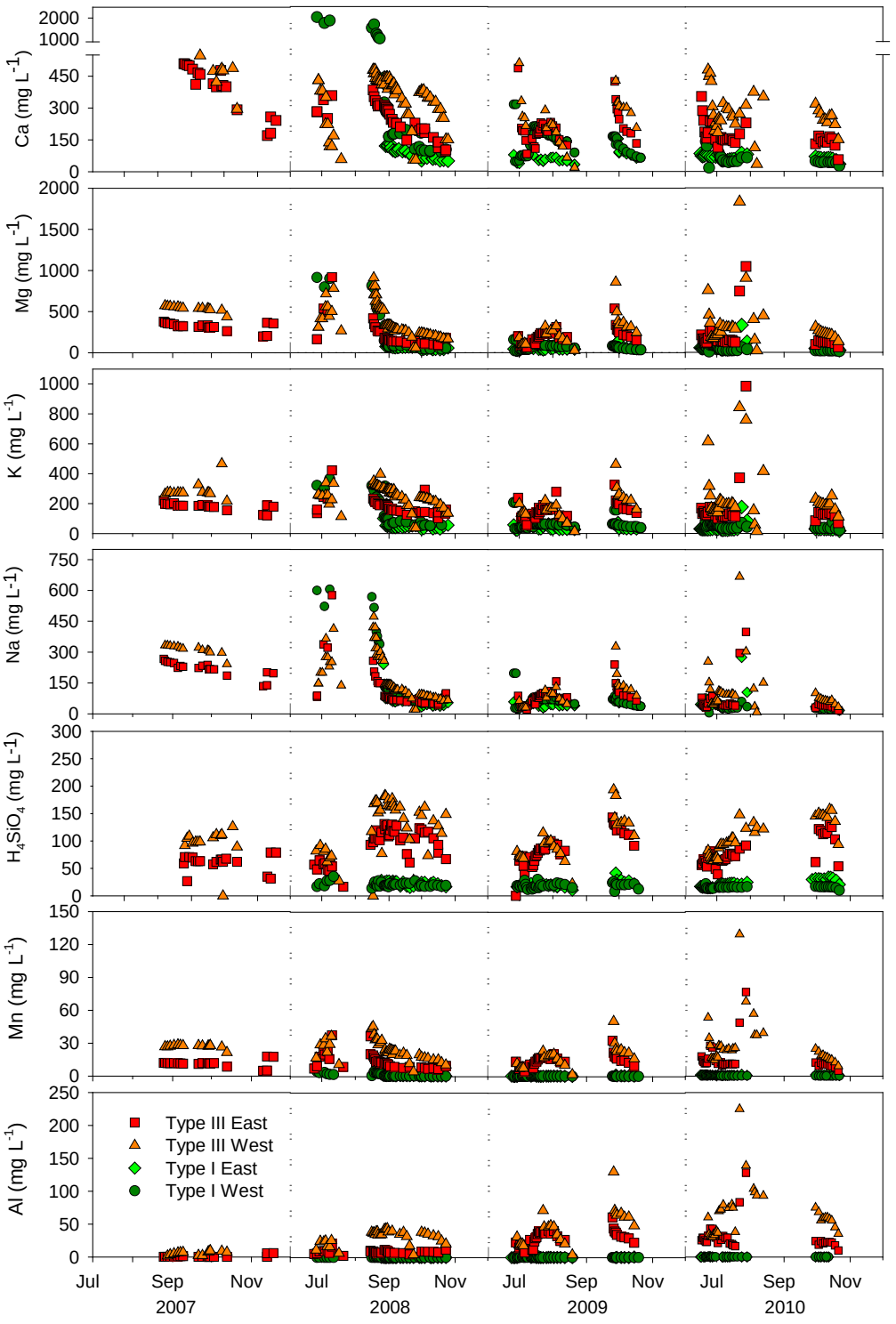

Figure 3.5 Time series plots presenting the major ion water chemistry for each sample location. The dashed line represents a break in time during dry periods over the frozen months.

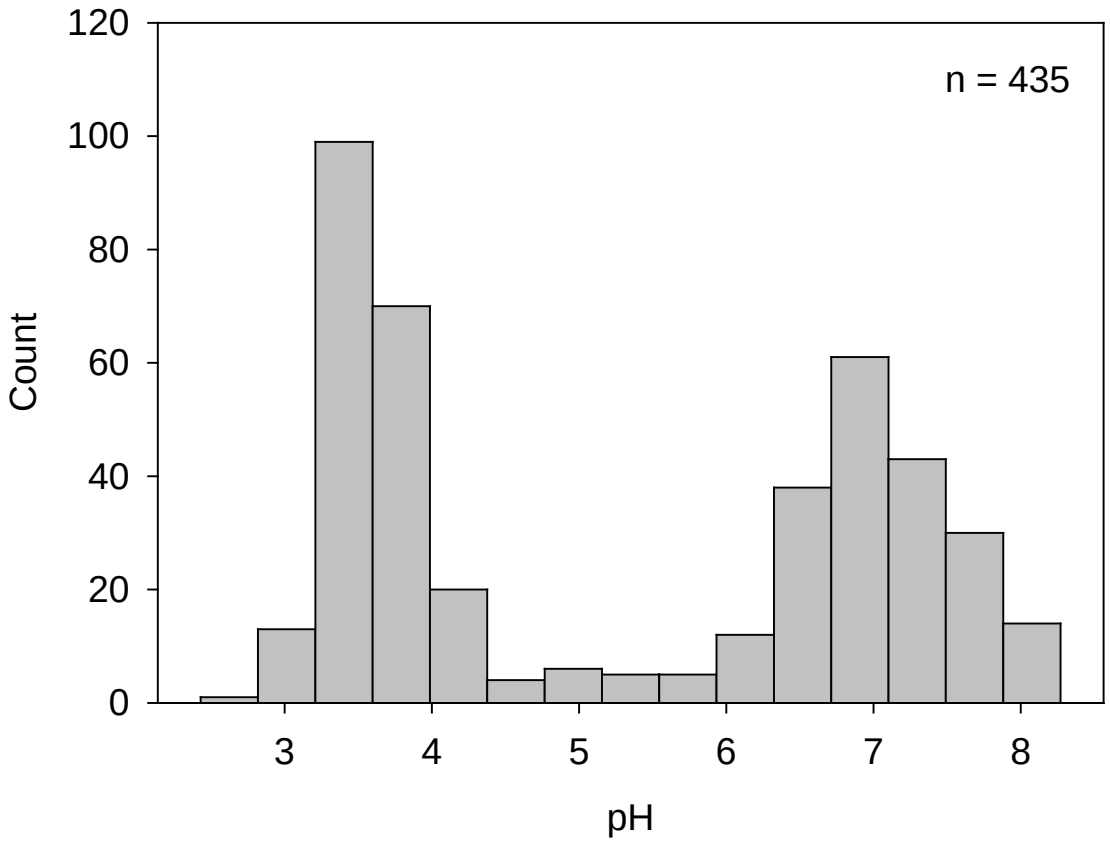

Figure 3.6 The distribution of pH from the Type I and Type III AZLs from 2007 to 2010 showing a bimodal distribution of near-neutral drainage and acidic drainage.

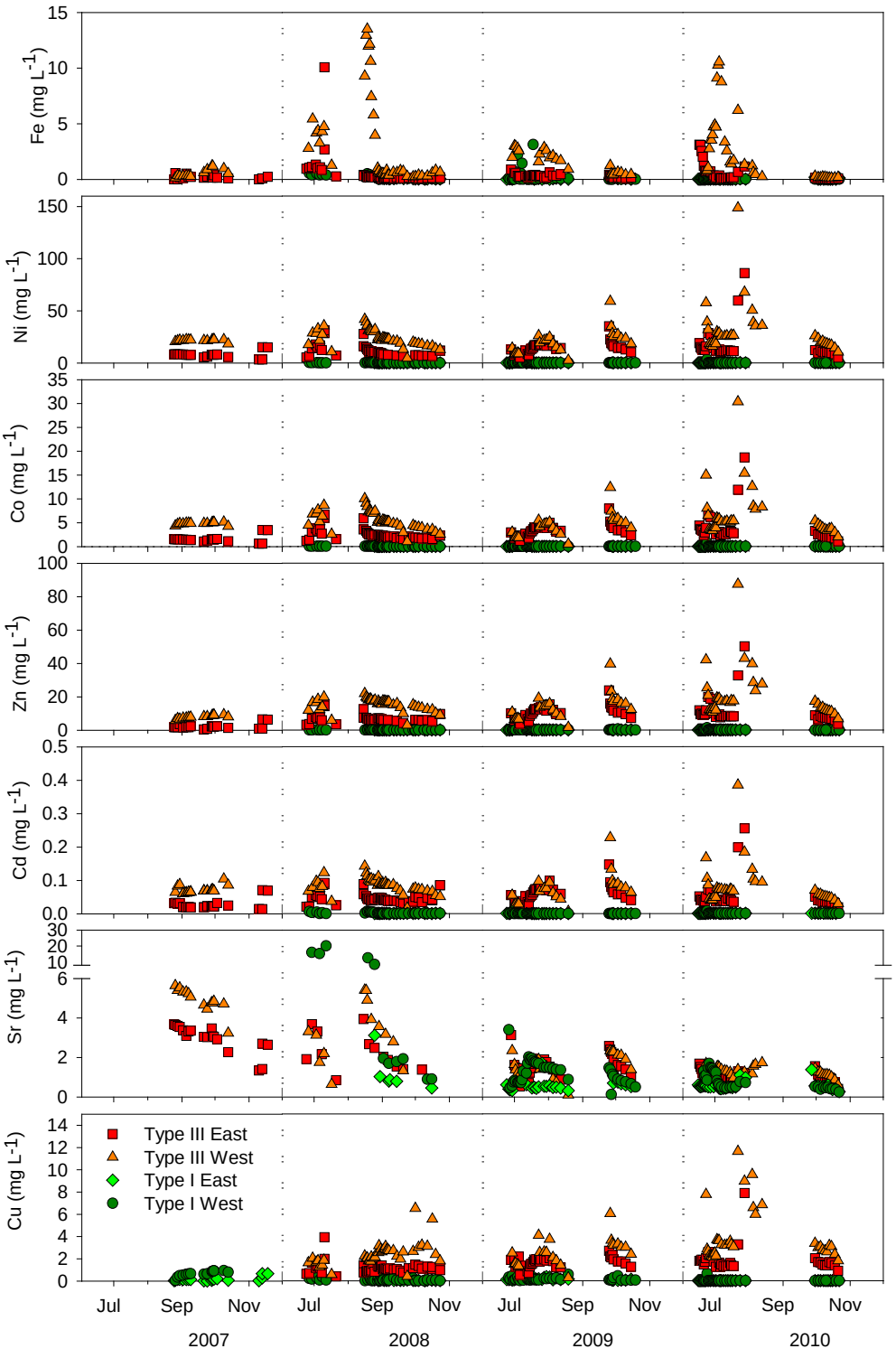

Figure 3.7 Time series plots presenting the major ion water chemistry for each sample location. The dashed line represents a break in time during dry periods over the frozen months.

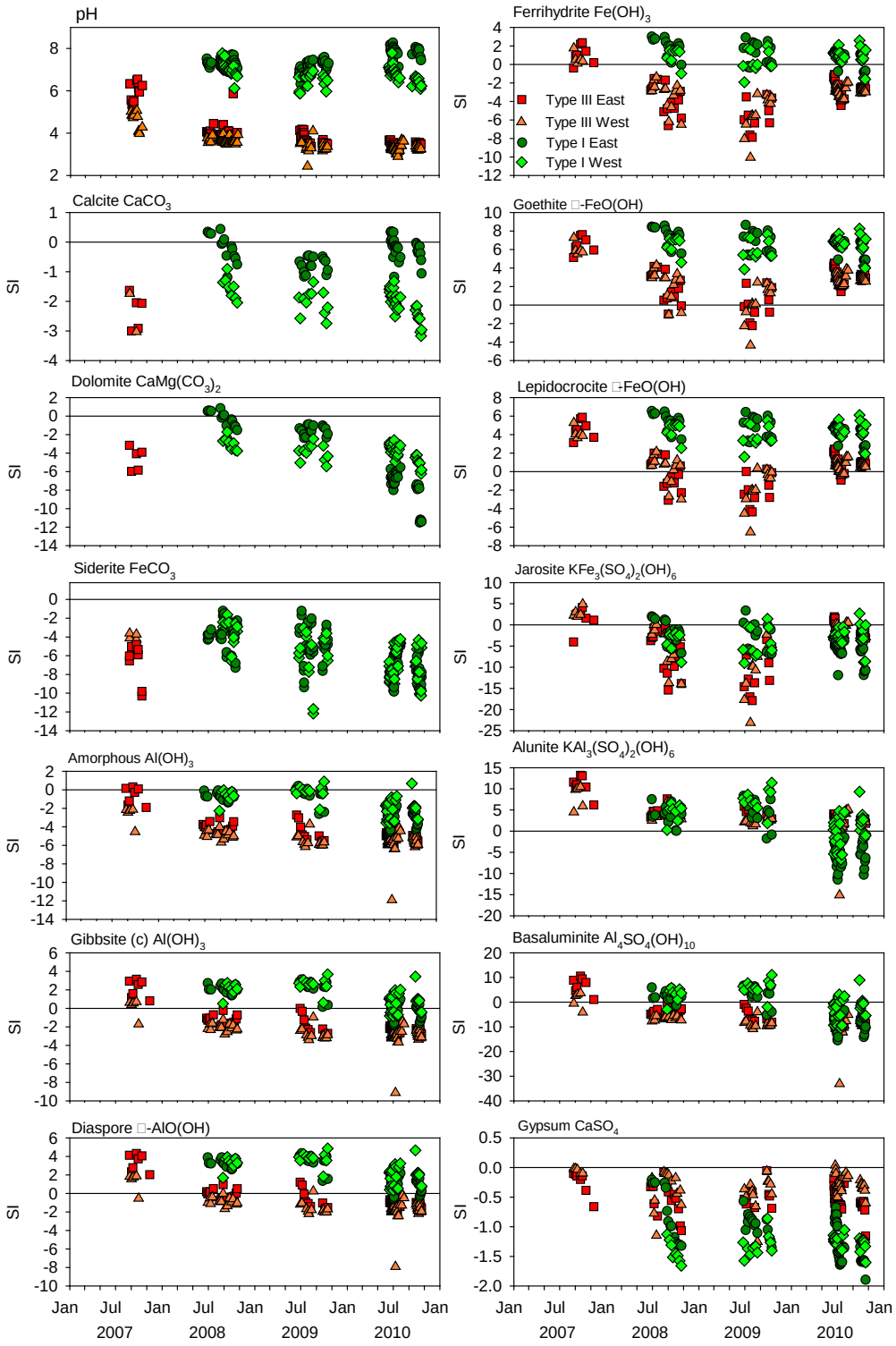

Figure 3.8 Time series of calculated saturation indices (SI), using MINTEQA2, for each sample location over time. The solid line at 0 represents equilibrium.

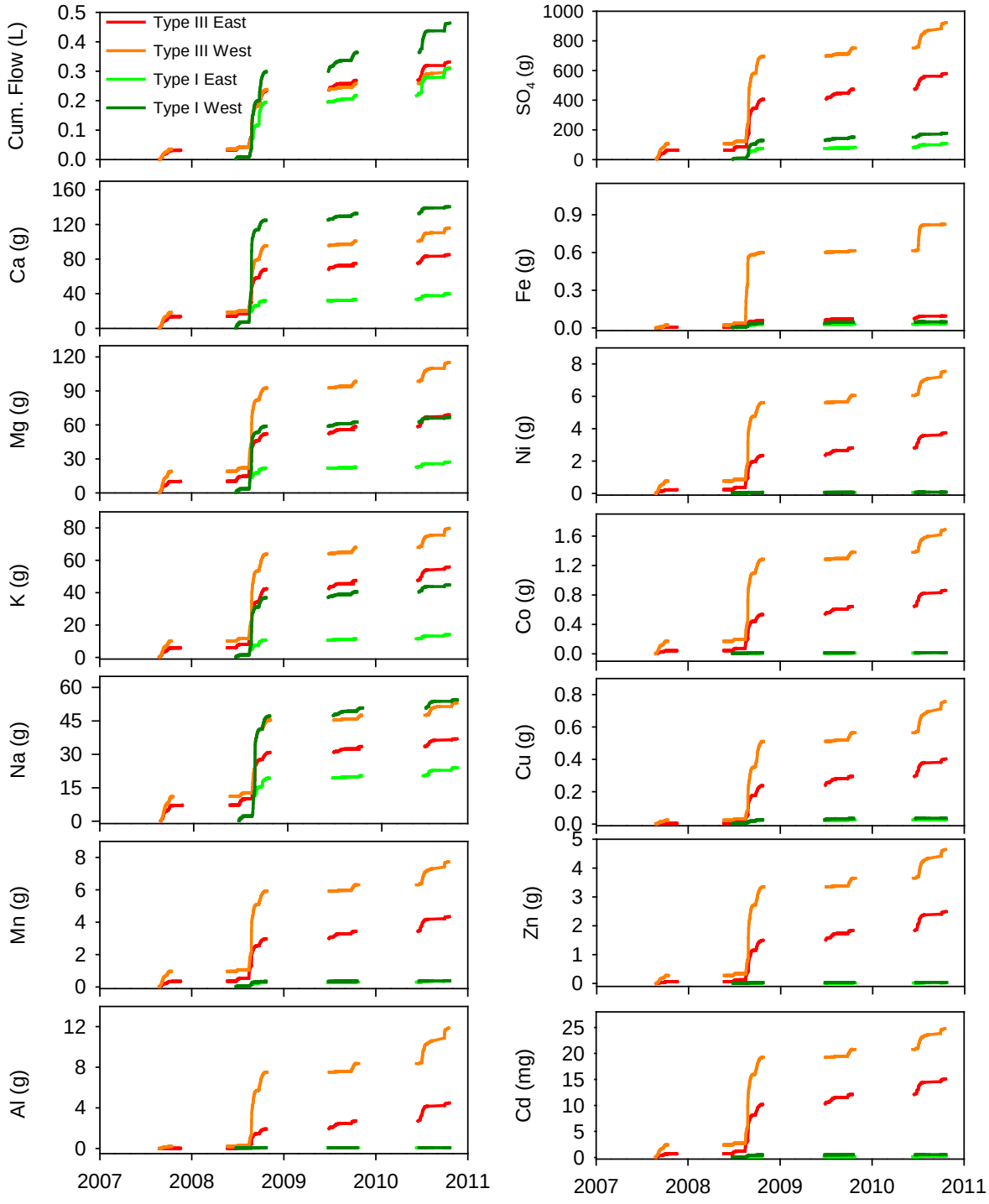

Figure 3.9 Cumulative release of major ions and metals (g, except Cd in mg) as a function of time for all sampling locations. Cumulative flow (L) is also presented as a function of time.

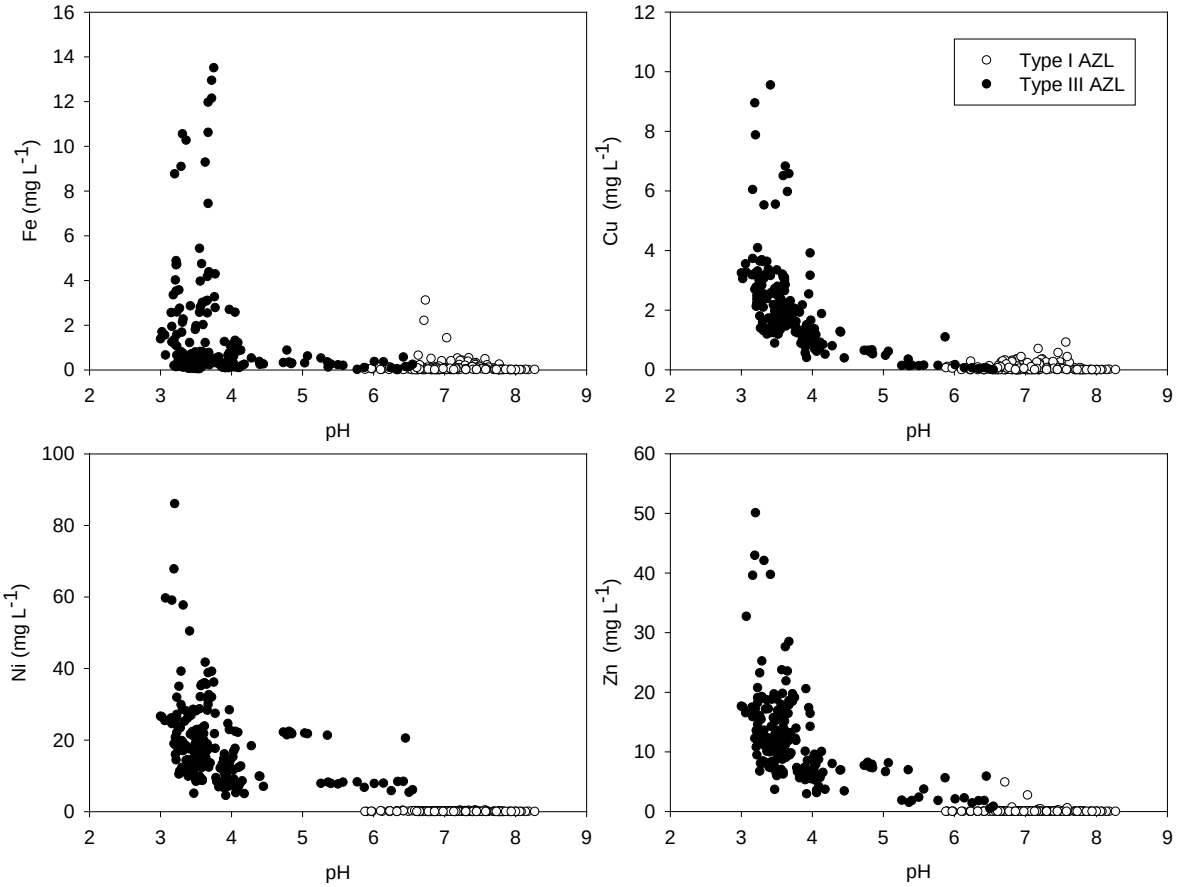

Figure 3.10 Concentration of metals in mg L^{-1} (Fe, Ni, Cu and Zn) as a function of pH in effluent from the Type I and III AZLs.

Chapter 4*:*

Geochemical and microbiological characterization of drainage from low-sulfide content waste rock: large-scale test piles

4.1 Executive Summary

Two test-scale waste-rock piles (15 m in height × 60 m × 50 m) were constructed at the Diavik diamond mine to study the behaviour of low-sulfide content waste rock, with an equally low acid-neutralization potential, in a continuous permafrost region. One test pile with an average of 0.035 wt. % S (referred to as Type I) and a second test pile with an average of 0.053 wt. % S (referred to as Type III) were constructed in 2006. The average C content of the Type I test pile was 0.031 wt. % C and the NP:AP ratio was 8.08, suggesting this test pile was non-acid generating. The average C content of the Type III test pile was 0.030 wt. % C and the NP:AP ratio was 1.60 suggesting this test pile had an uncertain acid-generating potential. The Type I test pile maintained near-neutral pH for the duration of the study. Sulfate and dissolved metal concentrations were low, with the exception of Ni, Zn, Cd, and Co in the fourth year following construction (2010). The pore water in the Type III test pile contained higher concentrations of SO_4^{2-} and dissolved metals, with a decrease in pH to < 4.7 and depletion of alkalinity. Maximum concentrations of dissolved metals corresponded to decreases in flow rate, which were observed at the end of each field season when the contribution of the total outflow from the central portion of the test pile was greatest. The microbial community within the Type I test pile included a population of neutrophilic S-oxidizing bacteria. Each year, the changes in the water quality of the Type III test-pile effluent were accompanied by changes in the microbial populations. Populations of acidophilic S-oxidizing bacteria and Fe-oxidizing bacteria became more abundant as the pH decreased through the duration of each year. The geochemical and microbiological results are consistent with other acid mine drainage studies, indicating that a series of mineral dissolution−precipitation reactions controls pH and metal mobility.

4.2 Introduction

4.2.1 Background

Waste rock is the non-economic grade of rock excavated in order to gain access to economic ore deposits. The construction of waste-rock piles exposes sulfide minerals to atmospheric oxygen and water, leading to sulfide-mineral oxidation and the potential for the release of acid mine drainage (AMD). AMD is characterized by high concentrations of H^+, SO_4^{2-}, and dissolved metals such as Zn, Fe, Ni, Co, and Cu. The metals released from waters impacted by AMD are known to cause environmental damage (US EPA, 1994); however, the release of AMD from low-S content waste-rock stockpiles with low acid-neutralization potential in the Arctic is not well understood.

Waste rock consists of large, boulder-size fragments down to fine-grained sand and silt, which is segregated through depositional processes, with a rubble zone at the base of the pile and a larger proportion of the finer fraction remaining near the top of the pile (MEND, 1995; Chi, 2010). The coarse nature of these piles allows for rapid flow of water through waste-rock piles (Ritchie, 1994) and low residual-moisture content. At the Diavik test-pile site, water flow through the waste rock occurs predominantly as continuum flow through the fine-grained matrix rather than as macropore or by-pass flow (Neuner *et al*., 2012). The greatest proportion of waste-rock surface area also is associated with the fine-grained matrix of the waste rock (Stromberg and Banwart, 1999; Hollings *et al*., 2001; Chi *et al.*, 2010; Smith *et al.*, in press). Understanding the interaction between hydrological and biogeochemical processes in waste-rock piles is fundamental to quantifying the extent and duration of environmental impacts of waste-rock stockpiles.

One of the objectives of the Diavik Waste Rock Project is to characterize the geochemical characteristics of water from large-scale waste-rock test piles with differing sulfide content over time, and to examine the microbial evolution of the waste-rock test piles in terms of type and abundance of different groups of Fe- and S-oxidizing bacteria in a continuous permafrost region. This paper focuses on the (bio)geochemical evolution of low-S content waste rock in large-scale waste-rock test piles at Diavik over 4 years from 2007 to 2010. Effluent samples were collected and analyzed to evaluate the metal release rates, the extent of acidity in the drainage water, and the microbial activity.

4.3 Methods of Investigation

4.3.1 Waste-Rock Characterization

During the construction of the Type I and Type III test piles, waste-rock samples were collected for particle size and S and C analysis (Smith *et al*., in press). A subset of samples from the < 4-cm fraction was collected for whole-rock analysis for this study. Whole-rock analysis was completed using 10-g samples analyzed as powders that were firmly compressed in cups with a polyester X-ray film using an energy dispersive X-ray fluorescence spectrometer (EDXRF; Minipal4; Panalytical, The Netherlands). The instrument was calibrated against granite, granodiorite and granite gneiss certified reference material (CRM) standards.

4.3.2 Sample Collection and Analysis

4.3.2.1 Field Methods

Water samples for chemical analysis were collected from the Type I basal drain, Type III north and south basal drains, and Type III basal lysimeters. Effluent from each test-pile basal drain was collected in a series of flow-through cells and directed to a calibrated tipping-bucket flow gauge to measure the flow rate and volume. Water samples were collected from the first cell in the flow-through cell series as described in Chapter 3.

Pore-water samples were collected from *in situ* soil water solution samplers (SWSSs). The SWSSs consisted of porous ceramic cups, which were used to extract pore water from the matrix of the unsaturated waste rock. SWSSs were encapsulated within fine-grained waste rock (< 25-mm fraction), either Type I (for the Type I test pile; average 0.037 wt. % S) or Type III (for the Type III; average 0.057 wt. % S), held in Nitex nylon screen bags (175 × 325 mm) to ensure hydraulic contact between the ceramic cup and matrix material. The SWSSs were distributed to align vertically above the basal lysimeters. Tubes connecting the SWSSs to the surface were strung through 50-mm flexible PVC protective conduits that contained either mineral-insulated or self-regulating heat trace.

The SWSSs (model e-127-1920F1L12-B02M2; Hoskin Scientific, Canada) were used to extract pore-water samples under an $N_{2(g)}$ atmosphere and an initial vacuum of 40–50 kPa. Water from the SWSSs was collected in a flow-through cell and samples were retrieved with sterile polyethylene (PE) syringes. Water was stored in pre-washed HDPE bottles which were triple-rinsed with the sample water.

Field and laboratory procedures for analysis of basal-drain effluent and pore-water samples are described in Chapter 3. Analysis included the pH, redox potential relative to the standard hydrogen electrode (E_h), EC, temperature, alkalinity, orthophosphate, Fe(II), H_2S, NH_3, anion concentrations, and total and dissolved cation concentrations. Quality control and quality assurance were assessed by evaluating several standards covering the range of measured concentrations, and by incorporating both field replicates and laboratory blanks into the protocol (Appendix A). Speciation calculations, as described in Chapter 3, were conducted for samples collected from Type I and Type III north and south drains, and Type I and Type III SWSSs with a complete suite of field and laboratory analyses, and these calculations were undertaken to assist in the identification of the potential phases controlling aqueous concentrations.

Unfiltered, unpreserved water samples were collected from the Type I, Type III north and south drains, and from selected basal lysimeters for microbial enumerations, following the methods described in Chapter 3.

4.4 Results and Discussion

4.4.1 Whole-Rock Analysis

The Type I and III test piles were constructed with waste rock with an elemental composition dominated by SiO_2 and Al_2O_3, followed by K_2O, Ba, and Na_2O (n = 31 for Type III; n = 6 for Type I; Table 4.1). The Type I and Type III rock types were dominated by granite and granite pegmatite lithologies, similar to the AZLs (Chapter 3) and previously characterized country rock at the Diavik site (Jambor, 1997). Each of these rock types has a characteristic sulfide mineralogy. Pyrite, present in trace amounts, is the principal sulfide mineral

associated with the granite and pegmatitic granite rock (Jambor, 1997). Pyrrhotite is the most abundant sulfide mineral (ranging from 0.02 to 0.42 wt. % S) associated with the biotite schist component of the country rock, which also contains lower abundances of sphalerite and chalcopyrite.

The Type III material contained an average of 495 ppm of S, whereas the Type I material only had 114 ppm S. The Type III material had higher proportions of metals (Zn = 41 ppm, Ni = 27 ppm, Cu = 9.9 ppm, and Co = 5.5 ppm; Table 4.1) than the Type I material (Zn = 27 ppm, Ni = 15 ppm, Cu = 4.7 ppm, and Co = 4.0 ppm; Table 4.1). The relative proportions of sulfide minerals can be estimated on the basis of the concentrations of these metals. Electron-microprobe analysis of Diavik waste rock indicates that the composition of the pyrrhotite within the biotite schist component of the waste rock is $(Fe_{0.0852}Ni_{0.004}Co_{0.001})_{\sum 0.857}S_{1.000}$ (Jambor, 1997), indicating a Ni:Co ratio of 4:1. Whole-rock analysis shows an average Ni to Co ratio of 4.4 (n = 31) in the Type III waste rock and 3.4 (n = 6) in the Type I waste rock. The finer fractions (< 5 mm) had a higher ratio of 4.6 in the Type III waste rock and 4.8 in the Type I waste rock than the coarser fractions. The main sources of Cu and Zn are chalcopyrite [$CuFeS_2$] and sphalerite [(Zn,Fe)S], respectively (Chapter 3; Smith *et al*., 2012). The total mass of Cu in the Type III waste rock was 4.7 ppm (0.17 mmol kg^{-1}) and the total mass of Zn in the Type III waste rock was 27 ppm (0.71 mmol kg^{-1}). Assuming that the mass of S in the Type III waste rock, as determined by whole-rock analysis, was from pyrrhotite, chalcopyrite and sphalerite, then the difference between the total moles of S (15 mmol kg^{-1}), with the contributions of S from chalcopyrite (0.34 mmol kg^{-1}; assuming 2 moles of S for every mole of Cu) and sphalerite (1.42 mmol kg^{-1}; assuming 2 moles of S for every mole of Zn) being known, mean that the mass of S from pyrrhotite can be estimated (residual S =

13.24 mmol kg^{-1}; Table 4.2). The estimated mass of pyrrhotite accounts for the total mass of both Ni and Co present in the Type III waste rock based on the molar ratios from the pyrrhotite formula of $(Fe_{0.0852}Ni_{0.004}Co_{0.001})_{\sum 0.857}S_{1.000}$ (Table 4.2). In addition, the mass of Fe from each sulfide mineral was estimated and the total mass of Fe from sulfide minerals was 14.12 mmol kg^{-1}, which represents 9 % of the Fe in the Type III waste rock.

Iron can substitute for Mg in the lattice structure of biotite and the mineral formula of biotite was assumed to be $K(Mg,Fe)_3(AlSi_3O_{10})(F,OH)_2$. The mass of K (500 mmol kg^{-1}) in the Type III waste rock was assumed to all be from biotite. Therefore, an estimated mass of Mg (based on the molar ratios of K to Mg) of 187 mmol kg^{-1} was from biotite, with only 25 % residual Mg from other mineral sources (Table 4.3). The mass of Fe in biotite was estimated to be 93.5 mmol kg^{-1}. Therefore, the biotite (63 %) and sulfide minerals (9 %) account for 72 % of the total Fe present in the Type III waste rock with the remaining Fe from other minerals (Table 4.2 and Table 4.3).

4.4.2 Geochemistry of Waste-Rock Test-Pile Pore Water and Effluent

Soil-water solution samplers were installed on two tip faces (Faces 1 and 2) in the Type I test pile and on three tip faces in the Type III test pile (Faces 1, 2, and 3) to collect pore water from the interior portion of the waste-rock test piles. Over the period between 2007 and 2010, samples were obtained from 13 SWSSs, at depths ranging from 1 m to 9 m below the test pile surface in the Type I test pile and from 18 SWSSs, at depths ranging from 2 m to 9 m below the Type III test pile surface. The frequency of sample collection from the SWSSs was irregular because the potential for a SWSS to yield a sufficient volume for a sample was dependent on the antecedent moisture conditions, temperature, and on the integrity of the

SWSS porous ceramic cups. Moreover, at times, there was insufficient moisture available for the collection of a full sample volume and limited geochemical analysis was completed on these individual samples.

Pore-water samples were collected, using suction, from a small area of influence (centimetres to tens of centimetres) around the porous ceramic cup (Smith *et al*., 2012). Nichol *et al*. (2005) suggest pore-water samples are considered as flux-averaged samples of the pore water based upon the flux generated by the applied suction and the geometry of the ceramic cup, rather than flux-averaged or volume-averaged concentrations. The pore-water samples, therefore, are discrete point measurements from within the matrix material, rather than the integrative samples provided by the basal drains, and to a lesser degree, by the basal lysimeters.

The basal lysimeters were constructed to observe the composition of water that migrated over a limited cross-sectional area from the top of the test pile to the base. The basal lysimeters collect water from a greater surface area and collect a greater volume of water, which has been in contact with a larger volume of waste rock, than the SWSSs. Furthermore, the basal-lysimeter samples integrate matrix flow and macropore flow for that section of waste rock. There are six 2 m by 2 m basal lysimeters under each test pile, with two located under the batters and four located below the crest of the test pile, and there are six 4 m by 4 m lysimeters, all of which are located below the crest.

The basal-drain system is designed to collect all the water that reaches the base of the test pile, and it integrates both the matrix flow and macropore flow for the entire waste-rock test pile. The water chemistry observed at the basal drain is a combination of flow from all areas

of the pile, including shorter flows paths along the batters of the pile with little potential for water–rock interaction and the longer flow paths in the centre of the pile with more extensive water rock interaction. The basal-drain effluent chemistry is a reflection of the physical and chemical processes that occur in a large volume of waste rock over time.

4.4.3 Sulfide Oxidation: The Release and Transport of Oxidation Products

The < 50-mm fraction of waste rock in the Type III test pile ranges from 0.0085 wt. % S to 0.27 wt. % S with an average of 0.053 wt. % S (Smith *et al*., in press). The < 50-mm fraction of waste rock used to construct the Type I test pile ranges from 0.0028 wt. % S to 0.26 wt. % S with an average of 0.035 wt. % S (Smith *et al*., in press). The oxidation of sulfide minerals contained in the granite and biotite schist lithologies present in the Diavik waste rock releases SO_4^{2-}, H^+, dissolved Fe and other metals (Chapter 3). The oxidation of pyrrhotite, the primary sulfide mineral in Diavik waste rock, by atmospheric can be represented by equation 4.1.

$$Fe_{17}S_{20(S)} + 28Fe^{3+} + 80H_2O \rightarrow 45Fe^{2+} + 20SO_4^{2-} + 160H^+ \quad (4.1)$$

Iron(II) can be further oxidized to Fe^{3+} and under mildly acidic to near-neutral pH conditions, Fe^{3+} may precipitate as Fe^{3+} oxyhydroxides, such as ferrihydrite [$Fe(OH)_3$ or nominally $5Fe_2O_3{\cdot}9H_2O$] and goethite [αFeOOH)]. Non-sulfide minerals contained within waste rock can neutralize H^+ generated during the oxidation of sulfide minerals. The concentration of SO_4^{2-} and blasting residuals in the pore water, basal lysimeters and basal drains can be used to describe to release and transport of oxidation products in waste rock.

4.4.3.1 Type III Test Pile

4.4.3.1.1 Pore Water

Sample collection from the SWSSs in the Type III test pile began in 2007. The volume of water available for sample collection was limited during the wetting up period in 2007 and 2008. Neuner *et al*. (2012) estimate pore water migrates at a rate of $< 10^{-2}$ to 3×10^{-2} m day^{-1} in response to common rainfall events and up 0.7 m day^{-1} in response to high intensity rainfall events. In 2007, the wetting front had migrated to a depth of 7 m below the crest of the test pile and samples were collected at the 3-m and 5-m depths. Insufficient moisture was available for sample collection from the SWSSs at 7-m and 9-m depths until 2008.

The dissipation of blasting residuals, such as NO_3^--N and Cl^-, can be used to observe the first flush of the matrix material (Bailey *et al*., 2012). The application of the LiCl tracer test on the Type III test pile in 2007 precludes the use of Cl^- as a resident tracer. The concentration of SO_4^{2-} in pore water during the first flush of the matrix material is influenced by SO_4^{2-} derived from sulfide-mineral oxidation during blasting and from *in situ* sulfide-mineral oxidation (Bailey *et al*., 2012; Chapter 2). After the first flush of the upper matrix material, the majority of SO_4^{2-} is derived from *in situ* sulfide-mineral oxidation or from the dissolution of secondary mineral assemblages (Bailey *et al*., 2012; Chapter 2).

Nitrate, from blasting, in the pore water from the Type III test pile increased in 2007 to the maximum observed concentrations at the 3-m and 5-m depths. Concentrations of NO_3^--N at the 3-m and 5-m depths decreased by the end of 2008, and remained low for the remainder of the study, flushing the upper matrix of blasting residuals (Figure 4.1 and Figure 4.2). The concentrations of SO_4^{2-} at the 3-m and 5-m depths increased through 2007 from a minimum

of 10 mg L^{-1} to a maximum of 2600 mg L^{-1}. By the end of 2008, the concentrations of SO_4^{2-} decreased following a similar trend as NO_3^--N concentrations, suggesting the SO_4^{2-} was derived from sulfide-mineral oxidation during blasting (Bailey *et al*., 2012;Chapter 2). Unlike NO_3^--N, the concentration of SO_4^{2-} further increased through 2009 and 2010. The maximum concentration of SO_4^{2-} (4500 mg L^{-1}) was observed in 2010 in near surface pore water indicating SO_4^{2-} probably was released from *in situ* sulfide mineral oxidation.

The pore water at the 7-m and 9-m depths had increasing SO_4^{2-} and NO_3^--N concentrations through 2007, and concentrations remained elevated through 2008 (Figure 4.3 and Figure 4.4). By 2009, low concentrations of blasting residuals in the pore water were observed at the 7-m depth, whereas the 9-m depth remained high through 2009 and subsequently decreased in 2010. The SO_4^{2-} concentrations at the 7-m and 9-m depths remained elevated through 2009 and 2010. By 2009, water at the 7-m and 9-m depths have an increased contribution of SO_4^{2-} from the upper portions of the test pile; therefore there are three main sources of SO_4^{2-} that results in increased concentrations over time including: 1) water migrating downwards that previously flushed the upper matrix material, 2) blasting residuals in the vicinity of the SWSS; and, 3) from *in situ* sulfide-mineral oxidation in the vicinity of the SWSS. In 2010, the matrix material surrounding the SWSSs at the 9-m depth had been flushed of blasting residuals. These observations suggest that by 2010, constituents derived from blasting activities were displaced beyond the 9-m sample depth and solutes present in the matrix pore water were derived entirely from *in situ* chemical reactions.

4.4.3.1.2 Basal Lysimeters

Flow first reported to one 2 m by 2 m and two 4 m by 4 m basal lysimeters in the Type III test pile in 2008. In 2009, flow was observed in an additional 4 m by 4 m basal lysimeter. No flow has reported to the remaining locations between 2007 and 2010. Two SWSSs, located at 3 m and 7 m, are located directly above one 4 m by 4 m basal lysimeter located in the central portion of the test pile under the crest. This is the only basal lysimeter in the Type III test pile discussed in this chapter. Water first reported to the basal lysimeter in the Type III test pile in August 2008 and sample collection commenced at that time.

In the Type III basal lysimeter, the concentrations of NO_3^--N (ranging from 240 mg L^{-1} to 770 mg L^{-1}), NO_2^--N (ranging from below detection to 27 mg L^{-1}), and NH_3-N (ranging from 0.50 mg L^{-1} to 14 mg L^{-1}) decreased through 2008, increased in early 2009, and subsequently decreased through late 2009 (Figure 4.5). In 2010, concentrations of nitrogen species were variable, but were within the concentration ranges previously observed at this location. Measurable concentrations of blasting residuals in the basal lysimeters suggest the matrix material above this basal lysimeter has not yet been fully flushed.

Between 2008 and 2010, sulfate concentrations ranged from 1300 mg L^{-1} to 2800 mg L^{-1} with the exception of the maximum SO_4^{2-} concentration of 4100 mg L^{-1} observed in September 2010 (Figure 4.5). In 2008, SO_4^{2-} concentrations were moderately-well correlated to NO_3^--N concentrations, but by 2009, SO_4^{2-} concentrations remained constant while NO_3^--N concentrations decreased, suggesting that the contribution of SO_4^{2-} from sulfide mineral oxidation during blasting was less than that from *in situ* sulfide-mineral oxidation. Geochemical equilibrium modeling suggests the effluent was at or near saturation with

respect to gypsum, alunite, and, at times, jarosite, potentially controlling the SO_4^{2-} concentrations (Figure 4.6).

4.4.3.1.3 Basal Drain

The pH in the Type III test-pile basal drain decreased in 2007 from near-neutral in May to acidic conditions in October (Figure 4.7). The same trend was observed in each subsequent year. As the pH in the Type III test pile decreased (to pH 4.5), concentrations of SO_4^{2-}, Fe and other dissolved metals increased. Alkalinity was detected in 2007, but the concentration progressively decreased with the decrease in pH through the field season (Figure 4.7). A similar trend was observed in each subsequent year; however, the maximum pH observed in May decreased each year from 2008 through 2010. By 2010, only modest carbonate acid-neutralization capacity remained.

The initial sulfate concentrations in the Type III test-pile effluent increased from < 500 mg L^{-1} in May 2007, to a maximum of 1500 mg L^{-1} in the south drain and 2000 mg L^{-1} in the north drain in September 2007. Concentrations subsequently decreased from September through November when flow ceased. In 2007, SO_4^{2-} concentrations were highly correlated with the concentrations of NO_3^- and Cl (NO_3^-:$R^2 = 0.87$; Cl^-: $R^2 = 0.81$), suggesting that the blasting residuals were an important source of SO_4^{2-}. From 2008 onward the correlation between the concentrations of dissolved sulfate and the concentrations of NO_3^-, and Cl^- declined as the proportion of SO_4^{2-} derived from *in situ* oxidation increased (discussed in Chapter 2; Bailey *et al*., 2012).

In 2008, SO_4^{2-} concentrations increased from 100 - 550 mg L^{-1} early in the summer to 800 mg L^{-1} in September, near the end of the season. During this phase, the majority of SO_4^{2-}

was derived from *in situ* oxidation. The increase in dissolved SO_4^{2-} concentrations observed late in the field season probably reflects increasing flow volumes from the central portions of the test pile, which had not previously contributed to the test-pile drainage. A maximum SO_4^{2-} concentration of 1300 mg L^{-1} was observed at the end of October 2008 when flow ceased. Water derived from the central portion of the test pile probably resulted in the increased concentrations of blasting residuals, including SO_4^{2-}, observed late in the year.

In 2009 and 2010, SO_4^{2-} concentrations followed a trend that was similar to that observed in 2008. The maximum concentrations of 2800 mg L^{-1} in the south drain and 1300 mg L^{-1} in the north drain were observed in October 2009. Increases in concentrations of NO_3^- and Cl^- suggest that portions of the test pile that had not previously contributed flow to the basal drain became active late in the year. During the period between May and September, variations in SO_4^{2-} concentrations followed trends in internal test-pile temperatures, with increasing concentrations as the test pile warmed. Ahonen and Tuovinen (1992) observed that the rate of pyrrhotite oxidization is dependent on temperature following the Arrhenius equation. The low temperatures prevalent in the spring probably result in lower rates of pyrrhotite oxidation, resulting in lower SO_4^{2-} concentrations. The total mass of S released from the Type III test pile (cumulative mass of both the north and south drains) from 2007 to 2010 was 129 kg. This SO_4^{2-} mass corresponds to an estimated oxidation rate of 1.05×10^{-10} kg (O_2) m^{-3} s^{-1}. This rate is higher than the observed rate in field test-pad measurements made at the Diavik mine site (3×10^{-13} kg (O_2) m^{-3} s^{-1}) during baseline characterization of the mine site (Blowes *et al.*, 2000). Oxidation rates range from 5×10^{-10} kg (O_2) m^{-3} $s^{-1}$to 5×10^{-6} kg (O_2) m^{-3} s^{-1}, with typical rates of 5×10^{-8} kg (O_2) m^{-3} s^{-1} (Ritchie, 2003). The difference in

oxidation rates could be a result of heterogeneities in the distribution of sulfides in the waste rock (Ritchie, 2003).

4.4.3.2 Type I Test Pile

4.4.3.2.1 Pore Water

Unlike the Type III test pile, the Type I test pile was not irrigated through infiltration experiments or through tracer tests. Neuner *et al*. (2012) suggest there was no net infiltration into the Type I test pile in 2007. Due to limited infiltration, the moisture content of the waste rock was insufficient to allow sample collection from each SWSS every year, and therefore, sampling was sporadic. There were only a few pore-water samples collected from the Type I test pile in 2007. Pore-water samples were collected in 2008 at an increased number of sample locations, and sampling continued through 2010; however, there was an insufficient volume of water from select pore-water samples to complete all geochemical analyses.

The maximum concentrations of blasting residuals, including SO_4^{2-} (1400 mg L^{-1}), Cl^- (380 mg L^{-1}), NO_3^--N (1300 mg L^{-1}), NO_2^--N (11 mg L^{-1}), and NH_3-N (140 mg L^{-1}), were observed in the first few samples collected from pore water at 1 m in 2008 (Figure 4.8). At the 1-m depth, the concentrations of these blasting residuals dissipated from June to October 2008, and remained low for the remainder of the study, with the exception of SO_4^{2-} which increased with decreasing pH. Concentrations of blasting residuals at the 2-m depth reached maximum concentrations in 2010, whereas the pore water at the 5-m depth showed elevated concentrations in 2008 and 2009 (Figure 4.9 and Figure 4.10). The concentrations of blasting residuals in the 7-m depth progressively increased from 2007 through 2009 and 2010, with maximum concentrations (SO_4^{2-} = 2700 mg L^{-1}, NO_3^--N = 1700 mg L^{-1}, NO_2^--N = 26 mg L^{-1},

NH_3-N = 30 mg L^{-1}, and Cl^- = 580 mg L^{-1}) observed in 2010. These concentrations are much higher than observed at the 1-m depth, with the exception of NH_3-N (Figure 4.11). Because the Type I test pile has not reached residual saturation, it is difficult to ascertain if there is a progressive increase in concentrations from the top of the test pile to the base of the test pile at all depths and all sample locations. However, the pore-water concentrations observed at the top of the test pile at the 1-m depth were lower than at the 7-m depth. Both of these locations had a high frequency of success in sampling pore water and can be assumed to represent the migration of water from the top of the test pile to the base of the test pile. Neuner *et al*. (2012) suggest that flow through the fine-grained matrix appears to dominate the flow mechanisms, rather than macropore or by-pass flow at the Diavik test piles. The progressive increase in concentrations at the base of the test pile was consistent with the migration of water through the matrix material within the Type I test pile. The effluent chemistry at the base of the test pile is consistent with matrix-dominated flow, rather than macropore or by-pass flow.

4.4.3.2.2 Basal Drain

Due to a defect in the basal drain of the Type I test pile, only one water sample was collected in 2007. The effluent from the Type I test pile maintained near-neutral pH (ranging from 5.8 to 8) with low concentrations of SO_4^{2-} (< 500 mg L^{-1}), Fe (< 1.4 mg L^{-1}) and other dissolved metals (Figure 4.12), with the exception of late 2010 when flow decreased and concentrations of SO_4^{2-} (1440 mg L^{-1}, Fe (5 μg L^{-1}) and Cd (16 μg L^{-1}) increased to concentrations similar to those observed in the Type III test-pile effluent. Measurable alkalinity was present in the Type I test pile for the duration of the period from 2007 to 2010; however, alkalinity

concentrations decreased through each field season as the pH decreased, with minimum concentrations of < 5 mg L^{-1} (as $CaCO_3$).

In 2008 and 2009, the effluent from the Type I test pile contained lower concentrations of SO_4^{2-} (10 - 410 mg L^{-1}) than those observed in the Type III test-pile effluent. Dissolved SO_4^{2-} concentrations increased as the flow rate decreased in October of each year. In 2010, SO_4^{2-} concentrations increased from July to November, reaching a maximum of 1800 mg L^{-1}, as a larger portion of the test pile contributed to the outflow, releasing blasting residuals. The maximum SO_4^{2-} concentration correlates to high concentrations of other blasting residuals, suggesting limited contribution of *in situ* sulfide oxidation. The total mass of S released from the Type I test pile from 2007 to 2010 was 12 kg corresponding to an estimated global oxidation rate of 4.0 x 10^{-11} kg (O_2) m^{-3} s^{-1}. The global oxidation rate of the Type I material is slightly slower than that observed in the Type III material, but it is greater than that observed in the field barrel tests.

4.4.4 Microbial Populations

Sulfide-mineral oxidation is catalyzed by bacteria, including *Thiobacillus* species and *Acidithiobacillus* species. Three groups of Fe- and S-oxidizing bacteria (*Acidithiobacillus ferrooxidans* and related species, *Acidithiobacllus thiooxidans* and related species and *Thiobacillus thioparus* and related species) were monitored in effluent from the Type I and Type III waste-rock test piles and enumerated (Figure 4.13).

Neutrophilic S-oxidizing bacteria (nSOB) were observed in both Type III basal drains in 2008. The number of nSOB decreased in late 2009 as the pH decreased (Figure 4.13). Populations of nSOB were also present in the Type I basal drain, with populations ranging

from 9.6×10^2 bacteria mL^{-1} to 1.1×10^6 bacteria $mL^{-1}$from 2008 through 2010. The pH in the Type I test pile remained near neutral for the duration of the study – ideal for neutrophilic S-oxidizing bacteria.

In 2008, acidophilic S-oxidizing bacteria (aSOB) were not detected in the Type III test pile; aSOB were detected in 2009, but not in 2010. Iron-oxidizing bacteria (aFeOB) were observed in the Type I basal drain in June 2009 and in 2010. In the Type III basal drains the populations of aFeOB increased with decreasing pH. A comparison of the population numbers to pH shows the abundance of aFeOB is highest when pH was below 6 and nSOB show higher populations when the pH was above 5.5 (Figure 4.14).

Sulfur- and Fe-oxidizing bacteria play an important role in the biogeochemical evolution of waste-rock test piles, accelerating the rate of sulfide oxidation and increasing the release rate of sulfate and other typical AMD constituents. These results are consistent with studies conducted on the upper 2 m of waste rock studied at Diavik (Chapter 3) and on mine tailings (*e.g.*, Blowes *et al.*, 1995) that had low populations of Fe- and S-oxidizing bacteria where sulfide-mineral oxidation was limited, and that had higher population numbers where sulfide-mineral oxidation was occurring and acidic conditions were prevalent. Continued monitoring and a more detailed analysis of the microbial population are required to further understand the biogeochemical evolution of these waste-rock test piles (Chapter 6).

4.4.5 pH, Alkalinity and Acid Neutralization

Although the pore-water from the test piles contains high concentrations of SO_4^{2-}, the pH of the pore water in the Type I test pile has remained near neutral, and the pH of the effluent from the Type III test pile varies throughout the year. These observations suggest that a

portion of the H^+ generated by sulfide oxidation is consumed by reaction with the non-sulfide mineral assemblage. Acidity generated from the oxidation of sulfide minerals in waste-rock piles is neutralized by the dissolution of primary and secondary minerals (Stromberg and Banwart, 1994; Stromberg and Banwart, 1999; Ritchie and Bennett, 2003; Stockwell *et al*., 2006). Acid neutralization in mill-tailings impoundments has been observed to result from a sequence of mineral-dissolution reactions, leading to a characteristic series of pH-neutralization plateaus. On the basis of laboratory column results, Jurjovec *et al*. (2002, 2003) observed acid-neutralization plateaus associated with the following phases: calcite (pH 6.5-7.5), siderite (4.8-6.3), $Al(OH)_3$ (4.0-4.3), and $Fe(OH)_3$ (2.5<3.5). A similar series of pH plateaus has been observed in inactive mill-tailings impoundments and in underlying aquifers (Morin *et al*., 1988; Blowes and Jambor, 1990; Blowes and Ptacek, 1994a). Chapter 3 described the acid-neutralization sequence observed within the Type III AZLs and suggests two pH plateaus, the first at a pH of 6.3-5.5, corresponding to the dissolution of carbonate minerals, and the second, ranging from a pH of 3.0 to 4.2, associated with the dissolution of secondary Al- and Fe-hydroxide phases. In addition, the kinetically limited dissolution of aluminosilicate minerals, principally biotite and plagioclase, occurs concurrently with the dissolution of the carbonate and (oxy)hydroxide minerals (Chapter 3). The pH of the effluent from the Type I AZLs remained near neutral for the duration of the study, suggesting that the pH is maintained by dissolution of carbonate minerals (Chapter 3).

4.4.5.1.1 Type III Test Pile

Measurements of pore-water pH in the Type III test-pile effluent showed a neutralization sequence similar to that observed in the AZLs (Chapter 3). In 2007, the pore-water pH was near neutral at both the 3-m and 5-m depths, with measurable alkalinity, suggesting the H^+

generated by sulfide-mineral oxidation at these depths was consumed by the dissolution of carbonate minerals (Figure 4.1 and Figure 4.2). Each subsequent year the pore-water pH and concentrations of alkalinity gradually decreased at each depth. Geochemical equilibrium modeling suggests the pore water was undersaturated with respect to all carbonate minerals in 2007 and saturation indices decreased with decreasing pH and alkalinity. At the 3-m depth, the pore-water pH decreased from near neutral to pH 5.0 by the end of 2007 and decreased to pH 4.7 by the end of 2008 (Figure 4.1). In 2009, the pH continued to decrease to pH 4.3, and in 2010, it reached a minimum of pH 3.5. Similar to the Type III basal drains, the decrease in pH to < 4.5 corresponded to increased concentrations of Al, suggesting that the dissolution of secondary Al-hydroxide phases buffers the pore-water pH. The pore water at the 5-m and 7-m depths followed a similar trend with slightly higher initial pH values (up to 6.9 at the 5-m depth and 6.3 at the 7-m depth), decreasing to a pH of 4.0 by the end of 2010 (Figure 4.2 and Figure 4.3). The pore water at 9 m below the surface remained near neutral, ranging from a pH of 6.5 to 7.5 through 2010, with the exception of one 9-m SWSS that decreased to 4.7 (Figure 4.4).

Water was first sampled from the basal lysimeter in the Type III test pile in August 2008 had a pH of 7.5 with alkalinity concentrations of ~20 mg L^{-1} as $CaCO_3$. The pH decreased to 4.8 concomitantly with a decline in the alkalinity to < 5 mg L^{-1} as $CaCO_3$ by the end of the first season (Figure 4.7). In 2009, the pH remained above 5.0 with measurable alkalinity (ranging from 2.8 to 11 mg L^{-1} as $CaCO_3$). In 2010, the pH decreased to 4.7 and had low concentrations of alkalinity (< 2 mg L^{-1} as $CaCO_3$).

The pH of the Type III test-pile effluent decreased from 7.5 to 5.0 between May and September 2007 and the pH remained at 5.0 until the end of October. The initial near-neutral pH and the presence of detectable alkalinity suggest that the H^+ generated by sulfide oxidation was consumed by the dissolution of carbonate minerals. Measurements of the carbon content of the < 50-mm fraction of Type III waste rock indicate a weighted mean carbon content of 0.030 wt. % (σ = 0.038) and that higher concentrations of carbonate minerals are associated with the fine fraction of the waste rock (Smith *et al*., in press). Alkalinity concentrations were highest (35 mg L^{-1} as $CaCO_3$) in early 2007 and decreased with decreasing pH. Similar trends in pH and alkalinity were observed in 2008, 2009 and 2010; however, the pH decreased earlier each year. In 2008 and 2009, the alkalinity decreased from 40 mg L^{-1} (as $CaCO_3$) to below the method detection limit (< 0.5 mg L^{-1}). In 2010, the alkalinity was lower, decreasing from 20 mg L^{-1} (as $CaCO_3$) in May to below detection. Geochemical equilibrium modeling suggests the effluent was undersaturated with respect to all carbonate minerals. Acid generation in the Type III test pile exceeded the neutralizing capacity available from carbonate minerals at the end of each field season (Figure 4.15). The Type III AZL (Chapter 3) had a distinct change in pH from near-neutral condition to pH < 4.5 in one year and the pH remained low for the duration of the study. Due to the large volume of waste rock in the test piles and the longer wetting-up period of the matrix material compared to the AZL (Chapter 3), this same trend was not observed in the Type III test pile.

The concentrations of Al remained low in all pore-water sample locations in 2007 and 2008, with the exception of one 5-m SWSS location. The pore water was at equilibrium or slightly below saturation with respect to amorphous $Al(OH)_3$, and was supersaturated with

respect to gibbsite and boehmite when the pH was above 5.0 and alkalinity concentrations were above detection (Figure 4.1 to Figure 4.4). Similar to the effluent from the Type III test-pile basal drains, concentrations of Al in the pore water increased slightly in 2009 and further increased in 2010. The pore water at 9 m had the lowest Al concentrations. In general, as the pH fell below 5.0, the pore water was undersaturated with respect to gibbsite and boehmite between 2009 and 2010.

The pH in the Type III basal drains decreased from near neutral to a secondary pH plateau of 5.0 that corresponded to an increase in Al concentrations from < 2 mg L^{-1} in 2007 to a range of 6 to 16 mg L^{-1} at the end of 2008, 2009 and 2010. A maximum Al concentration of 11 mg L^{-1} was observed in the Type III south-drain effluent in 2009. In 2010, concentrations increased from May through August and subsequently decreased. Concentrations of Al increased in the Type III north drain at the end of 2010 to 17 mg L^{-1}, the maximum concentration reported at this drain. The total mass loading of Al from 2007 to 2010 in the Type III test pile was 475 g (Figure 4.16).

Dissolved Al is derived from the dissolution of aluminosilicate and aluminum hydroxide minerals. A mineralogical study was conducted on weathered samples obtained from humidity-cell experiments conducted on the Diavik waste rock (Blowes and Logdson, 1998). Samples of biotite schist obtained from humidity-cell experiments that were acidic showed alteration of biotite grains, with depletion of K and Mg and enrichment of Al and Si on the edges of biotite laths. Early each year, the Type III test-pile effluent approached equilibrium with respect to amorphous $Al(OH)_3$, and was supersaturated with respect to gibbsite and boehmite when the pH was above 5.0 and alkalinity concentrations were above detection.

Near the end of the field season, as the pH fell below 5.0, effluent was undersaturated with respect to these minerals. Geochemical speciation modeling indicates that effluent from the Type III test pile was at equilibrium with respect to boehmite and basaluminite in 2007, and was supersaturated with respect to both of these minerals for the remainder of the period between 2008 and 2010, with the exception of a few select samples. Although discrete aluminum-bearing phases have not been isolated in sites impacted with AMD, it is commonly assumed that the dissolution of the Al-bearing phases buffer the pH in the region of 4.0–4.5 (Gunsinger *et al*., 2006 and references therein). At other locations, increases in Al concentrations were attributed to aluminosilicate or Al-hydroxide dissolution acid-neutralization reactions (Blowes and Jambor, 1990).

Dissolved Fe concentrations in the pore water were low (< 2 mg L^{-1}) in 2007, with the exception of one 3 m SWSS that had an elevated concentration of 4.2 mg L^{-1} in August 2007. The pore-water at 3 m remained low through 2009 and concentrations of Fe increased in 2010 up to 5.5 mg L^{-1}. The pore-water at 5 m also remained low for the duration of the study with a slight increase in concentrations in 2010 (to a maximum of 1.5 mg L^{-1}). The Fe concentrations remained low (< 0.87 mg L^{-1}) at both the 7-m and 9-m depths, with the exception of elevated concentrations in a few samples in 2008 (up to 14 mg L^{-1} at 7 m and 15 mg L^{-1}at 9 m). Pore water was supersaturated with respect to ferrihydrite in 2007 and in some samples in 2008, and became undersaturated with respect to ferrihydrite as the pH decreased below 5.0 (Figure 4.17 to Figure 4.20). In addition, the pore water was supersaturated with respect to goethite over the entire period between 2007 and 2010, with the exception of a few select samples. The calculated saturation indices for jarosite fluctuated between 5 and –5 from 2007 and 2010, with more samples supersaturated with respect to

jarosite than undersaturated (Figure 4.17 to Figure 4.20). Similar to the Type III basal-drain effluent, these observations suggest that formation of secondary Fe(III) (oxy)hydroxides and hydrosulfates controls the dissolved Fe concentrations from the Type III test pile (Figure 4.15).

Dissolved Fe concentrations at the base of the pile in the Type III basal drain were less than 1.0 mg L^{-1} throughout the period between 2007 and 2010. The Type III test-pile effluent was supersaturated with respect to ferrihydrite at the beginning of each year, and became undersaturated with respect to ferrihydrite at the end of each year as the pH fell below 5.0. The effluent remained supersaturated with respect to goethite over the entire period between 2007 and 2010. The effluent was occasionally supersaturated with respect to jarosite between 2007 and 2009, and approached saturation with respect to jarosite in 2010. Mineralogical studies of biotite schist column material from humidity tests indicate the presence of patchy, ochreous coatings of jarosite [$KFe_3(SO_4)_2(OH)_6$] (Blowes and Logdson, 1998). Although mineralogical characterization of the secondary minerals from the test piles has not yet been completed, it is likely that similar phases are present. Similar to the pore water, geochemical equilibrium modelling suggests that the formation of secondary Fe(III) (oxy)hydroxides and hydroxysulfates controls the dissolved Fe concentrations from the Type III test pile. Mineralogical studies of AMD-impacted sites have observed the formation of secondary Fe(III) (oxy)hydroxide and hydroxysulfate minerals (Moncur *et al*., 2005) and further mineralogical work at the Diavik test piles is required to determine if these minerals are present.

4.4.5.1.2 Type I Test Pile

Pore water in the Type I test pile at all depths ranged from pH 4.5 to 7.6 for the duration of the study. The pH at the 1 m depth decreased from 5.9 in 2007 to 5.0 in 2010 with a decrease in alkalinity from 10 mg L^{-1} (as $CaCO_3$) in 2007 to 1.1 mg L^{-1} (as $CaCO_3$) by 2010 (Figure 4.8). The pore-water pH at the 2 m depth remained near neutral for the duration of the study and few samples for geochemical analysis were collected (only 3 of 13 samples; Figure 4.9). The 5-m depth had four SWSSs produce water at various times throughout the study period (Figure 4.10). The Face 1 East and West 5-m SWSSs remained near neutral (ranging from pH 7.6 to 7.1) with measurable alkalinity (ranging from 16 mg L^{-1} as $CaCO_3$ to 40 mg L^{-1} as $CaCO_3$) for the duration of the study, while the pH observed at the Face 2 West 5 m SWSS decreased from 5.9 in 2008 to 4.9 in 2009, with low, but measurable alkalinity (ranging from 2.5 mg L^{-1} (as $CaCO_3$) to 8 mg L^{-1} (as $CaCO_3$); Figure 4.10). The pore water at the Face 2 West 7-m depth SWSS had a decrease in pH from near neutral in 2007 to 4.5 by 2010 (Figure 4.11). The pore water retrieved from the Face 2 West 7-m SWSS exhibited an increase in pH from 4.7 in 2007 to near neutral in 2009, and variable pH in 2010 ranging from 4.8 to 7.2. The Face 1 East 7 m SWSS was only sampled in 2007 and 2008, and had near neutral pH. Due to the limited sample volume, there were no alkalinity measurements made for this SWSS. The Face 2 East 7 m SWSS remained near neutral for the duration of the study, with measurable alkalinity ranging from 17 mg L^{-1} (as $CaCO_3$) to 27 mg L^{-1} (as $CaCO_3$).

Few samples were collected from SWSSs at the 9-m depth. Samples were obtained from the Face 1 East 9-m SWSS in 2007 and 2008, and samples were obtained from the Face 2 West 9-m SWSS in 2009 and 2010 (Figure 4.21). The pore water on Face 1 East at 9 m had near-neutral pH and measurable alkalinity (only one sample at 4.1 mg L^{-1} as $CaCO_3$) in 2007.

Alkalinity samples were not collected from this location in 2008. The pore water on Face 2 West at 9 m also was near neutral and had measurable alkalinity that ranged from 19 to 41 mg L^{-1} (as $CaCO_3$) in 2009 and 2010.

Similar to the Type I basal-drain effluent, geochemical equilibrium modeling suggests pore water in the Type I test pile was undersaturated with respect to all carbonate minerals at all depths (Figure 4.22 to Figure 4.26). The near-neutral pH at most locations suggests that any H^+ generated by the oxidation of the modest sulfide content of the waste rock was consumed by the limited neutralization potential of the waste rock in the Type I test pile.

Effluent from the Type I test pile began to flow in 2008, and maintained a circum-neutral pH (pH ~ 7) for the duration of this study. In early 2008 alkalinity concentrations increased from 30 mg L^{-1} (as $CaCO_3$) in May to 60 mg L^{-1} (as $CaCO_3$) in June, and decreased through the remainder of the field season to < 5 mg L^{-1} (as $CaCO_3$). The alkalinity concentration returned to 50 mg L^{-1} (as $CaCO_3$) when flow commenced in 2009 and decreased over the field season to < 8 mg L^{-1} (as $CaCO_3$). Alkalinity concentrations were elevated in two samples collected in early 2010, but the drain lines were frozen from late May through early July. After flow re-commenced in late July, concentrations had decreased to 15 mg L^{-1} (as $CaCO_3$), following a similar trend to 2009, ending the field season at 5 mg L^{-1} (as $CaCO_3$).

Geochemical equilibrium modeling suggests the Type I test-pile effluent was at equilibrium with respect to calcite for a short period at the beginning of 2008, then fell below saturation from 2008 through to 2010. The neutral pH of the effluent suggests that the limited neutralization potential of the Type I rock (NP_{avg} = 0.031 wt. % C, σ = 0.036; Smith *et al.*, in press) was sufficient to consume the H^+ generated by the oxidation of the modest sulfide

content of the waste rock. The effluent from the Type I test pile remained undersaturated with respect to siderite, suggesting no potential for the formation of secondary siderite. These observations are consistent with measurements made on the effluent from the Type I AZLs (Chapter 3).

Dissolved Al concentrations remained low at most depths within the Type I test pile (< 0.5 mg L^{-1}). Pore-water concentrations of Al increased with decreasing pH at the 1-m and 7-m depths from 2007 to 2010, with maximum concentrations of 1.9 mg L^{-1} at 1 m depth in 2009 and 1.3 mg L^{-1} at 7 m in 2010 (Figure 4.8 and Figure 4.11). Geochemical equilibrium modeling suggests pore water was at or near saturation with respect to amorphous $Al(OH)_3$ in 2007, and below saturation from 2008 through 2010 when the pH decreased below 6.0 (Figure 4.22 to Figure 4.26). Pore water was supersaturated with respect to gibbsite and boehmite from 2007 through 2010 and calculated saturation indices decreased over time; with the exception of one 7 m SWSS in 2010 that was below saturation with respect to boehmite (Figure 4.22 to Figure 4.26).

The differences in pH and alkalinity may be attributed to differences in S content in the small area of influence around each SWSS. The 1-m and 7-m depth may have been influenced by higher concentrations of sulfide minerals compared to other SWSSs. Although the Type I waste rock contains a low concentration of sulfide minerals, heterogeneities in the rock and the presence of a small quantity of biotite schist can cause variability in pore-water concentrations.

The Type I test pile had very low Al concentrations, with maximum concentrations of < 1.0 mg L^{-1}. The Type I test pile had a total mass loading of 26 g Al from 2007 to 2010

(Figure 4.16). Aluminosilicate dissolution provides limited acid neutralization at near-neutral pH (Jambor *et al*., 2007). The low concentrations of Al in the effluent suggest that Al released from aluminosilicate dissolution was modest, and that secondary Al-bearing minerals may be forming. Geochemical calculations indicate that the Type I test-pile effluent is near saturation or undersaturated with respect to amorphous $Al(OH)_3$ and consistently supersaturated with respect to the more crystalline Al oxides including gibbsite and boehmite. However, discrete aluminum-bearing phases have not been isolated in sites impacted with AMD (Blowes *et al*., 2003). Saturation with respect to the Al hydroxysulfate minerals, alunite and basaluminite, was variable, suggesting that there was little potential for significant accumulation of these minerals.

4.4.6 Major Cations

4.4.6.1 Type III Test Pile

The dissolution of carbonate and aluminosilicate minerals releases major ions (Ca, Mg, K, Na and Mn), and can play an important role in the formation of secondary minerals, such as gypsum and jarosite (Blowes and Jambor, 1990). Some K may be released from $KClO_4$ that is used during blasting but the concentrations are considered to be minor, as described in Chapter 3. Calcium, Mg, K and Na concentrations in the Type III pore water were elevated in 2007 at the 3-m and 5-m depths as water from the top of the test pile migrated downward (Figure 4.1 and Figure 4.2). Concentrations subsequently decreased in 2008, corresponding with the decrease in pH, and further decreased each subsequent year, with the exception of slight increases in concentrations at the 5-m depth. Few pore-water samples were collected in the 7-m and 9-m depths in 2007, as the wetting front remained at 7 m by the end of 2007

(Figure 4.3 and Figure 4.4). Concentrations of Ca, Mg, K, and Na were elevated at 7 m and 9 m in 2008, indicating water at the 3-m and 5-m depths from 2007 had migrated downward. Concentrations subsequently decreased similar to the trend observed in the upper portions of the test pile, with the exception of a few samples that were elevated in 2009 and 2010.

The concentrations of Ca and Mg in the basal lysimeter were elevated at the beginning of each field season, when the pH was near neutral, and subsequently decreased through to the end of the field season with decreasing pH and alkalinity (Figure 4.5). Maximum concentrations of Ca, Mg, K, and Na were observed in 2010, suggesting that water from the top of the test pile reached the basal lysimeter through matrix flow. The Ca concentrations ranged from 280 mg L^{-1} to the maximum concentration of 780 mg L^{-1}. The concentrations of Mg in the basal-lysimeter effluent ranged from 190 mg L^{-1} to 940 mg L^{-1} for the duration of the study. The concentrations of Na ranged from 78 mg L^{-1} to 350 mg L^{-1} and the K concentrations ranged from 88 to 200 mg L^{-1} from 2008 through 2010. The basal lysimeter showed the maximum concentrations of Ca (780 mg L^{-1}), Mg (940 mg L^{-1}), K (200 mg L^{-1}), and Na (350 mg L^{-1}) in 2010. The concentrations of Ca, Mg, K, and Na in the pore water and the basal lysimeters were similar to, or slightly lower than those of the Type III test-pile basal drains, suggesting that solute transport in the waste-rock test pile was matrix dominated.

Geochemical equilibrium modeling suggests the pore water was supersaturated with respect to alunite for the duration of the study and jarosite at various times. The precipitation of these minerals may provide a limit to dissolved K concentrations. Geochemical equilibrium modeling suggests Ca and SO_4^{2-} concentrations in the pore water may have been limited by the precipitation of gypsum for the duration of the study.

Calcium concentrations in the Type III north and south drains increased with increasing temperature and decreasing pH, to a maximum of 250 mg L^{-1} in August 2007, and subsequently decreased (Figure 4.27). The concentrations of Ca in 2008 were variable with an increasing trend from May through August. During this time, the pH and alkalinity over the period from May to August 2008 were the highest reported in the Type III test pile and concentrations of Ca increased through the end of 2008 as pH and alkalinity decreased. In 2009 and 2010, Ca concentrations were low in May, gradually increased until August and then sharply increased in September through October. The maximum Ca concentration was 420 mg L^{-1}, observed at the end of 2009 and 2010. The total mass of Ca released from the combined Type III basal drains was 63 kg. Geochemical speciation modeling suggests effluent from the Type III test pile was undersaturated with respect to gypsum, with the exception of the last few samples collected at the end of each field season, when the flow rate significantly decreased.

Magnesium and K are likely released by the kinetically limited dissolution of biotite (Chapter 3). The maximum concentration of Mg was 760 mg L^{-1} in the Type III south drain at the end of 2009 and 300 mg L^{-1} in the north drain at the end of 2010 (Figure 4.27). The total mass of Mg released from the combined Type III basal drains was 82 kg. In 2008, 2009, and 2010, K concentrations were low in May of each year and increased through the field season. The concentrations of K in the Type III south drain in 2007 and 2008 reached a similar maximum at 75 mg $L^{-1}$and 71 mg L^{-1}, respectively, and in 2009 and 2010, K concentrations reached 140 mg L^{-1} (Figure 4.27). The maximum concentration was 120 mg L^{-1} in the Type III north drain in 2007. The total masses of K released were 26 kg from the combined Type III basal drains and 6.9 kg from the Type I basal drain.

The cumulative ratio of Mg:K in the Type III basal drain was 3.1, with an average of 2.85, and the ratios for individual samples range from 0.21 to 5.35. The ideal molar ratio of Mg:K in biotite [$KMg_3AlSi_3O_{10}(OH)_2$] is 3:1. The range of ratios in the Type III basal drain suggests there was another source of Mg, or that K was preferentially removed from the effluent. In addition, K may be released from $KClO_4^-$ during blasting, however, the mass is considered to be low compared to the proportion released from aluminosilicate dissolution (Chapter 3). Geochemical modeling indicates that the effluent from the Type III basal drains was at saturation with respect to jarosite at the beginning of 2008 and 2009, thus the precipitation of jarosite may provide a limit to dissolved K concentrations.

Dissolved Na and Mn are derived from weathering of aluminosilicate minerals (Chapter 3). The concentrations of Na in 2007 and 2008 reached a similar maximum of 140 mg L^{-1} in the Type III south drain. In 2009 and 2010, concentrations further increased to 270 mg L^{-1} (Figure 4.27). The maximum Na concentration in the Type III north drain was 220 mg L^{-1} in 2007. Sodium concentrations remained low in 2008 through 2009. In 2010, the concentration of Na followed a similar trend to Mg and Ca, and significantly increased to 640 mg L^{-1}. The total mass of Na released from the Type III basal drain was 28 kg. The concentration of Mn followed a similar trend to Na, Mg, and Ca. The maximum Mn concentrations occurred in 2009 at 29 mg L^{-1} in the Type III south drain and 24 mg L^{-1} in the Type III north drain. The total Mn from the Type III basal drains was 2.3 kg.

4.4.6.2 Type I Test Pile

The concentrations of Ca, Mg, K, and Na in the Type I test-pile pore water were variable over time and with depth (Figure 4.8 to Figure 4.21). The average concentrations of Ca

(590 mg L^{-1}), Mg (450 mg L^{-1}), K (180 mg L^{-1}), and Na (400 mg L^{-1}) observed in the Type I test-pile SWSSs from 2007 to 2010 were within the range of concentrations observed in the Type I basal drain (Ca ranged between 11 to 2100 mg L^{-1}; K ranged between 2.8 to 230 mg L^{-1}; Mg ranged between 4.0 to 1200 mg L^{-1}; Na ranged between 1.1 to 640 mg L^{-1}). However, the maximum concentration of K (730 mg L^{-1}) and Na (2300 mg L^{-1}) in the pore water was significantly higher than in the Type I basal drain. The concentrations of Ca and Mg were not significantly different from the range of concentrations observed in the pore water (P = 0.351 for Ca and P = 0.210 for Mg; Mann–Whitney rank sum test; SigmaPlot, Systat Software Inc.).

Geochemical equilibrium modeling suggests the Type I test-pile pore water was supersaturated with respect to alunite for the duration of the study, with the exception of the 2-m SWSS, and individual samples from the 5-m, 7-m, and 9-m depths (Figure 4.22 to Figure 4.26). The calculated saturation indices for jarosite were variable at all depths over time, ranging from above to below saturation. Pore water was also below saturation with respect to gypsum for the duration of the study (Figure 4.22 to Figure 4.26). The precipitation of secondary minerals, such as alunite and jarosite, may provide a limit to SO_4^{2-} and/or dissolved K concentrations.

The Type I basal drain followed a similar trend to the Type III south drain in 2007 and reached a maximum Ca concentration of 320 mg L^{-1} (Figure 4.27). In 2008 and 2009, concentrations also followed a similar seasonal trend to the Type III south drain, but with lower concentrations. In 2010, the Ca concentrations were significantly higher and increased to 2100 mg L^{-1}. The Type I test pile had detectable alkalinity for the duration of the study.

The effluent from the Type I basal drain was undersaturated with respect to gypsum throughout the period from 2007 to 2010. The total mass of Ca released from the Type I basal drain over the four-year study period was 35 kg.

The Type I basal drain had lower Mg concentrations than the Type III basal drains through 2008 and 2009, but in 2010 concentrations increased to 750 mg L^{-1} similar to the maximum concentrations observed in the Type III basal drain. The total mass loading of Mg in the Type I basal drain was 16 kg. The molar ratio of Mg:K in the Type I basal drain effluent was 2.29 with an average of 1.79, and the Mg:K molar ratio in individual samples ranged from 0.23 to 3.42. These values are slightly lower than the ideal 3:1 molar ratio of Mg:K in biotite.

Type I effluent was undersaturated with respect to K-bearing minerals, suggesting that the lower molar ratio may have been a result of an additional source of K, or that Mg was preferentially removed from the effluent. A total of 6.9 kg of K was released from the Type I basal drain.

The Type I basal-drain effluent had low concentrations of Na through 2008 and 2009, and concentrations steadily increased in 2010 to 20 mg L^{-1}. The total mass loading of Na from the Type I drain was 9.0 kg (Figure 4.16).

4.4.7 Dissolved Metals

4.4.7.1 Type III Test Pile

The dissolved SO_4^{2-} concentrations suggest that, after viable populations of S-oxidizing bacteria became established, the rate of sulfide-mineral oxidation increased as the temperature within the test piles increased. The release of SO_4^{2-} also increased as larger

portions of the test piles contributed flow to the basal drainage system. The concentrations of dissolved metals followed a similar pattern.

Increases in Fe, SO_4^{2-}, and most dissolved metal concentrations coincided with the decrease in pH from the top of the test pile through to the base of the test pile. Concentrations were low at all depths in 2007 (Ni < 5 mg L^{-1}, Co < 2 mg L^{-1}, Zn < 4 mg L^{-1}, Cu < 1 mg L^{-1}, and Cd < 30 μg L^{-1}) with the exception of one SWSS at 5 m that had Ni concentrations ranging from 13 mg L^{-1} to 20 mg L^{-1} and Co concentrations ranging from 4 mg L^{-1} to 6 mg L^{-1}); however, the pore water at 3 m and 5 m had slightly higher concentrations than the 7-m and 9-m depths. The metal concentrations at the 3-m and 5-m depth increased slightly in 2008. The maximum concentrations observed at the 7-m depth in 2008 were similar to those observed at the 3-m and 5-m depths in 2007. In 2009, concentrations at the 3-m and 5-m depths further increased and in 2010, concentrations at 3-m, 5-m and 7-m depths sharply increased (Figure 4.1, Figure 4.2, and Figure 4.3). High concentrations of SO_4^{2-} (4500 mg L^{-1}), Al (79 mg L^{-1}), Ni (25 mg L^{-1}), Cu (6.6 mg L^{-1}), Zn (19 mg L^{-1}), and Co (5.5 mg L^{-1}) were observed by 2010 in near-surface pore water. The concentrations observed in the Type III test-pile pore water were lower than those observed in the effluent from the Type III 2 m by 2 m scale active zone experiments (Chapter 3).

The pore water at the 9-m depth did not exhibit the same decrease in pH or increases in SO_4^{2-} and dissolved metals observed in upper portions of the Type III test pile (Figure 4.4). Because of the variability in the Type III waste rock and the small zone of influence of the SWSSs, it is possible that the waste rock in the area of the 9-m SWSS may have been lower

in S content then in other regions within the test pile. It is also possible that contact water migrating downwards through the waste rock by-passed the 9-m SWSS.

Effluent reporting to the base of the test piles in the basal lysimeters and the basal drains exhibited decreases in pH, increases in SO_4^{2-} and in most dissolved metals similar to the pore-water samples at 3 m, 5 m, and 7 m. The effluent and pore-water concentrations of Al, Ni, Co, Zn, Cd, and Cu increased, corresponding to decreases in pH, over time. The concentrations of dissolved metals were low at the 3-m and 7-m depths in 2007 (Al < 0.15 mg L^{-1}, Ni < 1.7 mg L^{-1}, Co < 0.010 mg L^{-1}, Zn < 0.13 mg L^{-1}, Cd < 4 μg L^{-1}, and Cu < 0.010 mg L^{-1}; Figure 4.5). The concentrations increased with decreasing pH from 2008 through 2010 at both depths, with higher concentrations at the top of the test pile (3-m depth) than close to the base (7-m depth). The maximum pore-water concentrations at the 3-m depths (Al = 79 mg L^{-1}, Ni = 19 mg L^{-1}, Co = 4.0 mg L^{-1}, Zn = 18 mg L^{-1}, Cd = 110 μg L^{-1}, and Cu = 6.6 mg L^{-1}) and 7 m (Al = 30 mg L^{-1}, Ni = 14 mg L^{-1}, Co = 3.9 mg L^{-1}, Zn = 9.5 mg L^{-1}, Cd = 57 μg L^{-1}, and Cu = 4.1 mg L^{-1}) were reported in 2010. This observation indicates that solute transport is through matrix flow, and that concentrations deeper in the test pile are likely to increase over time, similar to the upper zone of the pile.

The basal-lysimeter effluent remained above pH 5.0 and concentrations of dissolved metals remained low, compared to the 3-m and 7-m depths, and only slightly increased over time (Figure 4.5). The concentrations of dissolved metals in the basal-lysimeter effluent increased with decreasing pH, and maximum concentrations of 0.76 mg L^{-1} Al, 10 mg L^{-1} Ni, 1.4 mg L^{-1} Co, 1.1 mg L^{-1} Cu, 0.73 mg L^{-1} Zn, and 15 μg L^{-1} Cd were observed when the pH decreased below 5.0 in 2010 (Figure 4.5). The maximum concentration of Fe was observed at 2.4 mg L^{-}

[1] in 2009. Geochemical equilibrium modeling suggests the basal-lysimeter effluent was supersaturated with respect to Fe oxyhydroxides (goethite, lepidocrocite, and, at times, ferrihydrite), suggesting that the accumulation of these secondary minerals may have limited the Fe concentrations (Figure 4.6). The maximum concentrations of dissolved metals in the basal lysimeter are expected to increase over time as the water moves from the top of the test pile through to the base, and with a decrease in effluent pH.

The concentrations of dissolved metals in the Type III basal drains were different between the north drain and south drain in 2007. The north-drain effluent showed a trend of increasing metal concentrations from May through September when flow ceased. The dissolved metal concentrations in south-drain effluent also increased, but reached lower maximum concentrations. The volume of flow was larger for the south basal drain and flow continued until late October. In subsequent sampling seasons, the concentrations and trends were similar for both drains; higher metal concentrations with increased temperatures within the test pile and with larger contributions of outflow from the central portions of the test pile. Maximum concentrations were observed in 2009. The concentrations of all dissolved metals in the Type I test-pile effluent were lower than for the Type III test-pile effluent, but followed seasonal trends that were similar to those observed in the Type III test-pile effluent.

The oxidation of pyrrhotite releases dissolved Ni and Co in the test-pile effluent (Chapter 3). The concentrations of Ni were highly correlated to the concentrations of Co in the Type III south drain ($R^2 = 0.98$) and Type III north drain ($R^2 = 0.96$). Effluent ratios of Ni to Co concentrations in the Type III test-pile effluent averaged 4.9 and this is slightly higher than the ratios observed in the whole-rock analysis (4.63) and the electron microprobe analysis of

pyrrhotite grains [$(Fe_{0.852}Ni_{0.004}Co_{0.001})_{\sum 0.857}S_{1.000}$] (Jambor, 1997), suggesting pyrrhotite oxidation is the primary source of Ni and Co. In addition, the ratios suggest Ni and Co have consistent release rates, or alternatively, that they could be removed from the effluent through coprecipitation or adsorption mechanisms in equal proportions.

The maximum Ni concentration in the Type III south (20 mg L^{-1}) and north drains (19 mg L^{-1}) were observed in 2009, similar to the maximum concentrations observed in the pore water and basal lysimeter. The total mass of Ni released from the Type III basal drains was 1800 g between 2007 and 2010 (Table 4.4). The maximum Co concentrations were observed in 2009 in the Type III south drain (3.8 mg L^{-1}) and in the Type III north drain (2.8 mg L^{-1}). The total mass loading of Co from 2007 to 2010 was 324 g (Table 4.4 and Figure 4.16).

The Zn in the effluent was derived from the oxidation of sphalerite (Chapter 3). The concentrations of Zn increased from 2007 through 2008, but the maximum in both the Type III basal drains occurred in 2009. The maximum Zn concentration in the Type III south drain was 3.7 mg L^{-1} and 3.0 mg L^{-1} in the Type III north drain in 2009 (Figure 4.12), lower than in the pore water and the basal lysimeter. Concentrations of Zn in 2010 followed a similar trend to concentrations in 2009; however, lower concentrations were observed. An increase in the total flow from the Type III basal drains in 2010 (2.10×10^5 L) relative to 2009 (1.10×10^5 L), resulted in a total mass load in 2009 of 110 g, approximately half of the 2010 total mass loading (210 g). The cumulative mass of Zn released from the combined Type III basal drains was 406 g from 2007 to 2010 (Figure 4.16).

Cadmium, Fe^{2+}, Cu, and Mn can be found at trace concentrations in sphalerite. The maximum concentration of Cd was 35 μg L^{-1} in the Type III south basal drain and 29 μg L^{-1} in the Type III north basal drain in 2009: slightly lower than in the pore water, but greater than in the basal lysimeter. The Cd concentrations were low in 2008 and 2009, but increased through 2010 from non-detectable to 16 μg L^{-1}. The total mass of Cd released from the combined Type III basal drains was 2.7 g.

Trace amounts of chalcopyrite have been found in the Diavik waste rock and chalcopyrite is the primary source of Cu in the waste-rock effluent. The maximum Cu concentration in the Type III south basal-drain effluent was 1.7 mg L^{-1} and in Type III north basal-drain effluent it was 2.3 mg L^{-1}, similar to the basal lysimeter, but lower than in the pore water. The total mass of Cu released between 2007 and 2010 from the combined Type III basal drains was 164 g.

Geochemical equilibrium modeling suggests the effluent from the Type III test-pile pore water and basal-drain effluent was undersaturated with respect to all secondary Ni, Zn, Cd, and Cu minerals included in the WATEQ4F database , suggesting there are no secondary mineralogical constraints on Ni, Zn, Cd, and Cu concentrations (Figure 4.15). Alternatively, metals such as Ni, Zn, Cd, Cu and Co have been observed to coprecipitate with, and adsorb to Fe(III)-oxyhydroxides at near-neutral pH conditions, and the increase in metal concentrations corresponded to the decrease in pH (Dzombak and Morel, 1990; Ribet *et al*., 1995; McGregor *et al*., 1998; Carlsson *et al*., 2002; Dold and Fontbote, 2002; Moncur *et al*., 2005; Gunsinger *et al*., 2006). Similar to the AZLs discussed in Chapter 3, the dissolved metal concentrations at all sampling locations (pore water and effluent) in the Type III test

pile increased with decreasing pH below 5.0 and the maximum dissolved metal concentrations were observed at the lowest pH (pH < 4), suggesting dissolved metal concentrations in the Type III test pile were controlled by coprecipitation or adsorption reactions. Mineralogical work is required to further understand the weathering patterns in the waste-rock test piles, the formation of secondary minerals, and the processes controlling metal concentrations.

4.4.7.2 Type I Test Pile

The concentrations of dissolved metals in the Type I SWSSs were highly variable, ranging from low minimum concentrations (minimum concentrations of 0.040 mg L^{-1} Ni, 0.004 mg L^{-1} Cu, 0.006 mg L^{-1} Co and below detection for Zn, Fe, and Cd) to maximum concentrations (maximum concentrations of 3.2 mg L^{-1} Fe, 13 mg L^{-1} Ni, 4.0 mg L^{-1} Cu, 3.2 mg L^{-1} Co, 18 mg L^{-1} Zn, and 50 μg L^{-1} Cd) that were greater than the average concentrations observed in the Type III test-pile basal drain (average concentrations of 0.14 mg L^{-1} Fe, 3.2 mg L^{-1} Ni, 0.37 mg L^{-1} Cu, 0.59 mg L^{-1} Co, 0.72 mg L^{-1} Zn, and 35 μg L^{-1} Cd). The average concentrations of dissolved metals in the Type I pore-water samples were 0.35 mg L^{-1} Fe, 1.5 mg L^{-1} Ni, 0.50 mg L^{-1} Co, 0.50 mg L^{-1} Cu, 1.4 mg L^{-1} Zn, and 13 μg L^{-1} Cd (Figure 4.8 to Figure 4.21).

Concentrations of dissolved Ni, Zn, Cu and Cd in the Type I basal-drain effluent were lower than in the Type III basal drains, with maximum concentrations of Fe = 0.99 mg L^{-1}, Ni = 1.1 mg L^{-1}, Co = 0.13 mg L^{-1}, Cu = 1.3 mg L^{-1}, Zn = 0.55 mg L^{-1}, and Cd = 16 μg L^{-1}. The concentrations of Ni were highly correlated to the concentrations of Co in the Type I basal drain ($R^2 = 0.98$), similar to the Type III test pile and the ratios observed in pyrrhotite

(Jambor, 1997). The Type I test-pile pore water and effluent was undersaturated with respect to Ni-, Cu-, Cd-, and Zn-bearing phases included in the WATEQ4F database (Figure 4.15). No secondary Ni-, Cu-, Cd-, or Zn-bearing minerals were identified in mineralogical studies of waste rock from the Diavik site (Jambor, 1997). Pore water and effluent were supersaturated or near equilibrium with respect to ferrihydrite and goethite, suggesting that the formation of secondary Fe(III) (oxy)hydroxides and hydrosulfates may control the dissolved Fe concentrations (Figure 4.22 to Figure 4.26). Maximum metal concentrations were observed at minimum pH, suggesting that metal concentrations were probably controlled by adsorption or complexation reactions, and that metals were released through acid-neutralization reactions.

4.4.8 Summary

The observed SO_4^{2-} concentrations indicate that although the sulfide-mineral content of the Diavik waste rock is low (Type III = 0.053 wt. % S; Type I = 0.035 wt. % S), the total mass of S within the test piles is sufficient to generate dissolved SO_4^{2-} concentrations that exceed 2800 mg L^{-1}. The low volume of water that migrated through the waste-rock pile was characterized by a high concentration of oxidation products, suggesting matrix-dominated flow. Similarly, at the Doyon mine in Quebec, Canada, maximum concentrations were observed during dry periods in unsaturated waste-rock piles, and decreased concentrations were observed during recharge periods (Sracek *et al*., 2004). Mass loadings of oxidation products such as SO_4^{2-} and dissolved metals can remain within waste-rock piles as components of secondary minerals and be remobilized later in the evolution of the waste-rock pile (MEND, 1995). The accumulation of weathering products was observed in low-S

content (0.7–1.7 % S) waste-rock piles at the Aitik mine in Sweden (Stromberg and Banwart, 1999). These observations have important implications with respect to the management of waste rock at other mine sites and the ability to predict the quality of mine drainage.

Other studies have also shown field oxidation rates to be lower than those observed in the laboratory by order(s)-of-magnitude (Malmstrom *et al*., 2000 and references therein). Preliminary results of calculations scaling the measured sulfide-mineral oxidations from humidity cells up to small-scale, field-based studies (Chapter 7) based on measured physical and chemical characteristics, such as temperature, grain size, sulfur content, and surface area, have shown good correlation between S release rates in the laboratory and in the field. Further investigation is required to ascertain whether humidity-cell experiments can achieve similar results for larger scale waste-rock test piles, such as the Type I and III test piles.

In addition to low pH, high metal loadings are frequently associated with mine wastes. In spite of the very low sulfide-mineral content of the Diavik waste rock, high concentrations of some metals, notably Cu, Zn, Ni and Co, were observed. The magnitude of the potential impact of these metals on surface water adjacent to the full-scale waste-rock pile will depend on a number of factors, including the amount of precipitation and the surface area of the catchment, and the volume of water discharged from the waste rock. Although estimates of metal concentrations released to the receiving water bodies are beyond the scope of the current study and will be addressed in future investigations, it is possible to estimate the degree of dilution required to meet regulatory guideline concentrations.

The SO_4^{2-} and dissolved metal concentrations observed in the Type III and Type I test piles are much lower than well-known AMD-impacted sites, such as pore waters in the Camp

tailings impoundment at Sherridon, Manitoba, (maximum SO_4^{2-} = 280 g mL^{-1}, Cu = 1.6 g mL^{-1}, and Zn = 55 g mL^{-1}; Moncur *et al*., 2005) and underground workings in the Richmond mine at Iron Mountain, California (maximum SO_4^{2-} = 760 g mL^{-1}, Cu = 4.76 g mL^{-1}, and Zn = 23.5 g mL^{-1}; Nordstrom *et al*., 2000). However, the metal concentrations at the base of the Type III and Type I test piles are high compared to Canadian water-quality guidelines for the protection of aquatic life (CEQG, 1999). This suggests, that if not managed appropriately, the waste rock at Diavik has the potential to have an impact on the local environment in terms of metal loadings, in addition to low pH and high SO_4^{2-}. The Type III test-pile mass loadings were compared to the estimated maximum metal loading to Lac de Gras, and was estimated using the test-pile flow rates and the metal concentrations from the Canadian water-quality guidelines for the protection of aquatic life (CEQG, 1999; DDMI, 2011). A 23-dilution factor was applied to the loadings to consider the mixing of discharge in Lac de Gras (DDMI, 2011). The mass loading of dissolved metals generated from the Type III test piles are higher than would be considered acceptable, indicating careful management planning is required prior to closure of the waste-rock piles at the Diavik site. In choosing a site-specific remediation plan, the contributions from metal loadings must be considered over concentrations, because the highest concentrations do not always have the greatest impact (Kimball *et al*., 2009).

In feasibility studies, Diavik anticipated the potential to exceed regulatory guideline concentrations for some metals and proposed closure strategies that have the potential to mitigate these loadings by maintaining freezing conditions in the central portion of the full-scale piles (DDMI, 2011). The objective of these strategies is to maintain low temperatures within the full-scale piles by preventing advective gas transport through the waste rock,

providing more uniform sub-freezing temperatures throughout the year. One of these strategies is currently being evaluated on the Covered test pile (Chapter 5).

The configuration of the test piles affects the timing and origin of flow reporting to the basal drains of the test piles. Both the Type III and Type I test piles are 60 m by 50 m at the base and 15 m high, and extend from a central platform (Chapter 1). The flat surface at the top of each of the test piles measures approximately 20 m by 30 m (Chapter 1). Angle of repose (1.3H:1V) slopes, varying in thickness from < 50 cm to 15 m, form the test-pile batters (sloped sides). Although water has been observed to pond at some locations of the test piles during natural and simulated rainfall events, there have been no observations of overland flow on the test-pile batters (Neuner *et al*., 2012). Neuner *et al*. (2012) estimate a downward pore-water flux of $< 10^{-2}$ to 3×10^{-2} m day^{-1} in response to common rainfall events and up to 0.7 m d^{-1} in response to intense rainfall on the level surface at the top of the test pile. In the absence of overland flow, it is reasonable to assume that the downward water flux through the batters will be similar. Because of the variable thickness of the batters, the time required for water to move from the level surface at the top of the test pile to the geomembrane at the base of the test pile is much longer than the time required for water to migrate from the batter surface to the geomembrane. Furthermore, batter flow also contacts less rock than flow through the full thickness of the test pile, resulting in less water–rock interaction. This difference is most pronounced for infiltration near the sides of the test piles.

The thermal regime also profoundly impacts the flow system within the test piles. Although the interior temperatures throughout both the test piles fall below 0°C every winter, the cooling process is not uniform (Pham *et al*., 2012). In the spring, the test piles thaw from

the margins inward, with temperatures rising above 0^{o}C at the outer surfaces of the test pile and a thawing front migrating inward and downward to the centre and base. In the fall, this process reverses, with cooling from the surface inward, and temperatures initially fall below 0°C at the test-pile surface, and the freezing front migrates inward (Pham *et al*., 2012). As a consequence of the test-pile configuration and the annual thermal cycle, flow derived from the test-pile batters dominates the test-pile effluent in the spring of each year, with increasing contributions from the central portions of the test piles through the summer. Late in the year, flow from the centre of the test pile becomes more dominant as frost migrates inward from the batters.

The chemical composition of the water reporting to the test-pile drains is consistent with this conceptual model of flow. The first flush of water through the finer grained matrix of the waste rock is characterized by high concentrations of blasting residuals, including SO_4^{2-}, NO_3^-, and NH_4^+ (Chapter 2; Bailey *et al*., 2012). The concentrations of blasting residuals progressively increase to maximum values during displacement of the first pore volume of flow through the fine-grained matrix, then subsequently decrease and remain low (Chapter 2; Bailey *et al*., 2012). In the lysimeter experiments (AZLs; Chapter 3), the volume of water that displaced the resident tracers corresponds to the matrix volume within the lysimeter (Chapter 2; Bailey *et al*., 2012). In the large-scale test piles, the release of blasting residuals reflects the relative contributions from the test-pile batters, and the central portions of the test piles. In the Type III test pile, for example, in 2007, the concentrations of blasting residuals increased with increasing ambient air temperature from May through to late September. The concentrations of blasting residuals then decreased from September through the end of the field season. This pattern suggests that the water first reporting to the basal drain was derived

from the batters of the test piles, where the flow path is shortest. In all subsequent years, the initial concentrations of components associated with blasting residuals were low, suggesting that this water was probably derived from the well-flushed test-pile batters. A subsequent increase in blasting concentrations, observed at the end of the field season, probably indicates that water moving along longer flow paths, originating in the central portion of the test pile, provided greater contributions to the outflow late in the season. The pattern of release of the blasting residuals, therefore, is consistent with the hypothesis that the water first released to the basal-drain systems each year was derived from the margins of the test pile, and flow observed later in the year was derived from a greater proportion of the test pile.

4.5 Conclusions

The effluent and pore water from the Type I waste-rock test pile (0.035 wt. % S) and the Type III waste-rock test pile (0.053 wt. % S) were monitored from their initial construction and for the subsequent four years after waste-rock placement. The pronounced variations in ambient air temperature influenced the concentrations of SO_4^{2-} and dissolved metals in effluent from the waste-rock test piles. Increased rates of sulfide-mineral oxidation were observed at higher temperatures within the test piles. In addition, the migration of water from the top of the test pile to the base of the test pile influenced the flushing of blasting residuals and oxidation products.

Pore-water concentrations were elevated compared to the effluent samples in both the Type I and Type III test piles. The concentrations of blasting residuals were high in the early time samples in the upper portion of each test pile. As pore water migrated downward, blasting residuals were flushed, and the concentrations increased in the deeper SWSSs, and in the

test-pile basal drains, suggesting flow is matrix dominated, rather than flow through the macropores or by-pass flow. Pore water at the top of the test pile had the highest reported concentrations of dissolved metals and lowest reported pH (3.24) in 2010. The effluent from the base of the Type III test pile is characterized by a low pH (< 4.5), and elevated concentrations of SO_4^{2-} (maximum of 2800 mg L^{-1}) and dissolved metals (maximum of 20 mg L^{-1} Ni, 2.3 mg L^{-1} Cu, 3.7 mg L^{-1} Zn, 35 μg L^{-1} Cd, and 3.8 mg L^{-1} Co), suggesting sulfide-mineral oxidation is occurring in the waste rock. The rate of sulfide-mineral oxidation in the Type III test pile exceeded the rate of acid consumption, resulting in the generation of acidic drainage. An acid-neutralization sequence observed in the Type III test-pile pore water and basal effluent was similar to the AZLs (Chapter 3) of other AMD studies, indicating a series of mineral dissolution-precipitation reactions control pH and metal mobility; carbonate mineral dissolution buffered the acidity generated from sulfide-mineral oxidation at near-neutral pH and the dissolution of Al and Fe (oxy)hydroxides buffered the effluent and pore water at pH < 5.0. The pore water and basal-drain effluent had similar mineralogical controls. Geochemical calculations suggest that the concentrations of Fe were limited by the formation of secondary minerals such as goethite, lepidocrocite, and at times, ferrihydrite in both pore water and basal-drain effluent. No secondary mineralogical controls for dissolved metals in the WATEQ4F database were identified. Dissolved metal concentrations were probably controlled by coprecipitation with, or adsorption to Fe(III)-oxyhydroxides at pH > 5.0.

The Type I test-pile effluent was characterized by near-neutral pH, and low concentrations of SO_4^{2-} (< 500 mg L^{-1}) and dissolved metals (average concentrations of 0.12 mg L^{-1} Fe, 0.16 mg L^{-1} Ni, 0.14 mg L^{-1} Cu, 0.062 mg L^{-1} Zn, 2.2 μg L^{-1} Cd, and 0.026 mg L^{-1} Co). The maximum dissolved metal concentrations in the Type I pore water were highly variable and

greater than the average concentrations observed in the Type III test-pile basal drain. However, sulfide-mineral oxidation in the Type I test pile was balanced by acid neutralization through carbonate mineral dissolution over time and near-neutral pH conditions prevail in the basal-drain effluent.

The initial results from this study showed near-neutral effluent in the Type I test pile corresponded to a population of neutrophilic S-oxidizing bacteria. The evolving effluent in the Type III test pile was accompanied by changes in the microbial populations. Elevated populations of acidophilic S-oxidizing bacteria and Fe-oxidizing bacteria were present each year. The microbial populations evolved with changes to the effluent chemistry; increased populations were observed with decreasing pH and increases in dissolved metals in the Type III test pile.

Table 4.1 Average elemental composition of waste rock used to construct the Type I (n = 6) and Type III (n = 31) waste-rock test piles determined by XRF.

%	Type III	Type I
SiO_2	70.9	73.7
Al_2O_3	15.9	15.0
Fe_2O_3	2.5	1.4
TiO_2	0.27	0.12
MgO	0.88	0.38
MnO	0.03	0.02
CaO	0.95	0.94
Na_2O	3.8	3.6
K_2O	4.8	5.0

Ppm	Type III	Type I
Ba	445	455
Rb	123	109
Sr	169	153
Pb	45	36
Cr	123	95
Cu	9.9	4.7
S	495	114
Zn	41	27
As	0.80	0.03
V	30	12
Ni	27	15
Co	5.5	4.0

Table 4.2 Estimates of sulfide minerals in the waste rock used to construct the Type III waste-rock test pile. Average moles per unit mass of metals (mmol kg^{-1}) for chalcopyrite, sphalerite, and pyrrhotite.

mmol kg^{-1}	Mass	Moles in Chalcopyrite	Moles in Sphalerite	Moles S remaining	Moles Pyrrhotite	Residual Ni, Co, Fe
		$CuFeS_2$	(Zn,Fe)S		$Fe_{0.0852}(Ni_{0.004}Co_{0.001})S$	
Total S	15	0.34	1.42	13.24	13.24	
Total Cu	0.17	0.17				
Total Zn	0.71		0.71			
Total Ni	0.52				0.62	-0.10
Total Co	0.11				0.16	-0.05
Total Fe	150	0.17	0.71		13.24	136.76

Table 4.3 Estimate of the average moles per unit mass (mmol kg^{-1}) for K, Fe, and Mg from biotite in the waste rock used to construct the Type III waste-rock test pile.

	Mass (mmol kg^{-1})	Moles of Biotite (mmol kg^{-1})	Residual K, Fe and Mg (mmol kg^{-1})
		$K(Mg,Fe)_3(AlSi_3O_{10})(F,OH)_2$	
Total Fe	150	93.5	43.3
Total Mg	250	187	63
Total K	500	502	-2.0

Table 4.4 Calculated mass loadings for parameters of interest from the Type I and Type III test piles (2007 to 2010).

Type III test pile	2007	2008	2009	2010	Total
Ca (kg)	8.5	12	13	29	63
K (kg)	3.0	6.0	6.2	11	26
Mg (kg)	9.3	13	21	39	82
Na (kg)	3.9	4.5	6.6	13	28
Al (g)	21	30	140	300	491
Fe (g)	28	18	22	20	88
Co (g)	19	46	89	170	324
Ni (g)	110	230	460	1,000	1800
Cu (g)	5.5	46	51	61	164
Zn (g)	22	64	110	210	406
S (kg)	17	27	19	66	129
Flow (x10^3 L)	49	130	110	210	499

Type I test pile	2007	2008	2009	2010	
Ca (kg)	0.0084	6.3	0.51	28	35
K (kg)	0.0022	2.3	0.19	4.4	6.9
Mg (kg)	0.003	3.6	0.32	12	16
Na (kg)	0.0017	2.2	0.14	6.7	9.0
Al (g)	0.043	15	1.5	9.6	26
Fe (g)	1.8	8.9	0.62	5.0	16.3
Co (g)	nd	0.6	0.093	2.5	3.2
Ni (g)	0.0065	4.6	1.0	17	23
Cu (g)	0.46	20	1.5	0.74	23
Zn (g)	0.070	6.2	0.11	1.7	8.1
S (kg)	0.026	3.8	0.46	7.6	11.9
Flow (x10^3 L)	4.0	76	9.1	44	133

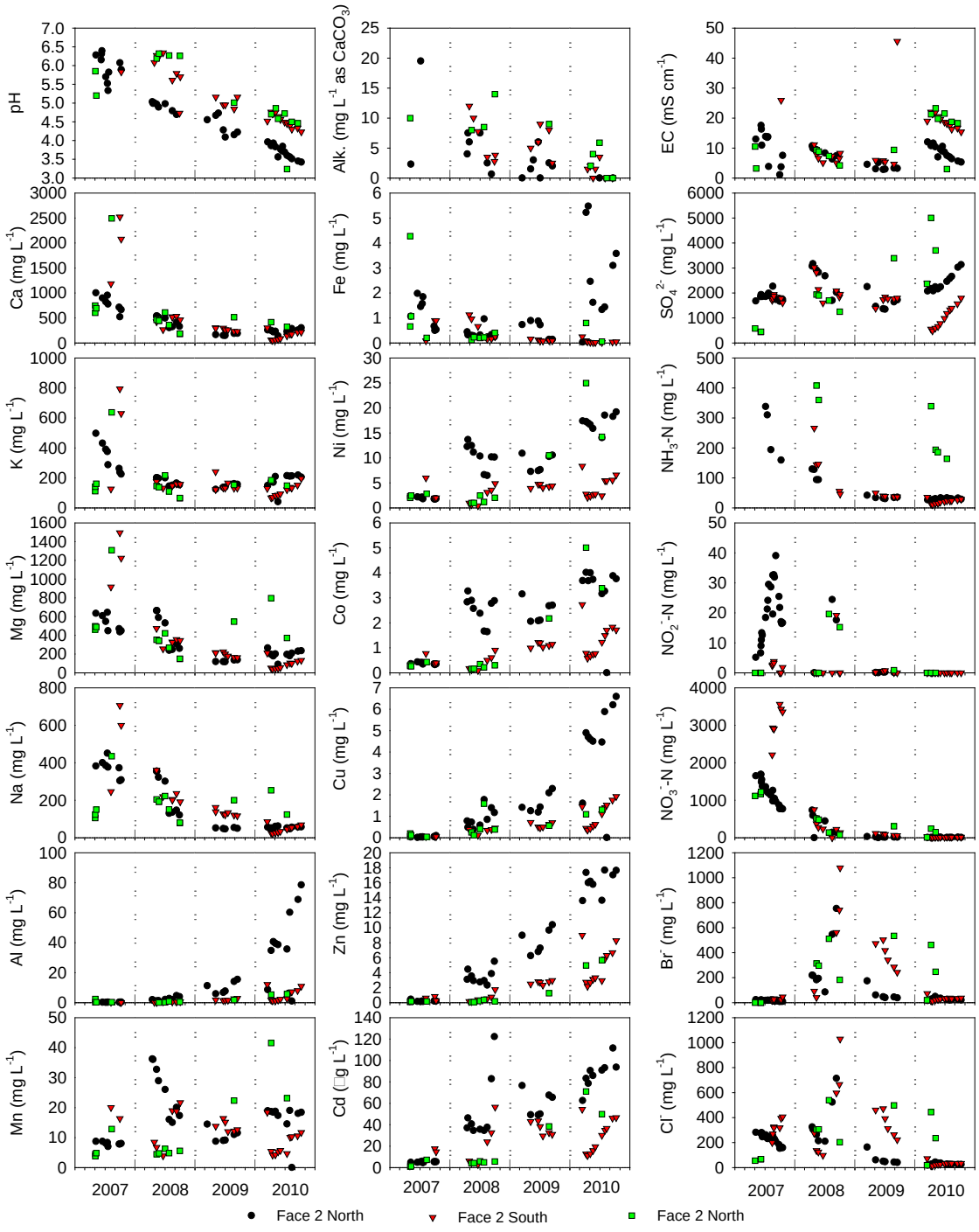

Figure 4.1 Pore-water chemistry in the Type III test pile at 3-m depth.

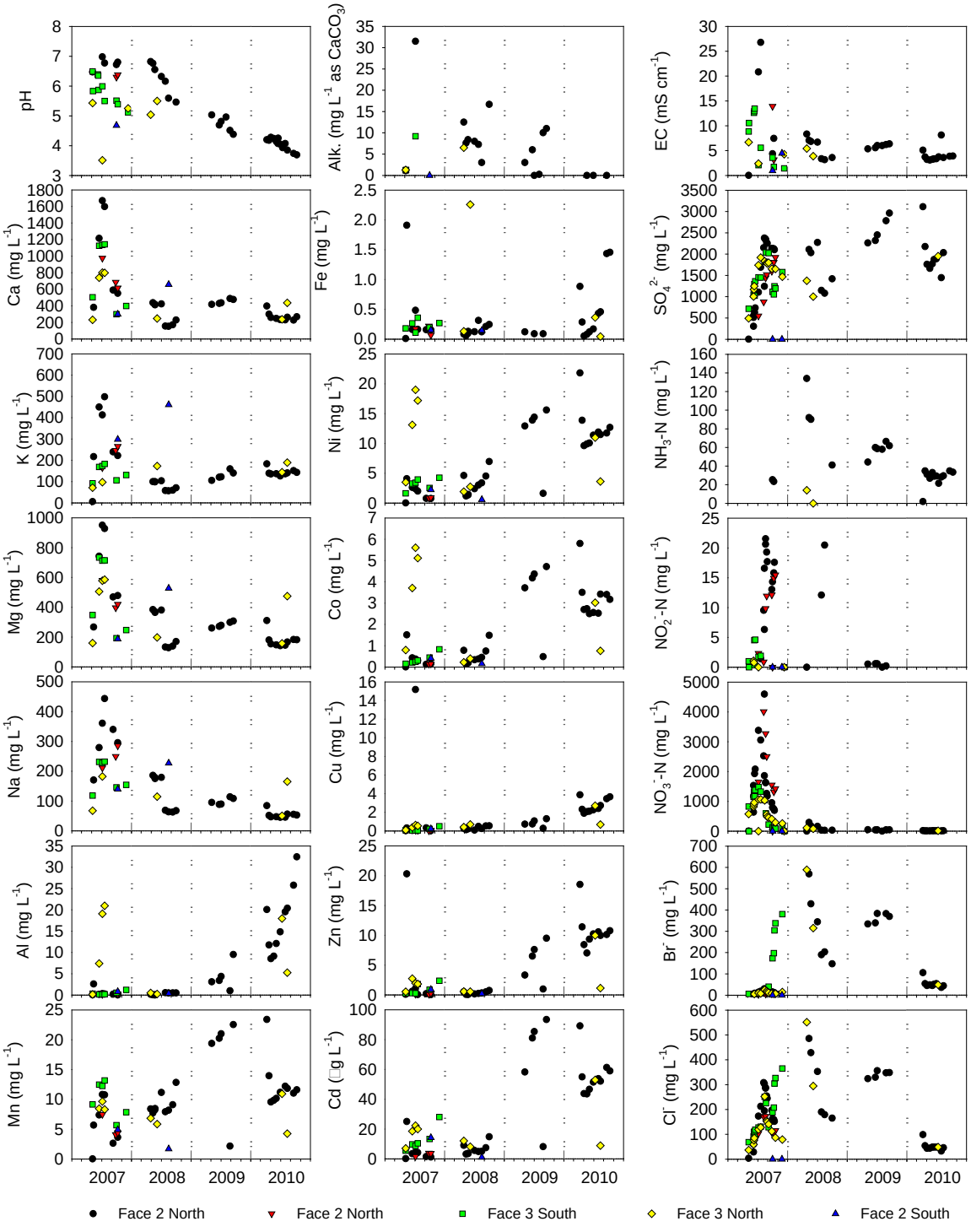

Figure 4.2 Pore-water chemistry in the Type III test pile at 5-m depth.

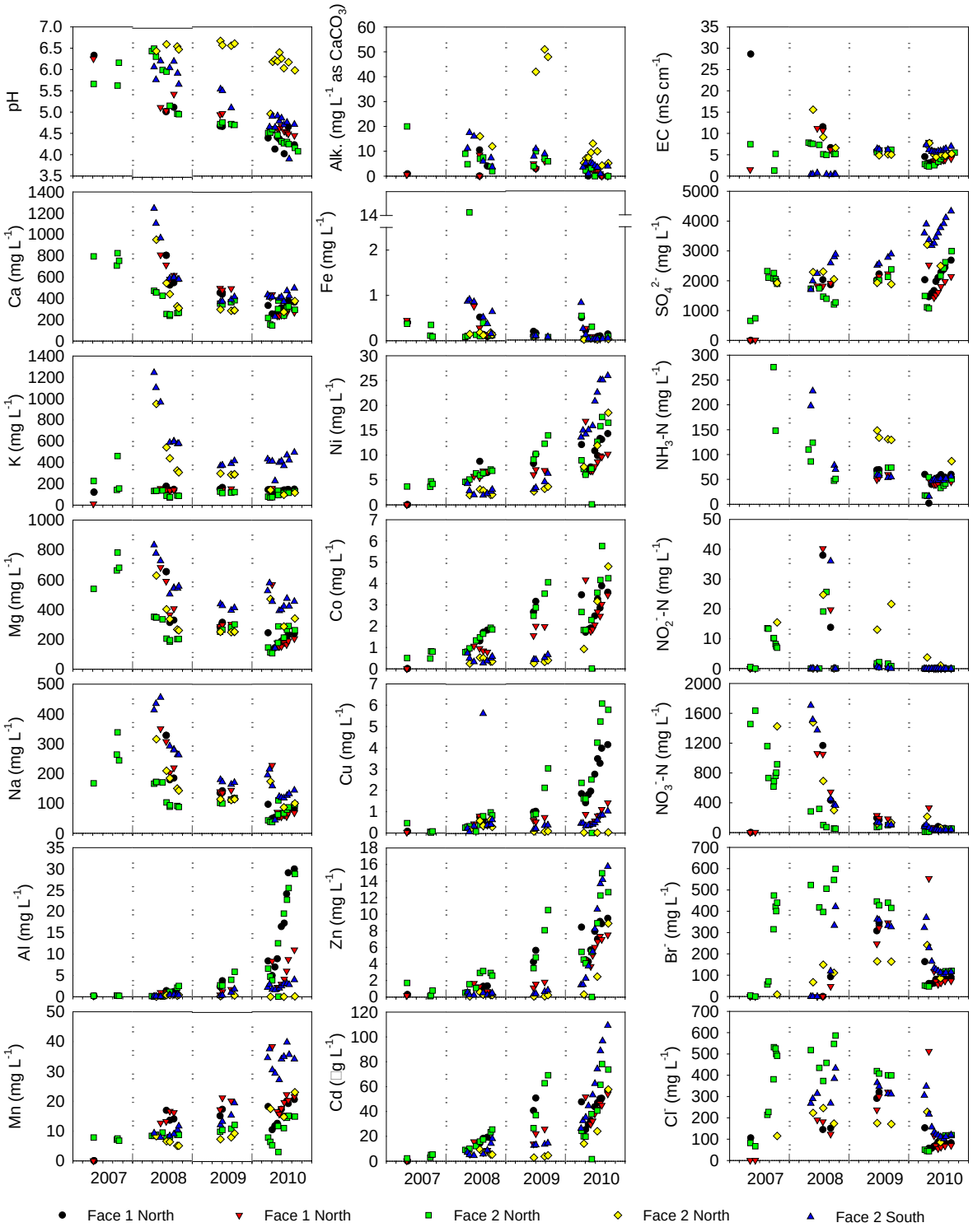

Figure 4.3 Pore-water chemistry in the Type III test pile at 7-m depth.

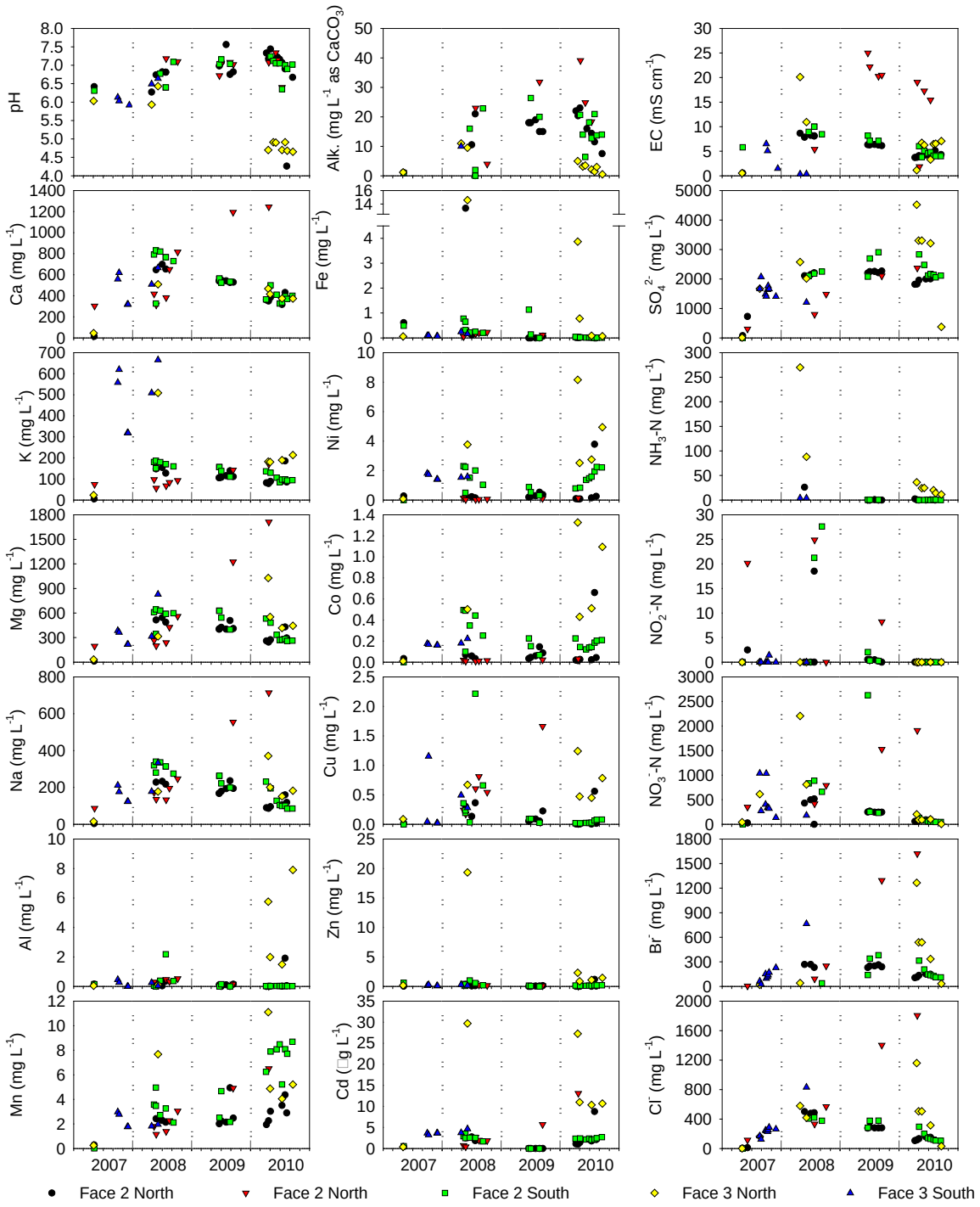

Figure 4.4 Pore-water chemistry in the Type III test pile at 9-m depth.

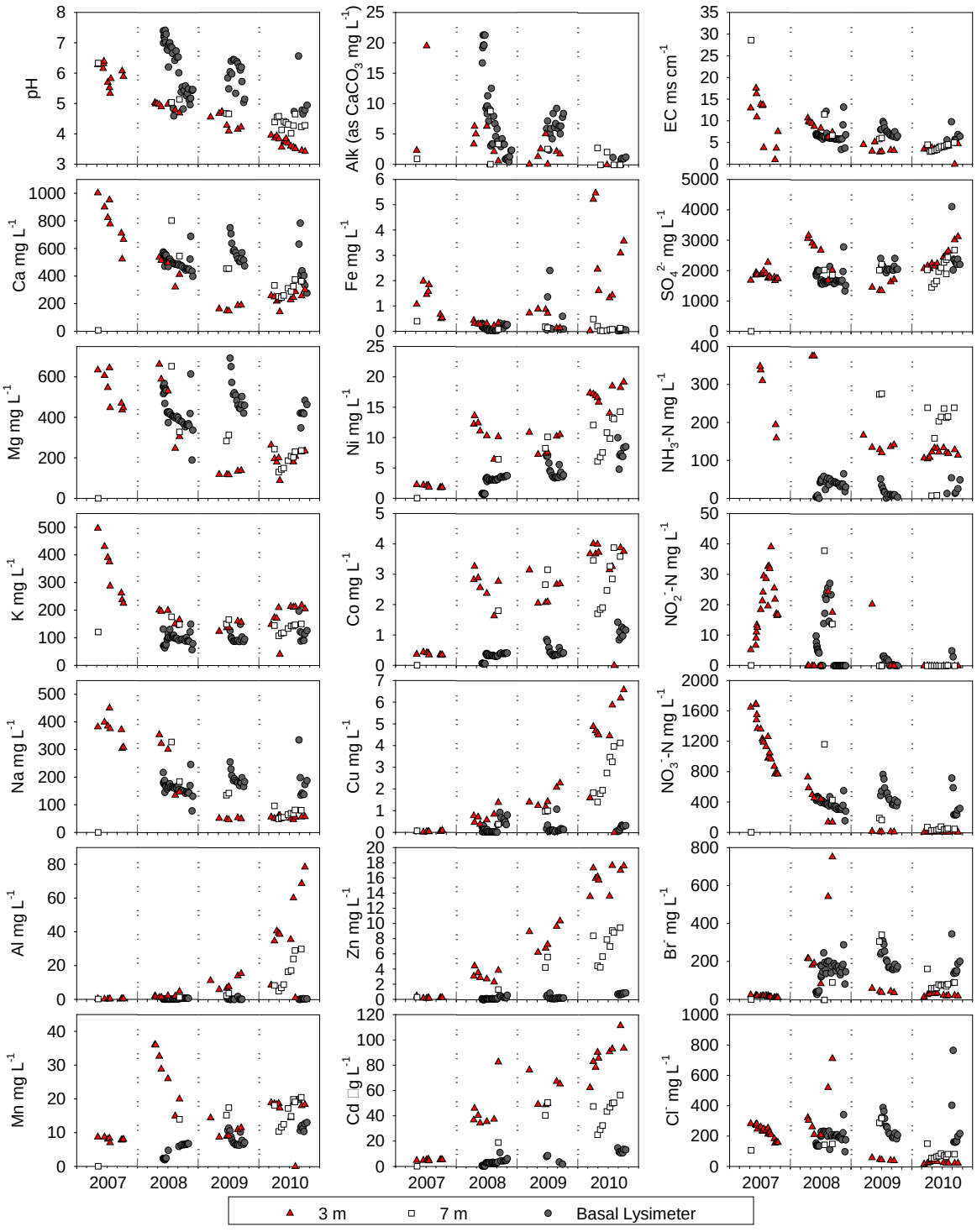

Figure 4.5 Pore-water chemistry samples collected from the centre of the pile at 3-m and 7-m depths in the Type III test pile and in the 4 m by 4 m basal lysimeter.

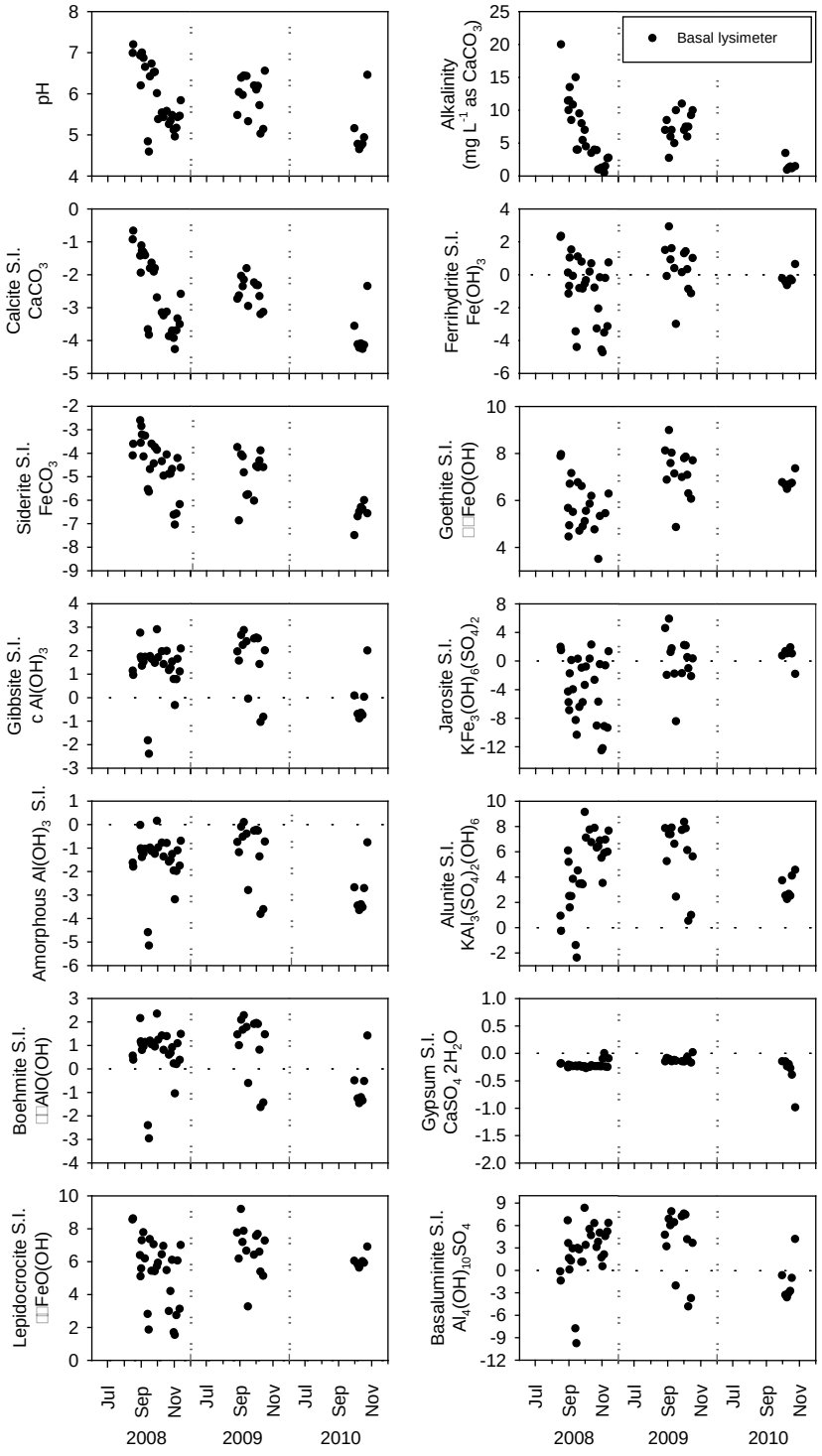

Figure 4.6 Time series plots of calculated saturation indices (SIs) using MINTEQA2 for effluent from the basal lysimeter in the Type III test pile. The dashed black line at 0 represents equilibrium.

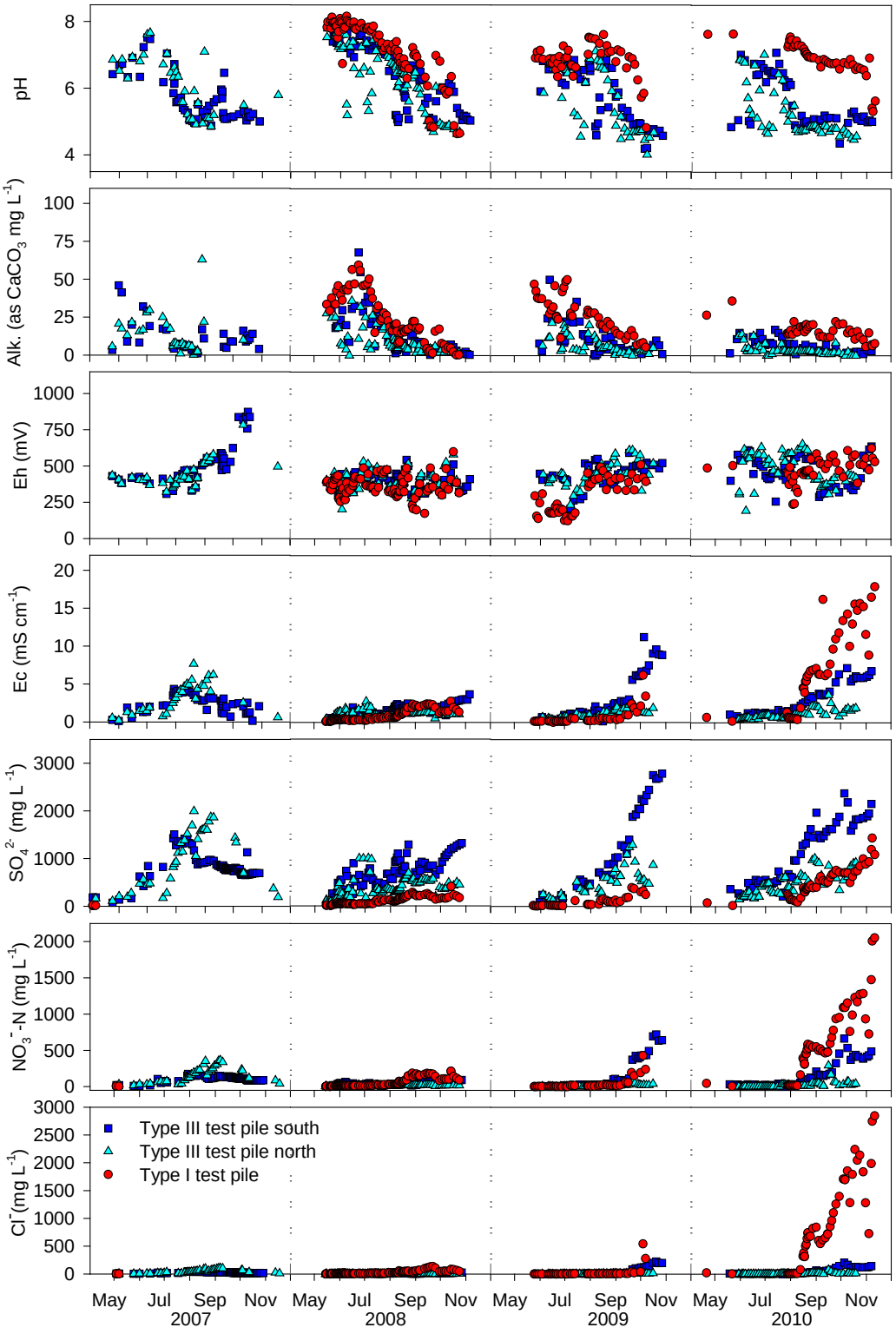

Figure 4.7 Type I test-pile drain and Type III test-pile north and south drain water chemistry.

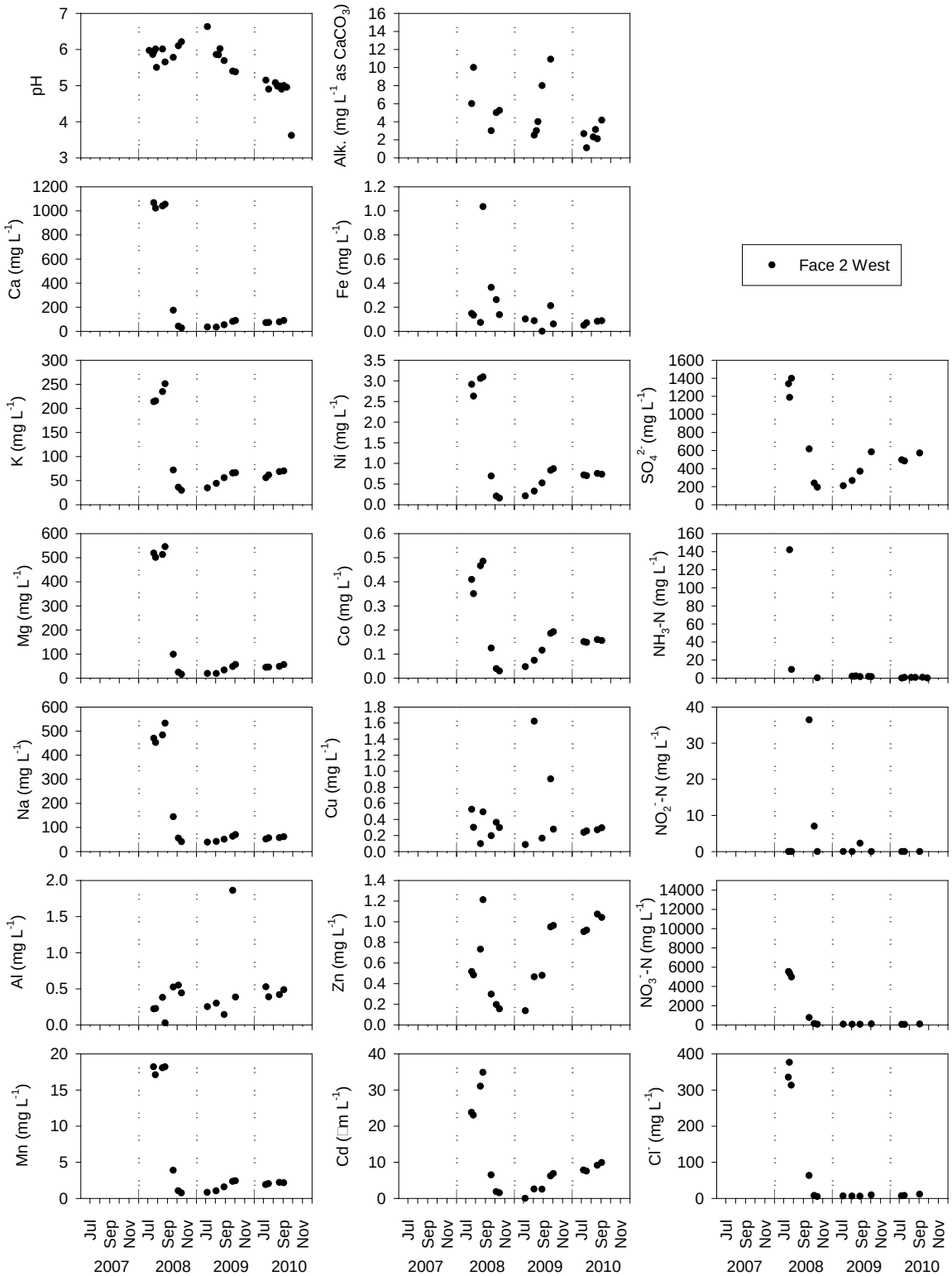

Figure 4.8 Pore-water chemistry in the Type I test pile at 1-m depth.

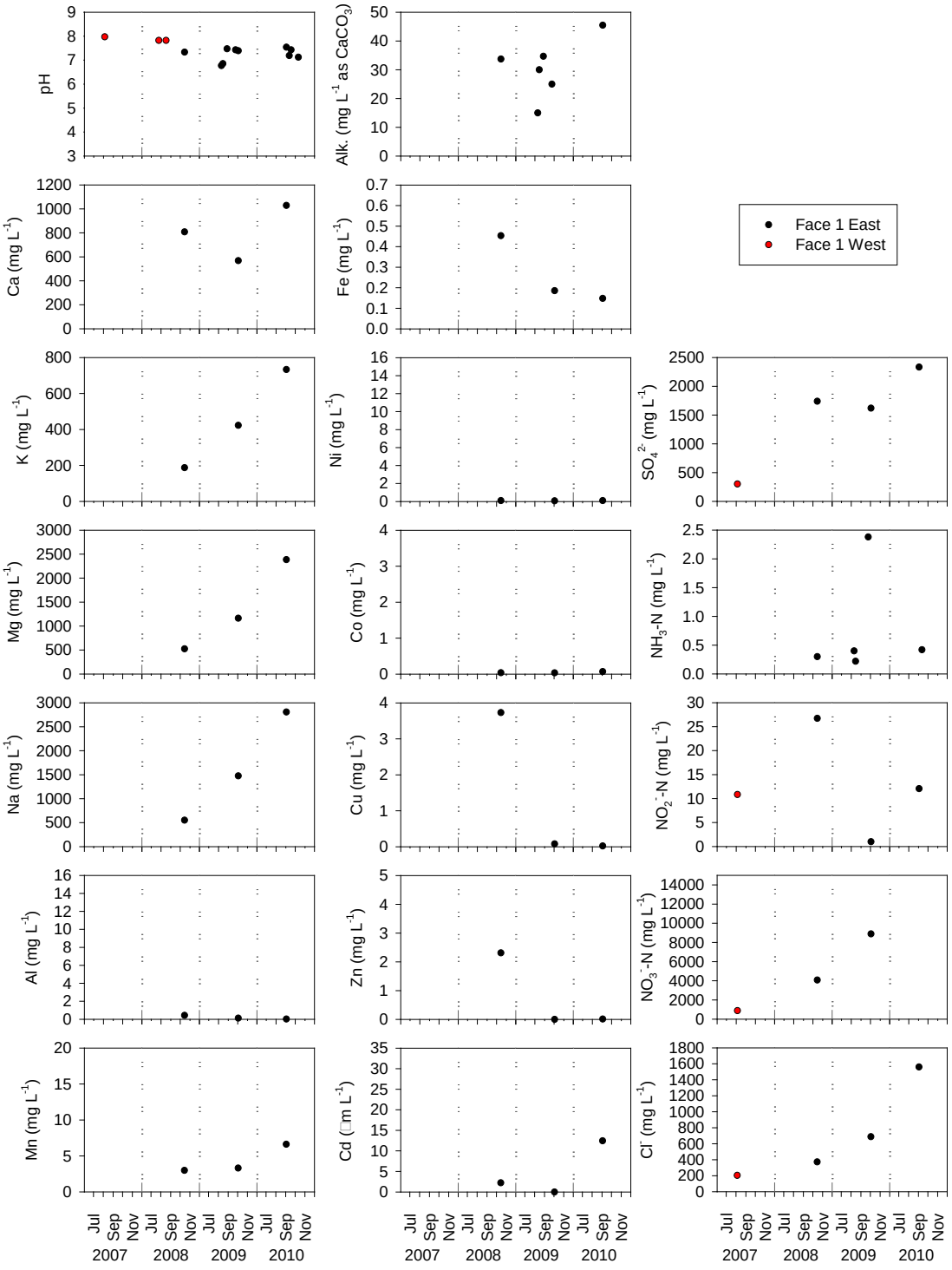

Figure 4.9 Pore-water chemistry in the Type I test pile at 2-m depth.

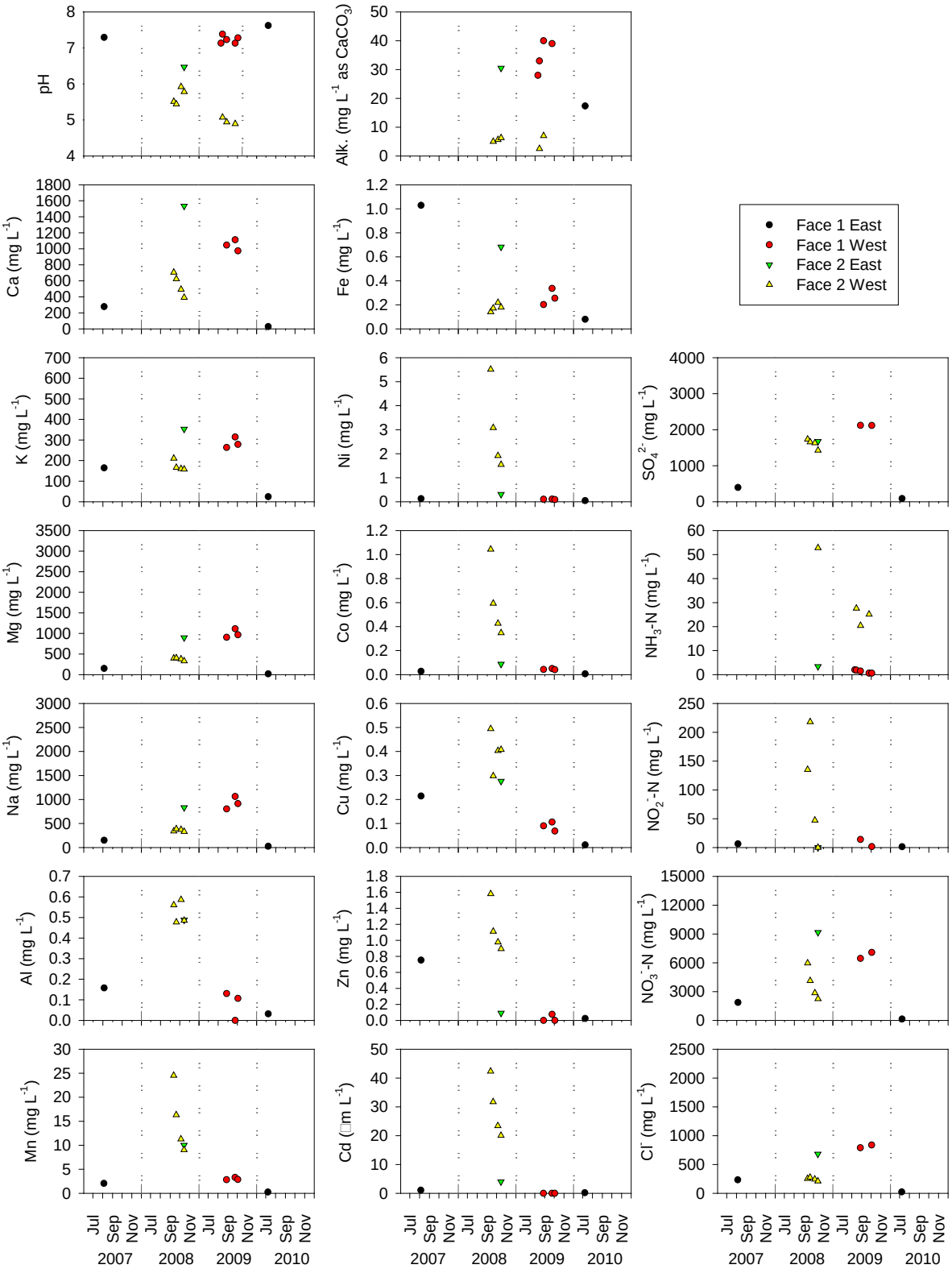

Figure 4.10 Pore-water chemistry in the Type I test pile at 5-m depth.

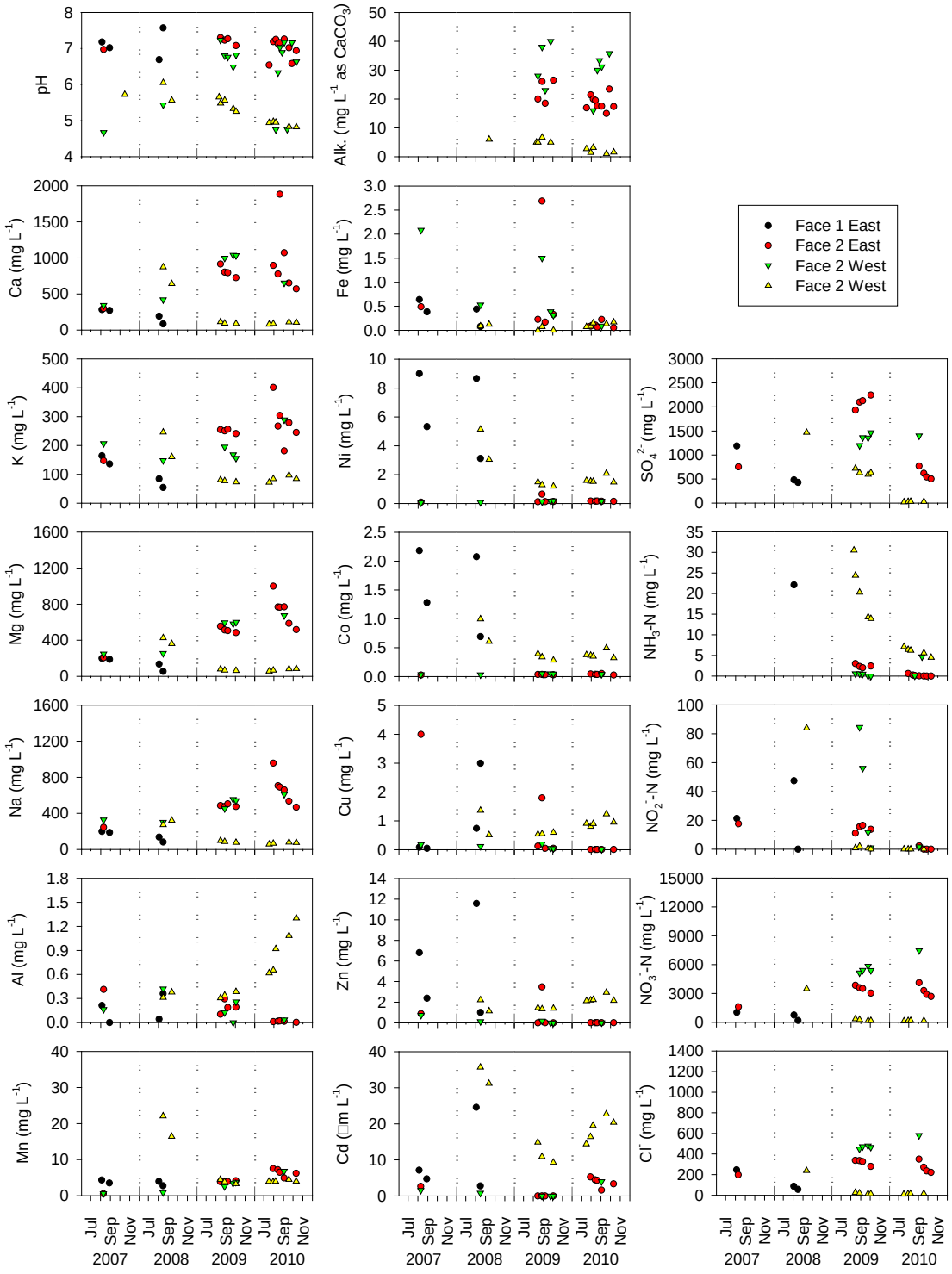

Figure 4.11 Pore-water chemistry in the Type I test pile at 7-m depth.

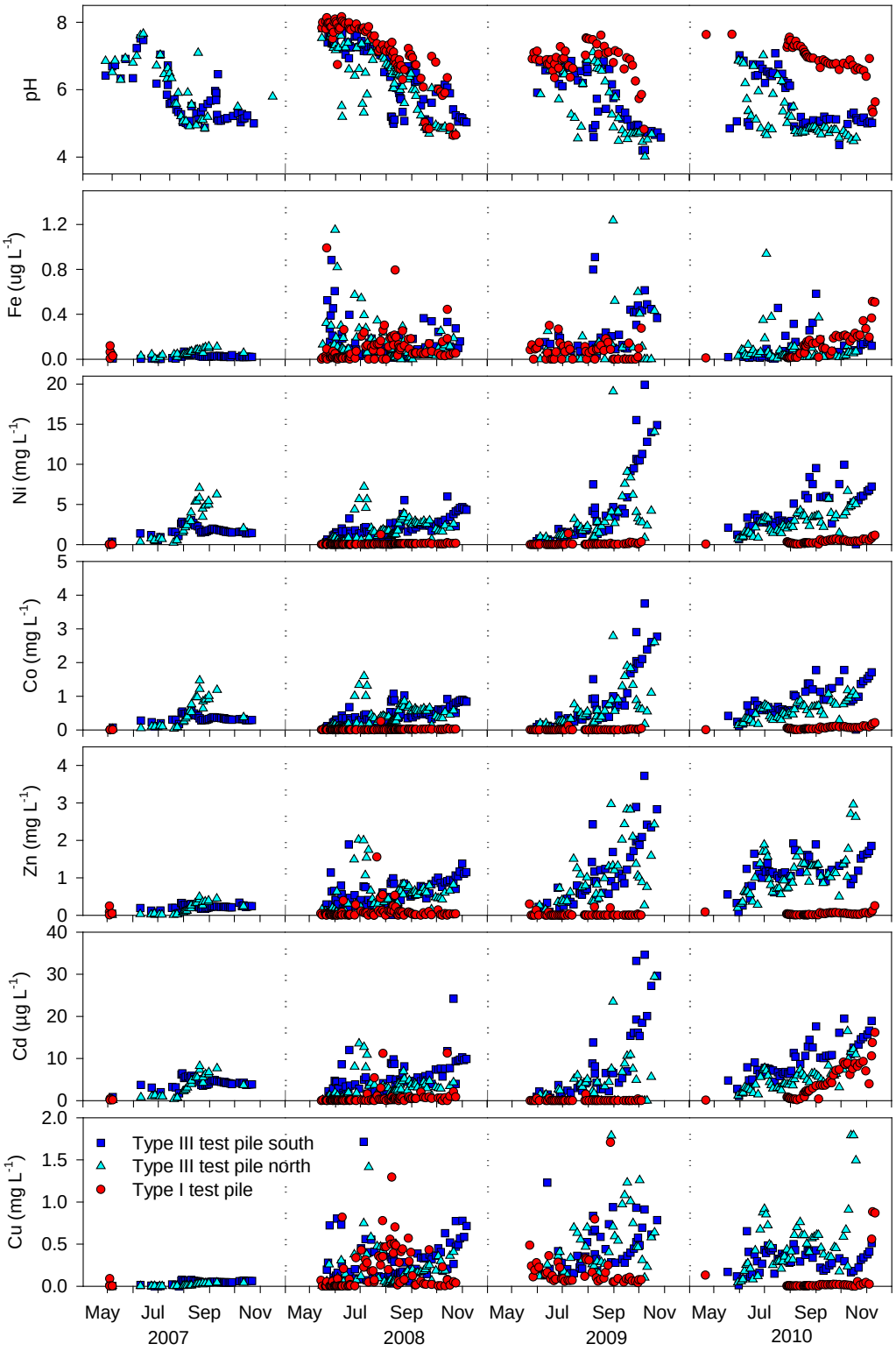

Figure 4.12 Concentrations of dissolved metals in Type I test-pile drain and Type III test-pile north and south drains.

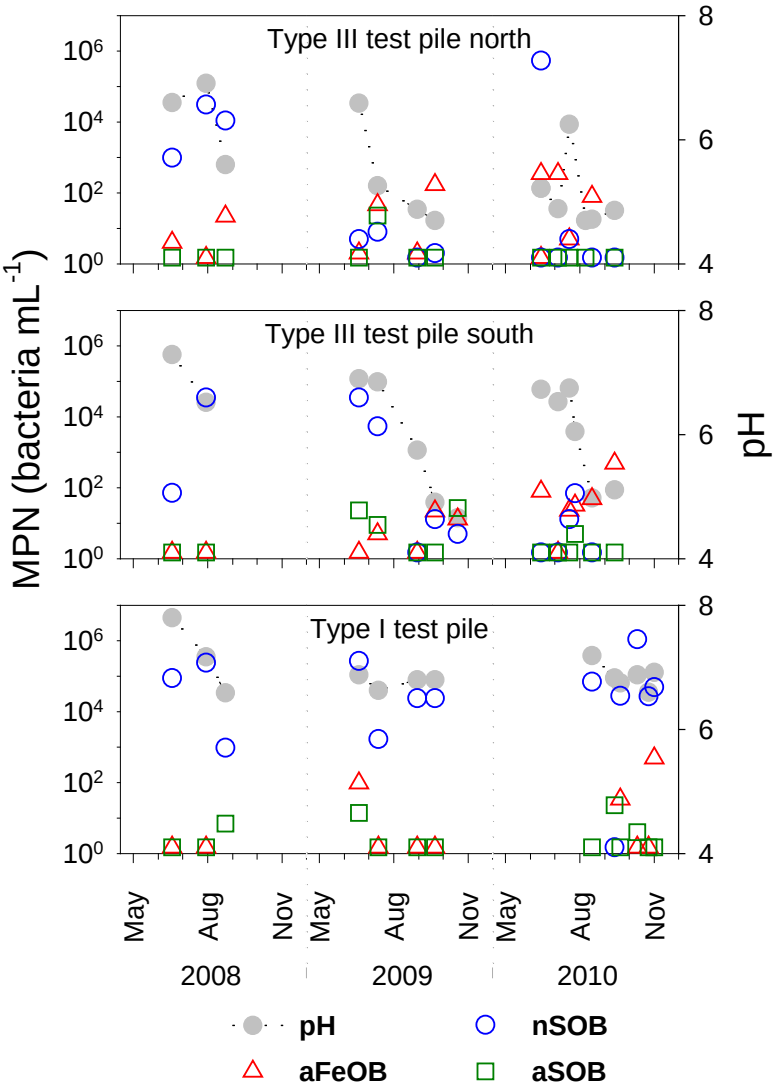

Figure 4.13 Populations of aFeOB, nSOB, and aSOB in the Type I test-pile drain and the Type III test-pile north and south drains.

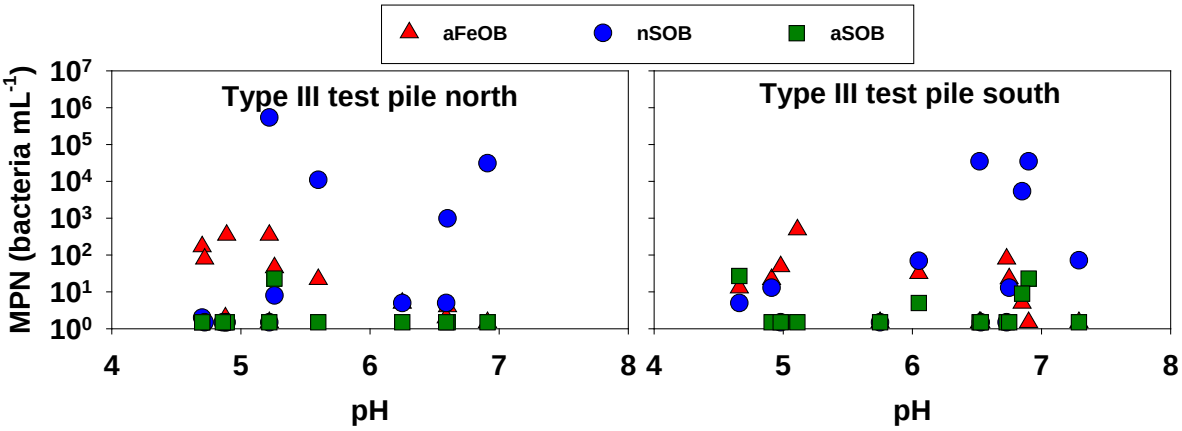

Figure 4.14 Populations of aFeOB, nSOB, and aSOB in the Type III test-pile north and south drains compared to pH.

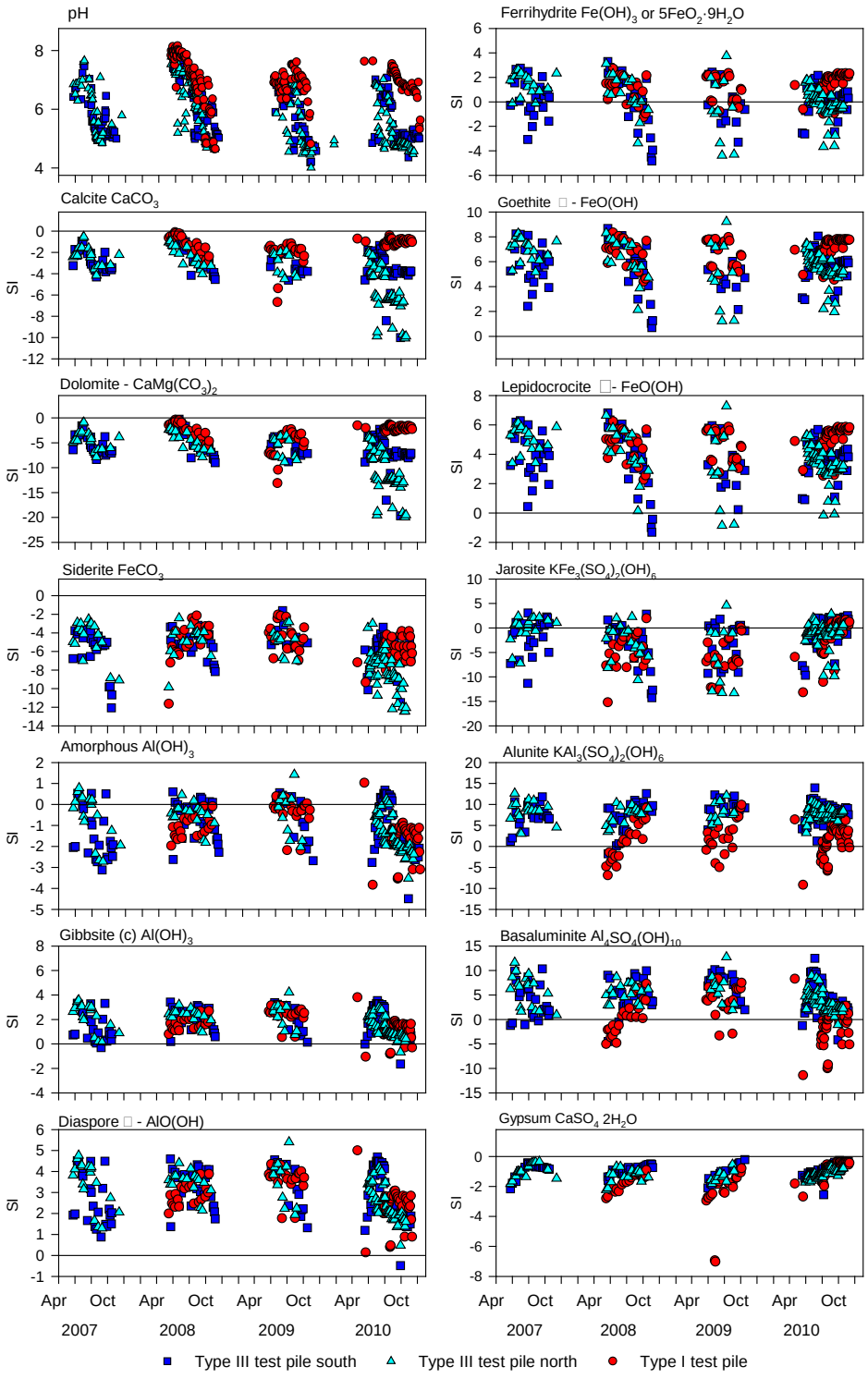

Figure 4.15 Time series plots of calculated saturation indices (SIs), using MINTEQA2 for the Type I test-pile drain and Type III test-pile north and south drains. The solid black line at 0 represents equilibrium.

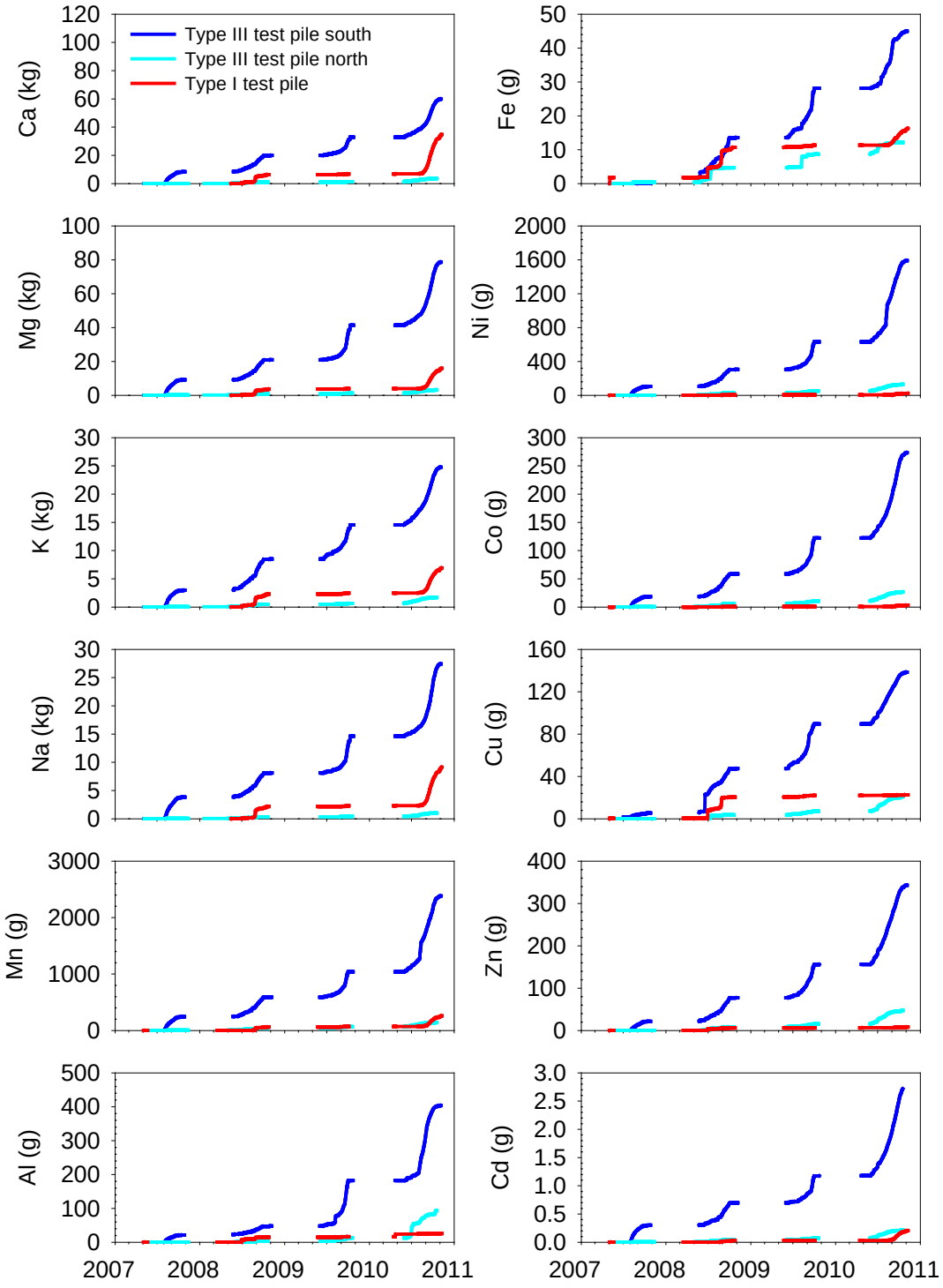

Figure 4.16 Type I test-pile drain and Type III test-pile north and south drains cumulative mass loading for select elements.

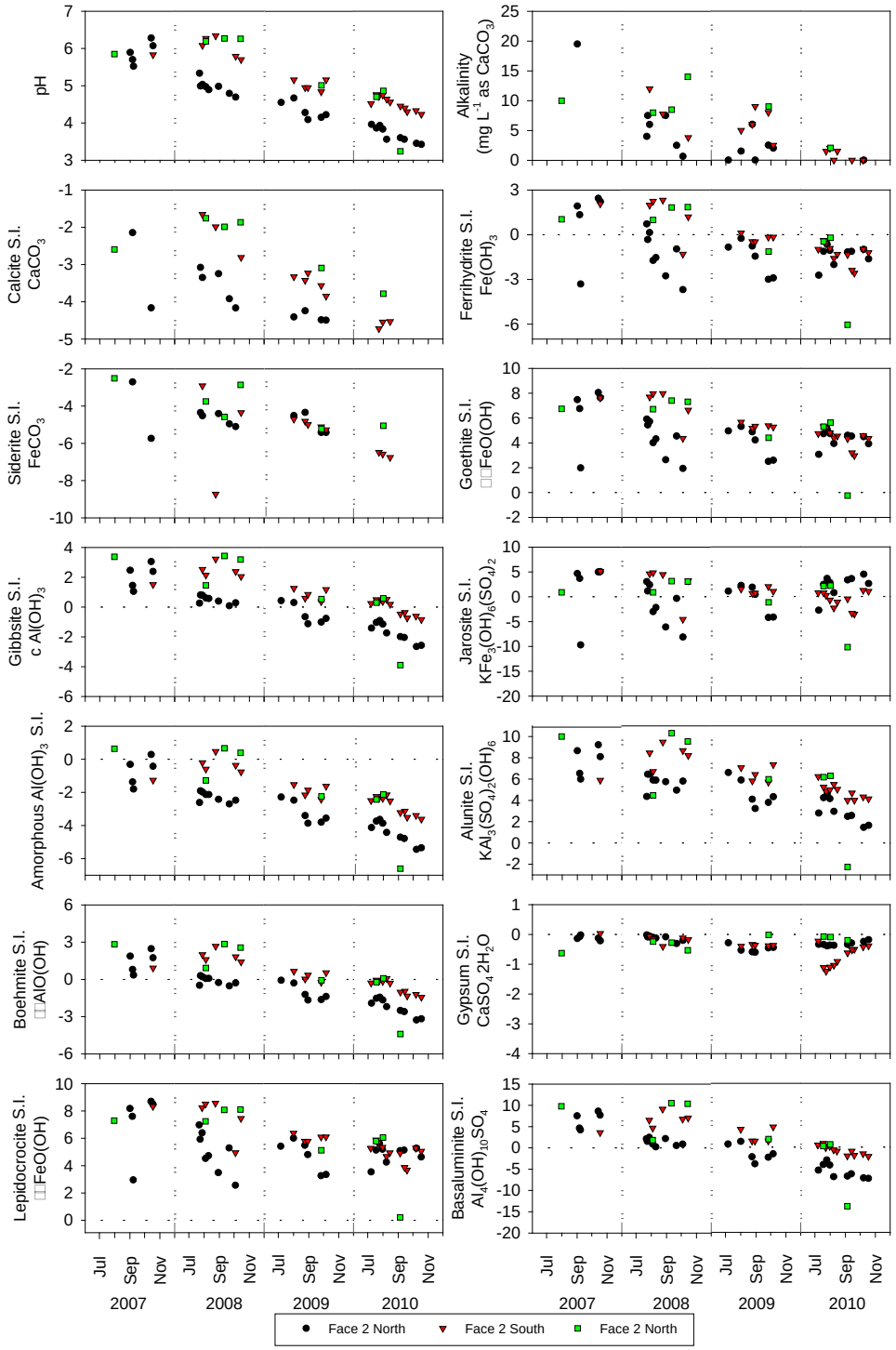

Figure 4.17 Time series plots of calculated saturation indices (SI) using MINTEQA2 for pore water at the 3-m depth in the Type III test pile. The dashed black line at 0 represents equilibrium.

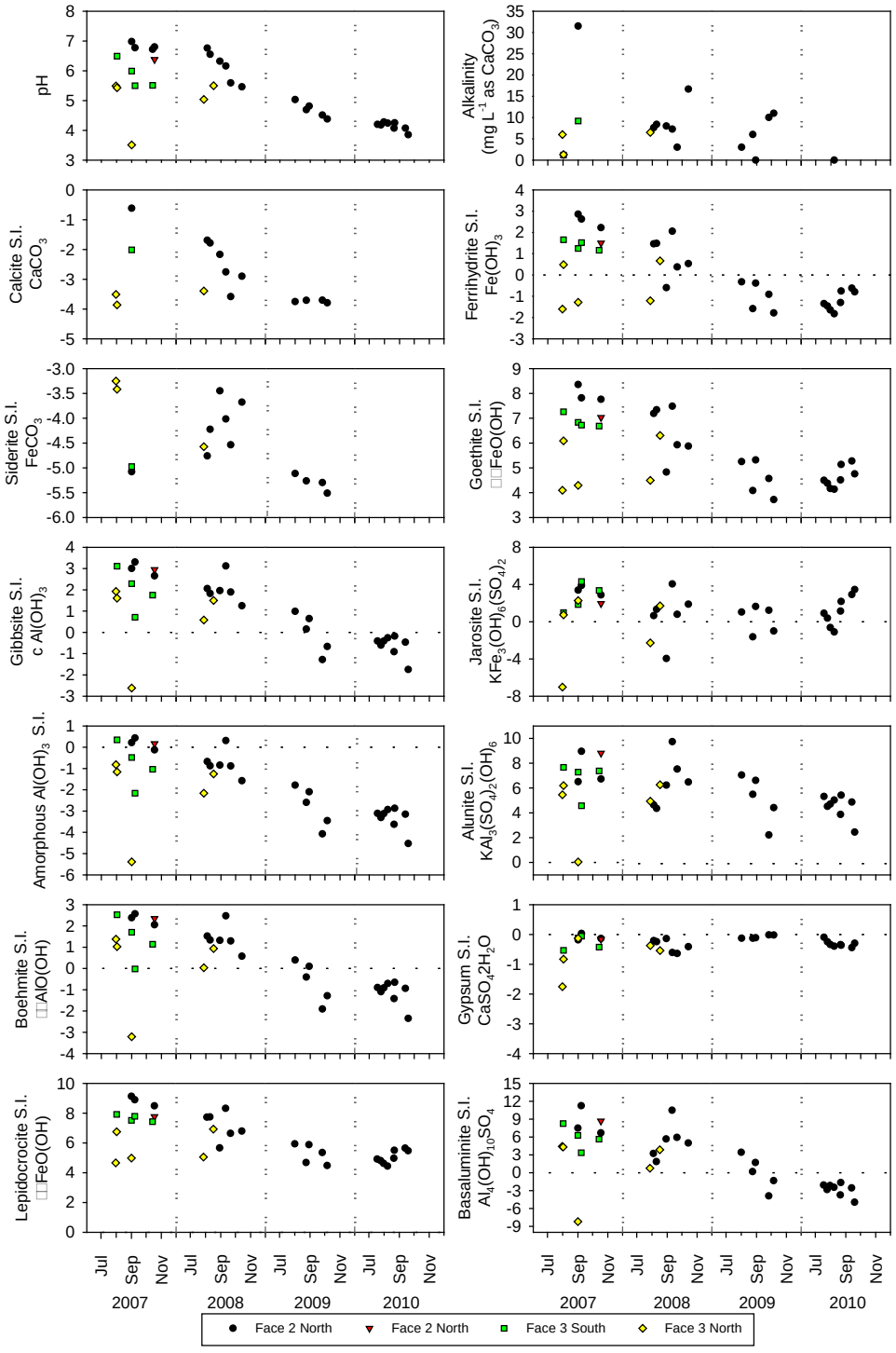

Figure 4.18 Time series plots of calculated saturation indices (SIs) using MINTEQA2 for pore water at the 5-m depth in the Type III test pile. The dashed black line at 0 represents equilibrium.

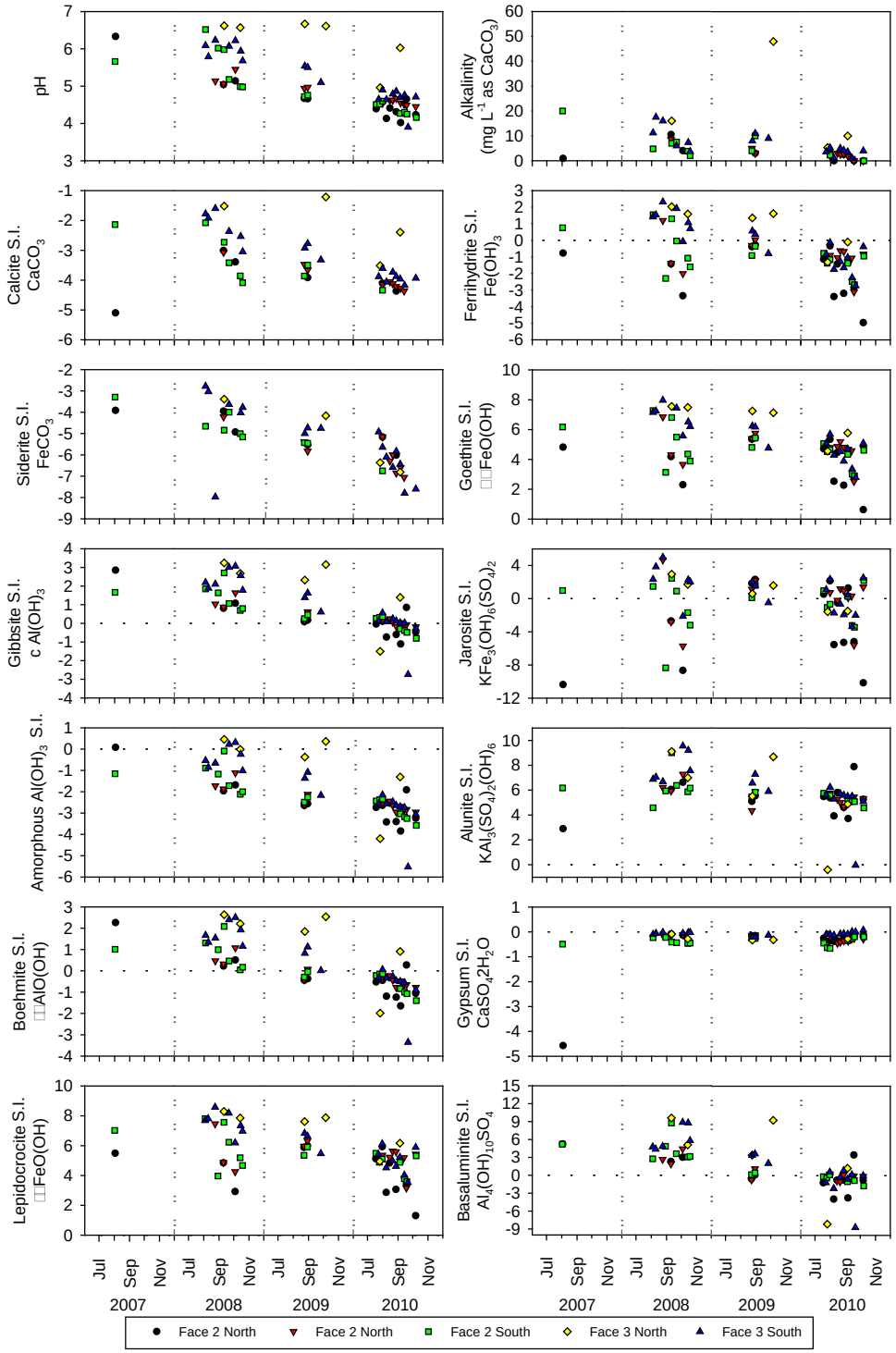

Figure 4.19 Time series plots of calculated saturation indices (SIs) using MINTEQA2 for pore water at the 7-m depth in the Type III test pile. The dashed black line at 0 represents equilibrium.

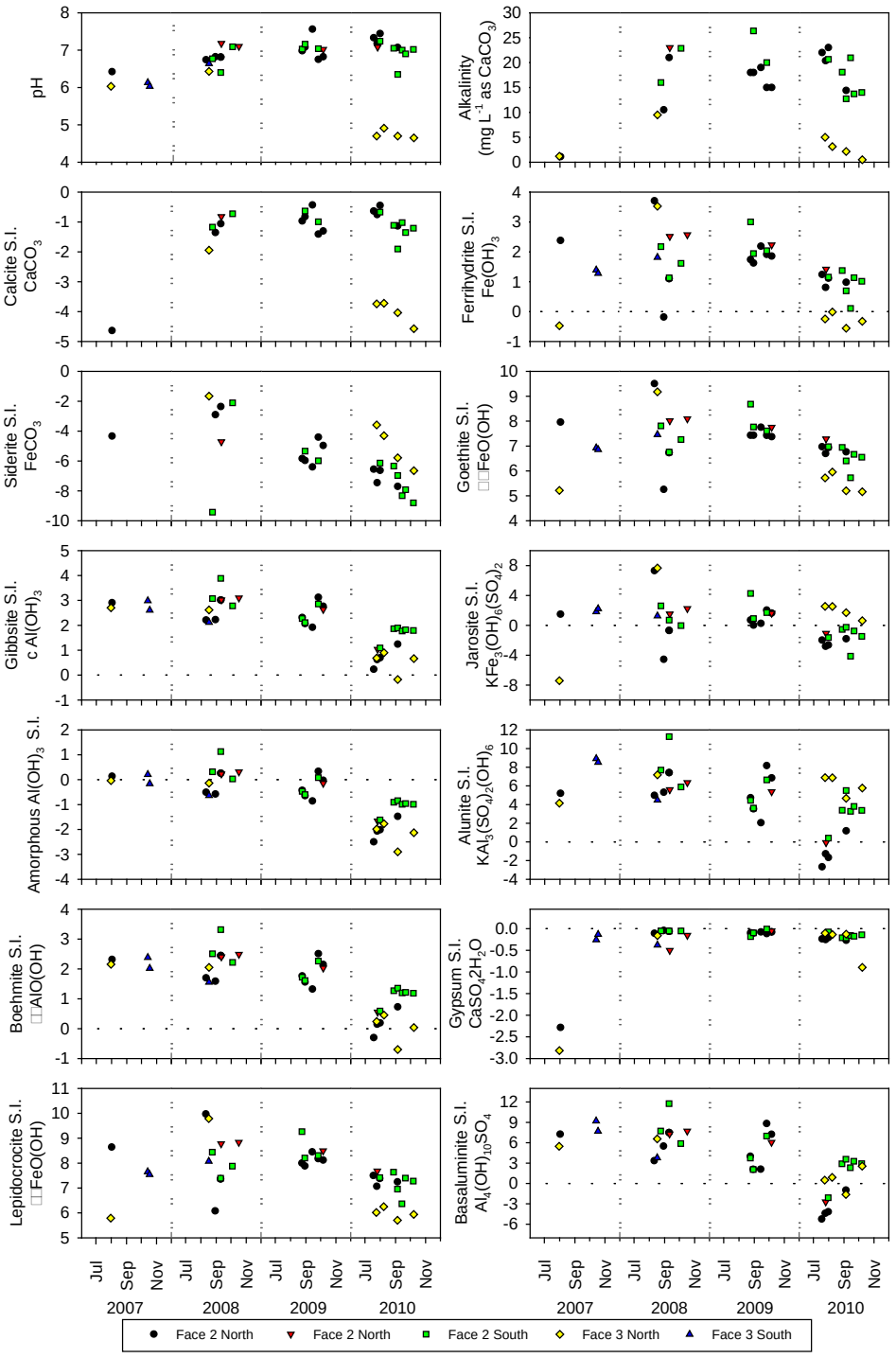

Figure 4.20 Time series plots of calculated saturation indices (SIs) using MINTEQA2 for pore water at the 9-m depth in the Type III test pile. The dashed black line at 0 represents equilibrium.

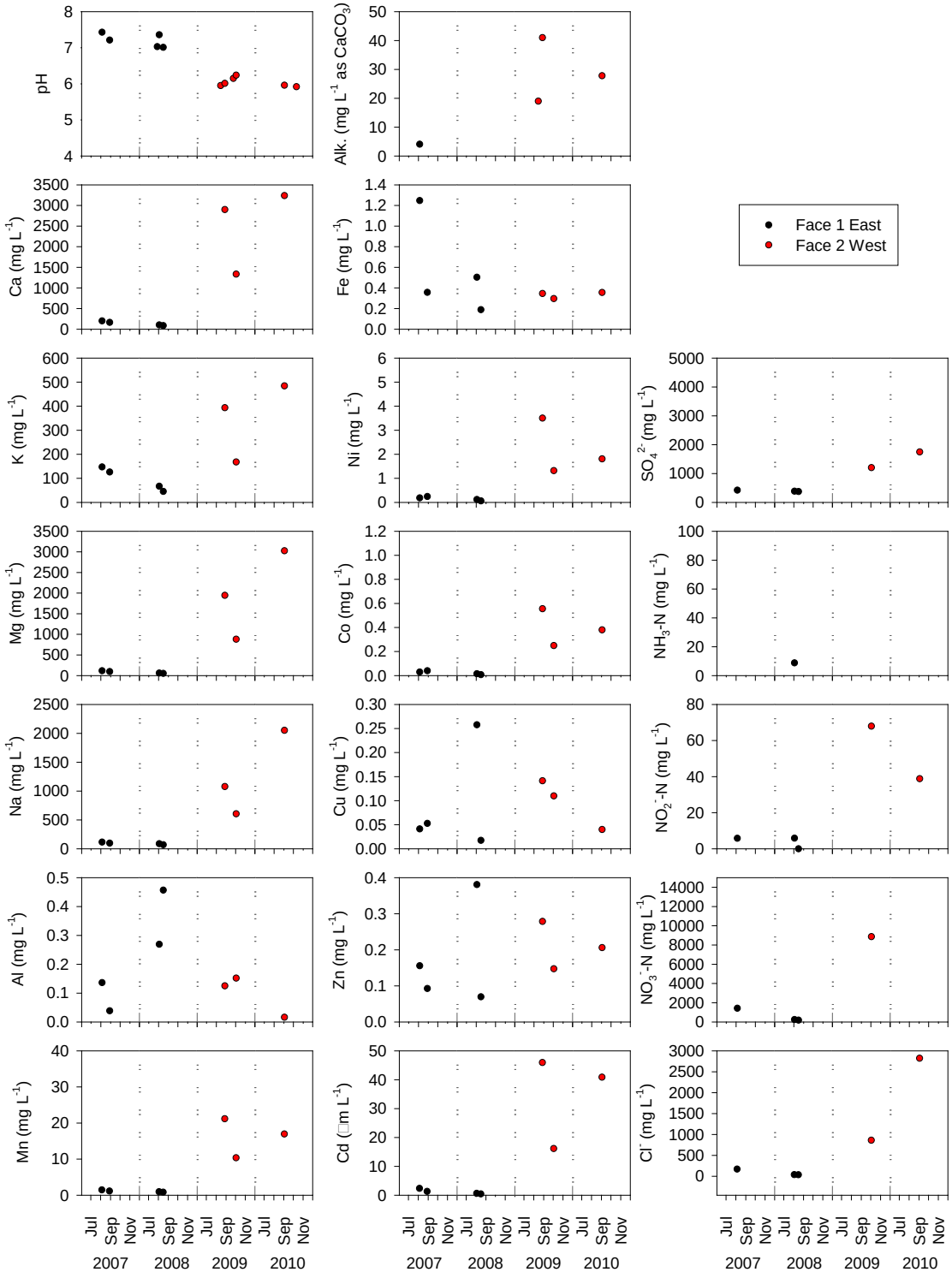

Figure 4.21 Pore-water chemistry in the Type I test pile at 9-m depth.

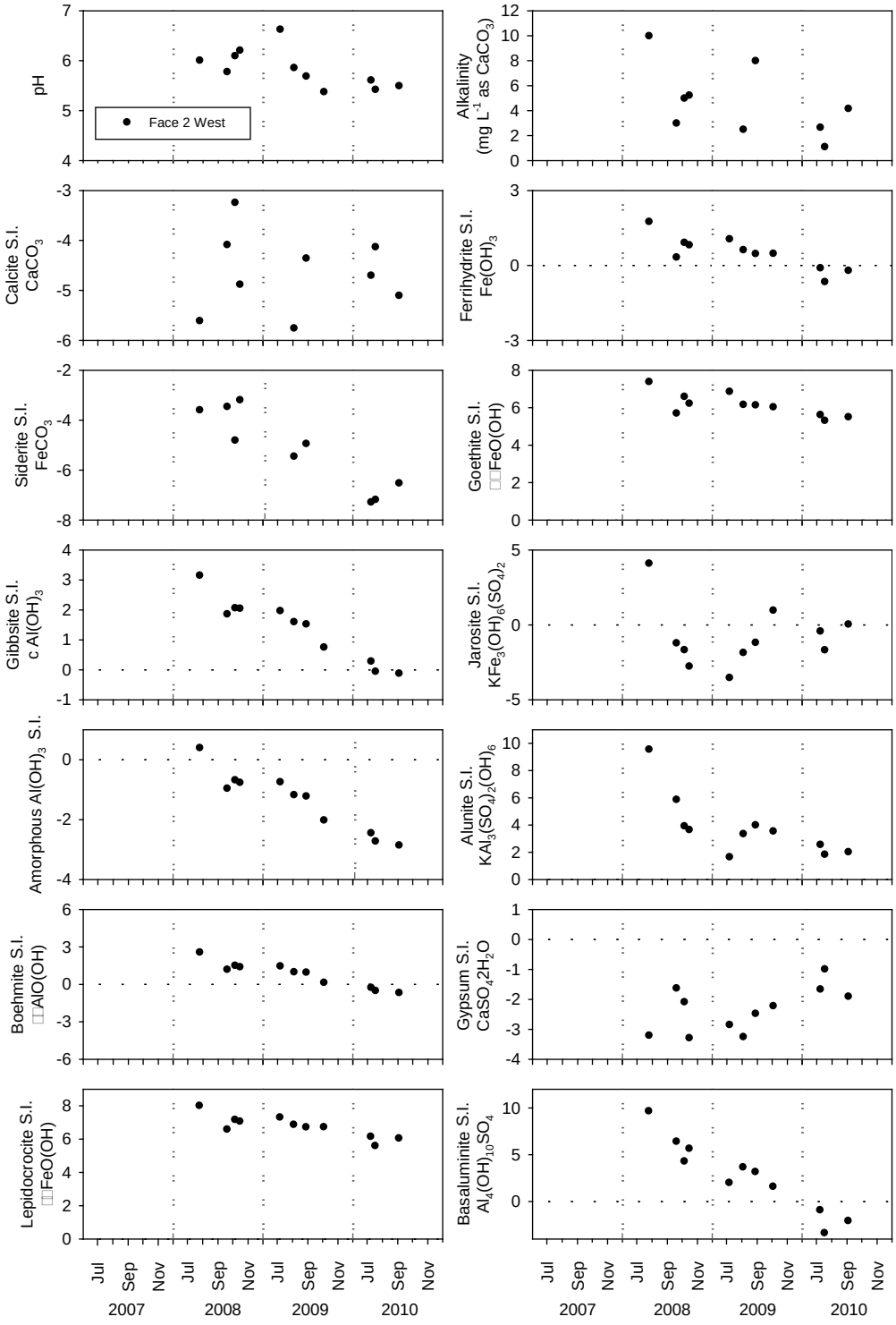

Figure 4.22 Time series plots of calculated saturation indices (SIs) using MINTEQA2 for pore water at the 1-m depth in the Type I test pile. The dashed black line at 0 represents equilibrium.

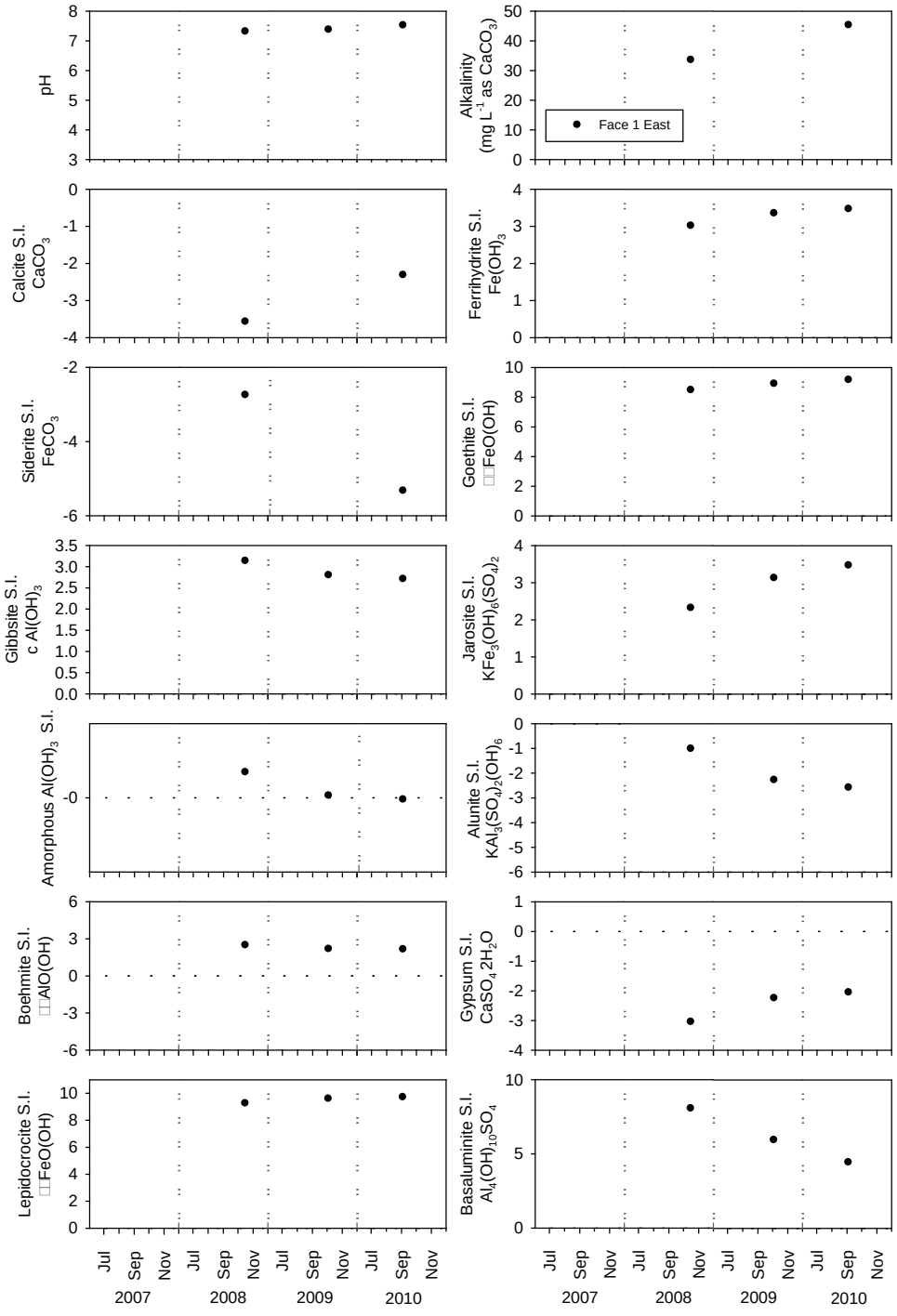

Figure 4.23 Time series plots of calculated saturation indices (SIs) using MINTEQA2 for pore water at the 2-m depth in the Type I test pile. The dashed black line at 0 represents equilibrium.

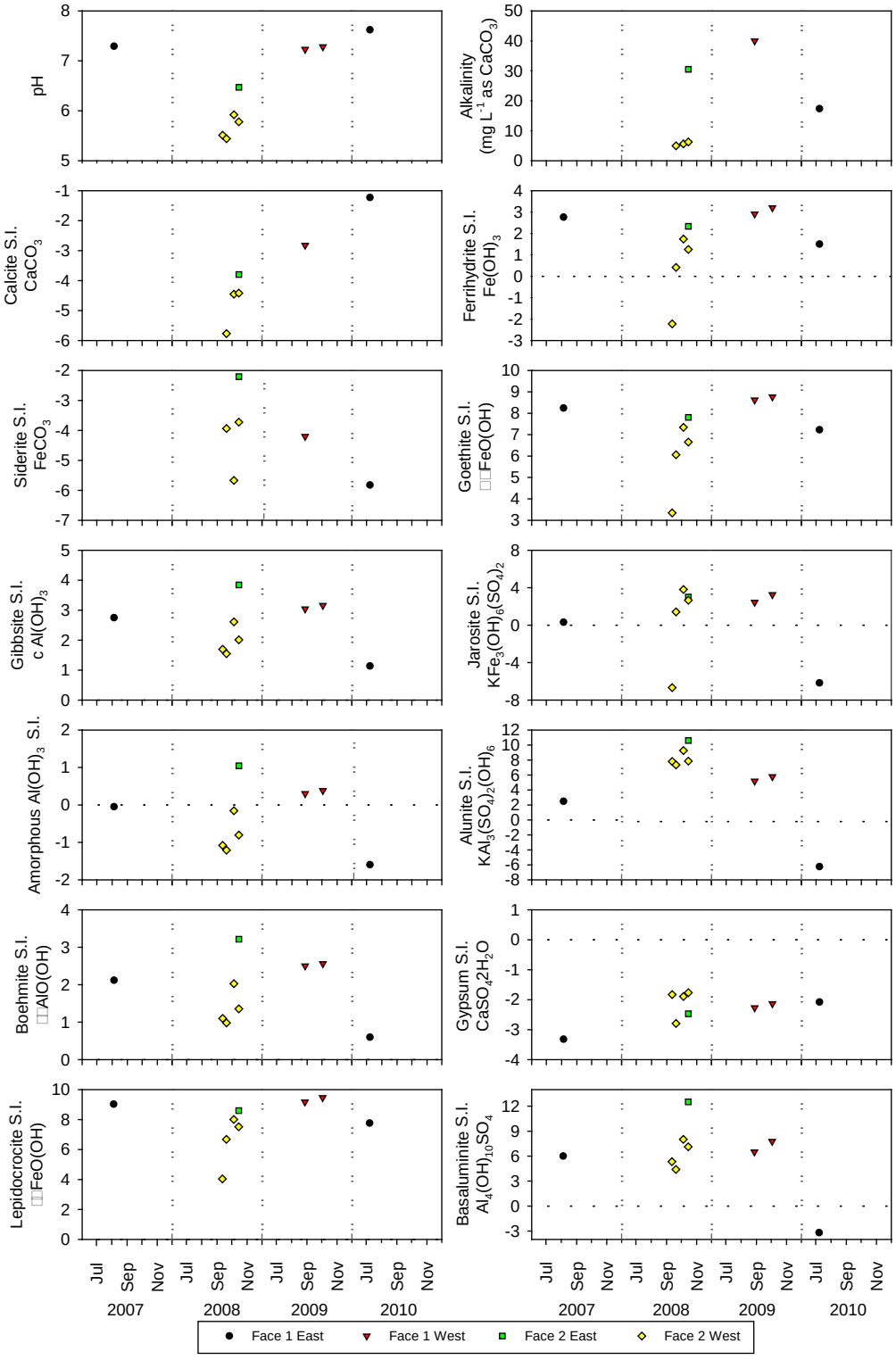

Figure 4.24 Time series plots of calculated saturation indices (SIs) using MINTEQA2 for pore water at the 5-m depth in the Type I test pile. The dashed black line at 0 represents equilibrium.

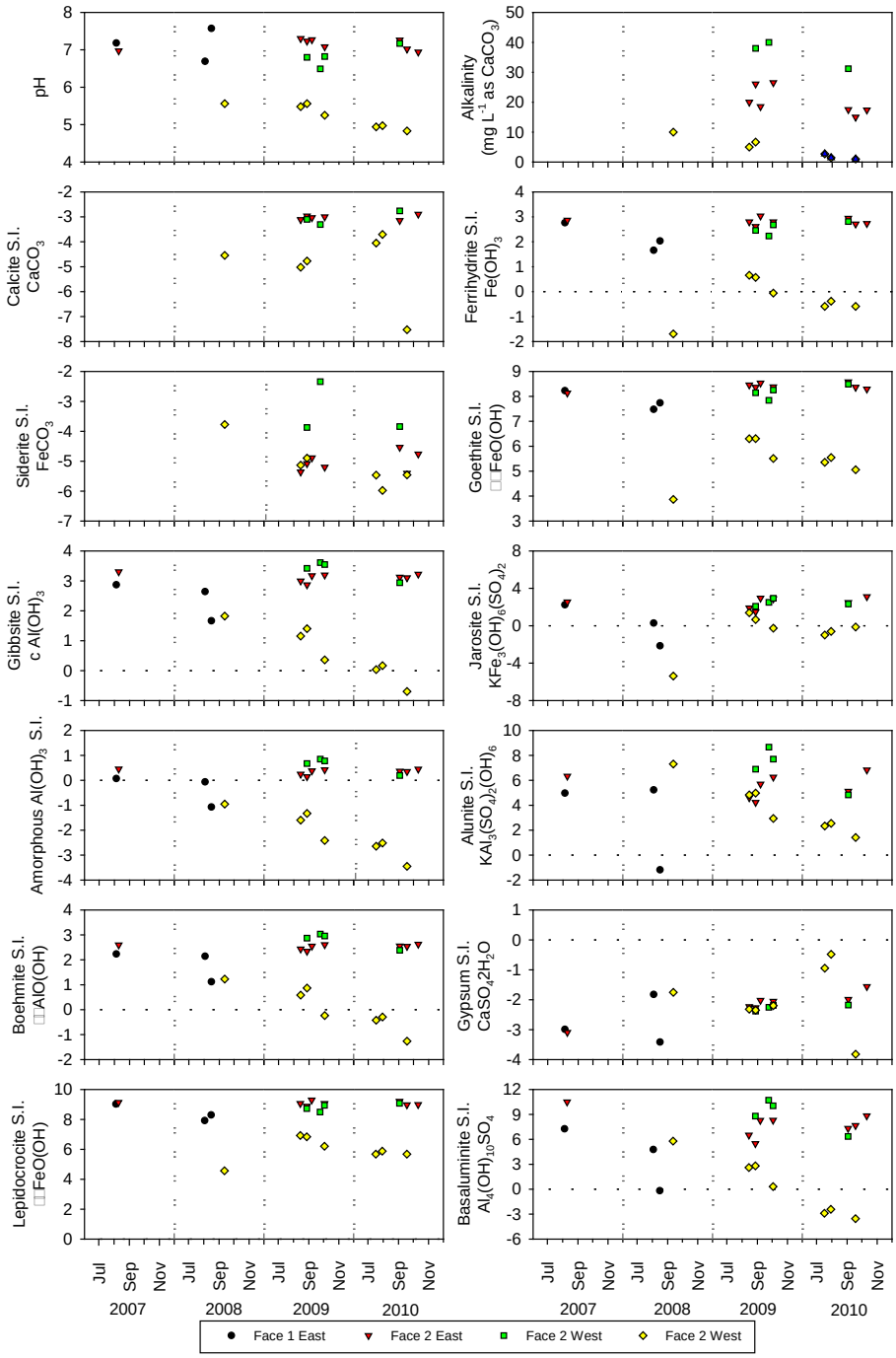

Figure 4.25 Time series plots of calculated saturation indices (SIs) using MINTEQA2 for pore water at the 7-m depth in the Type I test pile. The dashed black line at 0 represents equilibrium.

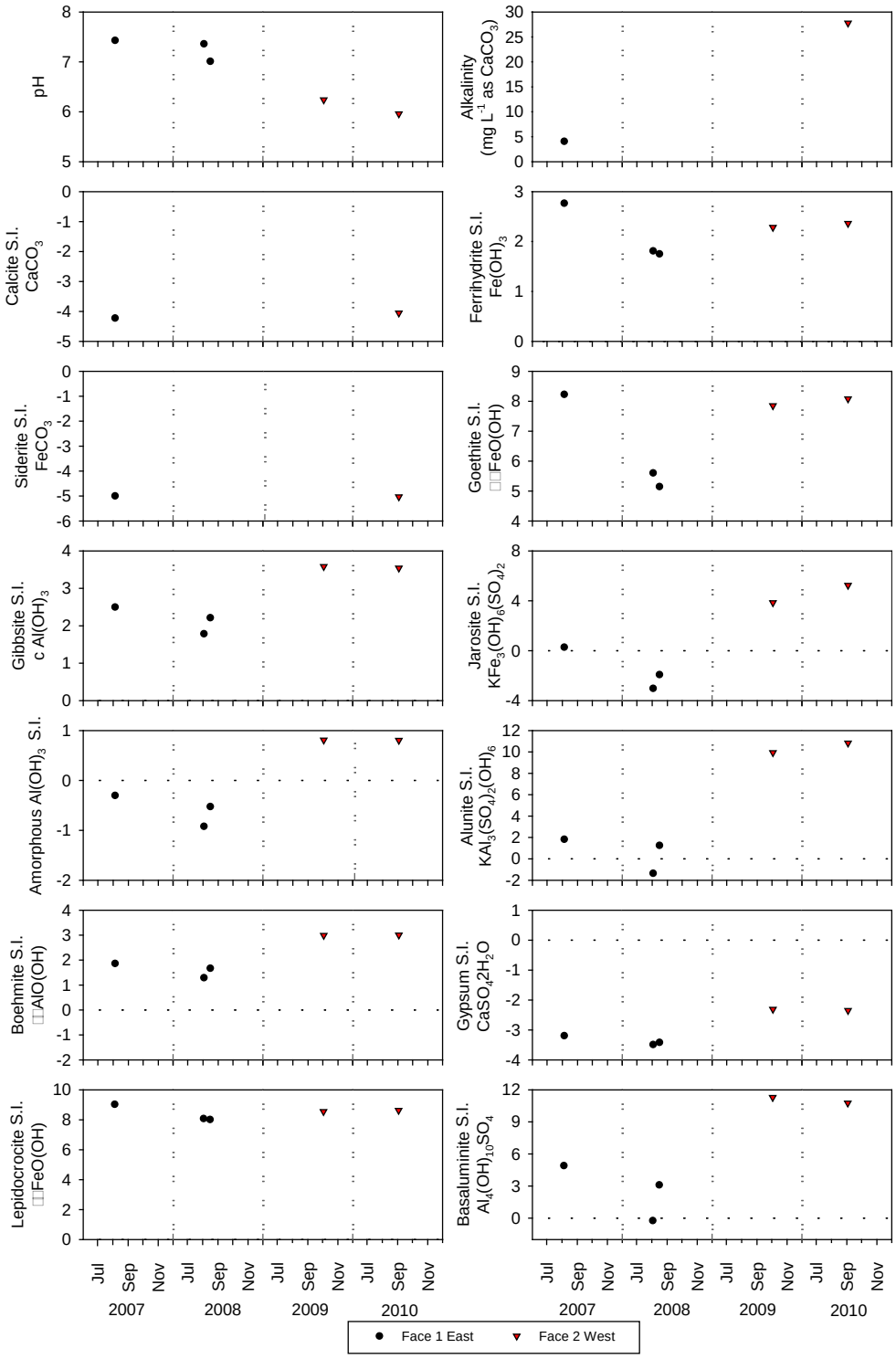

Figure 4.26 Time series plots of calculated saturation indices (SIs) using MINTEQA2 for pore water at the 9-m depth in the Type I test pile. The dashed black line at 0 represents equilibrium.

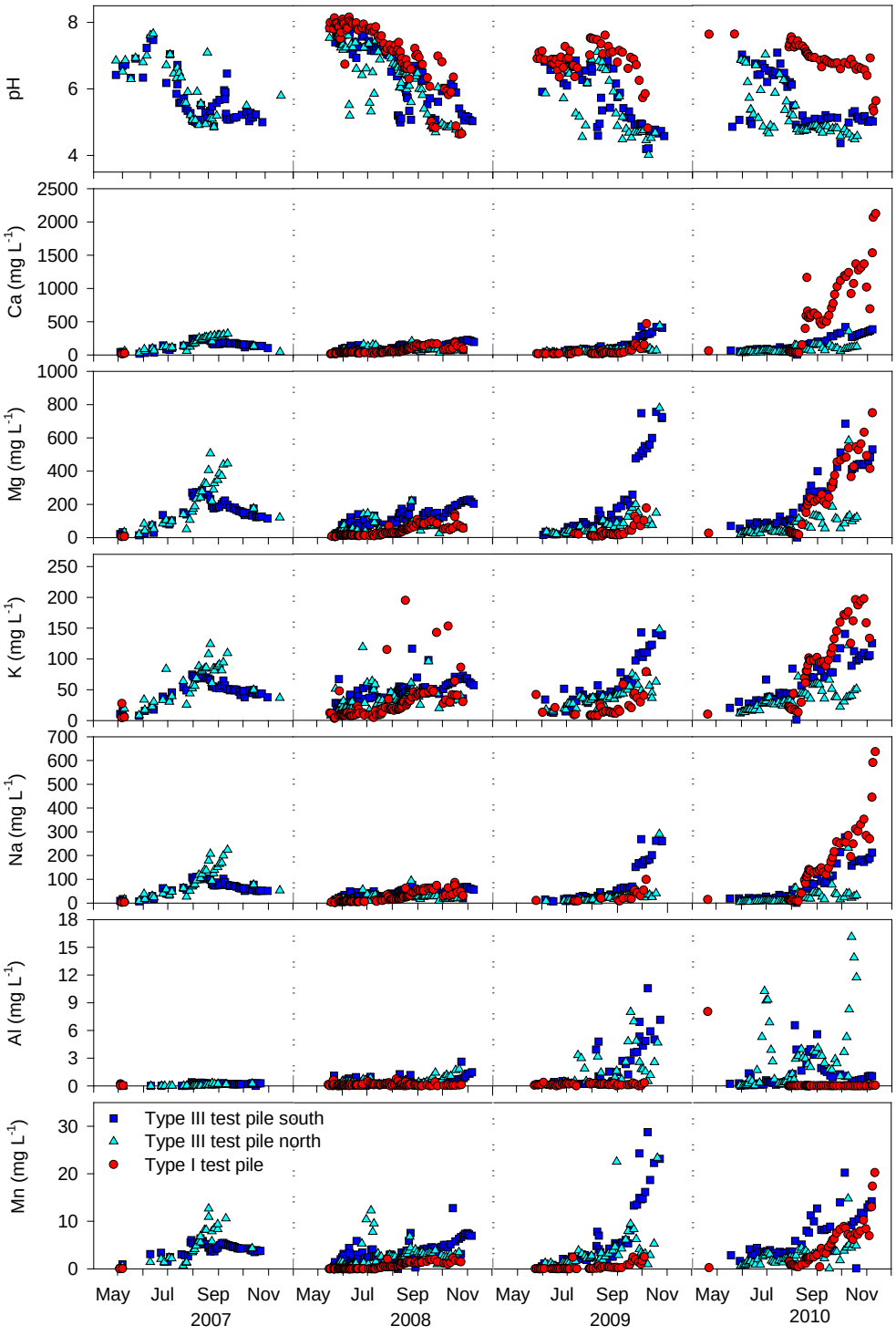

Figure 4.27 Major cation concentrations in the Type I test-pile drain and Type III test-pile north and south drains.

Chapter 5:

Geochemical and microbiological characterization of drainage from low-sulfide content waste rock: cover system performance

5.1 Executive Summary

The prevention and remediation of acid mine drainage (AMD) is one of the most costly environmental issues for the mining industry and regulatory agencies. This paper evaluates the potential performance of a proposed reclamation cover system for a waste-rock test pile at the Diavik Diamond Mine to minimize the release of sulfide-mineral oxidation products. An experimental waste-rock pile (0.082 wt. % S; Covered test pile) was constructed, re-sloped, and capped with a 1.5 m layer of lower permeability till (1.5×10^{-10} m^2) to reduce the ingress of oxygen and water infiltration. The test pile was covered with 3 m of non-acid generating waste rock to act as the active freeze-thaw layer. Differences in the effluent quality and microbial populations between the Covered test pile and an uncovered waste-rock test pile (0.053 wt. % S; Type III test pile) were examined over 4 years. The results show internal test pile temperatures influence the rate of sulfide-mineral oxidation and the release of oxidation products such as SO_4^{2-} and dissolved metals, including Ni, Co, Zn, Cd, and Cu. Measurements made in the Covered test pile showed uniform internal temperatures (~2 °C) and a relatively gradual decrease in the water flow rate, leading to a slow release of sulfide-mineral oxidation products. In contrast, the high permeability and porosity of the uncovered test pile resulted in more extreme temperature fluctuations (-15 to +15 °C) based on ambient air temperatures, and more variable discharge rates, in response to large recharge events. High concentrations of oxidation products, such as SO_4^{2-}, NO_3^-, NO_2^-, NH_3, ClO_4^-, and Cl^{-1}, were observed during periods of high flow rates. The cover system had no measurable effect on microbial populations compared to the uncovered test pile. Neutrophilic S-oxidizing bacteria (10^3 bacteria mL^{-1}) were present when effluent pH was near neutral in both the Covered test pile and uncovered Type III test pile. Iron-oxidizing bacteria population

numbers increased over time to 10^4 bacteria mL^{-1} as the pH decreased. Acidophilic S-oxidizing bacteria were low in abundance (< 10^2 bacteria mL^{-1}) in both test piles.

5.2 Introduction

5.2.1 Background

Sulfide-mineral oxidation in mine wastes can produce high concentrations of SO_4^{2-}, Fe, and H^+ that are transported in drainage (acid mine drainage; AMD) to the surrounding surface water and groundwater. Typically, the dissolution of non-sulfide minerals contained within mine wastes neutralizes H^+ generated during the oxidation of sulfide minerals to near neutral pH (Jurjovec *et al*., 2002). However, the potential for acid generation may be greater than the neutralization potential available in the mine wastes leading to AMD that can persist for decades, or even centuries (Environment Canada, 2004). The mining industry faces the challenge of managing the generation of AMD and the remediation of impacted sites.

Cover systems are applied to mine wastes to prevent the infiltration of rainwater or snowmelt into mine tailings impoundments or waste-rock stockpiles, restricting the migration of oxidation products (MEND, 2001). Furthermore, some cover systems can limit the ingress of O_2, decreasing the available O_2 for sulfide-mineral oxidation. By preventing the infiltration of water and the ingress of oxygen into waste-rock piles the rate of sulfide-mineral oxidation and the extent of contaminant release can be reduced (Ritchie, 1994).

Typical cover systems for waste rock materials consist of a single layer or multiple layers of one or more of the following materials: native soils, overburden, non-reactive tailings, non-reactive waste rock, geosynthetic materials, water, and oxygen consuming materials (MEND 2004). Specifically, the low-permeability covers are designed to create a layer of

material with a lower hydraulic conductivity between reactive waste material and the atmosphere. Modelling, laboratory and field based studies of cover systems applied to tailings and waste rock have been completed (e.g., Yanful *et al*., 1993; Yanful *et al*., 2000; Shurniak and Barbour, 2002; Bussiere *et al*., 2003 Aachib *et al*., 2004; Adu-Wusu and Yanful, 2006; Miller *et al*., 2006; Wagner *et al*., 2006; Marcoline, 2008; Taylor *et al*., 2009; Song, 2010; Demers *et al*., 2011; MEND, 2012), however, few studies have compared an uncovered waste-rock pile to covered waste-rock pile at a large scale.

A 30-cm low-permeability cover of fine-grained waste rock (< 10 cm) was placed on the surface of an experimental waste-rock pile (8 m by 8 m) at the Cluff Lake mine site in Saskatchewan (Wagner, 2004; Marcoline, 2008). The application of the low-permeability cover resulted in decreased outflow volumes with lower concentrations of dissolve metals compared to 2 years of prior monitoring the uncovered experimental pile. It was suggested the results were due to decreased oxygen concentrations and the aging of the pile (Wagner, 2004).

Yanful *et al*. (1993) studied a cover system at the Heathe Steele mine near Newcastle, New Brunswick on an experimental waste-rock pile that consisted of a 30 cm thick sand base, a 60 cm thick compacted glacial till layer, a 30 cm granular layer and a final 10 cm thick gravel layer. Results from this experiment indicate O_2 decreased from 20% before the application of the cover to 3% after the cover application, and infiltration rates were 2- 2.5% of precipitation when rainfall was heavy (Yanful *et al*., 1993). The authors concluded that although these results suggest reduced oxygen flux and acid production, the seepage quality must be monitored to confirm the reduction in acid production.

A study of three engineered test soil covers was completed at the Whistle mine near Capreol, Ontario to select a suitable cover for full-scale decommissioning of waste rock in a backfilled pit (Adu-Wusu and Yanful, 2006). The soil covers were effective in reducing percolation into the underlying waste rock over the course of this 3 year study. Concentrations of ions varied with seasons, increasing during wet periods in the spring and fall, and decreasing during dry periods when soluble minerals usually formed. The stored solutes were then released during the subsequent wet periods, resulting in increased concentrations in the spring (Adu-Wusu and Yanful, 2006). Hydroxides, oxide and sulfate phases generally controlled Al, Ca, Mg, and Fe^{3+} concentrations and Cu, Cd, Zn, Ni, Pb, As and Be were probably controlled by coprecipitation and adsorption with Fe and Al hydroxides and sulfates (Adu-Wusu and Yanful, 2006). Adu-Wusu and Yanful (2006) suggest that the quality of percolated water from the covered waste rock was much better than that of the percolated waster from the uncovered waste rock.

At the Diavik diamond mine (Diavik), the approved reclamation concept for the potential 120 Mt waste-rock stockpile includes re-sloping the waste rock to 18° (3H:1V), capping with a 1.5 m layer of lower permeability till as a barrier to water infiltration, and a 3 m cover of Type I waste rock to act as a thermal barrier. An experimental covered waste-rock test pile (Covered test pile) using the approved reclamation concept was constructed at Diavik as part of an ongoing study, to compare the hydrology, thermal transport, geochemistry, microbiology, and gas transport to an uncovered waste-rock test pile composed of Type III waste rock (Type III test pile). This paper described the effluent geochemistry and microbiology of the Covered test pile, and compares the results to the uncovered Type III test pile (Chapter 4).

5.3 Methods of Investigation

5.3.1 Waste Rock Characterization

Waste-rock samples were collect from most haul truck loads used to construct the Covered test-pile core. The particle-size distribution of samples of the < 50 mm fraction of the waste-rock material (n = 26) and S content of the < 50-mm fraction (n = 183) were determined following the methods described by Smith *et al*. (2012b). Subsamples of the < 10-mm fractions (10, 5, 2.5, 1.25, 0.625, 0.315, and 0.160 mm, and a pan for smaller size fractions) from 11 samples were collected for measurements of the S and C content and whole-rock analysis. Each fraction was pulverized using a four-position Fritsch Pulverisette Analysette planetary ball mill. Samples were further spilt for S and C analysis, and whole-rock analysis. Sulfur and C content was measured using a resistance furnace (CS-2000; Eltra, Germany) as described in Chapter 3.

5.3.2 Water Sample Collection and Analysis

Water samples were collected from the Covered test-pile basal drain system following the sampling procedures described in Chapter 3. Pore-water samples were collected from *in situ* soil water solution samplers (SWSS; model e-127-1920F1L12-B02M2; Hoskin Scientific, Canada) as described in Chapter 4.

At each sampling location (basal drains and SWSS), the pH, redox potential relative to the standard hydrogen electrode (E_h), EC, temperature, and alkalinity were determined using methods in Chapter 3. Field measurements were conducted using a Hach spectrophotometer DR/8400 for the determination of orthophosphate (o-PO_4; Ascorbic Acid method), Fe(II) (Phenanthroline method), H_2S (Methylene Blue method) and NH_3 (NH_3-N; Salicylate

method) concentrations for select samples (SMEWW, 2005). Concentrations of anions, and total and dissolved metals were determined following the methods described in Chapter 3. Quality control and quality assurance were assessed by evaluating several standards covering the range of measured concentrations, and incorporating both field replicates and laboratory blanks into the protocol (Appendix A).

Effluent samples were collected from the Covered test-pile drain for microbiological enumerations using the techniques described in Chapter 3. The enumeration of neutrophilic S-oxidizers (T. *thioparus* and related species), acidophilic S-oxidizers (A. *thiooxidans* and related species), and acidophilic Fe-oxidizers (A. *ferrooxidans* and related species) was completed following the most probable number (MPN) technique (Cochran, 1950) using media described by Hulshof *et al*. (2006).

The equilibrium/mass-transfer model MINTEQA2 (Allison *et al*., 1990), with a modified database for consistency with the WATEQ4F (Ball and Nordstrom, 1991), was used to calculate the saturation indices (SI) for discrete solid phases to assist in the interpretation of aqueous geochemistry data. Speciation calculations were conducted for samples collected from the Covered test pile using a complete suite of field and laboratory analyses following the procedures described in Chapter 3.

5.4 Results and Discussion

5.4.1 Sulfur Content and Acid-Base Accounting Calculations

The S content of the < 50-mm fraction of the waste rock used to construct the Covered test-pile core ranged from 0.006 to 0.38 wt. % S and averaged 0.082 wt. % S (n = 183, σ = 0.053; Smith *et al*., 2012b). The < 10-mm fraction had an average S content of 0.12 wt. % S (n = 11,

σ = 0.098) and the < 5-mm fraction S content was 0.14 wt. % S (n = 11, σ = 0.12), ranging from 0.019 to 0.44 wt. % S. The S content followed a trend of increasing sulfide content with finer particle size for particle sizes ≤ 1.25 mm, similar to the waste rock used in the Type III test pile (Smith *et al*., 2012b). The < 50-mm fraction of waste rock in the Type III test pile had an average S content of 0.053 wt. % S (n = 270, σ=0.037), and ranged from 0.0085 to 0.27 wt. % S (Smith *et al*., 2012b). The S content of the Covered test pile was more variable than in the Type III test pile (Smith *et al*., 2012b).

The average C content, present as $CaCO_3$, of the < 10-mm fraction in the Covered test pile was 0.047 wt. % C (n = 11, σ = 0.037), ranging from 0.018 to 0.12 wt. % C, and the < 5-mm fraction was 0.050 wt. % C (n = 11, σ = 0.046), ranging from 0.019 to 0.15 wt. % C. The finer fractions had a higher C content, which is consistent with the results from the Type III test pile (Smith *et al*., 2012b). The < 5-mm fraction of waste rock had an average C content of 0.029 ± 0.005 wt. % C (n = 10; Chapter 4).

Acid-base accounting was used to chemically predict the behaviour of the Covered test-pile waste rock during weathering. The acid-producing potential (AP) was determined using the S content of the waste rock, assuming that the S was present as pyrite or pyrrhotite. Every mole of S generates $2H^+$. The neutralization potential (NP) was determined assuming that the analytically-determined wt. % C consisted entirely of $CaCO_3$ (Smith *et al*., 2012b). The ratio of NP to AP is used to evaluate the acid generating potential; a NP:AP ratio of < 1 is considered to be potentially acid generating, > 3 is considered to be non-acid generating, and > 1 and < 3 remains uncertain (Smith *et al*., 2012b).

The average calculated AP value for the < 10-mm fraction was 3.81 ± 3.05 kg t^{-1} $CaCO_3$ and the average calculated NP was 3.92 ± 3.08 kg t^{-1} $CaCO_3$. The ratio of NP:AP for the < 10-mm fraction was 1.51 ± 0.96, suggesting the Covered test-pile core waste rock has an uncertain acid generating potential.

5.4.2 Microbial Populations

Three groups of Fe- and S-oxidizing bacteria (*At. ferrooxidans* and related species, *At. thiooxidans* and related species, and *T. thioparus* and related species) were monitored in effluent from the Covered test pile and enumerated in order to examine the processes associated with the oxidation of sulfide minerals over time. Neutrophilic S-oxidizers were observed in the Covered test pile in January 2009, populations decreased by May of 2009 when Fe-oxidizers were detected (Figure 5.1). The populations of Fe-oxidizers were detected for the remainder of 2009 and populations increased in 2010 (Figure 5.1) similar to the Type III test pile (Chapter 4). By 2010, Fe-oxidizers were the most abundant bacterial species in the effluent from the Covered test pile. The low pH in the Covered test pile was optimal for acidophilic S-oxidizers and Fe-oxidizers. Concentrations of dissolved metals associated with the oxidation of sulfide minerals, such as Ni, Co, Zn, and Cd, increased in 2010 when populations of iron oxidizers also increased. Acidophilic S-oxidizers were only detected in a few samples with populations < 10^2 bacteria mL^{-1} in 2009 and 2010 (Figure 5.1), whereas, the population of Fe-oxidizers was stable over the duration of the study. The populations of Fe-oxidizing bacteria in the Covered test pile were consistent over time, whereas low populations of Fe-oxidizing bacteria were present in the effluent of the Type III test pile at the beginning of each field season. It is not clear if the cover system or the heat trace had a

measurable effect on the populations over time; however, it appears as though the population was more stable than in the Type III test pile.

5.4.3 Sulfide-Mineral Oxidation

The uniform internal temperatures (~2 °C; with some influence from the heat trace) within the Covered test pile year round dampened the extreme temperature variations and resulting effects on sulfide-mineral oxidation rates and the release of acidity, SO_4^{2-} and dissolved metals. In contrast, the variable internal temperatures from -15 °C to +15 °C in the Type III test pile affected the rates of sulfide oxidation and the release of acidity, SO_4^{2-} and dissolved metals, with higher sulfide-oxidation rates at increased temperatures (Chapter 4). The SO_4^{2-} concentrations in the Type III test pile were more variable than the Covered test pile.

Sulfate can be released by the oxidation of sulfide minerals within the waste-rock test pile and through the oxidation of sulfide minerals during the blasting of waste rock (Chapter 3). Sulfate concentrations in the Covered test pile followed a similar trend to other blasting residuals, such as NO_3^- (Figure 5.2) and Cl^-, for the duration of the study (Bailey *et al*., 2012). The concentrations of SO_4^{2-} in the Covered test pile increased during sporadic flow in 2007 from 1000 mg L^{-1} to 1800 mg L^{-1} in January 2008 when flow ceased. Concentrations of SO_4^{2-} were elevated when flow recommenced in July 2008 at 3000 mg L^{-1} and decreased to 2500 mg L^{-1} by October 2008. Sulfate concentrations remained between 2000 mg L^{-1} and 3000 mg L^{-1} for the duration of the study with two exceptions: concentrations in July and August 2009 when flow decreased and ceased; and in April and May 2010 when flow also decreased and ceased. Geochemical modeling suggests the effluent was at equilibrium with

respect to gypsum [$CaSO_4 \cdot 2H_2O$] for the duration of the study, suggesting secondary mineral precipitation may limit the maximum SO_4^{2-} concentration.

The ratio of SO_4^{2-} to N_{Total} in the effluent can be used to estimate the proportion of S released from the oxidation of sulfide mineral during blasting *versus* S released from *in situ* sulfide-mineral oxidation (Chapter 2; Bailey *et al*., 2012). No coprecipitation or adsorption reactions that affect N_{Total} concentrations have been identified. It is assumed, therefore, that transport of N_{Total} through the test piles is conservative (Chapter 2, Bailey *et al*., 2012). The SO_4^{2-} to N_{Total} ratios measured in water samples collected from the Covered pile were similar to ratios in water samples collected from the Type III test pile in 2007 (Chapter 2, Bailey *et al*., 2012). Leaching of rock samples collected shortly after blasting suggest that water samples collected from the Type III test pile during 2007 have a modest contribution from *in situ* sulfide-mineral oxidation. The SO_4^{2-} to N_{Total} ratio steadily increased from 4 to 11 from 2007 to 2009. The mass of SO_4^{2-} derived from blasting can be estimated by multiplying the initial ratio of SO_4^{2-} to N_{Total}, observed in 2007, by the concentration of N_{Total}. Calculations conducted for the period post-2007 overestimate the observed SO_4^{2-} concentrations in the Covered test-pile effluent. These results suggest that the total mass of SO_4^{2-} in the effluent is probably limited by gypsum precipitation, or another SO_4^{2-}containing mineral. As a consequence, estimates of the rate of sulfide-mineral oxidation based on the concentration of SO_4^{2-} in the effluent from the Covered test pile probably underestimate the *in situ* oxidation rates.

Pyrrhotite is the primary sulfide mineral in the Type III waste rock (Smith *et al*., 2012). Electron-microprobe analysis of Diavik waste rock indicates that the composition of

pyrrhotite is $(Fe_{0.852}Ni_{0.004}Co_{0.001})_{\sum 0.857}S_{1.000}$ (Jambor, 1997). Nickel is released from the oxidation of pyrrhotite at a ratio of 0.004 moles of Ni for every 1 mole of S, (Chapter 4; Jambor, 1997). Precipitation and adsorption of Ni is limited under the low pH conditions that prevail in the Covered test-pile effluent. Therefore, Ni concentrations can be used to estimate the total concentrations of SO_4^{2-} due to pyrrhotite oxidation both *in situ* and from blasting. These calculations indicated that the total SO_4^{2-} concentrations estimated by Ni concentrations were higher than the measured SO_4^{2-} concentrations (Figure 5.3). In addition, *in situ* sulfide-mineral oxidation can be estimated as the difference between total SO_4^{2-} concentrations determined from Ni concentrations and that estimated from blasting as determined from N_{Total} concentrations. The results show that the total SO_4^{2-} concentration estimated from Ni were higher than the measured SO_4^{2-} concentrations, suggesting that SO_4^{2-} concentrations were limited by secondary mineral formation (Figure 5.4). Geochemical equilibrium modelling indicates there are no secondary mineralogical controls for Ni, however, at the pH > 4.5 Ni was probably controlled by adsorption reactions (Chapter 3 and 4). The pH in 2010 was less than 4.5; therefore, Ni concentrations in 2010 are probably a good analogue for total SO_4^{2-} concentrations and the proportion from *in situ* sulfide-mineral oxidation can be used to estimate the sulfide-mineral oxidation rate from the Covered Test pile.

The total mass of S released from the Covered test pile was 170 kg, approximately 0.19 % of the total initial mass of S in the test pile, similar to the Type III test pile. This mass loading suggests an oxidation rate of 2.71×10^{-10} kg (O_2) m^{-3} s^{-1}. Although the total mass of S released was low in comparison to the total mass of S in the waste-rock test piles, the available sulfide for oxidation is held within the finer fractions of the waste rock and consists

of approximately 40 % of the test-pile volume (Smith *et al*., 2012b). This suggests 0.81 % of available S was released from the Covered test pile. The sulfide-mineral content of the Diavik waste rock is low (Covered test pile = 0.082 wt. % S), however; the observed SO_4^{2-} concentrations in the Covered test-pile effluent (maximum of 3200 mg L^{-1}) indicates the mass of available S within the test piles is sufficient to generate high dissolved SO_4^{2-} concentrations.

The estimated total S released based on Ni concentrations suggests the total mass of S released by sulfide oxidation over the four year period was 335 kg, indicating that up to 178 kg has been stored as solid-phase precipitates within the test pile. The estimated proportion of the total mass due to *in situ* sulfide-mineral oxidation is 202 kg and the mass due to blasting is 133 kg. The sulfide-mineral oxidation rate from *in situ* sulfide-mineral oxidation therefore is estimated to be 3.23×10^{-10} kg (O_2) m^{-3} s^{-1}. Similar calculations can be made using Co. The estimated total mass of S released based on Co was 284 kg over the four year study period, with a sulfide oxidation rate of 4.05×10^{-10} kg (O_2) m^{-3} s^{-1}, which is slightly lower than the estimate by Ni. Both the Ni and Co estimated S oxidation rates are lower than the rate determined by humidity-cell experiment of the Type III material (1.69×10^{-7} kg (O_2) m^{-3} s^{-1} at 22°C; Chapter 3). The *in situ* sulfide-mineral oxidation rate of the Type III test pile was 7.50×10^{-12} kg (O_2) m^{-3} s^{-1}which is 2 orders of magnitude lower than the Covered test pile, suggesting the constant temperatures maintained by the cover system, and the higher sulfide content of the Covered test pile, influenced the sulfide-mineral oxidation rates.

The cover system resulted in lower amplitude changes in temperature, primarily driven by conductive heat flow, compared to the uncovered Type III test pile, which was affected by

conductive heat flow and advective gas transport (Pham *et al*., 2012). Heat trace was placed in the Covered test-pile basal lysimeters and basal drain to allow sample collection and to prevent freezing and rupturing of the drainage conduits at the base of the test pile. The low permeability of the till layer retained within the Covered test pile through the winter months. As a result, the Covered test pile maintained uniform internal temperatures (~2 °C) in the Type III core year round. The heat trace at the base of the uncovered Type III test pile did not have the same affect due to the porosity and permeability of the waste rock, and conductive heat flow and advective gas transport. The heat trace to the basal lysimeters in the Covered test pile was turned off in June 2011 and thereafter, only the heat trace in the basal drain has operated.

5.4.4 Water Chemistry

The flow rate from the Type III test-pile basal drain was correlated to external temperatures (Chapter 4). In contrast, the rate of basal outflow from the Covered test pile was limited by the rate of infiltration through the till layer. In addition, the Covered test pile had maximum discharge rates in the winter months and a relatively gradual decrease in the flow rate, whereas the Type III test pile was frozen during the winter, leading to maximum flow rates in the summer and variations in discharge rates in response to large recharge events. The Covered test-pile effluent contained relatively uniform concentrations of blasting residuals over the measurement period, with a gradual decrease over time (Chapter 2; Bailey *et al*., 2012). In addition, a gradual release of sulfide-mineral oxidation products was observed.

5.4.4.1 pH, Alkalinity and Acid Neutralization

Acid generation in the Covered test pile generally exceeded the neutralizing capacity available from carbonate minerals. The cover system maintained near-constant above-freezing internal temperatures within the Covered test pile. As a result, sulfide-mineral oxidation continued at a relatively uniform rate throughout the year, depleting the carbonate minerals within 1 year, in contrast to the annual pH cycles observed in the Type III test pile (Chapter 4). Between September 2007, when flow in the Covered test pile began and January 2008 when flow ceased, the pH decreased from 7.0 to 5.2 (Chapter 1). Few measurements of alkalinity were made in 2007, but the limited number of measurements indicated that alkalinity concentrations decreased from a maximum of 81 mg L^{-1} (as $CaCO_3$) to 15 mg L^{-1} (as $CaCO_3$) by January 2008. The pH was 5.5 when flow resumed in September 2008 and further decreased over time (ranging from pH 4.1 to 4.7) with slight fluctuations with changes in the flow rate. The alkalinity remained low (ranging from below detection to 10 mg L^{-1} as $CaCO_3$) for the remainder of the study. Geochemical equilibrium modeling suggests the effluent was undersaturated with respect to all carbonate minerals.

In 2007 the pH decreased as the alkalinity declined. In 2008, and the pH ranged from 4.1 to 4.7 (Figure 5.2) and remained in this range for the duration of the study. The concentration of Al in the effluent of the Covered test pile was low in 2007 through January 2008 (< 2 mg L^{-1}) when flow ceased.When flow resumed in August 2008, Al concentrations sharply increased from 0.23 mg L^{-1} to 7.3 mg L^{-1} by October 2008. Concentrations of Al continued to increase for the duration of the study, with decreased concentrations after dry periods in June 2009 and June 2010. Aluminum concentrations reached a maximum of 18 mg L^{-1} at the end of 2010 when flow was at its maximum. The total Al released from the Covered test pile was

1.8 g. Saturation indices suggest effluent was at or near equilibrium with respect to gibbsite [$Al(OH)_2$], boehmite [AlO(OH)] and basaluminite [$Al_4SO_4(OH)_{10}$] by November 2008, and was undersaturated with respect to amorphous Al hydroxide [$Al(OH)_3$] for the duration of the study. This suggests the dissolution of secondary Al minerals is neutralizing acidity to the pH plateau observed (4.1 to 4.7).

5.4.4.2 Major Ions

The dissolution of carbonate and aluminosilicate minerals releases major ions such as Ca, Mg, K, Na, Al, and Mn and can play an important role in the formation of secondary minerals such as gypsum and jarosite (Blowes and Jambor, 1990). Calcium concentrations in the Covered test pile were relatively constant over time and ranged from 380 to 520 mg L^{-1} for the duration of the study, with the exception of lower concentrations during periods of decreased flow rates (Figure 5.5). Geochemical modeling suggests effluent was at equilibrium with respect to gypsum and undersaturated with respect to all carbonate minerals for the duration of the study, suggesting the precipitation and dissolution of gypsum limited the concentrations of Ca and SO_4^{2-} (Figure 5.6). In contrast, the Type III test pile was undersaturated with respect to gypsum at most times, with the exception of a few samples at the end of the field season when concentrations of SO_4^{2-} were elevated. The total mass of Ca release from the Covered test pile was 101 kg (Table 5.1; Figure 5.7).

Magnesium and potassium are likely released by the kinetically limited dissolution of biotite. Concentrations of Mg, K, and Na in the Covered test pile followed similar trends for the duration of the study (Figure 5.5). The concentration of Mg in 2007 increased from 200 mg L^{-1} to 250 mg L^{-1} by January 2008 when flow ceased. Flow recommenced in August

2008 and Mg concentrations were elevated at 640 mg L^{-1}. Concentrations of Mg sharply decreased and remained between 380 mg L^{-1} and 520 mg L^{-1} for the duration of the study with the exception of increased concentrations during periods of decreased flow rates in June 2009 and June 2010. The maximum Mg concentration was 820 mg L^{-1} in July 2010. The total mass of Mg released from the Covered test pile from 2007 through December 2010 was 103 kg (Table 5.1; Figure 5.7).

The concentrations of K in the Covered test pile ranged between 75 and 180 mg L^{-1} for the duration of the study with a maximum of 230 mg L^{-1} observed in July 2010 (Figure 5.5). Increased K concentrations were observed during periods of reduced flow rate in June 2009 and June 2010. The total mass of K released was 35 kg (Figure 5.7). Geochemical modeling suggests the Covered test-pile effluent was supersaturated with respect to alunite [$KAl_3(SO_4)_2(OH)_6$] (Figure 5.6), an Al-bearing secondary mineral, which has been found in rims of pyrite or pyrrhotite grains in tailing hardpans (Moncur *et al*., 2005). Further mineralogical work is required to determine if secondary minerals were formed in the waste-rock test piles.

The average molar ratio of Mg:K in the Covered test-pile effluent was 3.1, with individual water samples ranging from 1.5 to 6.1. This average value was consistent with the ideal 3:1 molar ratio of Mg:K in biotite [$KMg_3AlSi_3O_{10}(OH)_2$]. The cumulative ratio of Mg:K in the Type III basal drain is 3.1 with an average of 2.85 for individual samples (ranged from 0.21 to 5.35), suggesting that there was another source of Mg or that K was preferentially removed from the pore water. Geochemical modeling indicates that the effluent from the Covered test pile was at saturation with respect to Al-hydroxides at various times. Similarly,

the Type III basal drains were at saturation with respect to jarosite at the beginning of 2008 and 2009, thus the formation of secondary minerals may provide a limit to dissolved K concentrations.

The concentrations of Na from the Covered test pile ranged between 112 mg L^{-1} and 200 mg L^{-1} for the duration of the study with a total mass of 36 kg released from 2007 through 2010 (Figure 5.5). Maximum Na concentrations were observed in June 2010 at 240 mg L^{-1}. Geochemical modeling suggests there were no geochemical controls on Na concentrations. Manganese concentrations increased when the flow rate decreased similar to the trends in Mg, K, and Na concentrations. The maximum Mn concentration of 39 mg L^{-1} occurred in July 2010 (Figure 5.5). The total mass of Mn released was 36 kg.

The major cations, Ca, Mg, K, Na and Mn, in the Type III test pile all followed a similar trend over time (Figure 5.5). Concentrations were low at the beginning of each field season in May and increased to maximum concentrations at the end of the field season in October or November when flow rates decreased and ceased. The maximum concentrations of Ca (420 mg L^{-1}), Mg (760 mg L^{-1}), K (140 mg L^{-1}), Na (270 mg L^{-1}), and Mn (29 mg L^{-1}) in the Type III test pile generally occurred in 2009 and were similar in concentration to the maximum observed in the Covered test pile in 2010. The maximum concentrations of Al (17 mg L^{-1}) occurred in 2010.

Calculated saturation indices suggest secondary mineralogical controls on the major cations in the Covered test pile were similar to the Type III test pile (Chapter 4). The calculated saturation indices indicated effluent from the Type III test pile was undersaturated with respect to gypsum, with the exception of SIs at equilibrium at the end of the field season

when concentrations of Ca and SO_4^{2-} were at their maximum (Figure 5.6). The Type III test-pile effluent was supersaturated with respect to alunite, and at times jarosite, suggesting a control on K concentrations. No secondary mineralogical controls were expected for Na and Mn. Further mineralogical work is necessary to confirm the presence of secondary mineral in Covered test pile.

The above freezing internal temperatures in the Covered test pile resulted in a relatively constant rate of major cation release through the dissolution of carbonate and aluminosilicate minerals. The mass loadings of cations were higher in the Covered test pile than the Type III test pile, probably due to the larger volume of waste rock in the Cover test pile.

5.4.4.3 Trace Metals

The concentration of Fe in the Covered test pile was variable over time with the maximum concentrations in January 2008 and January 2009 at 0.50 mg L^{-1} (Figure 5.5). Concentrations for 2010 remained low (< 0.03 mg L^{-1}). Concentrations of Fe were controlled by the rate of sulfide oxidation, and by the solubility and formation of secondary minerals, such as Fe(III) oxyhydroxides and Fe(III) hydroxysulfates (Figure 5.6). Geochemical modeling suggests effluent is supersaturated with respect to goethite, lepidocrocite [γ-FeO(OH)] and ferrihydrite [$Fe(OH)_3$ or nominally $Fe_2O_3.9H_2O$], therefore, the accumulation of these secondary minerals may coincide with variable Fe concentrations (Figure 5.5). Goethite and lepidocrocite were at or near equilibrium in January 2008 and 2009 when Fe concentrations were slightly elevated to the maximum observed concentrations.

Nickel and Co are released from the oxidation of pyrrhotite and Zn and Cd are released from the oxidation of sphalerite (Chapter 3). The concentrations of Ni and Co in the Covered

test pile followed a similar trend and were highly correlated (R^2=0.86). The ratio of Ni to Co was 5.2 ±0.7 which is higher than then ratio in pyrrhotite (Ni:Co = 4). Nickel concentrations generally followed a similar trend with each pulse of water migrating through the Covered test pile each year. After a peak in the flow rate, concentrations of Ni and Co increased until flow ceased. When flow resumed, concentrations decreased with increasing flow rate. The maximum Ni and Co concentrations were observed in June 2010 immediately before flow ceased for a short duration (Figure 5.5).

Zinc and Cd concentrations followed a similar trend as Ni; increased concentrations with decreasing flow rate and decreased concentrations with increasing flow rates (Figure 5.5). Zn and Cd were highly correlated (R^2 = 0.86). The maximum Zn concentration was 11 mg L^{-1} and maximum Cd concentration was 50 μg L^{-1} in June 2010 (Figure 5.5).

Geochemical modeling suggests waste-rock effluent was undersaturated with respect to secondary Ni minerals, which is consistent with other studies of waste rock that suggest discrete Ni secondary minerals have not been observed in tailings environments (Alpers, 1994). In addition, geochemical modeling suggests effluent was undersaturated with respect to both Zn and Cd secondary minerals and no secondary Zn- or Cd-bearing minerals were identified in mineralogical studies of waste rock from the Diavik site. However, Ni, Zn and Cd may undergo adsorption/complexation reactions with Fe(III) oxyhydroxides and hydroxysulfates removing them from the effluent (Webster *et al*., 1998; Galan *et al*., 2003; Gunsinger *et al*., 2006). Geochemical modeling suggests effluent from the Covered test pile is supersaturated with respect to Fe(III) oxyhydroxides and hydroxysulfates, such as, goethite, lepidocrocite and jarosite, at various times throughout the study. Covered test pile

had a total of 1,340 g of Ni, 284 g of Co, 909 g of Zn and 5.7 g of Cd released over the 4 year period (2007 to 2010; Table 5.1; Figure 5.7).

Chalcopyrite is found at trace concentrations in the Diavik waste rock and is the primary source of Cu in the effluent (Chapter 3). Similar to other metals in the Covered test pile, Cu increased during decreases in the flow rate and decreased with increases in flow rates; however, the increase in April 2010 was not as significant as with the other metals, such as Ni, Co, Zn and Cd (Figure 5.5). The maximum concentrations of Ni, Co, Zn, and Cd occurred in June 2010, whereas the maximum concentration of Cu was 2.7 mg L^{-1} in November 2010. The pH of the Covered test pile remained below 4.5 for much of the study. At a pH of 4.0, Cu has been shown to adsorb onto Fe (III) hydrous oxides, whereas Ni, Co and Zn remained in solution (Dzombak and Morel, 1990; Gunsinger *et al*., 2006). Copper also can be removed from effluent through adsorption reactions with Fe(III) oxyhydroxides and hydroxysulfates (Webster *et al*., 1998; Galan *et al*., 2003; Gunsinger *et al*., 2006). Effluent is undersaturated with respect to Cu metals such as covellite [CuS] or chalcocite [$CuFeS_2$]; however, Webster *et al* (1998) suggest MINTEQA2 underestimates the degree of Cu adsorption that occurs in AMD waters, in the presence of bacteria, by up to 50 %. The total mass of Cu released from the Covered test pile was 279 g.

The mass loading of dissolved metals, such as Ni, Co, Zn, Cd and Cu, from the Covered test pile were higher than the Type III test pile. This was probably a result of higher S oxidation rates in the Covered test pile and a function of the hydrology of the Covered pile.

5.4.4.4 Summary

Cover systems are used to limit the infiltration of atmospheric water, the ingress of atmospheric oxygen; to control erosion of waste materials, and upward movement of process-water constituents and oxidation products; and to provide a medium for revegetation (MEND, 2012). The constructed experimental Covered test pile discussed in this Chapter was affected by heat trace placed at the base of the test pile. The cover system was effective in trapping heat within the core of the Covered test pile, limiting the effects of low ambient temperatures experienced in the Arctic environment. The low-permeability layer was effective in limiting advective heat transport, thereby allowing sulfide-mineral oxidation to continue during the winter months. The heat source has since been turned off and future work will be completed to determine if the thermal layer and low-permeability layer are effective cover materials for waste rock at Diavik.

The low permeability of the Covered test pile prevented advective gas transport, and maintained constant internal temperatures within the test pile, which resulted in relatively uniform outflow chemistry in response to a relatively steady change in flow rate. The Covered test pile had maximum discharge rates in the winter months and a relatively gradual decrease in the flow rate. Concentrations of metals generally increased with decreasing flow rate with maximum concentrations observed immediately before flow ceased. Concentrations subsequently decreased with increasing flow rate. The amplitude of concentrations peaks for Ca and SO_4^{2-} were less dramatic than metals probably because gypsum precipitation controlled Ca and SO_4^{2-} concentrations during low flow periods. The sulfide-mineral oxidation rates were higher than those observed in the uncovered Type III test pile, which

resulted in a greater mass loading of oxidation products such as SO_4^{2-}, H^+ and dissolved metals.

These observations were not consistent with those of other cover system studies in which effluent chemistry was improved with the application of a cover system (Yanful *et al*., 1993; Wagner, 2004; Adu-Wusu and Yanful, 2006). The Covered test pile was artificially heated and the heat source has since been turned off. Over the coming years, it is expected that the sulfide-mineral oxidation rates will decrease due to lower internal temperatures, less water-rock interaction, and limited O_2 availability. Further work is currently being completed to investigate the changes in temperature, outflow chemistry, gas transport and flow rates due to the removal of the internal heat source.

5.5 Conclusions

This study compared geochemical and microbiological conditions in the Covered test pile constructed based on an approved reclamation concept to an uncovered Type III test pile. The cover system included a low permeability (1.5×10^{-10} m^2) layer of till to limit water infiltration, and was covered with non-reactive waste rock to act as the active freeze-thaw layer. The internal test-pile temperatures were influenced by the heat trace at the base of the Covered test pile. As a result, sulfide-mineral oxidation rates and the release rates of oxidation products, such as SO_4^{2-} and dissolved metals, including Ni, Co, Zn, Cd, and Cu were elevated compared to the uncovered Type III test pile. In the Covered test pile, the constant internal temperatures (~2°C) and a relatively steady change in flow rate led to a consistent release of sulfide-oxidation by products. In contrast, the high permeability and porosity of the uncovered Type III test pile resulted in temperature fluctuations (-15 to

+15 °C) based on ambient air temperatures and discharge rate changes in response to recharge events; with high concentrations of oxidation products during periods of high flow rates. The sulfide-mineral oxidation rates were higher in the Covered test pile due to the constant year round temperatures and higher sulfide content compared to the uncovered Type III test pile. Neutrophilic S-oxidizers (10^3 bacteria mL^{-1}) were present when effluent pH was near neutral in both the Covered and Type III test piles. The population of acidophilic Fe-oxidizers increased over time to 10^4 bacteria mL^{-1} with decreasing pH. Acidophilic S-oxidizers were low in abundance ($< 10^2$ bacteria mL^{-1}) in both test piles. The cover system and increased temperatures from the heat trace had no significant effect on microbial populations compared to the uncovered test pile.

Table 5.1 Calculated mass loadings for parameters of interest from the Covered test piles (2007 to 2010).

Covered Pile	Mass											Flow ($x10^3$ L)
	Ca (kg)	K (kg)	Mg (kg)	Na (kg)	Al (g)	Fe (g)	Co (g)	Ni (g)	Cu (g)	Zn (g)	S (kg)	
2007												500 L
2008	41	14	40	15	0.11	1.9	35	180	24	89	26	30
2009	18	5.9	17	6.5	0.2	7.0	39	200	65	110	39	46
2010	42	15	46	14	1.5	11	210	960	190	710	105	114
Total	101	34.9	103	35.5	1.81	19.9	284	1340	279	909	170	190

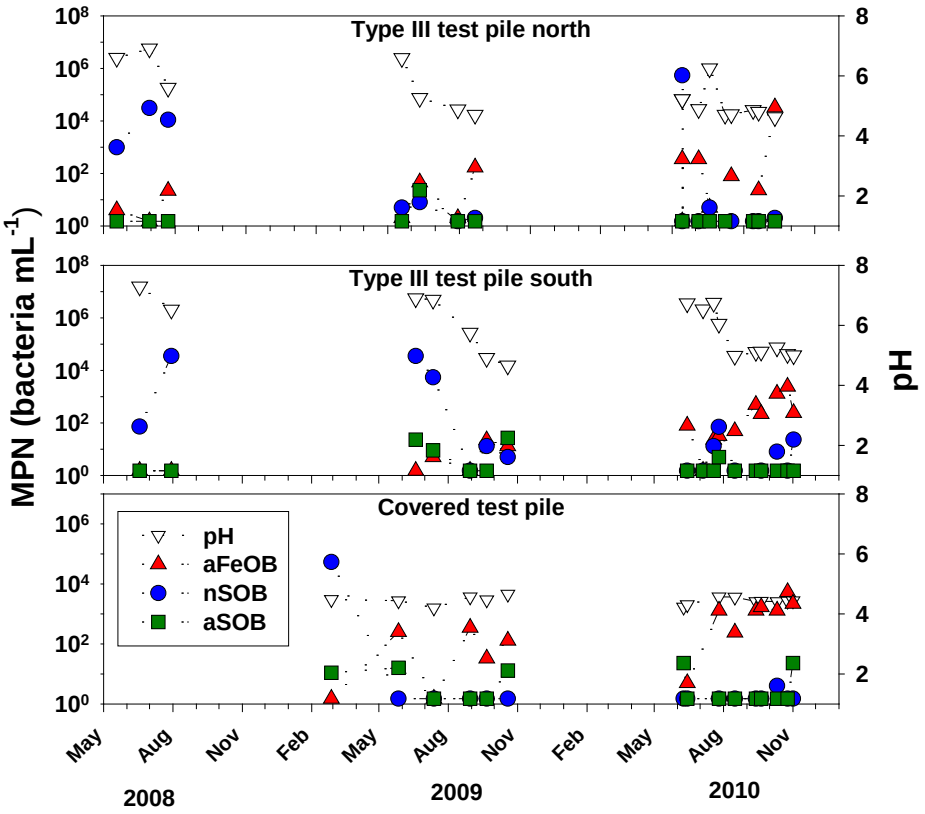

Figure 5.1 Most probable number (MPN) populations of Fe-oxidizing bacteria (aFeOB), neutrophilic S-oxidizing bacteria (nSOB), and acidophilic S-oxidizing bacteria (aSOB) for the Covered test pile compared to the Type III test pile results presented in Chapter 4.

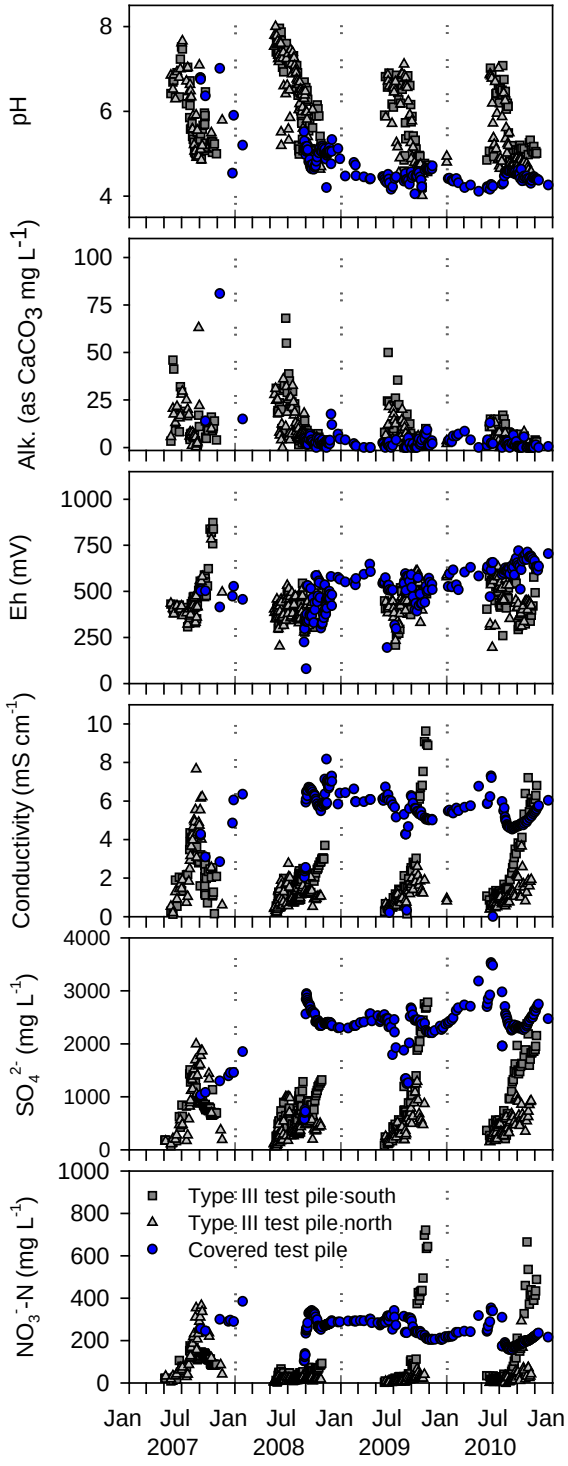

Figure 5.2 Time series plots presenting the pH, alkalinity (mg L^{-1} as $CaCO_3$), E_h (mV), conductivity (mS cm^{-1}), SO_4^{2-}, and NO_3^--N for each sample location.

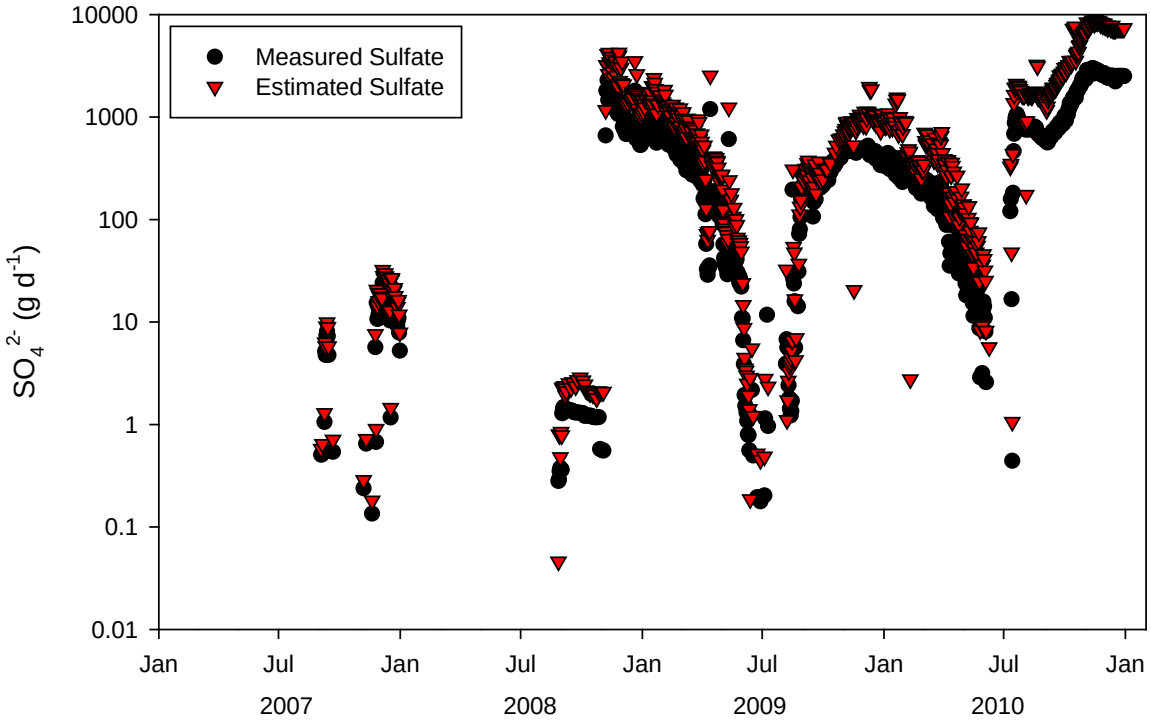

Figure 5.3 Measured daily SO_4^{2-} mass load (g d^{-1}) from the Covered test-pile drain and the estimated daily SO_4^{2-} mass load based on the Ni concentration and the ratio of Ni to S in pyrrhotite.

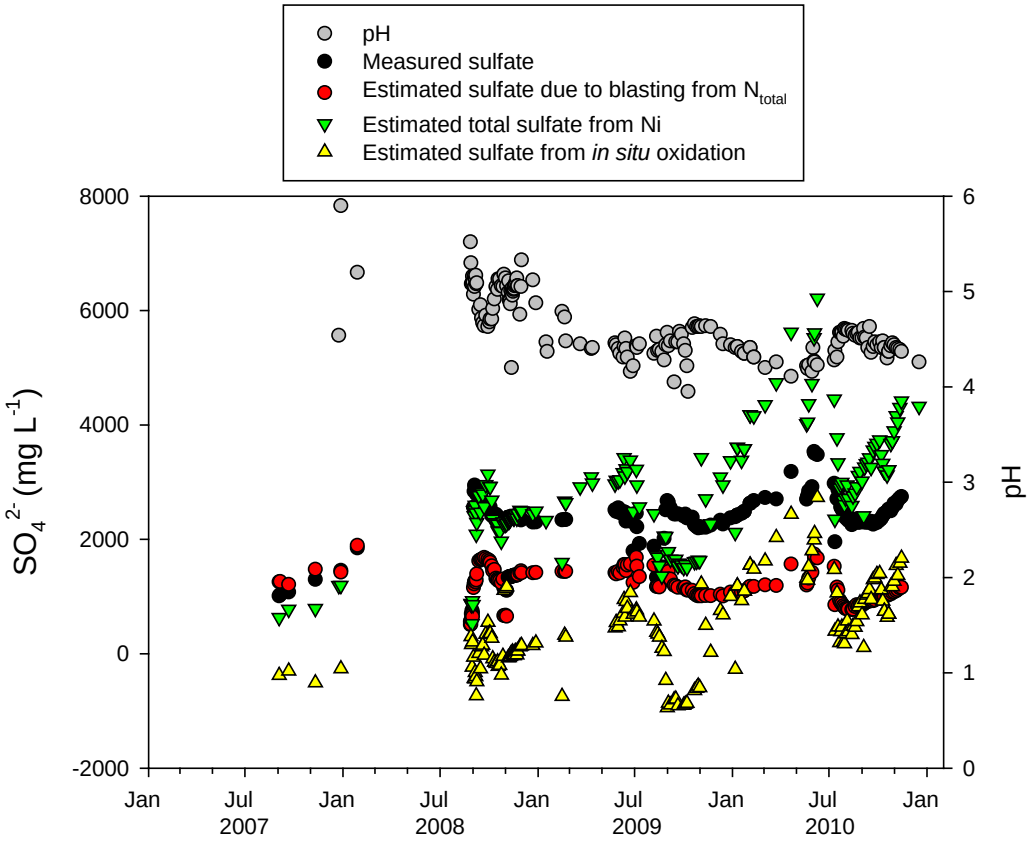

Figure 5.4 Measured SO_4^{2-} concentrations and pH in the Covered test-pile drain compared to 1) the estimated SO_4^{2-} concentrations due to blasting in based on N_{Total}, 2) the estimated SO_4^{2-} concentrations based on the Ni concentration and the ratio of Ni to S in pyrrhotite and 3) the estimated SO_4^{2-} concentration from *in situ* sulfide-mineral oxidation (SO_4^{2-} from Ni - SO_4^{2-} from N_{Total}).

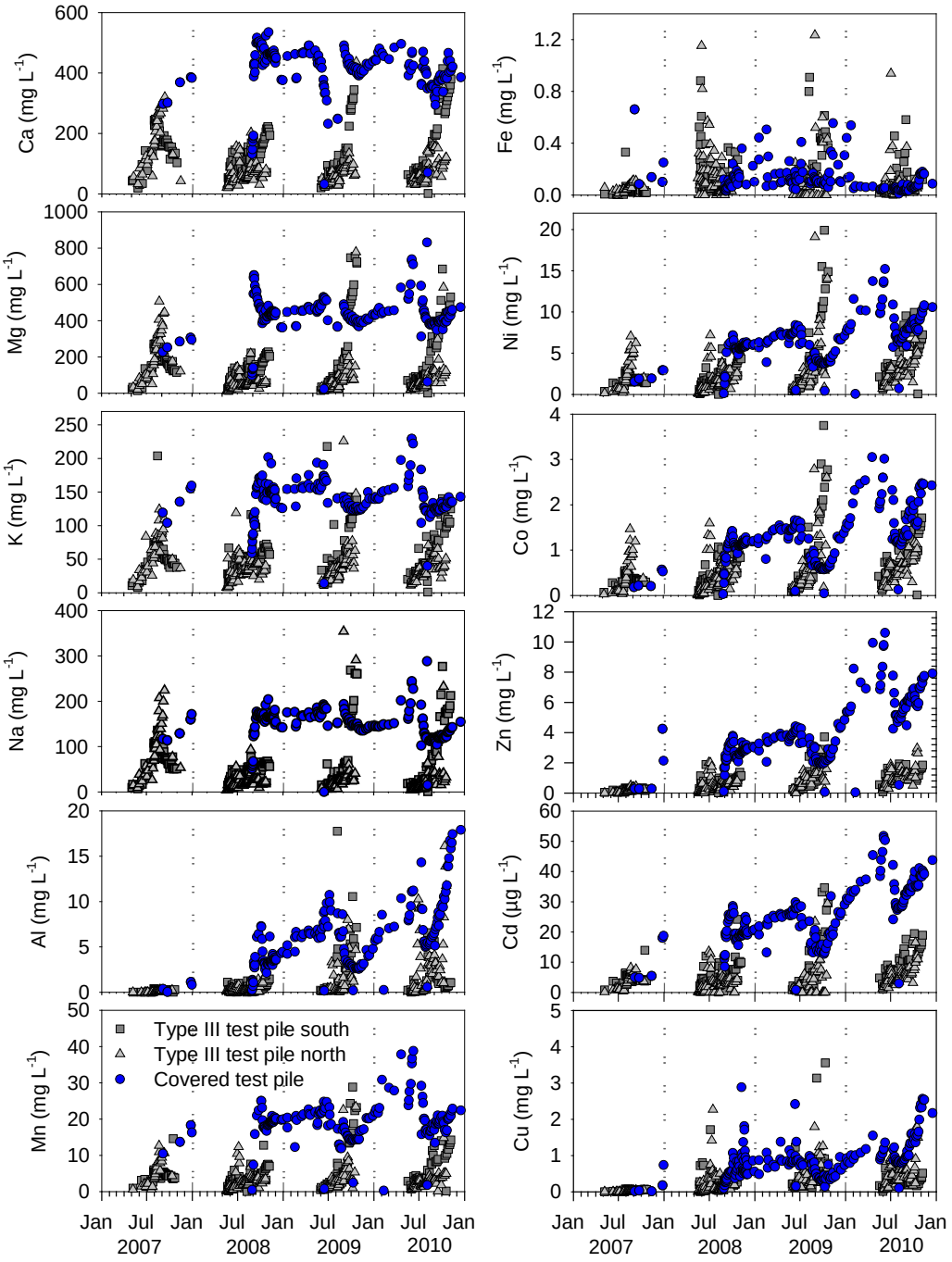

Figure 5.5 Time series plots presenting the major ion water chemistry for the Covered test pile and uncovered Type III test pile.

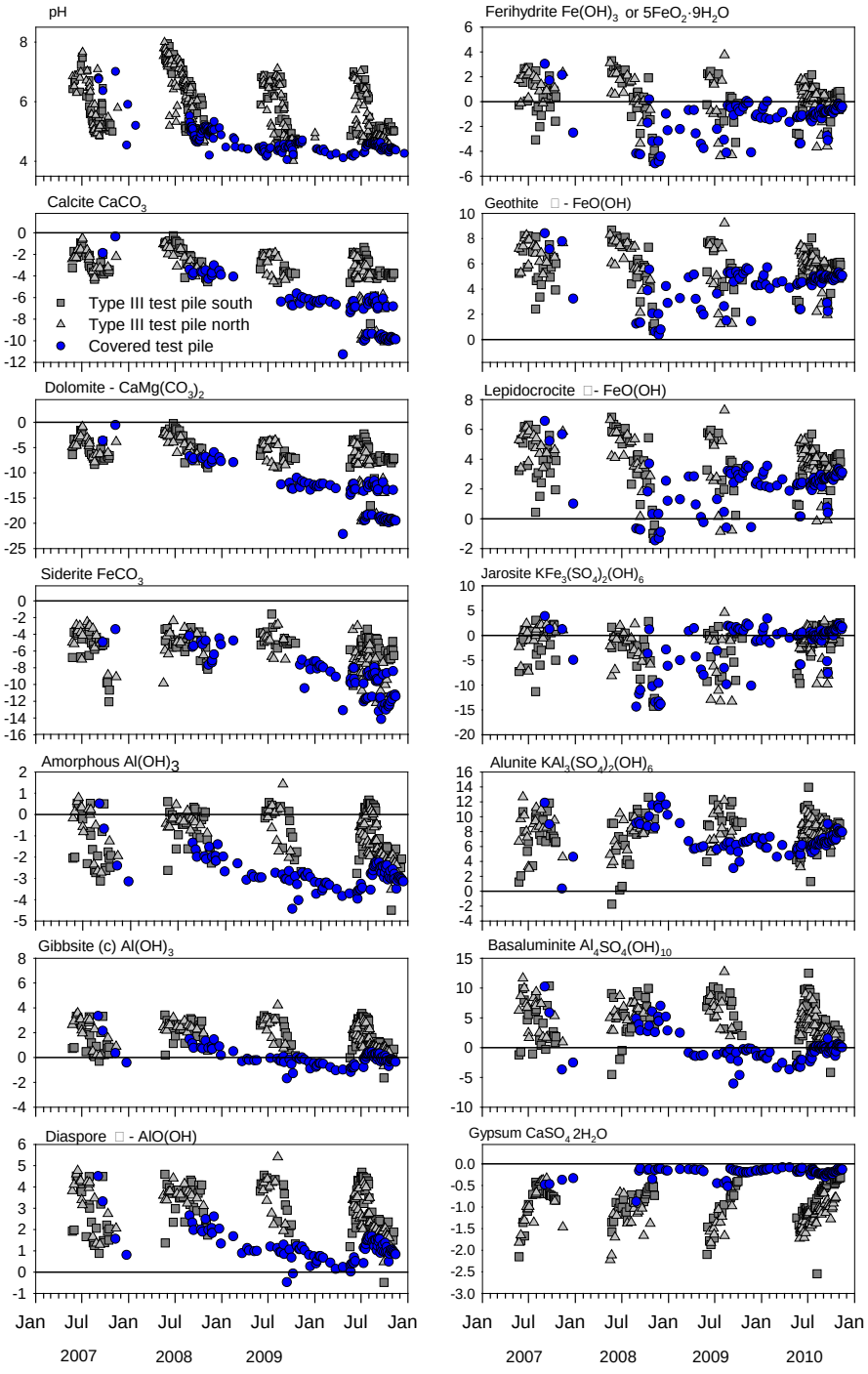

Figure 5.6 Time series plots of calculated saturation indices (SI), using MINTEQA2, for the Covered test-pile drain and Type III test-pile north and south drains. The solid black line at 0 represents equilibrium.

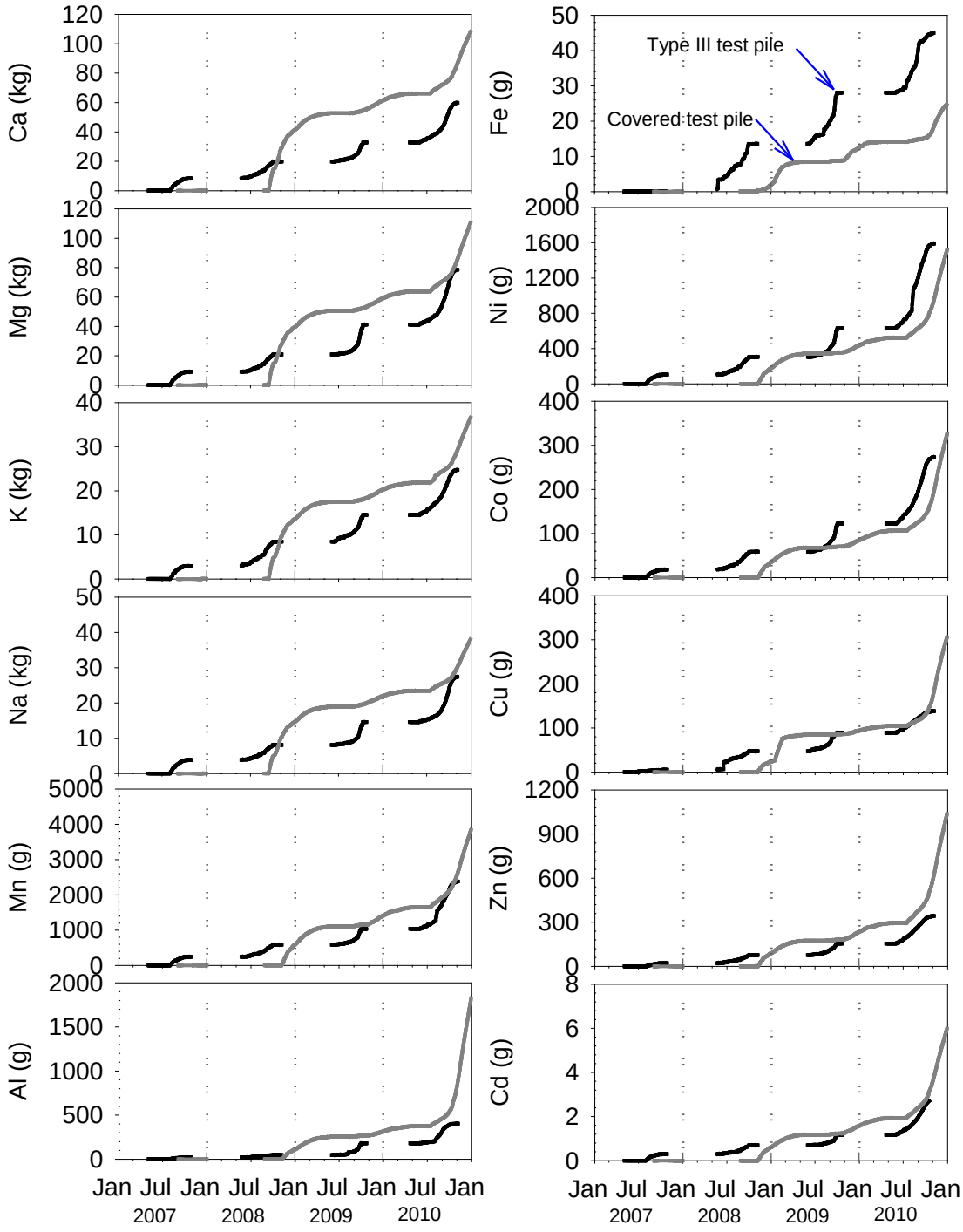

Figure 5.7 Cumulative release of major ions and metals as a function of time for the Covered test pile (grey line) and Type III test pile (black line).

Chapter 6:

The succession of bacterial communities in effluent from waste-rock test piles with a low-sulfur content in the Arctic

6.1 Executive Summary

The bacterial diversity of drainage from waste-rock lysimeters and test piles, with varying S content, at the Diavik Diamond Mine in the Canadian Arctic was examined using deep sequencing and a temporal comparison of the phylogenies at different scales. In addition, populations of neutrophilic and acidophilic S-oxidizers, and acidophilic Fe-oxidizers were enumerated using the most probable number technique. Drainage from waste-rock test piles and lysimeters with the lowest S content (lysimeters: 0.017 wt. % S and test pile: ~ 0.035 wt. % S) had near-neutral pH and contained the highest phylogenetic diversity. Alternatively, the waste-rock test piles and lysimeters with a slightly higher S content (lysimeters: ~0.035 wt. % S, uncovered test pile: ~ 0.053 wt. % S, and covered test pile: ~ 0.082 wt. % S) released acidic drainage and had a less diverse phylogenies. The *Hydrogenophilaceae* family, specifically the genus *Thiobacillus*, was dominant in drainage from most locations where elevated concentrations of sulfide-mineral oxidation products were present. The abundance of N-cycling bacteria increased when concentrations of dissolved N compounds, derived from blasting residuals, increased. The acidophilic Fe-oxidizer, *Acidithiobacillus* sp., was present in drainage from the sampling location where the pH decreased to 3.5 and the highest concentrations of sulfide-mineral oxidation products were observed. The temporal community profiles generated in this study provide a baseline for determining the succession of the microbial communities associated with different stages of sulfide-mineral oxidation in waste-rock stockpiles in the Arctic.

6.2 Introduction

Mining increases the surface area of rock exposing sulfide minerals to atmospheric conditions, including oxygen, water, and microorganisms, frequently leading to the generation of acid mine drainage (AMD). Waste rock from open pit and underground mining is typically stockpiled on the land surface. Runoff from large-scale waste-rock stockpiles undergoes geochemical transitions as the generation of AMD evolves, which can ultimately release high concentrations of SO_4^{2-}, dissolved metals, and H^+. This process is catalyzed by microorganisms, known to oxidize S and Fe containing minerals, increasing the rate of oxidation at both neutral and acidic pH. The oxidation of Fe^{2+} is the rate limiting step in abiotic pyrite oxidation (Singer and Stumm, 1970). *Acidithiobacillus ferrooxidans* and some other acidophiles oxidize Fe^{2+} resulting in mineral oxidation rates that are orders of magnitude faster than abiotic laboratory rates (Kirby *et al.*, 1999). A succession of bacterial species, capable of S oxidation with progressively lower pH resulting in ideal conditions for *Acidithiobacillus* spp., has been observed in a sulfide-rich mill tailings impoundment (Blowes *et al*., 1995). The microbial ecology of effluent from sulfidic waste-rock stockpiles is anticipated to evolve with the geochemistry of the effluent, from neutrophilic S- (e.g., *Thiobacillus* species) to acidophilic S- and Fe-oxidizers (e.g., *Acidithiobacillus* species).

The phylogenetic communities of AMD mine tailings impoundments have been shown to include the *Acidobacteria*, *Nitrospira*, *Firmicutes*, *Actinobacteria* and *Proteobacteria* phylotypes (Baker and Banfield, 2003; Mendez *et al*., 2008). In addition, a spatial and temporal analysis of the microbial community in a Pb-Zn mine tailings study found distinct microbial populations with the different oxidation stages of the mine tailings (Huang *et al*.,

2011). The phylogeny of an extreme AMD site (pH < 2) has been investigated to understand the microbial ecology and changes as a function of geochemical conditions, resulting in the discovery that 70 % of clones may represent new genera (Bond *et al*., 2000). Studies using the new generation of pyrosequencing for the phylogeny of communities found in mine tailings and pore water exist; however, no studies have been completed on runoff from waste-rock stockpiles with evolving geochemistry in northern climates.

In Polar Regions, soil microorganisms have adapted to a unique ecosystem that includes low temperatures and long periods of frozen conditions. These conditions, along with other physical and chemical conditions differ from temperate-region soils. Sattley and Madigan (2006) showed biological S cycling at pH 7 is occurring in Lake Fryxell, a polar lake located in Antarctica, and identified strains to be related to mesophilic *Thiobacillus* species, such as *Thiobacillus thioparus*. Additionally, studies have shown Fe- and S-oxidizing bacteria are present at low temperatures (e.g., Leduc *et al*., 1993; Liljeqvist *et al*., 2011) and can contribute to the sulfide-mineral oxidation at temperatures as low as -11 °C in the laboratory (Elberling, 2005). Chu *et al*. (2010) suggested that bacterial community composition in Arctic soils is structured based on soil pH and that the diversity and richness of microbial communities in Arctic soils is similar to those found in lower latitudes. However, there is little information on the total diversity of microorganisms in waste-rock piles located in polar climates.

In this study effluent from experimental waste-rock test piles located at a site in the Arctic were investigated to evaluate the evolution of the total bacterial diversity with changing geochemistry, and at different scales. The test piles had differing S contents and one test pile

was constructed with a proposed reclamation covered system (Chapter 4 and 5). In addition, four 2 m by 2 m experiments were used to examine the thermally active zone in the upper 2 m of the waste rock (Chapter 3). Bacterial diversity was assessed using culture-independent analysis including next-generation pyrosequencing of effluent samples. Culture-dependant analysis was used to assess the microbial activity of groups of microorganisms typically found in AMD environment, including MPN counts of neutrophilic S-oxidizers (nSOB), and acidophilic Fe- (aFeOB) and S-oxidizers (aSOB). The total diversity of microorganisms within these selective media cultures was also investigated.

6.3 Field Site Description

The Diavik Waste Rock Research Facility is located at the Diavik Diamond Mine (Diavik) on an island in Lac de Gras, an oligotrophic lake (64°29’ N; 110°18’ W; elevation 440 m) in the Northwest Territories, Canada. This research site has a semi-arid climate, with temperatures < 0°C for 8 months of the year. The mean annual air temperature between March 1998 and March 2007 was -9.0 °C and ranged from a maximum of 27 °C in July to a minimum of -44 °C in January/February (Environment Canada, 2010). The mean annual precipitation was 280 mm, of which 65 % occurs as snow (Environment Canada, 2010). A regional study of the local climate over 50 years, suggests the mean annual precipitation for the region is 351 mm, of which 53 % occurs as snow (187 mm) and 47 % occurs as rain (164 mm), and the mean annual air temperature was -10.1°C (Golder Associates, 2008). Over a 5 year period, 2007 through 2011, the mean annual rainfall measured at the test piles was 113 mm and the mean annual air temperature was -8.8°C.

Diavik is an open pit and underground diamond mining operation. At the end of mining Diavik will generate a 120Mt waste-rock stockpile (Smith *et al*., 2012). Waste rock at Diavik is segregate based on S content, rather than lithology into three types: Type I (< 0.04 wt. % S), Type II (0.04 wt. % S to 0.08 wt. % S) and Type III (> 0.08 wt. % S). Waste rock at Diavik predominantly consists of granite and pegmatite granite, and biotite schist, which occurs as irregular laths within the host granite (Jambor, 1997). The granites contain only trace sulfides, and are considered non-acid generating with little neutralization potential (Smith *et al*., 2012b). The biotite schist contains locally disseminated pyrrhotite with lesser amounts of pyrite, sphalerite and chalcopyrite (Jambor, 1997). The biotite schist contains < 0.42 wt. % S and little neutralization potential, therefore, it is considered potentially acid generating (Smith *et al*., 2012b).

6.3.1 Research Facilities

A detailed description of the design, construction, and instrumentation of the Diavik Waste Rock Research facilities is provided by Smith *et al*. (2012a). Geochemical and microbiological sampling procedures are described in Chapter 4. Four 2 m by 2 m scale experiments were constructed to examine the upper 2 m active freeze-thaw region of the waste rock. These experiments consist of 2 m diameter by 2 m in height high-density polyethylene (HDPE) tanks. The tanks were filled with and surrounded by waste rock (referred to as active zone lysimeters; AZLs). Two AZLs were filled with Type I waste rock with an average of 0.017 wt. % S (Type I East AZL and Type I West AZL) and two AZLs were filled with Type III waste rock with an average of 0.035 wt. % S (Type III East and Type III West AZL). Effluent reaching the bottom of the AZLs is gravity fed through a

drainage system, which is heated to prevent freezing, and directed to an instrumentation hut. Inside the instrumentation huts effluent flows through a series of flow-through cells, the first cell is used to collect water samples, the second to continuously measure pH, and the third for continuous measurements of temperature and electrical conductivity. Water is then directed to a calibrated tipping-bucket flow gauge to continuously measure the flow rate.

Three large-scale experimental waste-rock piles (test piles) were also constructed to monitor the hydrology, geochemistry, mineralogy, thermal regime, and gas transport of the waste rock. Two waste-rock test piles measure 15 m in height by 60 m by 50 m at the base. The first test pile consisted of 0.035 wt. % S (Type I test pile) and another with 0.053 wt. % S (Type III test pile). The third test pile was designed based on a reclamation concept proposed by the mine and consists of waste rock with 0.082 wt. % S, resloped and capped with a lower permeability till layer and freeze-thaw layer (Covered test pile; base of 80 m by 125 m based on contoured 18º (3H:1V) slopes and a 24 m wide crest). Each test pile was constructed on a graded base and lined with HDPE. Water reaching the base of each test pile flows by gravity through drainage systems, referred to as the basal drains, which is heated to prevent freezing over the winter. The basal drains connect to an instrumentation hut, which contains a series of flow through cells identical to the AZLs. The Type I and Covered test piles each have one drain line (Type I basal drain and Covered test-pile basal drain) leading to the discrete instrumentation huts, whereas the Type III test pile has two drain lines (Type III south and north basal drains) that also lead to discrete instrumentation huts.

6.4 Materials and Methods

6.4.1 Effluent Sample Collection for Microbial Analysis

Samples were collected at various times from 2008 through 2010 for most probable number (MPN) analysis as discussed in Chapters 3, 4 and 5. Samples were collected for MPN analysis in 2011 for this study following the methods described in Chapter 3. In addition, in 2010, samples were collected at various times for phylogenetic analyses from the basal drain lines of each test pile during periods of flow (Type I, Type III and Covered test-pile basal drains) and on October 11, 2010 from the AZLs. Effluent samples were collected using 0.64 cm polyethylene tubing attached to a sterile 60 mL PE syringe from flow through cells. Water was stored in sterile HDPE sample bottles at 4 °C until analysis was completed at the University of Waterloo. In the laboratory, a known volume of water from each sample was filtered through a sterile 0.2 μm cellulose-nitrate membrane (45mm diameter; Millipore, Bedford, MA, US). Filters were stored at -20 °C until DNA was extracted or processed immediately.

6.4.2 Microbial Enumerations

Microbiological enumerations were conducted for three physiological groups of bacteria using the MPN technique (Cochran, 1950). Techniques and media for the enumeration of neutrophilic S-oxidizers (*T. thioparus* and related species; nSOB), acidophilic S-oxidizers (*At. thiooxidans*; aSOB), and acidophilic Fe-oxidizers (*At. ferrooxidans*; aFeOB) are described by Hulshof *et al*. (2006).

6.4.3 Isolation of Solid Media

Samples collected from the Type III south basal drain and the Covered test-pile basal drain on October 19, 2009 were serially diluted in a sterile basal salts solution. Dilutions were spread onto solid media plates to enumerate acidophilic Fe- and S-oxidizing bacteria, acidophilic heterotrophs, and moderately acidophilic Fe-oxidizing bacteria as described by Johnson and Hallberg (2007) and Johnson *et al*. (2005). Plates were incubated for 10–15 days at 30 °C. Colonies were differentiated by morphological characteristics and representative colonies were repeatedly sub-cultured on fresh solid media to obtain pure cultures. One colony from each of the moderately acidophilic Fe-oxidizing pure culture plates for the Type III south drain and Covered test piles were lysed and their 16S rRNA genes amplified and sequenced, as described by Lindsay *et al*. (2011).

6.4.4 DNA Extraction

DNA extraction was carried out on samples collected in 2010 from the Type I and Type III AZLs, Type III south drain and Covered test-pile drain. In addition, samples from the Type III south drain were collected in 2011 for DNA extraction from effluent on July 5 and October 16. After aFeOB, nSOB, and aSOB MPN media were inoculated with the effluent from the Type III south drain on October 16, 2011, and incubated for four weeks, the 10^0 dilution cultures were filtered through cellulose-nitrate membranes for DNA extraction. All filters were processed immediately or stored at -20 °C until DNA was extracted. Prior to DNA extraction, the cellulose-nitrate membranes were removed from the freezer and allowed to thaw at room temperature. Genomic DNA was isolated from the cellulose-nitrate

membranes using the UltraClean Soil DNA Kit (MoBio, Carlsbad, CA, USA) as per the supplier's instructions. Purified DNA was stored at -20 °C until use.

6.4.5 Pyrosequencing and Data Analysis

Purified DNA was centrifuged at 10,000x to a final concentration of 20 ng μL^{-1}. DNA samples were quantified using an ND-1000 spectrophotometer (Nanodrop Technologies, Wilmington, DE). The characterization of the microbial community present in the effluent from each sample location was conducted via 16S rRNA pyrosequencing analysis. In 2010, the pyrosequencing was performed using primers 28F 5' GAGTTTGATYNTGGCTC and 519r 5' GWATTACCGCGGCKGCTG for bacterial populations with a Roche 454 FLX Genome Sequencer. In 2011, the analysis was performed using primers 27F 5'AGRGTTTGATCMTGGCTCAG and 519r 5' GWATTACCGCGGCKGCTG. All sequence analysis in 2010 was performed at Research and Testing Laboratory (Lubbock, Texas) as described by Dowd *et al*. (2008) and references therein, and all sequence analysis in 2011 was performed at Molecular Research LP (Shallowater, TX) following the same method.

All 16S rRNA read libraries were processed using the pyrosequencing pipeline of the Ribosomal Database Project (RDP) II website (http://pyro.cme.msu.edu/). Sequence alignments were constructed using the aligner tool provided by RDP and only sequences with $\geq$ 50 base pairs were retained. The aligned sequences were clustered according to the farthest neighbour clustering principle to group similar sequences. The RDP classifier software Release 10 (Wang *et al*., 2007) was used to identify a representative microorganism for each

cluster using default parameters (80 % confidence threshold). The relative abundance of each taxonomic group was determined by dividing the number of classified reads by the total read number of each sample. The sequences were compared against the National Center for Biotechnology Information online database using the Basic Local Alignment Search Tool nucleotide algorithm (BLASTn; Altschul *et al*., 1990). The community richness and diversity indices (Shannon's diversity index (H′); ChaoI estimator; rarefaction curves with a threshold of > 97 %) were determined using the RDP software.

6.5 Results

6.5.1 MPN Counts

The microbial enumerations from 2008 through 2010 in the Type I and III AZLs, Type I and III test piles, and the Covered test pile are described in Chapters 3, 4 and 5, respectively. Samples from each location were collected in 2011 for this study (Figure 6.1, Figure 6.2 and Figure 6.3).

The MPN values indicated that the microbial populations in Type I AZLs were dominated by neutrophilic S-oxidizers in 2011 and numbers increased from 2008 through 2011 (Chapter 3; Figure 6.1). The Type I AZLs had a small number of acidophilic S-oxidizing bacteria in all years. No acidophilic Fe-oxidizing bacteria were detected in the Type I AZLs from 2008 through 2011 (Figure 6.1).

Low populations of neutrophilic S-oxidizing bacteria were detected in the Type III AZLs in 2011, similar to previous sampling sessions in 2008 through 2010 (Chapter 3; Figure 6.1). Acidophilic S-oxidizing bacteria were the dominate species present in the Type III AZLs

throughout 2010 and were elevated at the beginning of 2011 (Figure 6.1). Populations of aSOB decreased as the pH decreased from 3.7 to 3.1 at the end of 2011. No acidophilic Fe-oxidizing bacteria were detected in the Type III East AZL from 2008 through 2010, whereas a measurable population was present in the Type III West AZL in November 2010 (Chapter 3). Acidophilic Fe-oxidizers were detected in both Type III AZLs in late 2011 as the population of acidophilic S-oxidizers decreased (Figure 6.1).

The Type I test-pile pH was near neutral for the duration of the study with slight decreases at the end of the field season (to approximately pH 5.5). The basal-drain effluent from the Type I test pile contained a population of neutrophilic S-oxidizers in 2011, similar to previous years (Chapter 4). Acidophilic S-oxidizers were only detected at very low numbers ($< 10^2$ bacteria mL^{-1}) from 2008 through 2011 (Figure 6.2). Low populations ($< 10^3$ bacteria mL^{-1}) of acidophilic Fe-oxidizers were detected in samples collected in June 2009, late in 2010 and in 2011.

The pH observed in the Type III test-pile basal drain decreased each year from near-neutral pH in May to less than 4.5 at the end of the field season (Figure 6.2). Numbers of nSOB were greatest in August 2011 when the pH was 4.7 (up to 5.4×10^5 bacteria mL^{-1}), and in October 2011 when the pH was 4.8 (2.4×10^4 bacteria mL^{-1}). Acidophilic S-oxidizers were detected with low numbers at the beginning of 2011 ($< 10^2$ bacteria mL^{-1}), similar to samples collected in 2008 through 2010. The population of aFeOB decreased in early 2011 concomitantly with pH, through September, and increased to the highest detected numbers at this location by November 2011 ($\sim 10^4$ bacteria mL^{-1}).

The pH in the Covered test pile ranged from 4.0 to 4.7 for all effluent samples collected for microbial analysis. In 2011, increased numbers of neutrophilic S-oxidizers were detected in August (3.5×10^4 bacteria mL^{-1}) and late November (7.9×10^3 bacteria mL^{-1}; Figure 6.3), compared to samples collected in 2008 through 2010 (Chapter 5). The population of aFeOB were the highest reported to date in 2011 (up to 5.0×10^4 bacteria mL^{-1}; Figure 6.3). Acidophilic S-oxidizers were only detected in a few samples with populations < 10^2 bacteria mL^{-1} in 2011, similar to previous years (Chapter 5; Figure 6.3).

6.5.2 Isolation of Indigenous Bacteria

Following inoculation with effluent from the Type III south drain, colonies of microbes grew on ferrous iron/thiosulfate overlay media at a pH of 3.8 after 10 - 15 days of incubation (80 CFU mL^{-1}). The most abundant colony was chosen for further study (isolate 3BS1). Only 4 CFUs were detected on the acidic heterotrophic overlay plate, and no CFU were detected on the acidophilic S-oxidizing overlay plate.

Innoculation with effluent from the Covered test pile resulted in growth of a population on the ferrous iron/thiosulfate overlay media after 10-15 days of incubation (1.47×10^2 CFU mL^{-1}). Two colonies were observed, the first, a small red Fe stained bacteria (isolate CB1), and the other had a “fried egg” morphology (isolate CB2). Both were selected for phylogenetic analysis. Limited CFU grew on the acidophilic heterotrophic and ferrous iron/tetrathionate overlay plates and no CFU grew on the acidophilic S-oxidizing overlay plate.

6.5.2.1 Phylogenetic Analysis of Isolates

Analysis based on 16S rRNA gene sequences showed that two of the isolates were closely related to known bacterial genera. The closest (99 %) 16S rRNA gene sequence in the public database for CB1 was an uncultured *Stenotrophomonas* bacterium of the *Xanthomonadaceae* family found in deep-granitic-fracture water in Colorado. The three closest recognised species were also from the *Xanthomonadaceae* family; *Frateuria* sp. a neutrophilic acetogenic microbe; *Dyella* sp. which has been found in plant roots (Weisskopf *et al*., 2011); and, *Rhodanobacter sp.* which has been isolated from uranium and nitrate contaminated subsurface sediment (Table 6.1).

There were no close relatives of 3BS1 in the database. The closest 16S rRNA gene sequence for isolate 3BS1 was an uncultured bacterial clone from a concrete sewer biofilm in the Cincinnati metropolitan area. The closest classified species was *Thiobacillus plumbophilus* (forward primer: 96% and reverse primer: 98%; Table 6.1) isolated from a uranium mine and named as such from its ability to oxidize galena (PbS), forming anglesite ($PbSO_4$) (Drobner *et al*., 1992). No Fe^{2+} was oxidized by this isolate and it grew between pH 4.0 and 6.5 at temperatures between 9 and 41 °C (optimum around 27 °C).

6.5.3 Culture-Independent Analysis

6.5.3.1 Pyrosequencing of Effluent Samples

6.5.3.1.1 Diversity

Rarefaction curves illustrating the sequence coverage of species diversity (by operational taxonomic unit; OTU) with diversity indices were generated for all sample locations (Figure

6.4 and Figure 6.5). The failure of the rarefaction curves to reach a plateau at OTUs estimated at a distance of 0.03, suggests the communities were incompletely sampled. The Chao1 minimum richness estimates indicated that no sample reached the observed number of OTUs and that they did not reach the plateau with the current sequencing efforts (Table 6.2). Approximately 50 - 70 % of the OTUs predicted by the Chao1 estimator were actually observed. The small amount of bacterial diversity remaining to be sampled was similar to other studies (Bolhuis and Stal, 2011).

Of the large-scale test piles, the Type I basal drain had the highest phylogenetic diversity (by OTU) in 2010 followed by the Type III south drain, and then the Covered test-pile basal drain (Figure 6.4). The Type III test-pile basal drains had the most number of sequences (with the exception of the October 25, 2010 sample), followed by the Covered test pile, and then the Type I test pile (Figure 6.4). Rarefaction curves showed similar levels of diversity for both samples from the Type I test-pile basal drain (Figure 6.4). The Chao1 for the Type I test-pile basal drain indicated both samples had similar richness (Table 6.2).

The Type III test-pile south drain 2010 samples had better coverage than the Type I test pile, with less OTUs from September through to the end of October. The sample collected in July 2011 from the Type III south test-pile drain had the highest diversity of all samples collected from this location (Table 6.2). The sample collected from the Type III south basal drain on October 25, 2010 had the highest richness with 103 of a possible 136 observed number of OTUs.

The Covered test-pile basal drain had similar rarefaction curves on all three sampling events with a similar number of sequences. The Chao1 for the Covered test-pile basal drain on September 9, 2010 (152) had the least agreement with the observed number of OTUs (254) resulting in a lower richness (60 % coverage). The other samples from this location had a similar level of coverage as the Type I test pile.

At the AZL scale, the rarefaction curves and the Shannon estimators indicated the Type I East AZL was more diverse than the Type I West AZL, and both had a higher diversity than the Type III AZLs that were similar to each other (Figure 6.5). The Type III East and West AZLs had the highest number of OTUs compared to the expected number, estimated by Chao1, suggesting these samples had a higher richness than the Type I AZLs (Figure 6.5). The rarefaction curves failed to plateau at all AZL locations; however, the slopes of the Type III AZLs were the steepest. The rarefaction curve did not become asymptotic with increasing sample size suggesting the sequencing effort was not sufficient to capture the complete diversity.

6.5.3.1.2 Phylogenetic Analysis

Bacterial sequences were identified and grouped by phylum, or in the case of *Proteobacteria* by class, using the RDP classifier. The Type I basal-drain samples had similar phylogenetic composition, dominated by *Proteobacteria*. The October 11, 2010 sample was dominated by *Betaproteobacteria* (78 %), whereas the October 25, 2010 sample had similar populations of *Alphaproteobacteria* (31 %), *Betaproteobacteria* (29 %), and *Actinobacteria* (36 %; Figure 6.6). A small percentage of *Firmicutes*, *Bacteroidetes* and TM7 were also observed in the

Type I test-pile drain, but in low numbers. No *Gammaproteobacteria* were observed in the Type I test-pile drain.

The Type III south basal-drain sample was dominated by *Betaproteobacteria* in 2010, with a decrease from 75 % in September to 64 % in late October. *Alphaproteobacteria* increased over time, and *Actinobacteria* decreased from September 13, 2010 to October 10, 2010 (Figure 6.6). In addition, *Bacteroidetes* were present on October 25, 2010. *Gammaproteobacteria* were highest in October 10, 2010 at 12 %. The community shifted in July 2011, the dominant phylum was *Actinobacteria* (68%) with lower proportions of *Betaproteobacteria* (14 %) and higher proportions of *Gammaproteobacteria* (18%) than previously observed. By October 2011, the community shifted back to a similar distribution previously observed in the fall of 2010; *Betaproteobacteria* (50 %) became the dominant phylum, with decreased *Actinobacteria* (6 %), similar *Gammaproteobacteria*, and the presence of *Alphaproteobacteria*.

The Covered test-pile basal drain was dominated by *Gammaproteobacteria* (62 %) on July 26, 2010, followed by *Betaproteobacteria* (30 %) and *Actinobacteria* (8 %; Figure 6.6). On September 20, 2010 and October 11, 2010 the Covered test-pile effluent was dominated by *Betaproteobacteria* (72 % and 68 %, respectively) with some *Gammaproteobacteria* (16 % and 23 %, respectively) and *Actinobacteria* (9 % and 7 %, respectively), and a small fraction of *Alphaproteobacteria* (1% on both dates).

The Type III West AZL effluent was dominated by *Proteobacteria*, specifically *Betaproteobacteria* (90 %) and *Gammaproteobacteria* (5 %; Figure 6.6). A small population

of *Actinobacteria* (3 %), and *Cyanobacteria* (1%) were also present. The sample from the Type III East AZL was dominated by *Actinobacteria* (82 %), with small amounts of *Proteobacteria* (16 %), *Bacteroidetes* (1 %), and *Cyanobacteria* (1%), similar to the Type III test pile in July 2011. The Type I East AZL was dominated by *Proteobacteria*, specifically *Betaproteobacteria* (51 %) and *Alphaproteobacteria* (7 %). *Actinobacteria* (30 %) were also abundant in the Type I East AZL samples, with lesser amounts of *Bacteroidetes* (5 %), *Firmicutes* (2 %), and TM7 (19 %). The samples from the Type I West AZL had a more diverse phylogeny with a more even spread of *Actinobacteria* (16 %), *Alphaproteobacteria* (14 %), *Betaproteobacteria* (29 %) and *Gammaproteobacteria* (12 %) compared to the Type I East AZL.

6.5.3.1.3 Taxonomic Classification at the Family Level

Bacterial reads were classified into the family taxonomic level based on a 70 % similarity threshold. If genera were specified, it was to a similarity threshold of 50 %. On October 11, 2010 the Type I basal drain effluent was dominated by *Hydrogenophilaceae*, specifically the genera *Thiobacillus* (Figure 6.7). Over time the population became more diverse and on October 25, 2010 the effluent was dominated by the *Microbacteriaceae* and *Bradyrhizobiaceae* families. The *Microbacteriaceae* family included the genera *Salinibacterium* sp., *Microbacterium* sp. and *Leisonia* sp., typical gram positive soil microorganisms. The family *Bradyrhizobiaceae* included the genera *Afipia* sp. and *Bradyrhizobium* sp. The *Bradyrhizobiaceae* family are known nitrogen fixing bacteria and were present when the concentrations of N-species increased from 120 mg L^{-1} NH_3-N,

4.3 mg L^{-1} NO_2^--N, and 760 mg L^{-1} NO_3^--N on October 12, 2010 to 160 mg L^{-1} NH_3-N, 7.4 mg L^{-1} NO_2^--N, and 1270 mg L^{-1} NO_3^--N on October 25, 2010.

The Type III south basal-drain effluent was dominated by *Hydrogenophilaceae,* specifically the genera *Thiobacillus* in 2010 (Figure 6.7). Other families included *Oxalobacteraceae*, *Xanthomonadaceae*, *Microbacteriaceae,* and *Bradyrhizobiaceae* (Figure 6.7). The population of *Microbacteriaceae* (*Frigoribacterium* sp.) and *Xanthomonadaceae* (*Rhodanobacter* sp. and *Thermomonas* sp.) decreased over time as the population of *Bradyrhizobiaceae,* including the genera *Nitrobacter* sp. and *Afipia* sp., increased. In July 2011, the Type III south basal-drain effluent was dominated by *Microbacteriaceae*, with a notably lower abundance of *Hydrogenophilaceae*. By October 2011, *Hydrogenophilaceae, Xanthomonadaceae, Oxalobacteraceae,* and *Comamonadaceae* increased and *Microbacteriaceae* decreased.

The Covered test-pile basal-drain effluent had an increase in *Hydrogenophilaceae,* specifically the genera *Thiobacillus* sp., and a decrease in the *Moraxellaceae* family (*Alkanindiges* sp.) from July through October 2010 (Figure 6.7). Other families present in all Covered test-pile effluent samples included *Oxalobacteraceae* (*Oxalicibacterium* sp.), *Xanthomonadaceae* (*Rhodanobacter* sp.), *Microbacteriaceae* (*Frigoribacterium* sp.), and *Rhodocyclaceae* (*Zoogloea* sp.). Minor families included *Bradyrhizobiaceae, Ectothiorhodospiraceae, Methylococcaceae, Legionellaceae, Intrasporangiaceae,* and *Comamonadaceae.*

The Type III West AZL effluent was dominated by *Oxalobacteraceae* (61 %; *Oxalicibacterium* sp.*),* followed by *Hydrogenophilaceae,* specifically *Thiobacillus* sp. (29 %; (Figure 6.8). Other families included small amounts of *Acidithiobacillaceae* (4 %, specifically *Acidithiobacillus* sp.), *Actinomycetales, Xanthomonadaceae* (*Rhodanobacter* sp.) and *Streptophyta*. The Type III East AZL was dominated by the phylum *Actinobacteria*, which included the family *Microbacteriaceae* (82 %; Figure 6.8). Other families included *Hydrogenophilaceae*, specifically *Thiobacillus* sp., *Xanthomonadaceae* (*Rhodanobacter* sp.), and *Oxalobacteraceae (Oxalicibacterium* sp and *Herbaspirillum* sp.).

The effluent from the Type I West AZL had a diverse phylogeny and was dominated by the families *Comamonadaceae,* TM7, *Legionellaceae*, and *Nocardiaceae* (Figure 6.8). Other families present in limited number included *Rickettsianceae*, *Oxalobacteraceae,* OD1, and *Caulobacteraceae*. The Type I East AZL also had a diverse phylogeny and was dominated by the families *Oxalobacteraceae, Comamonadaceae* and *Nocardianceae* (Figure 6.8). Other families present in limited number included *Microbacteriaceae,* TM7, *Rhodocyclaceae,* and *Streptophyta*. The family *Comamonadaceae* was the most abundant and included *Polaromonas* sp., *Hydrogenophaga* sp. and *Acidovorax* sp. All genera present were common soil microbes.

The representative sequences for each cluster of *Thiobacillus* spp., obtained from each sample, were compared to type strain *Thiobacillus* spp. using a phylogenetic tree (Figure 6.9). The *Thiobacillus* spp. observed in all samples were closely related to *Thiobacillus plumbophilus*.

6.5.3.2 Pyrosequencing of MPN Cultures

The Type III south basal-drain effluent was used to inoculate nSOB, aSOB and aFeOB MPN media to determine the population numbers of each group of bacteria. In addition, the 10^0 dilution from the inoculated MPN media was used to investigate the diversity of the microbial community present after the incubation period. The Chao1 minimum richness estimate indicated that aSOB and nSOB inoculated media reached the observed number of OTUs and the aFeOB inoculated media reached 67 %, similar Chao1 to the field samples (Figure 6.10). The aSOB inoculated media did not reach a plateau with the current sequencing efforts; whereas the nSOB and aFeOB inoculated media became asymptotic with increasing sample size, suggesting the sequencing effort was sufficient to capture the complete diversity for these samples (Figure 6.9).

The Shannon diversity index suggests the aFeOB inoculated media had a lower diversity than the nSOB and aSOB inoculated media. The aFeOB inoculated media was dominated by *Acidithiobacillus ferrooxidans*, which was not one of the dominant members in the sample (< 1 %; data not shown). The nSOB inoculated media had the highest number of sequences (24147) and was dominated by Hydrogenophilaceae, specifically the genera *Thiobacillus* sp. (Figure 6.11). The aSOB inoculated media had the lowest number of OTUs and sequences. In addition, the rarefaction curve did not become asymptotic with the current sampling size, suggesting the sequencing effort was insufficient to capture the total diversity. However, the initial samples used to inoculate the media had a slightly higher number of sequences and OTUs, but a similar coverage to the aSOB inoculated media, suggesting few new bacterial

cells grew during the incubation period. There were no dominant known acidophilic S-oxidizers present.

6.6 Discussion and Conclusion

Waste-rock piles have the potential to host microbes that catalyze the generation of AMD and mobilize metals. In this study, the bacterial diversity deduced by 454 pyrosequencing of metagenomic DNA extracted from waste-rock effluent was estimated. Specifically, changes in the total bacterial biodiversity with evolving effluent geochemistry was observed for waste-rock test piles at different scales. Moreover, the bacterial communities associated with differing S content were characterized by 16S rRNA gene libraries. These analyses were used to estimate the richness and dominant species colonizing waste rock in the Arctic. The community profiles observed in the waste-rock test piles and AZLs suggest typical AMD related species were present in acidic effluent with elevated concentrations of metals, whereas microbes typical of arctic soils were present in effluent with a near-neutral pH and lower concentrations of SO_4^{2-} and dissolved metals.

The Type I test-pile effluent had near neutral pH (ranging from 6.6 to 6.9) with low concentrations of SO_4^{2-} (average of 220 mg L^{-1}) and dissolved metals (Chapter 4), whereas the Type III test pile (pH ~ 5; Chapter 4) and the Covered test pile (pH ~ 4.2; Chapter 5) both had lower pH and higher concentrations of SO_4^{2-} (up to 3000mg L^{-1}) and dissolved metals (Ni, Zn, Cu and Fe). The concentration of N-species in the Type I and Type III test piles increased with each sampling session (Chapter 2). In contrast, the concentrations in the Covered test pile were lower and remained more uniform over time (Chapter 5).

The rarefaction and Chao1 analysis suggest the Type I test pile had the most diverse population of microorganisms, with five bacterial phyla detected including ~20 different families. The Type III test-pile effluent had a lower diversity, but was the richest dataset with a higher number of sequences. Similarly, the Covered test-pile effluent was less diverse than the Type I test-pile effluent, but had more sequences (higher OTUs), suggesting a richer community.

The effluent from the Type III test pile, Covered test pile, and the October 11, 2010 sample from the Type I test pile were dominated by *Hydrogenophilaceae* family, specifically the *Thiobacillus* genus. *Thiobacillus* derive their energy from the oxidation of S-containing electron donors, are known to be involved in the dissolution of metal sulfides through the oxidation of S, and are considered typical of AMD systems. The waste rock used in this experiment has a low organic C content (< 0.01 wt. % C) providing an ideal environment for the growth of some *Thiobacillus* species. Although *Betaproteobacteria* have been shown to be limited by low abundances of organic C (Fierer *et al*. 2007), a high abundance of *Betaproteobacteria* were observed in rhizospheric soils of pioneer plants contaminated with heavy metals and gold tailings and uranium mine sediments that had a low concentration of organic C (Navarro-Noya *et al.*, 2010, and references therein).

Species of *Thiobacillus* sequenced in this study were closely associated with *T. plumbophilus, T. thioparus,* and *T. denitrificans*. On October 11, 2010, the Type I test-pile effluent had a pH of 6.5 and had a high proportion of *Thiobacillus* sp. Some *Thiobacillus* spp. prefer near-neutral pH conditions (Drobner *et al*., 1992; Vlasceanu *et al*., 1997) and have been associated with S-oxidation in AMD related studies (Blowes *et al*., 1995). The

pure culture obtained from the Type III south test-pile drain was similar to *T. plumbophilus*, suggesting this is the main *Thiobacillus* species at this location.

The Type I test pile also had a population of the *Nitrosomonadaceae* family, including chemolithoautotrophic ammonia-oxidizing bacteria, and the family *Bradyrhizobiaceae*, including nitrite-oxidizing bacteria, but *Bradyrhizobiaceae* were more abundant on October 25, 2010 when the concentrations of NO_2^- increased. Similarly, the Type III south drain had increased populations of *Bradyrhizobiaceae* and *Xanthomonadaceae* with increased concentrations of N-species, whereas the the population in the Covered test-pile effluent increased slightly (Chapter 2). The increased concentrations of NO_3^- , NO_2^- and NH_4^+ in the effluent were related to the dissolution of ammonium nitrate used in blasting of the waste rock and the subsequent oxidation of NH_4^+ to NO_2^- and NO_2^- to NO_3^- (Chapter 2). As the concentrations of N-species increased in the effluent, the families of ammonia-oxidizing and nitrate-producing bacteria increased.

Similar to the Type I test pile, the effluent from the Type I AZLs had a near-neutral pH and low concentrations of metals and SO_4^{2-} (Chapter 3). The Type III AZLs had the lowest pH (< 3.5) and highest concentrations of dissolved metals and SO_4^{2-} of all locations (Chapter 3). Nitrogen species were not elevated in the AZLs because they were depleted during the first flush of water through the matrix material in the lysimeters in 2008 (Chapter 2). The Type I AZLs and Type III East AZLs were dominated by genera typical of most soils. A small population of N-cycling bacteria were detected, even though N concentrations were lower than in the test piles.

The Type III East AZL had a low pH similar to the Type III West AZL; however, it had slightly lower metal concentrations. The Type III East AZL was dominated by typical soil genera similar to the Type I AZLs, with the exception of the presence of a population of *Thiobacillus,* which is similar to the test piles. A population of *Thiobacillus* was present in the Type III West AZL, which also included the genus *Acidithiobacillus,* known for the oxidation of S- and Fe(II) containing minerals providing optimal conditions for the growth of this species. The Type III West AZL effluent had a pH < 4 for over 3 years.

The Type III test pile and Covered test pile have slightly higher pH and had a higher number of OTUs in the *Thiobacillus* genera. The microbial activity of bacteria in the aFeOB media suggests *Acidithiobacillus* were present in low numbers (< 10^3 bacterial mL^{-1}); in addition, *Acidithiobacillus* were found in the rare phylogeny (< 1 %) in the Type III basal drain effluent and the Covered test-pile effluent. As the Type III and Covered test piles evolve, it is anticipated that the pH will decrease and higher concentrations of SO_4^{2-} and dissolved metals will be released. The results from the Type III West AZL and other AMD mine tailings studies (Blowes *et al*., 1995; He *et al*., 2008; Mendez *et al*., 2008) suggest that *Acidithiobacillus spp.* may become more abundant when these conditions develop.

The phylogenetic composition and structure of the bacterial communities from waste-rock drainage with evolving geochemistry were characterized. Waste rock with near-neutral drainage and low concentrations of dissolved metals sustained a population of neutrophilic S-oxidizers and had the most diverse population. Soil bacterial diversity in the Arctic has been shown to be structured according to local variations in pH and the highest phylogenetic diversity of the bacterial communities at pH 6 (Chu *et al*., 2010). The phylogenetic

community observed in the Type I test pile included groups of bacteria found in typical healthy tundra soils (Janssen, 2006). Waste rock with low pH drainage was characterized by populations of acidophilic S- and Fe-oxidizers, and had less phylogenetic diversity. The phyla observed in acidic waste-rock drainage were similar to those observed in mine tailings with similar pH (Mendez *et al*., 2008); however, typical AMD microbes from the phylum *Nitrospira* (e.g., *Leptospirillum ferrooxidans*-group) were notably absent. This may be a result of 1) a low abundance and not being captured in the current sampling program, which focussed on aqueous samples, 2) *Leptospirillum ferrooxidans* adhere to mineral surfaces in the waste rock and were not flushed through with the effluent, or 3) the pH has not decreased low enough to maintain a viable population.

The sampling methods used in this experiment suggest good coverage of all microorganisms in the effluent of the waste-rock test piles and AZLs. The high diversity of the neutral pH locations (Type I AZLs and Type I test pile) and high richness of the acidic samples (Type III test pile, Covered test pile and Type III AZLs), are good preliminary results examining the succession of microorganisms in waste-rock test piles with low-S content in the Arctic. In addition, the observed results serve as a baseline for the succession of the bacterial community in waste rock at different stages of sulfide-mineral oxidation. As the waste-rock test piles evolved, the bacterial community adjusted to the evolving effluent chemistry. Further studies of the waste rock effluent and solid samples will aid in understanding the long-term succession of bacteria and archaea involved in the oxidation of sulfide minerals found in waste-rock stockpiles.

Table 6.1 Characterization of isolates from the Type III south and Covered test-pile basal drains.

Location	Primer	Nearest Relative (s) (Accession Number)	Gene Similarity (%) (Sequence Lengths (nt))
Covered test-pile drain	27F	*Frateuria* sp. KP1-34 (AB366186.1)	99 (434/439)
		Dyella sp. Z1-YC6845 (GQ369113.1)	99 (433/439)
	1387R	*Frateuria* sp. Bio32 (AB467342.1)	99 (388/391)
		Dyella sp. Sen1072 (JN590396.1)	99 (388/391)
		Rhodanobacter sp. 2APBS1 (JF719060.1)	99 (388/391)
Type III south drain	27F	*Thiobacillus plumbophilus* (AJ316618.1)	96 (601/627)
	1387R	*Thiobacillus plumbophilus* (AJ316618.1)	98 (620/635)

Table 6.2 Diversity indices for the Type I, Type III south, and Covered test-pile basal drains.

Location	Sample Date	N	Chao	H'	Coverage (%)
Type I	11-Oct-10	1642	387	3.96	62
	25-Oct-10	1839	328	4.10	66
Type III	13-Sep-10	2516	266	3.40	73
	11-Oct-10	2916	268	3.15	67
	25-Oct-10	1506	136	2.70	76
	5-Jul-11	10353	747	3.80	63
	16-Oct-11	5980	332	3.56	68
Covered Pile	26-Jul-10	2393	204	2.51	69
	20-Sep-10	2178	254	3.05	60
	11-Oct-10	2437	217	3.09	69

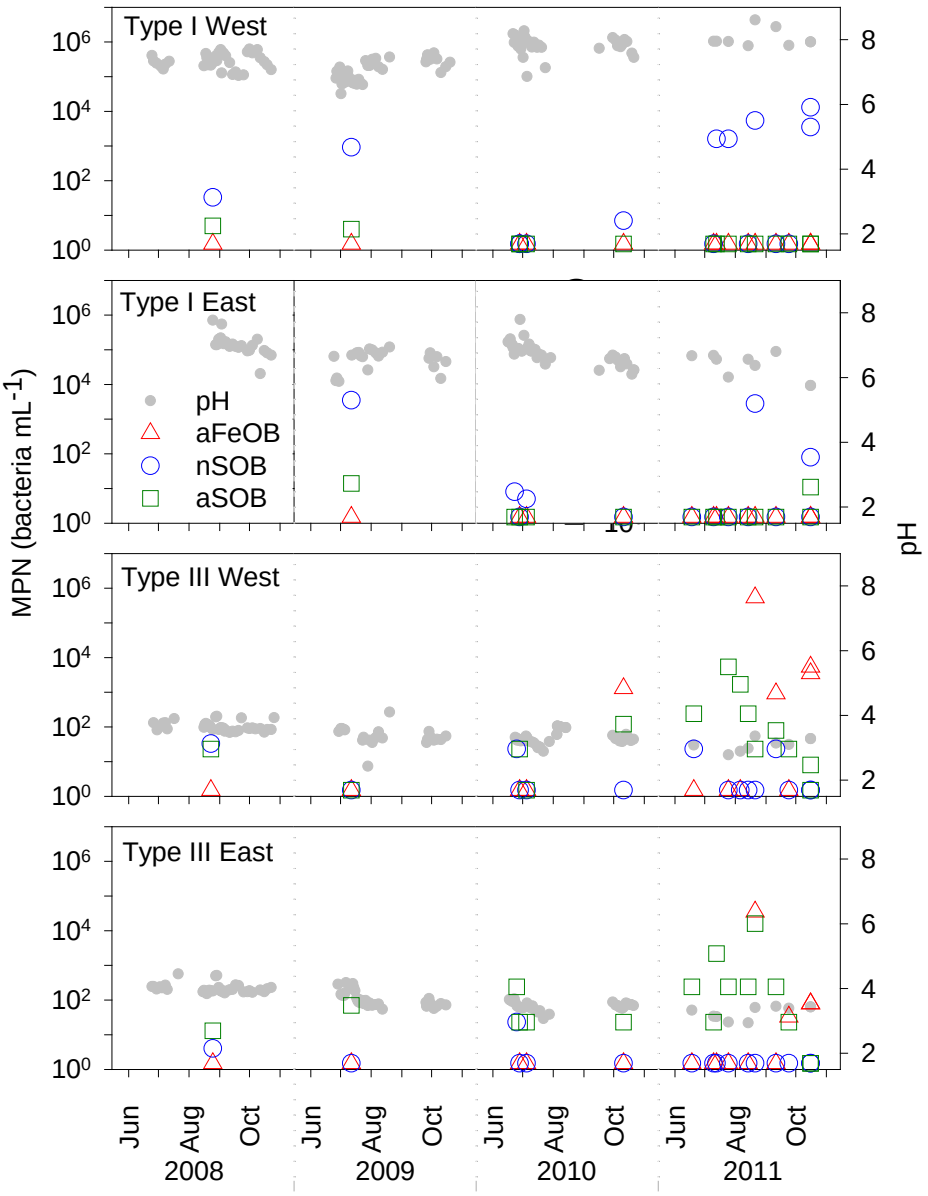

Figure 6.1 Most probable number (MPN) populations of acidophilic Fe-oxidizing bacteria (aFeOB; △), neutrophilic S-oxidizing bacteria (nSOB; ○), and acidophilic S-oxidizing bacteria (aSOB; □) for each AZL with pH (•) (2007 through 2010 data from Chapter 3).

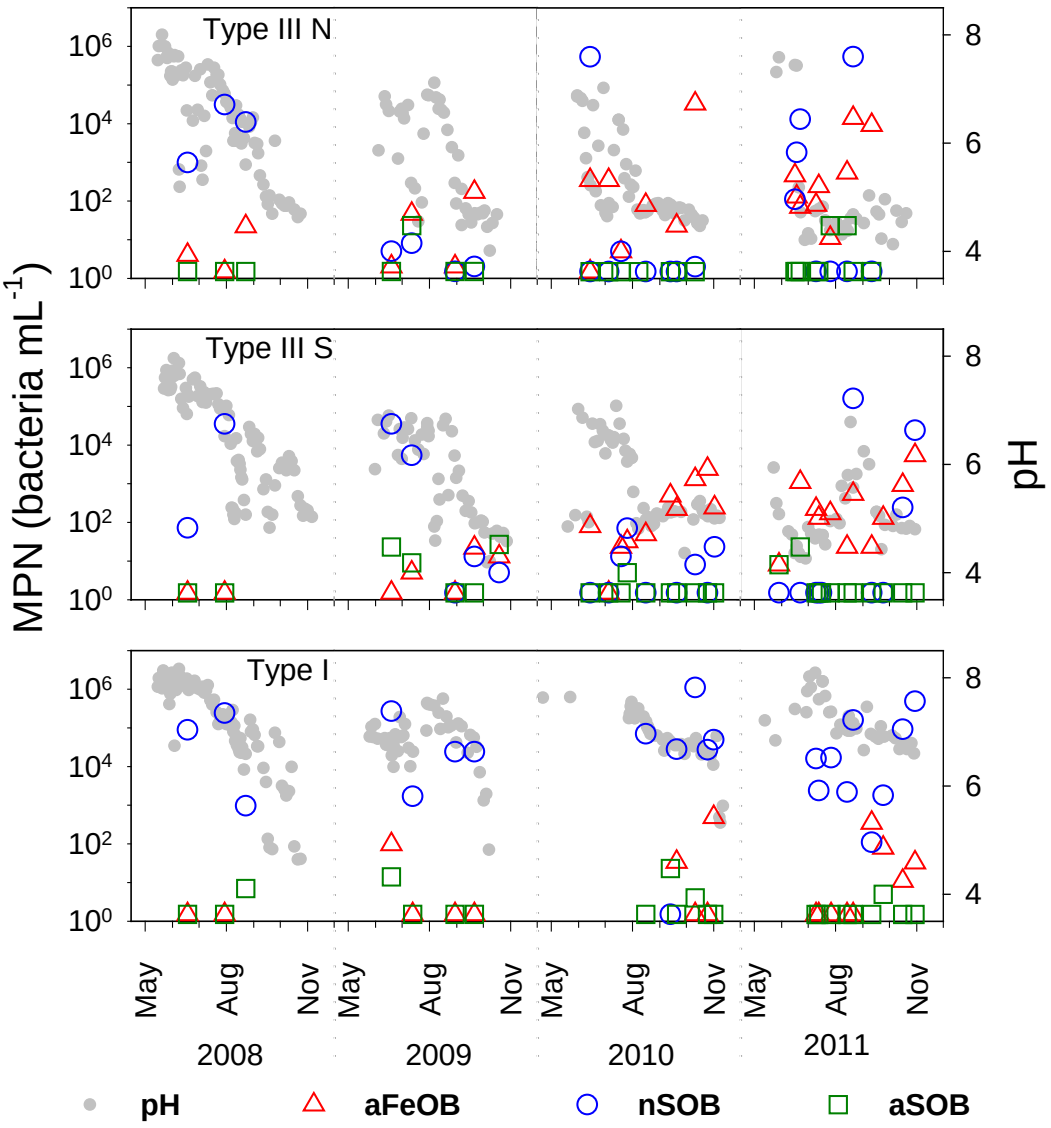

Figure 6.2 Most probable number (MPN) populations of acidophilic Fe-oxidizing bacteria (aFeOB;△), neutrophilic S-oxidizing bacteria (nSOB; ○), and acidophilic S-oxidizing bacteria (aSOB; □) for the Type I, Type III south and north basal drains with pH (•)(2007 through 2010 data from Chapter 4).

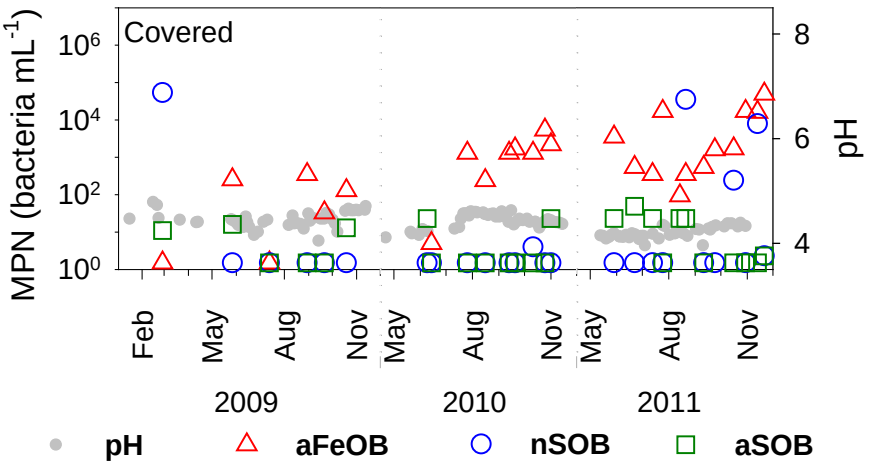

Figure 6.3 Most probable number (MPN) populations of acidophilic Fe-oxidizing bacteria (aFeOB; △), neutrophilic S-oxidizing bacteria (nSOB; ○), and acidophilic S-oxidizing bacteria (aSOB; □) for the Covered test-pile basal drain with pH (•) (2009 and 2010 data from Chapter 5).

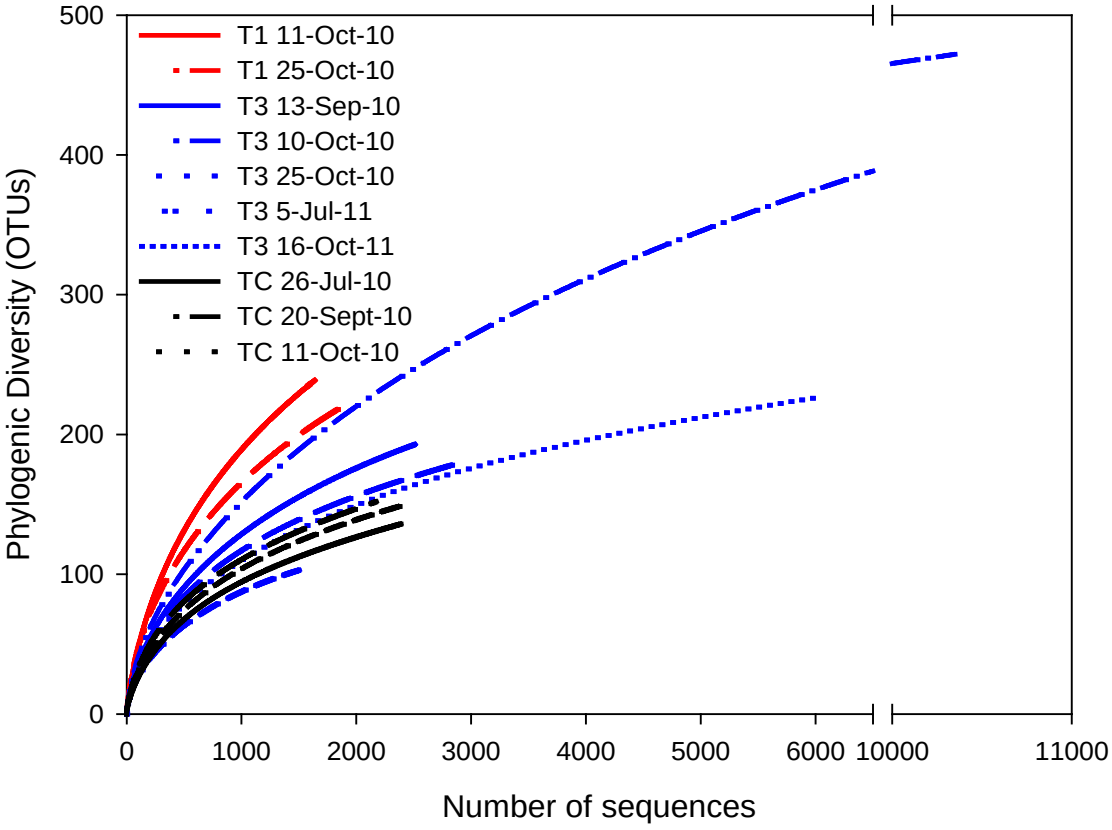

Figure 6.4 Rarefaction curves indicating the observed number of operational taxonomic units (OTUs) at a genetic distance of 3 % in the Type I, Type III and Covered test piles at different times. The Type I (T1), Type III (T3), and Covered test pile (TC) sampling sites are marked by the red, blue, and black color, respectively.

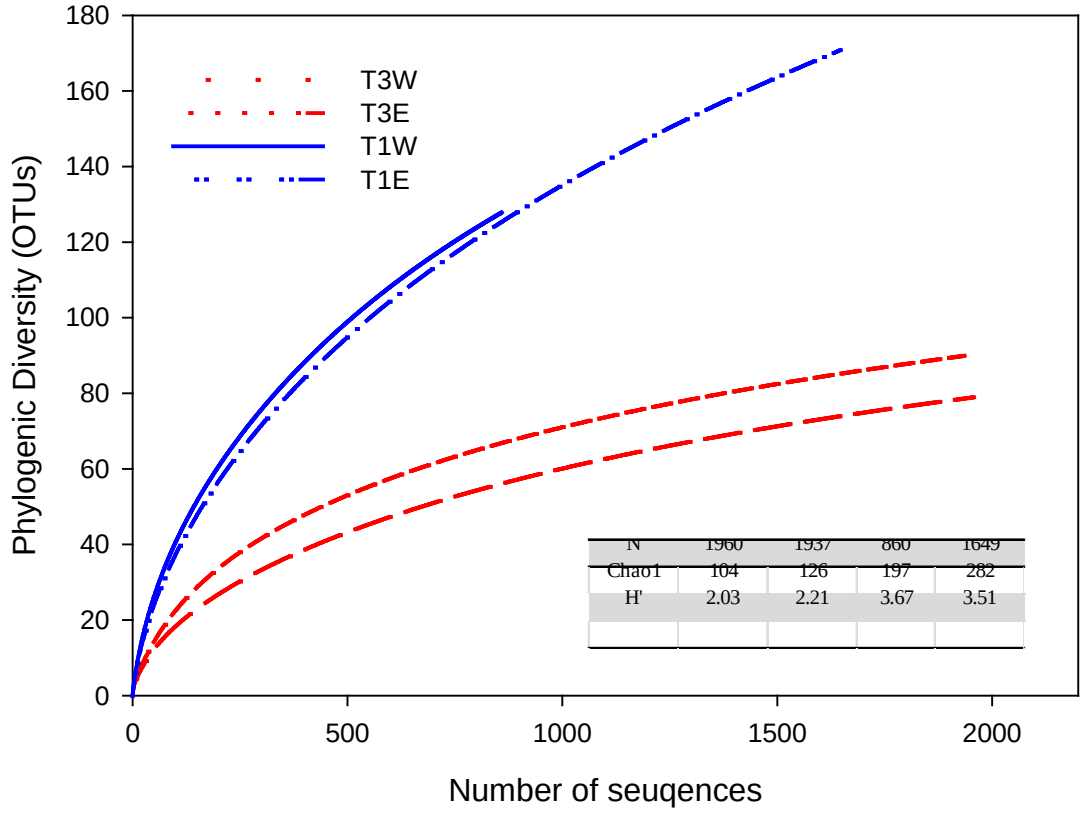

Figure 6.5 Rarefaction curves indicating the observed number of operational taxonomic units (OTUs) at a genetic distance of 3 % in the Type I and Type III AZLs on October 25, 2010. The Type I (1UE and 1UW) and Type III (3UE and 3UW) sampling sites are marked by the blue and red color, respectively.

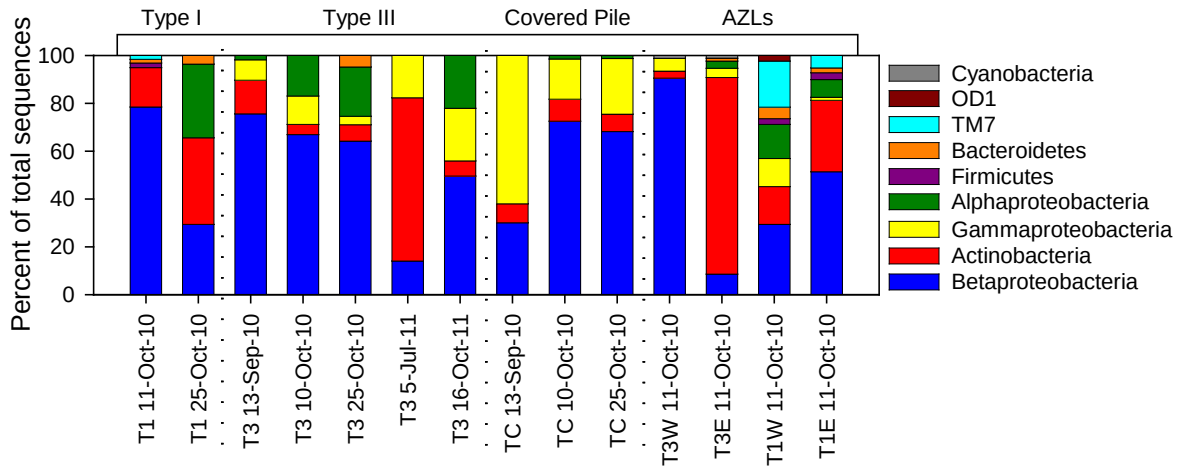

Figure 6.6 Relative abundance of bacterial reads from the Type I, Type III, and Covered test piles and AZLs at the phylum level, with the exception of *Proteobacteria* which is reported at the order level (*Alphaproteobacteria, Betaproteobacteria* and *Gammaproteobacteria*). Reads were classified in the RDP database using a threshold similarity of 50 %. Sample numbers indicating the sampling date and location are given below the graph.

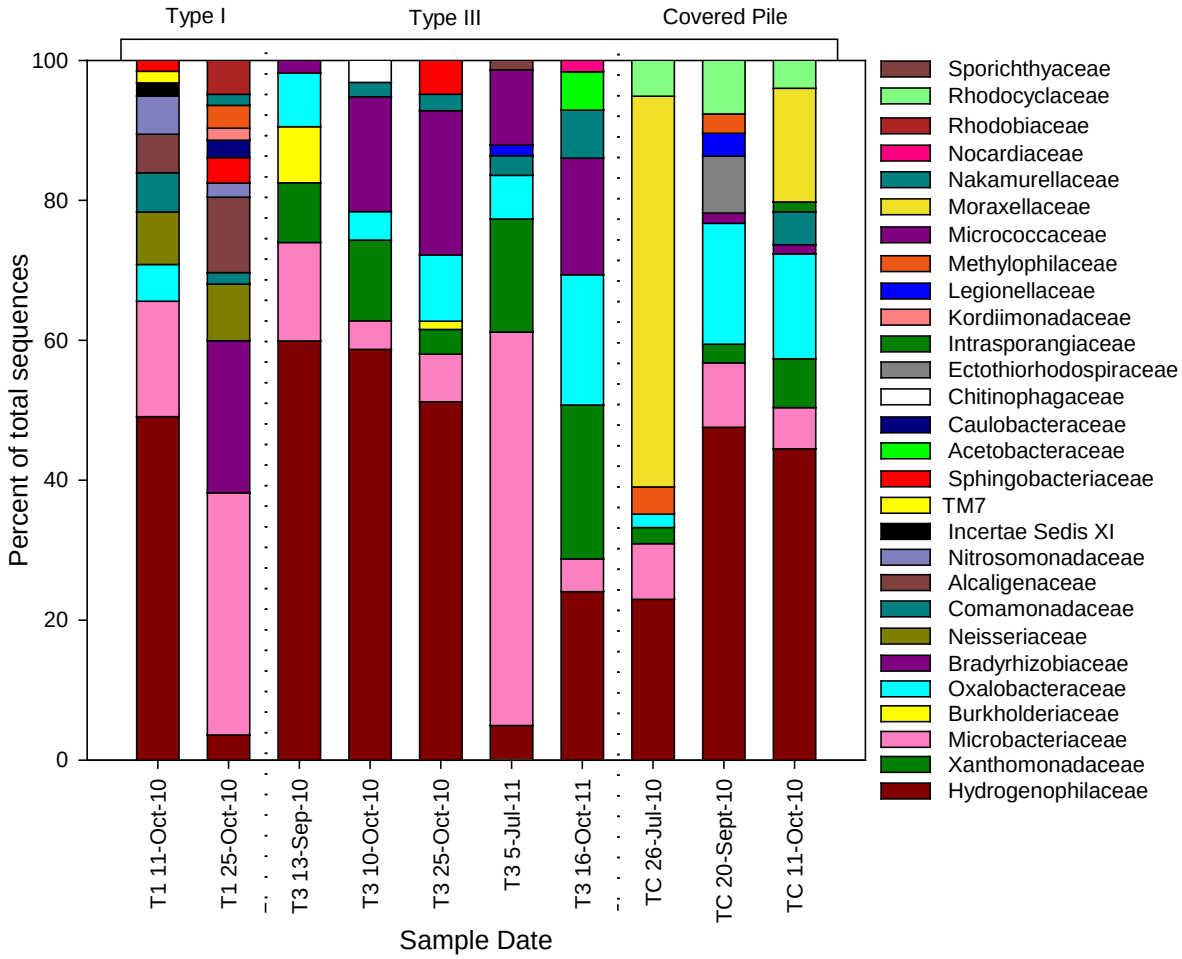

Figure 6.7 Relative abundance of bacterial reads from the Type I, Type III and Covered test pile at the family level. Reads were classified in the RDP database using a threshold similarity of 50 %. Sample numbers indicating the sampling date and location are given below the graph.

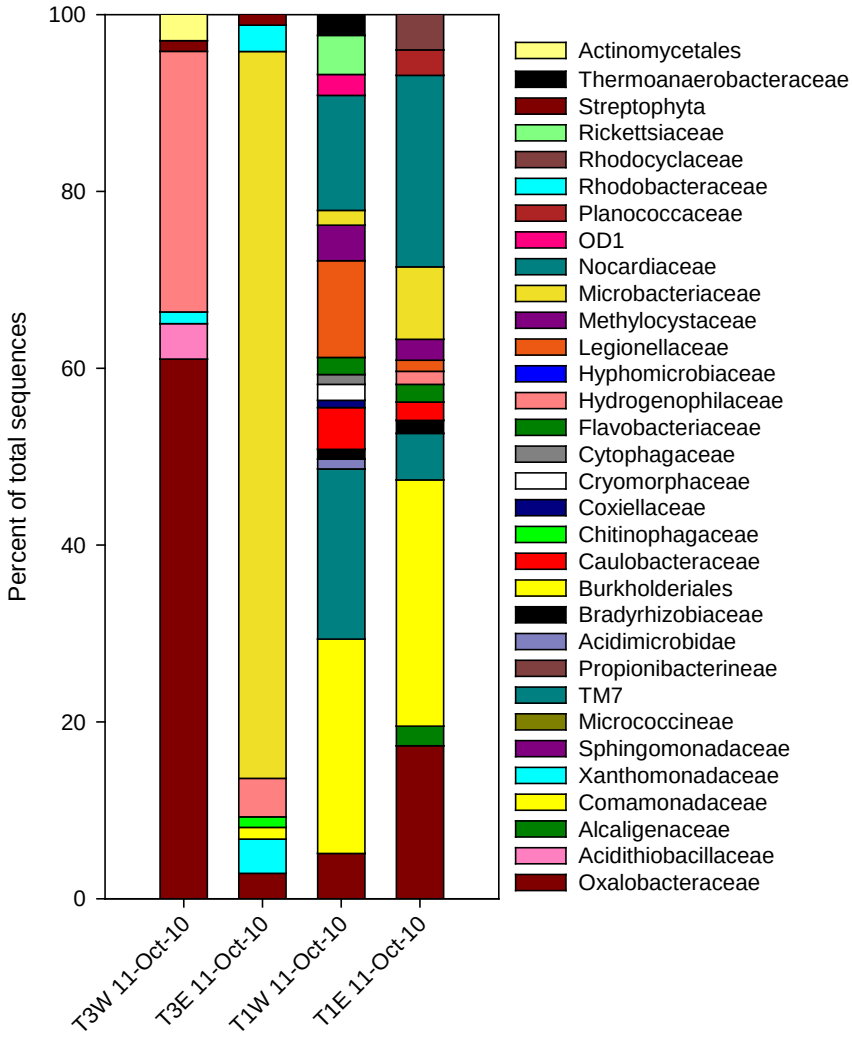

Figure 6.8 Relative abundance of bacterial reads from the Type I and Type III AZLs at the family level. Reads were classified in the RDP database using a threshold similarity of 50 %. Sample numbers indicating the sampling date and location are given below the graph.

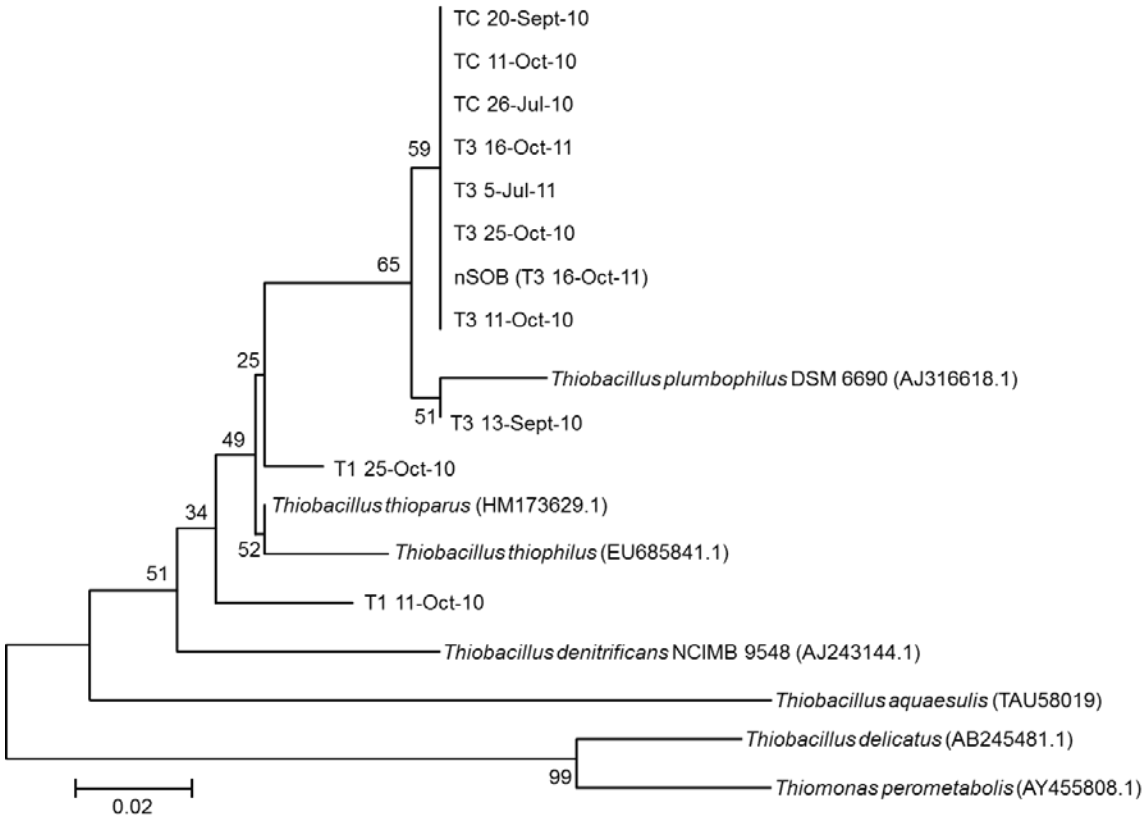

Figure 6.9 Neighbour-joining phylogenetic tree generated from 16S rRNA gene sequences from *Thiobacillus* sp. (GenBank) reference bacterial strains and unique phylotypes of bacteria in effluent from the Type I, Type III, and Covered test piles, in addition to the nSOB media. Bootstrap values (expressed as percentages of 1000 replications) are shown at branch nodes. Similar topologies were recovered in trees generated with the maximum-likelihood algorithm. Bar, 0.05 substitutions per nucleotide position. The database accession numbers are in parentheses.

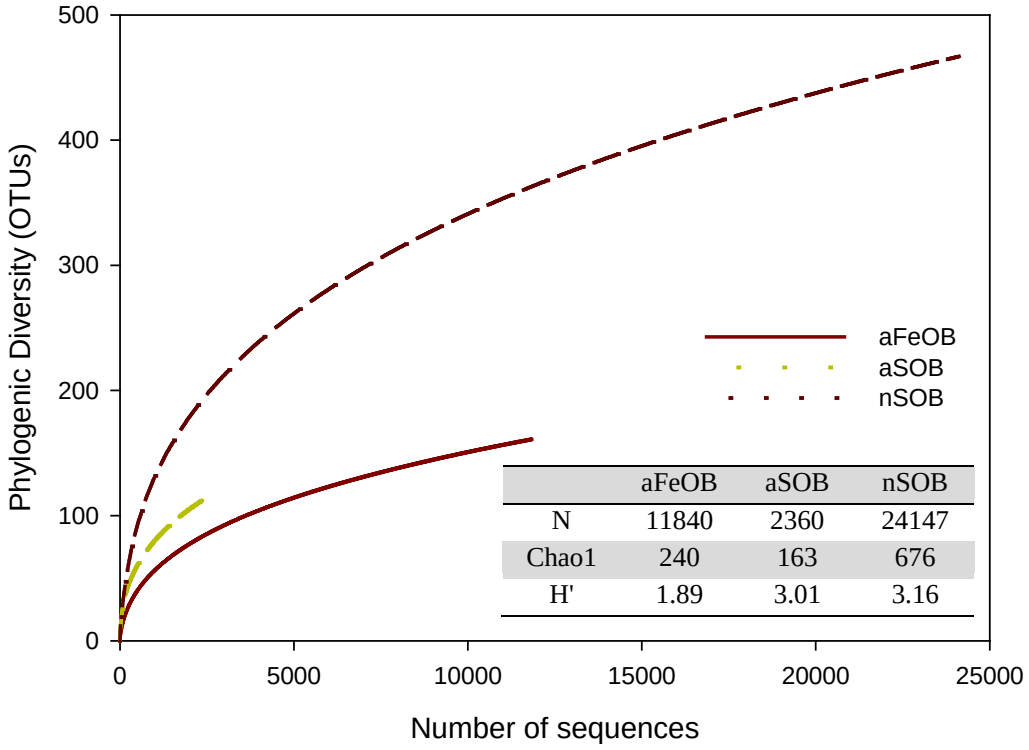

Figure 6.10 Rarefaction curves indicating the observed number of operational taxonomic units (OTUs) at a genetic distance of 3 % in MPN 10^0 dilution cultures for aFeOB, aSOB, and nSOB.

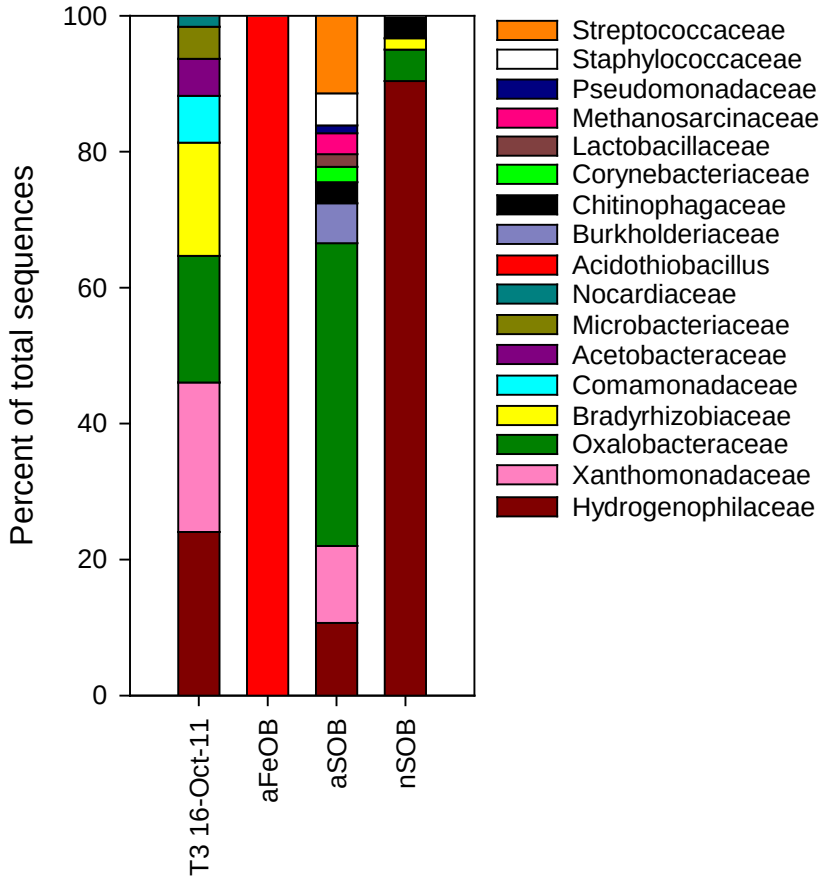

Figure 6.11 Relative abundance of bacterial reads from the Type III test pile on October 16, 2011, and the MPN 10^0 dilution cultures for aFeOB, aSOB, and nSOB at the family level. Reads were classified in the RDP database using a threshold similarity of 50 %. Sample numbers indicating the sampling date and location are given below the graph.

Chapter 7:

Scale-up: Predicting field-scale waste-rock drainage quality from humidity-cell experiments

7.1 Executive Summary

Humidity-cell experiments (1 kg sample) conducted at 4°C and 22°C were used to estimate the effluent quality and release rates of oxidation-products from small-scale (6 t) field-based lysimeters in a continuous permafrost region. A comparison between predicted total mass loadings from laboratory humidity cells and total mass loadings from field lysimeters (AZL) at Diavik Diamond Mine was completed for a 5-year period between 2007 and 2011. Measured values for temperature, S content, and surface area were used in these estimates. The release rate of SO_4^{2-} from humidity cells with varying S content (ranging from 0.02 to 0.18 wt. % S) were normalized to the surface area of S (mol m^{-2} S^{-1} sec^{-1}) from each humidity cell. The resulting variability in S-release rates for all waste-rock types fell within one order of magnitude for all waste-rock types. The release rates of dissolved metals from humidity cells with a S content of 0.18 wt. % S were used to estimate the release rates from waste rock in the field with 0.035 wt. % S. The results suggest the normalization to the surface area of S estimated annual total mass loads that were similar to measured annual total mass loadings in the field, with a few exceptions due to a low precipitation year (concentrations overestimated) followed by a year with high precipitation (concentrations underestimated). In addition, Fe and Al were over predicted in all years. Geochemical equilibrium modeling of the estimated concentrations suggested that Fe and Al concentrations were controlled by the solubility and formation of secondary minerals, including Fe oxyhydroxides, jarosite, and goethite. The results indicate that, at this scale, annual total mass loadings can be estimated if a thorough characterization of the waste rock is completed to better refine the release rates.

7.2 Introduction

The costs associated with reclamation and remediation of mine sites are high (Williamson, *et al*., 2008). It is essential to evaluate the potential environmental impacts of mine wastes prior to the development of a mining project and to implement adequate mine-waste management strategies. Estimates of the lag time and the longevity of poor quality effluent, from acid mine drainage (AMD) for example, are standard calculations required for permitting, implementation, and monitoring of new and closed mining sites (Price, 1999). There are many challenges and site specific issues that increase the complexity of extrapolating geochemical mass loadings from small-scale laboratory experiments to larger-scale field-based experiments, and ultimately, to full-scale operational waste-rock stockpiles. Parameters that influence the magnitude and duration of environmental impacts include: temperature, microbial activity, acidity, surface area of the waste rock, S content, inorganic carbon content, grain size, moisture content, and gas transport mechanisms.

Typical methods for AMD prediction include static tests and kinetic tests. Static tests, such as Acid-Base Accounting (ABA) tests, which consist of point measurements of the acid generating potential (AP; usually determined from S content) and the neutralization potential (NP; usually determined using an acid-digestion procedure), and Net-Acid Generating (NAG) tests, a titration to determine the acid-generation and acid-consumption potentials of geological materials (Benzaazoua, *et al*., 2004). Static tests are considered qualitative prediction methods. Although static tests are simple and rapid, these tests do not provide predictions of the quality of drainage over a long period of time (Garcia *et al*., 2005). Kinetic tests are used to confirm predictions of static tests, if they show uncertain results (Garcia *et*

al., 2005), and provide estimates of lag-time and the longevity of acid generation. Humidity-cell experiments are the most commonly used kinetic test, consisting of unsaturated conditions with wet/dry cycles to generate differing redox conditions and simulate unsaturated flow (Lapakko and White, 2000). The results from these types of studies are used to estimate the water quality from differing rock types using different methodologies (e.g., Benzaazoua *et al*., 2003; Garcia *et al.,* 2005; Sapsford *et al*., 2009; Plante *et al*., 2011).

The Diavik Waste Rock Research Project was initiated at the Diavik Diamond Mine (Diavik) in the Northwest Territories, Canada, to evaluate the potential to scale the geochemical, microbiological, hydrological, thermal and temporal data from standard laboratory testing procedures to field-based results. The construction of the Diavik Waste Rock Research Facility was previously described by Blowes *et al*. (2006) and Smith *et al*. (2012a). The specific objectives of this chapter were to assess the potential to use humidity-cell (1 kg) results to estimate the effluent quality and the rate oxidation-products are released from small-scale (6 t) lysimeters (active zone lysimeters; AZLs). The geochemistry and microbiology of the AZLs is described in Chapter 3. Measured values for temperature, S content, and surface area from both the small scale experiments and the AZLs were used in these estimates.

7.3 Methodology

7.3.1 Humidity-Cell Experiments

All experimental methods and results pertaining to the humidity-cell experiments were completed by Mandy Moore and are presented herein for completeness of this Chapter.

Interpretation of the humidity cell data used in this chapter was completed by the author of this thesis.

The laboratory-scale experiments (humidity cells) were conducted using waste rock collected from the Diavik diamond mine in October 2004 and November 2005. Waste-rock samples were collected based on the waste-rock segregation method used by Diavik, and included Type I, Type II, and Type III waste-rock each year. Waste-rock samples were submitted to external laboratories for whole-rock digestion and static ABA. Particle-size distribution, surface area and NAG potential analyses were completed at the University of Waterloo. Static ABA was conducted by three commercial laboratories (SGS Lakefield, Ontario, Actlabs, Ancaster, Ontario, and Canadian Environmental & Metallurgical Inc., British Columbia) using a modified Sobek method and included the analysis of paste pH, total S, sulfate S, sulfide S, neutralization potential, total carbon, and net acid generation. Whole-rock and bulk metal analyses were conducted at SGS Lakefield by X-ray fluorescence spectroscopy (XRF) and X-ray diffraction, and at Actlabs by inductively coupled plasma–mass spectrometry (ICP–MS) and fusion XRF.

Grain size was determined at the University of Waterloo. A 1-kg sample was riffle split to obtain representative samples. Unused splits were retained for future studies. Grain-size distribution was determined by dry sieving, utilizing US standard ¼', 8, 18, 35, 60, 120, 230, and 325 sieves (metric sieve sizes of 6.25, 2.36, 1.0, 0.5, 0.250, 0.125, and 0.063 mm), with the addition of 3/8 inch (9.53 mm) and 5/16 inch (7.94 mm) sieves when the particle size was greater than 2.54 cm (1 inch). Surface area was determined at the University of Waterloo using the BET Multipoint method (Brunauer *et al.*, 1938). Three replicate sample splits were

analyzed for each waste-rock type and collection date (either 2004 or 2005), with the mean value reported.

Twenty-four modified humidity-cell experiments were conducted following the ASTM D 5744 Standard Test Method for Accelerated Weathering of Solid Materials Using a Modified Humidity Cell Designation D 5744 – 96 – designated leach method (Reapproved 2001) ASTM (1998) using 1 kg of < 2.54 cm waste rock by Mandy Moore. Two cells of each Type I, Type II, and Type III waste rock from both 2004 and 2005 were tested at two temperatures, 22°C and 4°C (total of 24 humidity cells) for 250 weeks. Each week, air of varying relative humidity (RH) was circulated through the humidity cells. This included a 3-day dry period (0 % RH), a 3-day wet period (> 95 % RH) and a 1-day flood leach with 500 mL of distilled water. Samples of the leachate were collected for pH, redox potential relative to the standard hydrogen electrode (E_h), conductivity, alkalinity, anions, and cations. Methods of analysis are described in Chapters 3. Data interpretation was completed by examining the saturation indices (SI) of solid phases for samples with a complete suite of field and laboratory analyses as described in Chapter 3.

7.3.2 Field-Scale Experiments: 2 m by 2 m Active Zone Lysimeters

The AZLs are described in detail in Chapter 3. These experiments consist of four 2 m in diameter and 2 m in height high-density polyethylene (HDPE) tanks were filled, and surrounded by, waste rock in 2006 and are referred to as the active zone lysimeters (AZL; Chapter 3). Two AZLs were filled with Type I waste rock (Type I East AZL and Type I West

AZL) and two AZLs were filled with Type III waste rock (Type III East and Type III West AZL).

7.4 Results and Discussion

7.4.1 Laboratory Experiments

7.4.1.1 Acid-Base Accounting and Net Acid Generation

The acid-base accounting static tests, including the average S content, NP, AP, net-neutralization potential (NNP) and NP:AP ratio, were used to assess the acid generating potential of the material used to construct humidity cells (Table 7.1). The ratio of NP to AP is used to evaluate the acid generating potential; a NP:AP ratio of < 1 is considered to be potentially acid generating, > 3 is considered to be non-acid generating, and > 1 and < 3 remains uncertain (Smith *et al*., 2012b). The NAG pH values are also used to assess the acid generating potential; NAG pH > 4.5 is considered potentially non-acid forming, and ≤ 4.5 has a risk of being acid forming (Miller *et al*., 1991).

The S content of the 2004 and 2005 Type I material was similar with 0.02 wt. % S and 0.03 wt. % sulfide-S (Table 7.1). The Type II material collected in 2004 was similar to the Type I material (0.02 wt. % S; 0.03 wt. % sulfide-S) and the Type II material collected in 2005 had a slightly higher S content (0.04 wt. % S; 0.05 wt. % sulfide-S). The ABA (NP:AP > 3)and NAG pH (pH > 4.5) results suggest both the 2004 and 2005 Type I and Type II waste rock were unlikely to be acid generating (Table 7.1).

The average S content of the 2004 Type III material was 0.18 wt. % S, and the average sulfide-S content was 0.16 wt. % sulfide-S. The average NP:AP ratio was 2.97, suggesting

this material has an uncertain acid generating potential. The 2004 Type III material had a mean NAG pH value of 3.35±0.03 (n = 3) and it produced 4.50± 0.2 kg H_2SO_4 t^{-1} (n = 3), suggesting this material poses a low risk for acid generation. The results from both ABA and NAG tests indicate there was a potential for acid generation associated with the 2004 Type III waste rock.

The average S content of the Type III material collected in 2005 was lower than the 2004 Type III material with 0.04 wt. % S and the average sulfide-S content was 0.06 wt. % sulfide-S (Table 7.1). The 2005 Type III material was within the range for Type II material based on the Diavik waste-rock segregation classification. However, because this material was obtained from the Type III stockpile, the Type III designation has been retained for this study. The NP was determined to be 33.08 kg $CaCO_3$ t^{-1} with an AP of 0.77 kg $CaCO_3$ t^{-1} (Table 7.1). The average NNP for the 2005 Type III material was 32.29 kg $CaCO_3$ t^{-1} and the average NP:AP ratio was 121.33; therefore, this material was considered non-acid generating and had a substantial neutralization potential (Table 7.1). The 2005 Type III material had a mean NAG pH of 8.40 and it did not produce a measurable amount of acidity (< 0.01 kg H_2SO_4 t^{-1}); therefore, this material was considered non-acid generating.

7.4.1.2 Surface Area

The mean surface area measurement for the 2004 Type I material was 1.21 m^2 g^{-1}, and for the 2005 Type I material it was determined to be lower at 0.42 m^2 g^{-1}. The 2004 Type II material had a surface area of 0.73 m^2 g^{-1}, whereas the 2005 Type II material had a surface area nearly double of 1.61 m^2 g^{-1}. The greatest variation between the 2004 and 2005 samples was on the

Type III material. The 2004 Type III material had a mean surface area of 1.62 m^2 g^{-1}, whereas the 2005 Type III material had the highest surface area at 5.97 m^2 g^{-1}.

7.4.1.3 Sulfate Release Rates

The highest rate of sulfate release occurred in the first flush of the humidity cells, likely due to the release of oxidation products at the surfaces of grains contained in the column charge material that formed prior to the initiation of the humidity-cell experiments (Figure 7.1 and Figure 7.2; Ardau *et al*., 2009). This effect was anticipated and an increased number of humidity cell flushes were implemented for weeks 0, 1, 2 and 3 (Lapakko and White, 2000).

In general, the humidity cells, of the same waste-rock type, at 22°C had higher or nearly equal release rates of SO_4^{2-} to those at 4°C for the duration of the study. The 2004 and 2005 Type I materials had the lowest release rates of SO_4^{2-}. The 2004 and 2005 Type II materials had slightly higher release rates than the Type I material. The 2004 Type III humidity cells produced the highest release of SO_4^{2-}. Average SO_4^{2-} release for the two 2004 Type III humidity cells was 14.6 μg kg^{-1} wk^{-1} and 14.3 μg kg^{-1} wk^{-1} (σ = 3.7 μg kg^{-1} wk^{-1} for both samples), equivalent to an average molar SO_4^{2-} release rate of 3.8 x 10^{-10} mol kg^{-1} s^{-1}, (σ = 1.3 x10^{-10} mol kg^{-1} s^{-1}). The Type III 2005 material was characterized as Type II material and the release rates of sulfate were consistent with the Type II waste rock from 2004 and 2005.

7.4.1.4 Pyrrhotite Oxidation and Activation Energy

Sulfide-oxidation rates are affected by temperature in a manner that can be described by the Arrhenius equation (Ahonen and Tuovinen., 1992):

$$\ln \frac{k_2}{k_1} = \frac{E_a}{R \times 2.3} \times \left(\frac{1}{T_1} - \frac{1}{T_2} \right) \quad (7.1)$$

where k_1 and k_2 are the rate constants at temperatures T_1 and T_2; E_a is the activation energy of the reaction; and R is the gas constant. Seasonal temperature fluctuations, therefore, may influence the rate of release of SO_4^{2-} from waste rock. The release rate of sulfate from the Type III humidity cells at 22°C was an average of a factor of 2.04 higher than the rate at 4°C (Table 7.2). The activation energy calculated from the Type III humidity-cell experiments at 22°C and 4°C was determined to be 38 kJ mol^{-1} in the first two weeks, and 25 kJ mol^{-1} from weeks 2 to 20. In addition, the Type I humidity-cell experiments had an activation energy of 18 kJ mol^{-1} in weeks 0 to 2 and 24 kJ mol^{-1} in weeks 2 to 20. Similarly, Ahonen and Tuovinen (1992) determined a similar activation energy of 25 kJ mol^{-1} for the oxidation of pyrrhotite, the most abundant sulfide mineral at the Diavik site, based on a column leaching experiment conducted at a range of temperatures from 4 to 37°C, and suggested the rate is controlled by diffusion of reactants or products. The formation of oxidation rims may have an effect on pyrrhotite oxidation after week 2.

7.4.1.5 pH and Alkalinity

The pH in the Type I humidity cells at both 22°C and 4°C was near neutral for the duration of the study. The 2004 Type I material maintained a slightly higher pH at 22°C than at 4°C, whereas the 2005 Type I material at both temperatures remained similar. The pH of the 2005 Type I humidity-cell effluent decreased from 7.5 to 6.5 over 240 weeks. The humidity cells containing the 2004 and 2005 Type I material at both 22°C and 4°C released alkalinity at

concentrations > 4 mg L^{-1} (as $CaCO_3$) for the duration of the study (Figure 7.1 and Figure 7.2). The effluent from the 2004 and 2005 Type II humidity cells, at both 22°C and 4°C, also remained near-neutral ranging from pH 5.5 to 7.5. In addition, alkalinity concentrations remained > 2.44 mg L^{-1} (as $CaCO_3$) for the duration of the study.

The leachate from the 2004 Type III humidity cell followed similar trends at both 22°C and 4°C; however, at 22°C the pH was typically 0.2 to 0.8 pH units lower. At 22°C, the pH was near neutral for the first 18 weeks of the study then decreased to 4.3; the pH decreased to 5.0 in the 4°C humidity cells. The pH continued to decrease to a minimum of 3.9 ± 0.1 from week 57 to 95. The alkalinity decreased from 8.0 mg L^{-1} (as $CaCO_3$) at the initiation of the experiment to < 2 mg L^{-1} (as $CaCO_3$) by week 61.

The leachate from the 2005 Type III humidity cell remained near neutral pH for the duration of the study and had alkalinity concentrations > 22.4 mg L^{-1} (as $CaCO_3$). The NP/AP of the 2005 Type III material suggests it is non-acid generating. The discrepancy between the 2004 Type III material and the 2005 Type III material illustrates the heterogeneity of the waste rock and the need to complete many replicates in order to fully characterize waste rock.

7.4.1.6 Major Cation Release Rates

The release of dissolved Ca, Mg, K, Na, and SiO_2 in humidity cell leachate indicates the dissolution of carbonates, feldspar, and biotite. The rate of Ca and Mg release was highest for the Type III 2005 material, whereas the release rates were similar for the 2004 Type I, Type II, and Type III materials (Table 7.3). The release rate of K was also highest in the 2005

Type III humidity cells, but only slightly higher than the 2004 Type I, Type II, and Type III humidity cells (Table 7.3). The release rates of Na were similar for all humidity cells (Table 7.3). The increased concentrations in the 2005 Type III material was a result of higher dissolution rates at lower pH.

7.4.1.7 Dissolved Metals Release Rates

The release of dissolved Fe is affected by the rate of oxidation of pyrrhotite and other sulfide minerals, and by the rate of formation of secondary minerals such as Fe oxyhydroxides. The rate of Fe release reached a maximum within four to thirteen weeks for all humidity cells, with the exception of the 2004 Type III material (maximum of 2.65×10^{-11} mol kg^{-1} sec^{-1} on week 75) and 2005 Type III material (maximum of 1.76×10^{-13} mol kg^{-1} sec^{-1} on week 65) at 22°C, and the 2004 Type III material (maximum of 3.22×10^{-12} mol kg^{-1} sec^{-1} on week 75) and 2004 Type II material (maximum of 2.40×10^{-13} mol kg^{-1} sec^{-1} on week 27) at 4°C. The mean release rate of Fe for each material type was higher at 22°C than at 4°C (Table 7.4). The release rates for the 2004 Type III humidity cell at both 4°C and 22°C increased through the first 30 weeks after testing commenced reaching a plateau ranging from 7.19×10^{-13} mol kg^{-1} sec^{-1} to 3.22×10^{-12} mol kg^{-1} sec^{-1} at 4°C, and ranging from at 1.55×10^{-11} mol kg^{-1} sec^{-1} to 2.65×10^{-11} mol kg^{-1} sec^{-1} at 22°C. The precipitation of an orange ocherous coating on some of the material in the 2004 Type III humidity cells occurred as the pH decreased to below 4.5. This coating initially was limited to small areas, and expanded to the whole surface observed from the outside perimeter of the humidity cell.

The oxidation of pyrrhotite was the primary source of dissolved Ni and Co in effluent from Diavik waste rock (Jambor, 1997). The release rates of Ni and Co from the 2004 Type III

humidity cells increased through week 37 and slowly decreased over time at both 4°C and 22°C. The mean release rate of Ni was at 4.33×10^{-13} mol kg^{-1} sec^{-1} ($\sigma = 6.45 \times 10^{-13}$ mol kg^{-1} sec^{-1}) at 4°C and 2.68×10^{-12} mol kg^{-1} sec^{-1}($\sigma = 2.06 \times 10^{-12}$ mol kg^{-1} sec^{-1}) at 22°C from the Type III 2004 humidity cells. The average release rate of Co was 7.54×10^{-13} ($\sigma = 3.81 \times 10^{-13}$ mol kg^{-1} sec^{-1}) at 4°C and 7.49×10^{-13} mol kg^{-1} sec^{-1} ($\sigma = 5.85 \times 10^{-13}$ mol kg^{-1} sec^{-1}) at 22°C from the 2004 Type III humidity cells. Geochemical modeling indicates that the leachate was undersaturated with respect to Ni hydroxides, therefore, the decrease in release rate of Ni was not likely attributable to the precipitation of hydroxides on the surface of particles. The decline in these release rates was probably due to a decrease in surface reaction rate caused by the build-up of Fe (oxy)hydroxides on the surfaces of waste-rock particles. The release rates of Ni from all other humidity cells were variable in the first 10 weeks and release rates subsequently stabilized, with the exception of a slight increasing trend in the Ni release rate from the 2005 Type I and Type II humidity cells at 4°C after week 35; however, the release rates were one to two orders of magnitude lower than in the 2004 Type III material. The average Ni release rate for all other humidity cells ranged between 2.22×10^{-15} mol kg^{-1} sec^{-1} to 1.58×10^{-13} mol kg^{-1} sec^{-1}.

The oxidation of chalcopyrite and sphalerite were the primary sources of dissolved Cu and Zn, respectively, in the humidity cell leachate. Similar to Fe, the release rates of Cu and Zn increased overtime to week 30 reaching release rates of Cu ranging from 1.26×10^{-12} mol kg^{-1} sec^{-1} to 3.31×10^{-12} mol kg^{-1} sec^{-1} at 22°C and release rates of Zn ranging from 6.17×10^{-13} mol kg^{-1} sec^{-1} to 3.27×10^{-12} mol kg^{-1} sec^{-1} at 22°C. The release rate from the same material at 4°C also increased for the first 49 weeks and then stabilized with a slightly lower release rate.

The average release rate of Cu from the 2004 Type III humidity cells was $9.54x10^{-13}$ mol kg^{-1} sec^{-1} (σ=$1.05x10^{-12}$ mol kg^{-1} sec^{-1}) at 4°C and $1.56x10^{-13}$ mol kg^{-1} sec^{-1} (σ= $2.82x10^{-13}$ mol kg^{-1} sec^{-1}) at 22°C. The average release rate of Zn from the 2004 Type III humidity cells was $1.18x10^{-12}$ mol kg^{-1} sec^{-1} (σ = $8.81x10^{-13}$ mol kg^{-1} sec^{-1}) at 22°C and $3.20x10^{-13}$ mol kg^{-1} sec^{-1} (σ=$4.08x10^{-13}$ mol kg^{-1} sec^{-1}) at 4°C. The release rates of Cu and Zn were lower in all other humidity cells. Mineralogical studies of column experiments of the bioitite schist from baseline studies at Diavik indicate the presence of covellite [CuS], a secondary Cu sulfide, on the edges of biotite grains, and completely replacing pyrrhotite grains (Blowes and Logsdon, 1998). No Zn-bearing secondary minerals were identified in mineralogical studies of waste rock from the Diavik site. Geochemical equilibrium modeling suggests effluent was undersaturated with respect to both Cu and Zn secondary minerals; however, Cu and Zn may undergo adsorption/complextation reactions with Fe(III) oxyhydroxides and hydroxysulfates removing them from the effluent (Webster *et al*., 1998; Galan *et al*., 2003; Gunsinger *et al*., 2006). Further mineralogical work is planned for the humidity cells to investigate the weathering of primary minerals and formation of any secondary minerals.

7.4.2 Scale-Up of Humidity Cells to Estimate AZL Mass Loadings

Several methods can be used to extrapolate geochemical mass loadings from small-scale laboratory experiments to larger-scale field-based experiments, and ultimately, to full-scale operational waste-rock stockpiles. Release rates from humidity cells are typically expressed in terms of rock mass (mol kg $rock^{-1}$ sec^{-1}) or surface area of rock (mol m^{-2} sec^{-1}; e.g., Malmstrom *et al*., 2000). In this study, the S release rates from humidity cells were normalized to the mass of the rock (mol kg $rock^{-1}$ sec^{-1}; Figure 7.3 and Figure 7.4), the

surface area of the rock (mol m^{-2} sec^{-1}; Figure 7.5 and Figure 7.6), and estimated surface area of exposed S (mol m^{-2} S^{-1} sec^{-1}; Figure 7.7 and Figure 7.8). In addition, S mass loadings from each humidity cell and AZL were also normalized to the mass of the rock (g S kg $rock^{-1}$), the surface area of the rock (g S m^{-2} $rock^{-1}$), mass of S in the rock (g S kg S^{-1}) and estimated surface area of the S (g S m^{-2} S^{-1}).

The mass of rock in the AZLs (M_{AZL}) was calculated based on equation 7.2:

$$M_{AZL} = V_{AZL}(1-\varepsilon)\rho_s \tag{7.2}$$

where V_{AZL} is the volume of the AZL, ρ_s is the density of the waste rock and ε is the porosity within the waste rock. The volume of each barrel was estimated based on the as-built surveys. The Type I AZL barrels have a volume of 5.7 m^3 (Neuner, 2009) and the Type III barrels 3.4 m^3 (Neuner, 2009). The density of the blasted waste rock at Diavik is estimated to be 2060 kg m^{-3} with a porosity of 0.25±0.02 (Neuner *et al.*, 2012). The surface area of the waste rock in the AZLs was estimated based on the surface area measurements performed on the humidity cell material. The grain-size analysis of the waste rock at Diavik (Smith *et al.*, 2012b) suggests the grain-size fraction contained within the humidity cells (< 2.54 mm) accounts for approximately 16 % of the waste rock in the AZLs. In addition, the fine fraction of a waste-rock sample contains the vast majority of the surface area; therefore, it is assumed that the surface area in the humidity cells was 16 % of that measured in the AZLs on a per mass basis (Table 7.5). The mass of S was estimated based on the mass-weighted S content

of each grain-size fraction (Table 7.5). The surface area of exposed S in the AZLs ($M_{S_{AZL}}$) was determined as follows:

$$M_{S_{AZL}} = SA_{HC}\left(M_{AZL} \times f_{gs(AZL)} \times wt.\%S\right) \quad (7.3)$$

where SA_{HC} is the surface area of the humidity cell charges (< 2.54-mm fraction), M_{AZL} is the mass of waste rock in the AZLs, $f_{gs(AZL)}$ is the fraction of waste rock < 2.54 mm in the AZLs based on grain size analysis, and wt. % S is the S content of the AZL. This approach assumes that the surface area of the particle size fraction exceeding 2.54 mm is negligible.

Normalizing SO_4^{2-} release rates from the humidity cells to the mass of rock (mol kg rock^{-1} sec^{-1}; Figure 7.3 and Figure 7.4), and the measured surface area of the rock (mol m^{-2} sec^{-1}; Figure 7.5 and Figure 7.6) for each humidity cell resulted in the S release rates that were within two orders of magnitude for all of the waste-rock types. Normalizing SO_4^{2-} release rates to the estimated surface area of the S (mol m^{-2} S^{-1} sec^{-1}; Figure 7.7 and Figure 7.8) the resulting variability in the S release rates for all waste-rock types was within one order of magnitude. These calculations suggest that the S release rates in the humidity cells can be constrained to the degree that they may be used to estimate the release rates at larger scales. In this study, the release rates from the 2004 Type III were used to estimate the release rates from the Type III AZLs.

The average release rate of SO_4^{2-} from all room temperature humidity cells corrected for surface area of S, at each sample point, was multiplied by the ratio of the concentration of an

element (e.g., Ni) to SO_4^{2-} concentrations to estimate the release rates. For example, the Ni release rate from the 2004 Type III humidity cell at 22°C was estimated based on equation 7.4:

$$R_{Ni} = R_{SO4} \times \frac{[Ni]}{[SO_4^{2-}]} \quad (7.4)$$

where [Ni] is the concentration of Ni, $[SO_4^{2-}]$ is the concentration of SO_4^{2-}, R_{Ni} is the release rate of Ni, and R_{SO4} is the release rate of SO_4^{2-}.

The same calculation was applied to the 2004 Type III humidity cells at 4°C. The release rates at 4°C and 22°C were used with the Arrhenius equation (equation 7.1) to estimate the release rates at the average positive temperature within the AZLs (6.5°C; $R_{HC\ at\ 6.5°C}$). These release rates then were adjusted to account for variations in the mass of S within the AZLs to the estimate the annual total mass loadings from the Type III AZLs. These calculations implicitly assume that sulfide-mineral oxidation is minimal below freezing, therefore, the first 22 weeks in the humidity cells represents the release rates in Year 1 of the AZLs, considering that the average time the AZLs were thawed each year was 22 weeks. Furthermore, the release rate from 22 weeks to 44 weeks represents Year 2 of the AZLs, 44 weeks to 66 weeks represents the release rates in Year 3 of the AZLs, 66 weeks to 88 weeks represents the release rates in Year 4 of the AZLs and 88 weeks to 110 weeks represents the release rates in Year 5 of the AZLs. The annual precipitation in the area was below average in 2007, 2009, and 2010. The annual total mass loadings were estimated because annual loadings are less dependent on transient fluctuations in the flow rate in response to

precipitation events, which affects concentrations during isolated sampling events. In addition, the influence of $O_{2(g)}$ was assumed to be negligible based on the permeability and porosity of the waste rock, and because atmospheric concentrations were observed within the Type III test pile (Amos *et al*., 2009a).

The average annual release rates from the humidity cells corrected to a temperature of 6.5°C each year were used to estimate the average annual release rate from the AZLs:

$$R_{AZL} = R_{HCat\,6.5^{\circ}C} \times M_{S_{AZL}} \tag{7.5}$$

where R_{AZL} is the release rate in mol sec^{-1}, $R_{HC\ at\ 6.5°C}$ is the temperature corrected average release rate from the humidity cells in each year (mol m^{-2} S^{-1} sec^{-1}), and M_{SAZL} is the surface area of exposed S in the AZL (mol sec^{-1};). In addition, the release rates were estimated using the release rates at 22°C for an estimate of the maximum potential mass loadings from each AZL. The annual release rates were then converted to a total annual load:

$$M_{total} = R_{AZL} \times GFW \times \frac{3.1536 \times 10^{7}\ \text{sec}}{1 year} \tag{7.6}$$

7.4.2.1 Type III AZL Estimated Mass Loadings

7.4.2.1.1 Sulfide-mineral oxidation

The mass of S released from the AZLs was overestimated and underestimated in different years. For example, the estimated total mass loading of SO_4^{2-} in 2007 (131 g) at 6.5°C was

overestimated compared to the observed results (Type III East = 61 g; Type III West = 100 g), whereas in 2008 the total mass loading of SO_4^{2-} (188 g) was underestimated (Type III East = 340 g; Type III West = 690 g; Table 7.6). Limited outflow reported to the base of the Type III AZLs in 2007 (Type III East = 35 L; Type III West = 33 L) compared to 2008 (Type III East = 201 L; Type III West = 202 L; Table 7.6). It is possible the SO_4^{2-} derived from oxidation in 2007, did not report to the base until 2008 accounting for the difference in total mass loadings observed compared to the estimated total mass loadings in 2007 and 2008. Approximately 90 % of the first flush of the matrix material occurred in 2008, flushing SO_4^{2-} from the oxidation of sulfide minerals during blasting (Bailey *et al*., 2010; Chapter 2) and SO_4^{2-} from *in situ* sulfide-mineral oxidation in 2007. In 2009 and 2010, the mass loadings of SO_4^{2-} (Type III East: 2009 = 67 g, 2010 = 110 g; Type III West: 2009 = 56 g, 2010 = 170 g) were overestimated (2009 = 205 g; 2010 = 219 g; Table 7.6). Geochemical equilibrium modeling suggests the Type III AZL effluent was at or near equilibrium with respect to secondary minerals such as alunite, basaluminite, jarosite and gypsum at various times in 2009 and 2010, potentially controlling the release of SO_4^{2-} in the effluent (Chapter 3). In addition, it is possible not all the oxidation products generated in 2009 and 2010 were flushed from the AZLs due lower flushing rates; therefore S was overestimated compared to the concentrations in the effluent. This suggests that this method represents the upper limit of the S that could potentially be released from the AZLs, and at times, S may be lower and could report to the drain in a subsequent wetter year. This is consistent with the understanding that the accumulation of secondary minerals in the field where flushing rates are lower than in

humidity-cell experiments, thereby controlling field oxidation rates, and the release of oxidation products (MEND, 2009; Sapsford *et al*., 2009).

7.4.2.1.2 Major Cations

The pH in the humidity cells during the first 45 weeks was near neutral, whereas the Type III AZLs were acidic within the first field season. The differences in Ca and Mg total mass loadings between the estimated and actual values may be due to the dissolution of a greater mass of carbonate minerals in the Type III AZLs to buffer the pH, depleting the carbonates at a faster rate than predicted. The total mass loading of Ca and Mg released were underestimated in 2007 and 2008 (Figure 7.9). The measured Ca mass loading was lower than the estimated values in and in 2010 and 2011 the Ca masses were underestimated (Figure 7.9). The total mass loading of Mg was similar to the estimated value in 2009, but the total mass loading was underestimated in 2010. The discrepancies between the estimated and measured concentrations of Ca and Mg may result from the presence of carbonate minerals in the AZLs that were not present in the humidity cells.

The total mass loading of Na released followed a similar trend to Ca with two exceptions: the total Na mass loading was underestimated in 2010 in the Type III West AZL; and the Na in the Type III East AZL was overestimated in 2010. Cumulative five years mass loading of Na was similar to the estimated value. The mass loading of K was overestimated in 2007 and 2009, but underestimated in 2008. In 2010, the total mass loading of K (Type III East = 8.4 g and Type III West = 12 g) was overestimated and in 2011 it was underestimated (Figure 7.9). The cumulative five year mass loading of K released was 71 g in the Type III East AZL and 109 g in the Type III West AZL, compared to an estimated value of 67 g at 6.5°C and 79 g at

22°C (Table 7.7). The discrepancy between the Na and K total mass loadings may be a result of the low pH in the AZLs compared to the humidity cells, with more aluminosilicate dissolution at the low pHs.

7.4.2.1.3 Aluminum and Iron

The concentrations of Al and Fe in the Type III AZLs at times were potentially controlled by secondary mineral formation (Chapter 3), whereas the humidity cells were below saturation with respect to most Al and Fe secondary minerals. The total mass loading of Al was underestimated for the Type III East AZL in 2007, but overestimated for the Type III West AZL in 2007 (Figure 7.9 and Figure 7.10). In 2008, the total mass loading of Al was underestimated at 6.5°C (0.86 g), and overestimated in 2009 and 2010. In 2011, the total mass loading of Al was underestimated. The increased mass loading of Al in 2011 may have been a result of flushing of the oxidation products released in 2009 and 2010 retained within the AZL. The effluent from all of the humidity-cell experiments was undersaturated with respect to Al secondary minerals. Therefore, the overestimation of Al concentrations in the AZLs may be due to secondary mineral constraints on Al concentrations in the AZLs, which were not observed in the humidity cells (Chapter 3).

Iron, in general, was overestimated for all years (Figure 7.10). The total mass loading in the Type III East was 0.11 g and in the Type III West AZL it was 0.90 g, whereas the estimate at 6.5°C was 13 g and at 22°C it was 45 g (Table 7.6 and Table 7.7). Geochemical equilibrium modeling suggested that Fe concentrations in the Type III AZLs would be controlled by the solubility and formation of secondary minerals, such as ferrihydrite,

jarosite, and goethite (Chapter 3). Furthermore, the actual effluent from the Type III East and West AZLs was at or above saturation with respect to jarosite, and goethite (Chapter 3).

7.4.2.1.4 Dissolved Metals

No secondary mineralogical controls were identified for Ni, Zn, and Cu in effluent from both the humidity cells and the AZLs. In addition, at the low pH conditions observed in the Type III AZLs, adsorption of Ni and Zn is suggested to be minimal (Chapter 3). This suggests the dissolved metals will be released from the Type III AZLs proportional to the sulfide-mineral oxidation rates and can thus be estimated using the SO_4^{2-} release rates.

The estimated total mass loadings of Ni and Zn in 2007 were similar to the average total mass loading from the Type III East and West AZLs (Table 7.6; Figure 7.10). In 2008, the total mass loadings of both Ni and Zn were underestimated (Table 7.7; Figure 7.10). In 2009, the total mass loading of Ni and Zn was overestimated (Table 7.7 and Figure 7.10); however, precipitation in 2009 was 73 mm, 45 % of the mean annual rainfall (164 mm), suggesting not all of the oxidation products were flushed from the AZLs prior to freeze-up at the end of the year. Precipitation in 2010 was 95 mm, 56 % of the average annual rainfall. In 2010, the total mass loadings of Ni and Zn (Table 7.6) were almost equal to the estimated load. In 2011, the total mass loadings of Ni and Zn were substantially underestimated, and there was an average amount of precipitation. This observation suggests some of the residual oxidation products from previous years may have been flushed from the AZLs in 2011. The average AZL total mass loading of Ni after five years was 5.3 g in the Type III East AZL and 9.6 g in the Type III West AZL, compared to an estimated AZL total mass loading of 4.1 g. The average AZL total mass loading of Zn after 5 years was 3.6 g in the Type III East AZL

and 5.9 g in the Type III West AZL, compared to an estimated AZL total mass load of 3.6 g. Over the five year period of this study, the total mass estimates of dissolved metals agreed within a factor of two, suggesting that this approach can provide reasonable estimates of mass loadings for conservative dissolved metals.

The total mass loading of Cu released from the Type III AZLs was estimated in the same manner. However, at a pH of > 4.0, Cu has been has been shown to adsorb onto Fe (III) hydrous oxides potentially controlling Cu concentrations (Dzombak and Morel, 1990; Webster *et al*., 1998; Galan *et al*., 2003; Gunsinger *et al*., 2006). In 2007, 2009, and 2010, the annual total precipitation was below average and Cu loadings were overestimated. In 2008, the Type III East AZL (0.21 g) was nearly equal to the estimated mass loading at 6.5°C (estimate of Cu at 6.5°C = 0.31 g and estimate at 22°C = 1.5 g), whereas the Type III West AZL (0.49 g) was above the estimated mass loading at 6.5°C. In 2011, the total mass loading of Cu was higher than in previous years, but lower than estimated suggesting the oxidation products from low precipitation years (2009 and 2010) retained within the AZL were flushed in 2011. The total mass loading of Cu released from the Type III East AZL was 0.71 g and from the Type III West AZL it was 1.2 g. The estimated mass loading were higher with 3.2 g at 6.5°C and 7.5 g at 22°C indicating Cu may have been controlled by adsorption or coprecipitation reactions in the Type III AZLs (Table 7.6 and Table 7.7; Figure 7.10).

7.4.2.1.5 Summary

Currently, there is no standard method for scaling laboratory sulfide oxidation rates to the overall oxidation rate within a full-scale operational waste-rock pile (Sapsford *et al*., 2009). The ability to predict the lag time and longevity of acid mine drainage of full-scale

operational waste-rock piles would aid the mining industry in better understanding the environmental impacts of a proposed mine site before production and the development of an appropriate waste rock management strategy to minimize AMD (Bensaasoua *et al*., 2004 and references therein). Sapsford *et al*. (2009) indicate sulfate release rates can vary by an order of magnitude or more during a humidity-cell experiment and between tests for the same material, or in some incidences by altering the humidity cell protocol. Results of a study at the Aitik site in Northern Sweden show bulk-averaged physiochemical characteristics can be used to predict weathering rates within two orders of magnitude, similar to other studies (Malmstrom *et al*., 2000; Frostad *et al*., 2005).

In the study herein, the SO_4^{2-} release rates from humidity-cell experiments on waste rock with differing S content (ranging from 0.01 wt. % S to 0.16 wt. % S) and at different temperatures (4°C versus 22°C) were corrected for their physical and chemical characteristics. Results showed corrected sulfate release-rates were within an order of magnitude for all humidity cells. In addition, the release rate of S in the field AZLs (2 m x 2 m) studied were within one order of magnitude to the humidity cells S release rates when corrected for the same physical and chemical characteristics of the waste rock. Metal release rates were also estimated in this study and results indicated that the accumulation of secondary minerals and/or sorption reactions affected Al and Fe concentrations, but had minimal impact on the concentrations of Ni, Zn and Cu. The estimates made in the paper would benefit from the addition of solubility controls for elements that are found in secondary minerals after mineralogical work is completed. Al and Fe may have solubility controls that would better estimate Al and Fe concentrations in the AZL effluent.

Based on the reaction rates for the destruction of pyrite and pyrrhotite (Chapter 1, equations 1.10 and 1.11) in the presence of oxygen, pH should have an effect on the reaction rates and therefore release rates of SO_4^{2-} (Williamson and Rimstidt, 1994). The humidity cell S release rates were not adjusted for pH and the release rates adjusted to the surface area of S were within one order of magnitude. In addition, the estimate release rates of S in the AZLs were close to the measured values. This observation suggests pH was not a dominate factor in the release of S. Further investigation and the incorporation of pH into the scaling model will aid in refining the results of this study.

Humidity-cell experiments are designed to flush all of the oxidation products in each cycle (Sapsford *et al*., 2009). In contrast, full-scale operational waste-rock piles are flushed based on the local hydrology and infiltration properties of the waste-rock pile (MEND, 1995). The flushing rates in the field AZLs may be lower than in the humidity cells due to limited field precipitation. As a result, the release of oxidation products from the AZLs may have been overestimated compared to the controlled flushing of the humidity cells.

7.5 Conclusions

The release rate of SO_4^{2-} from humidity cells (1 kg) were used to estimate the effluent quality and release rates of oxidation products from small-scale (6 t) lysimeters in a semi-arid, continuous permafrost region. Measured values of temperature, S content, and surface area were used in these estimates. The results suggest humidity cells can be used to predict quality of drainage from small-scale field based studies as long as a thorough characterization of the waste rock accompanies the analysis to refine the release rates.

The release rates of SO_4^{-2} from humidity cells was normalized to the surface area of S in the waste rock to provide estimates of the release rates of various elements from a larger scale. Scaling from the humidity cells to small-scale field-based waste-rock lysimeters suggests the annual total mass loadings were similar for all years, with the exception of 2008 which had higher than predicted total mass loadings, in part due to a low precipitation year (2007) followed by a year with high precipitation (2008). Calcium, Mg, and SO_4^{2-} concentrations were underestimated from the humidity-cell experiments to the small-scale field tests (AZLs), possibly due to the difference in pH in the humidity cells for the first 45 weeks (pH < 5.0) compared to the field tests (pH < 4.5). Metal concentrations were also underestimated in 2007 and 2008 when the pH in the field cells was low (pH < 5.0) and the pH in the humidity cells was higher (pH > 5.0). The scale-up approach developed in the study suggests that humidity-cell results can be used to estimate the water quality from larger scale experiments if a thorough characterization of the waste rock accompanies the analysis to refine the release rates.

Table 7.1 Characteristics of Type I, Type II, and Type III waste rock used in the humidity-cell experiments (modified from Moore, in preparation)

		Type I		Type II		Type III	
	units	**2004**	**2005**	**2004**	**2005**	**2004**	**2005**
Sulfur	wt. % S	0.02	0.02	0.02	0.04	0.18	0.04
Sulfide-S	wt. % sulfide-S	0.03	0.03	0.03	0.05	0.16	0.06
Carbon	wt. % C	0.05	0.02	0.03	0.02	0.03	0.08
Surface area	m^2 kg $rock^{-1}$	1210	420	730	1610	1620	1120
Surface area S	m^2 S kg $rock^{-1}$	0.121	0.126	0.219	0.644	2.59	0.671
NP	kg $CaCO_3$ t^{-1}	9.32	8.57	9.17	10.48	9.34	33.08
AP	kg $CaCO_3$ t^{-1}	0.41	0.50	0.95	0.88	4.94	0.77
NP:AP		22.73	17.14	9.65	11.91	1.89	42.96

Table 7.2 Ratio of SO_4^{2-} release rates from the humidity-cell experiments at 22°C to 4°C.

	2004 Type I	2004 Type II	2004 Type III	2005 Type I	2005 Type II	2005 Type III
Overall rates	1.15	2.61	2.91	2.01	1.96	1.58
Rates after 8 weeks	1.36	3.05	2.66	2.08	2.10	1.52
Rates after 15 weeks	1.41	3.23	2.20	2.21	2.20	1.49

Table 7.3 Release rates of major cations from 2004 and 2005 Type I, Type II, and Type III humidity-cell experiments at 22°C and 4°C

	Ca (mol kg^{-1} sec^{-1})		Mg (mol kg^{-1} sec^{-1})		K (mol kg^{-1} sec^{-1})		Na (mol kg^{-1} sec^{-1})	
22°C	mean	σ	mean	σ	mean	σ	mean	σ
Type I 2004	$3.71x10^{-12}$	$2.78x10^{-12}$	$7.23x10^{-12}$	$8.10x10^{-12}$	$1.57x10^{-11}$	$9.45x10^{-12}$	$1.52x10^{-11}$	$1.03x10^{-11}$
Type II 2004	$8.49x10^{-12}$	$4.82x10^{-12}$	$1.28x10^{-11}$	$6.79x10^{-12}$	$2.86x10^{-11}$	$1.45x10^{-11}$	$1.04x10^{-11}$	$7.20x10^{-12}$
Type III 2004	$3.08x10^{-11}$	$2.30x10^{-11}$	$2.36x10^{-11}$	$2.12x10^{-11}$	$3.61x10^{-11}$	$1.89x10^{-11}$	$1.37x10^{-11}$	$8.38x10^{-12}$
Type I 2005	$7.70x10^{-12}$	$5.63x10^{-12}$	$7.40x10^{-12}$	$2.81x10^{-12}$	$2.79x10^{-11}$	$1.87x10^{-11}$	$2.71x10^{-11}$	$1.71x10^{-11}$
Type II 2005	$1.12x10^{-11}$	$7.02x10^{-12}$	$2.04x10^{-11}$	$1.27x10^{-11}$	$4.41x10^{-11}$	$2.71x10^{-11}$	$2.17x10^{-11}$	$1.32x10^{-11}$
Type III 2005	$8.96x10^{-11}$	$4.06x10^{-11}$	$1.75x10^{-10}$	$8.08x10^{-11}$	$6.78x10^{-11}$	$6.62x10^{-11}$	$3.99x10^{-11}$	$3.35x10^{-11}$
4°C								
Type I 2004	$5.37x10^{-12}$	$5.87x10^{-12}$	$4.78x10^{-12}$	$5.72x10^{-12}$	$1.22x10^{-11}$	$1.03x10^{-11}$	$2.13x10^{-11}$	$1.45x10^{-11}$
Type II 2004	$1.14x10^{-11}$	$1.25x10^{-11}$	$1.37x10^{-11}$	$1.65x10^{-11}$	$2.75x10^{-11}$	$3.60x10^{-11}$	$3.60x10^{-11}$	$5.71x10^{-11}$
Type III 2004	$1.49x10^{-11}$	$1.72x10^{-11}$	$1.14x10^{-11}$	$1.42x10^{-11}$	$1.70x10^{-11}$	$1.37x10^{-11}$	$2.08x10^{-11}$	$1.40x10^{-11}$
Type I 2005	$7.43x10^{-12}$	$9.35x10^{-12}$	$6.58x10^{-12}$	$8.46x10^{-12}$	$1.95x10^{-11}$	$2.72x10^{-11}$	$2.33x10^{-11}$	$3.13x10^{-11}$
Type II 2005	$6.07x10^{-12}$	$6.86x10^{-12}$	$1.10x10^{-11}$	$1.18x10^{-11}$	$2.23x10^{-11}$	$2.12x10^{-11}$	$1.76x10^{-11}$	$1.29x10^{-11}$
Type III 2005	$3.91x10^{-11}$	$2.41x10^{-11}$	$8.21x10^{-11}$	$5.65x10^{-11}$	$2.86x10^{-11}$	$2.49x10^{-11}$	$1.96x10^{-11}$	$2.43x10^{-11}$

Table 7.4 Release rates of select metals from 2004 and 2005 Type I, Type II, and Type III humidity-cell experiments at 22°C and 4°C

	Cu (mol kg^{-1} sec^{-1})		Zn (mol kg^{-1} sec^{-1})		Ni (mol kg^{-1} sec^{-1})		Fe (mol kg^{-1} sec^{-1})		Co (mol kg^{-1} sec^{-1})	
22°C	mean	σ	mean	σ	mean	σ	mean	σ	mean	σ
Type I 2004	1.65×10^{-13}	2.23×10^{-13}	1.05×10^{-13}	1.38×10^{-13}	6.80×10^{-14}	1.14×10^{-13}	6.39×10^{-12}	1.42×10^{-11}	7.28×10^{-14}	6.27×10^{-14}
Type II 2004	4.40×10^{-14}	2.26×10^{-14}	1.40×10^{-13}	8.11×10^{-14}	5.23×10^{-14}	2.81×10^{-14}	1.19×10^{-12}	3.50×10^{-12}	1.83×10^{-13}	2.67×10^{-13}
Type III 2004	9.54×10^{-13}	1.05×10^{-12}	1.18×10^{-12}	8.81×10^{-13}	2.68×10^{-12}	2.06×10^{-12}	6.58×10^{-12}	7.67×10^{-12}	7.49×10^{-13}	5.85×10^{-13}
Type I 2005	2.36×10^{-14}	1.50×10^{-14}	6.55×10^{-14}	6.12×10^{-14}	2.22×10^{-15}	6.75×10^{-15}	1.57×10^{-13}	7.47×10^{-14}	4.04×10^{-14}	4.53×10^{-14}
Type II 2005	3.01×10^{-14}	1.78×10^{-14}	1.95×10^{-13}	1.19×10^{-13}	9.55×10^{-14}	4.99×10^{-14}	7.49×10^{-14}	4.34×10^{-14}	1.32×10^{-13}	1.34×10^{-13}
Type III 2005	2.48×10^{-14}	1.81×10^{-14}	5.34×10^{-14}	6.76×10^{-14}	9.84×10^{-15}	7.09×10^{-15}	7.13×10^{-14}	3.48×10^{-14}	1.13×10^{-14}	1.06×10^{-14}
4°C										
Type I 2004	5.92×10^{-14}	4.47×10^{-14}	6.06×10^{-14}	5.57×10^{-14}	9.43×10^{-15}	6.26×10^{-15}	1.36×10^{-13}	1.12×10^{-13}	4.95×10^{-13}	5.46×10^{-13}
Type II 2004	2.50×10^{-14}	1.67×10^{-14}	1.11×10^{-13}	7.94×10^{-14}	1.58×10^{-13}	7.47×10^{-13}	1.01×10^{-13}	7.49×10^{-14}	6.33×10^{-13}	3.81×10^{-13}
Type III 2004	1.56×10^{-13}	2.85×10^{-13}	3.20×10^{-13}	4.08×10^{-13}	4.33×10^{-13}	6.45×10^{-13}	1.68×10^{-13}	3.53×10^{-13}	7.54×10^{-13}	3.81×10^{-13}
Type I 2005	2.25×10^{-14}	1.33×10^{-14}	1.40×10^{-13}	1.12×10^{-13}	2.78×10^{-15}	1.99×10^{-15}	1.43×10^{-13}	8.70×10^{-14}	1.21×10^{-13}	1.14×10^{-13}
Type II 2005	3.36×10^{-14}	3.47×10^{-14}	1.82×10^{-13}	1.51×10^{-13}	6.27×10^{-14}	6.35×10^{-14}	5.70×10^{-14}	2.82×10^{-14}	3.63×10^{-13}	3.00×10^{-13}
Type III 2005	2.14×10^{-14}	1.60×10^{-14}	8.41×10^{-14}	9.26×10^{-14}	1.67×10^{-14}	5.69×10^{-15}	5.74×10^{-14}	3.99×10^{-14}	7.73×10^{-14}	6.39×10^{-14}

Table 7.5 Characteristics of the Type I and Type III AZLs.

	Units	Type III	Type I
Volume of AZL	m^3	5.947	4.870
Volume of rock	m^3	3.866	3.166
Mass of rock	t	10.24	8.40
Mass of fines	t	1.64	1.34
Sulfur content	wt. % S	0.035 ± 0.015	0.014 ± 0.009
Mass of Sulfur	t S	0.39	0.12
Carbon Content	wt. % C	0.029 ± 0.003	0.039 ± 0.005
Mass of Carbon	t C	0.30	0.33

Table 7.6 Total component mass loadings released from the AZLs between 2007 and 2011 (2007 through 2010 data from Chapter 3).

	Mass (g)									
	Ca	**Mg**	**K**	**Na**	**Al**	**Fe**	**Ni**	**Zn**	**Cu**	**SO_4^{2-}**
Type III East										
2007	10	7.5	4.3	5.3	0.022	0.007	0.16	0.04	0.004	61
2008	48	36	32	20	1.9	0.051	1.9	1.3	0.21	340
2009	4.7	4.4	3.5	1.9	0.67	0.013	0.45	0.32	0.06	67
2010	10	10	8.4	3.4	1.9	0.022	0.94	0.65	0.11	110
2011	23	22	23	6.4	4.6	0.020	1.8	1.3	0.33	247
Total 5 year mass load	**96**	**80**	**71**	**37**	**9.1**	**0.11**	**5.3**	**3.6**	**0.71**	**825**
Average annual mass load	19	16	14	7.4	1.8	0.023	1.1	0.72	0.14	165
Type III West										
2007	16	16	8.7	10	0.19	0.021	0.72	0.26	0.022	100
2008	70	66	49	31	7.3	0.58	4.32	2.8	0.49	690
2009	5.3	5.6	4.0	2.1	0.85	0.015	0.26	0.18	0.054	56
2010	15	17	12	5.6	3.5	0.21	1.5	1.0	0.19	170
2011	33	25	35	7.7	9.6	0.070	2.8	1.7	0.45	290
Total 5 year mass load	**139**	**130**	**109**	**56**	**21**	**0.90**	**9.6**	**5.9**	**1.2**	**1306**
Average annual mass load	28	26	22	11	4.3	0.18	1.9	1.2	0.24	261
Overall AZL average total mass load	**118**	**105**	**90**	**47**	**17**	**0.50**	**7.4**	**4.8**	**0.96**	**942**

Table 7.7 Estimated annual mass loadings from the AZLs based on the scaling of release rates from humidity cells to the AZLs at the mean annual temperature in the AZLs (6.5°C) and at the maximum temperature (22°C) in the AZL.

	Mass (g)									
Rate at 6.5°C	**Ca**	**Mg**	**K**	**Na**	**Al**	**Fe**	**Ni**	**Zn**	**Cu**	**SO_4^{2-}**
2007	9.1	5.5	16	6.3	0.18	0.16	0.57	0.37	0.11	131
2008	18	9.3	14	6.3	0.86	0.5	0.95	0.65	0.31	188
2009	19	8.8	12	6.8	3.8	2.7	1.2	1.1	0.86	205
2010	13	6.7	15	6	6.9	5.4	0.93	0.98	1.1	219
2011	3.1	4.3	10	5.0	4.0	4.2	0.45	0.49	0.81	94
Total 5 year mass load	**62**	**35**	**67**	**30**	**16**	**13**	**4.1**	**3.6**	**3.2**	**837**
Average annual mass load	12	6.9	13	6.1	3.1	2.6	0.82	0.72	0.64	167

	Mass (g)									
Rate at 22°C	**Ca**	**Mg**	**K**	**Na**	**Al**	**Fe**	**Ni**	**Zn**	**Cu**	**SO_4^{2-}**
2007	17	9.4	22	3.9	0.56	0.92	1.2	0.39	0.2	290
2008	30	14	19	6.8	3.2	6.0	3.7	1.4	1.5	311
2009	14	6.6	12	8.0	6.0	16	1.8	1.7	2.5	236
2010	7.8	3.8	14	6.9	6.9	15	1.0	0.98	1.9	253
2011	2.6	3.0	12	6.6	4.6	7.3	0.46	0.53	1.4	112
Total 5 year mass load	**71**	**37**	**79**	**32**	**21**	**45**	**8.2**	**5.0**	**7.5**	**1202**
Average annual mass load	14	7.4	16	6.4	4.3	9.0	1.6	1.0	1.5	240

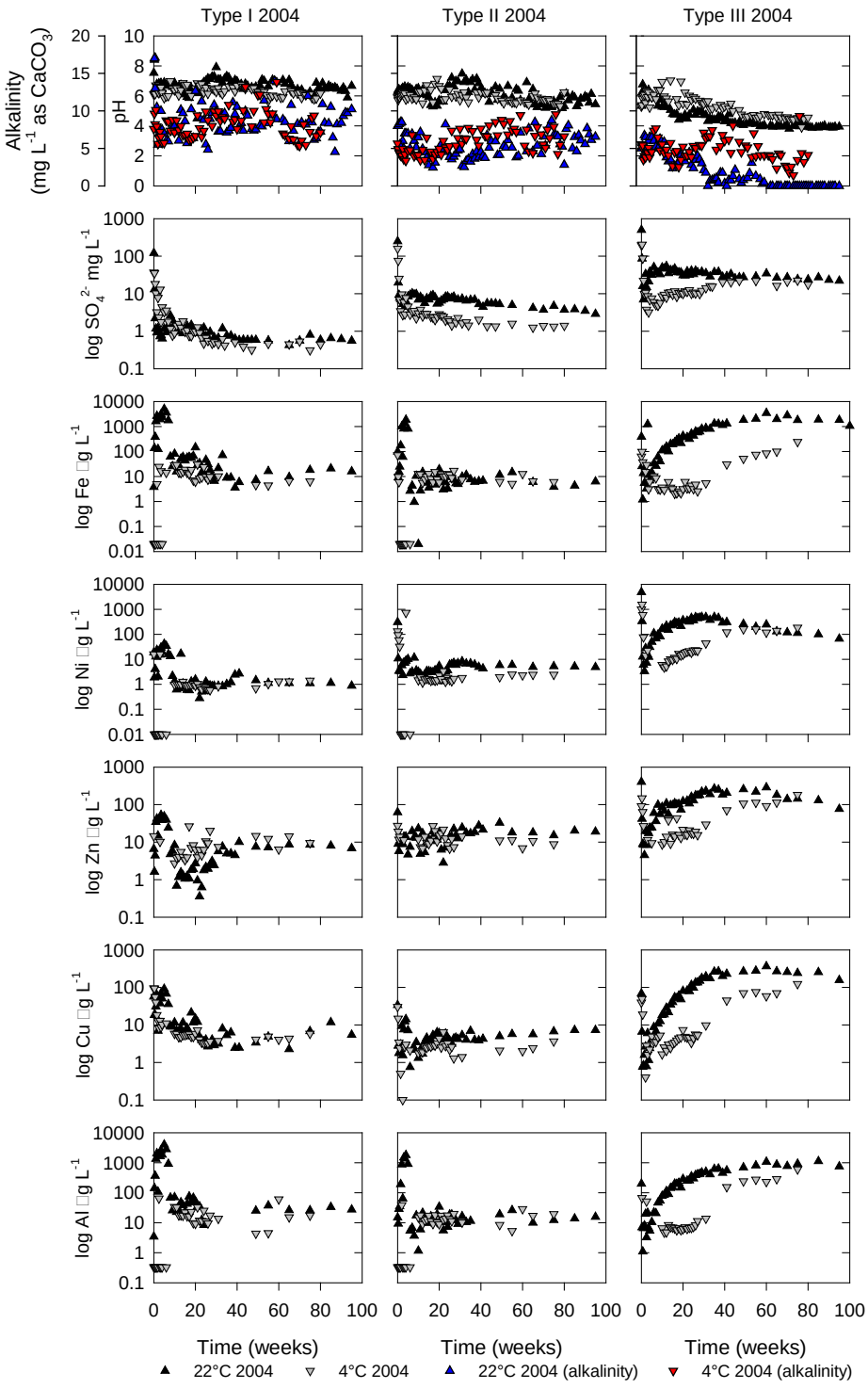

Figure 7.1 Time series plots presenting the pH and concentrations of Al, Cu, Zn, Ni, Fe, SO_4^{2-}, and alkalinity from humidity cells containing 2004 Type I, Type II, and Type III waste rock.

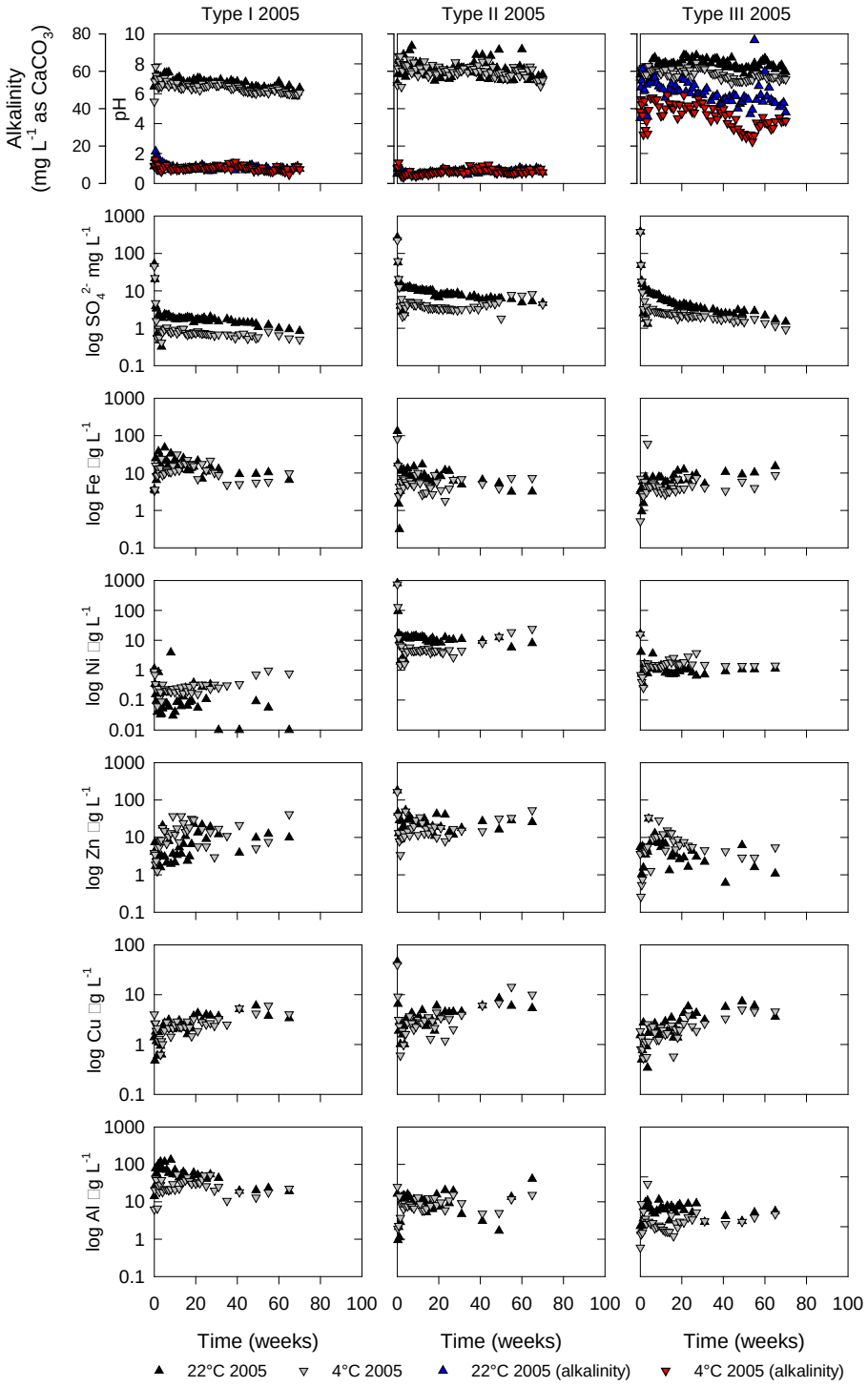

Figure 7.2 Time series plots presenting the pH and concentrations of Al, Cu, Zn, Ni, Fe, SO_4^{2-}, and alkalinity from humidity cells containing 2005 Type I, Type II, and Type III waste rock.

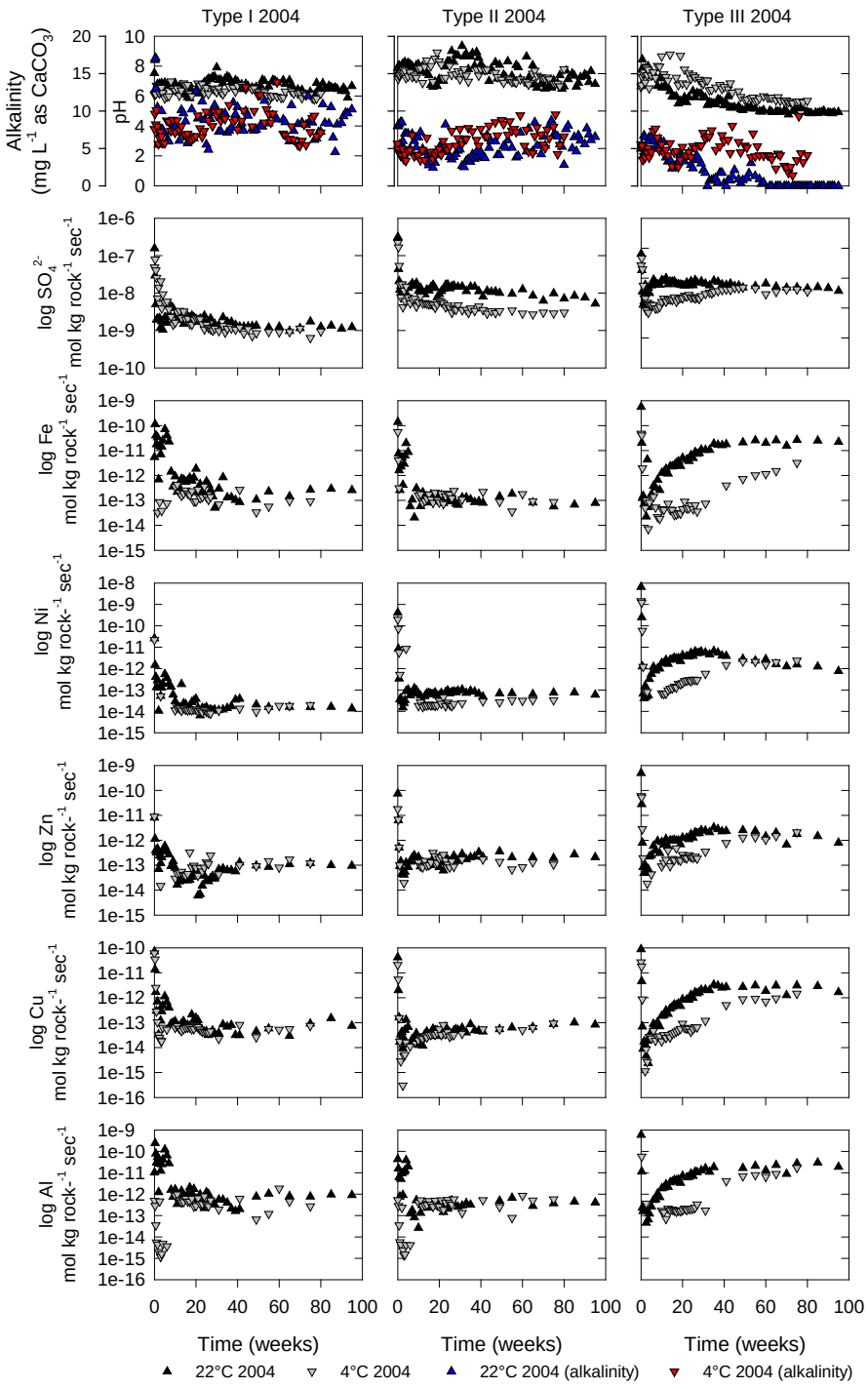

Figure 7.3 Release of SO_4^{2-}, Al, Fe, Ni, Zn, and Cu from the humidity cells normalized to the mass of rock (mol kg rock^{-1} sec^{-1}) for Type I, II, and III materials collected in 2004.

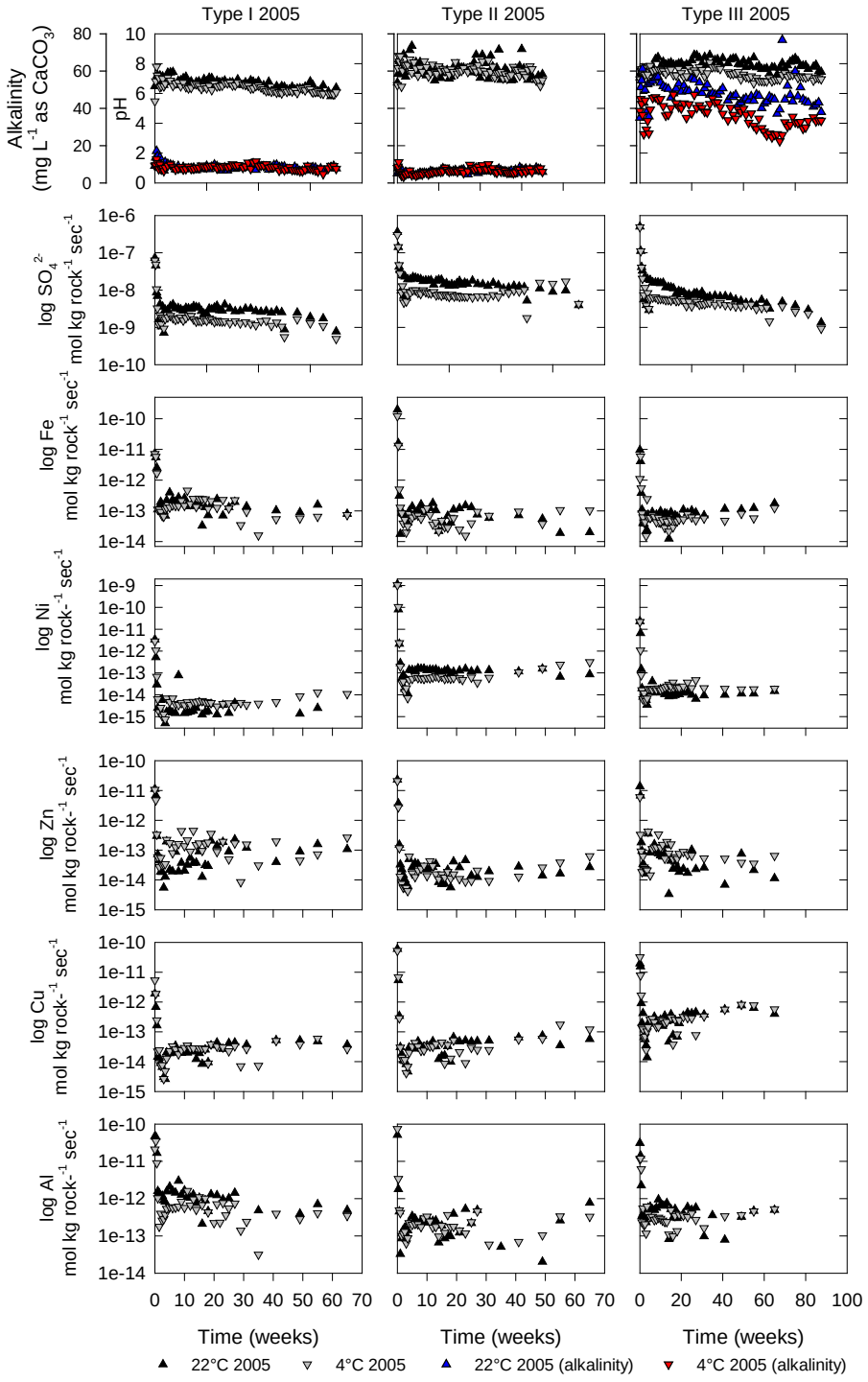

Figure 7.4. Release of SO_4^{2-}, Al, Fe, Ni, Zn, and Cu from the humidity cells normalized to the mass of rock (mol kg rock^{-1} sec^{-1}) for Type I, II, and III materials collected in 2005.

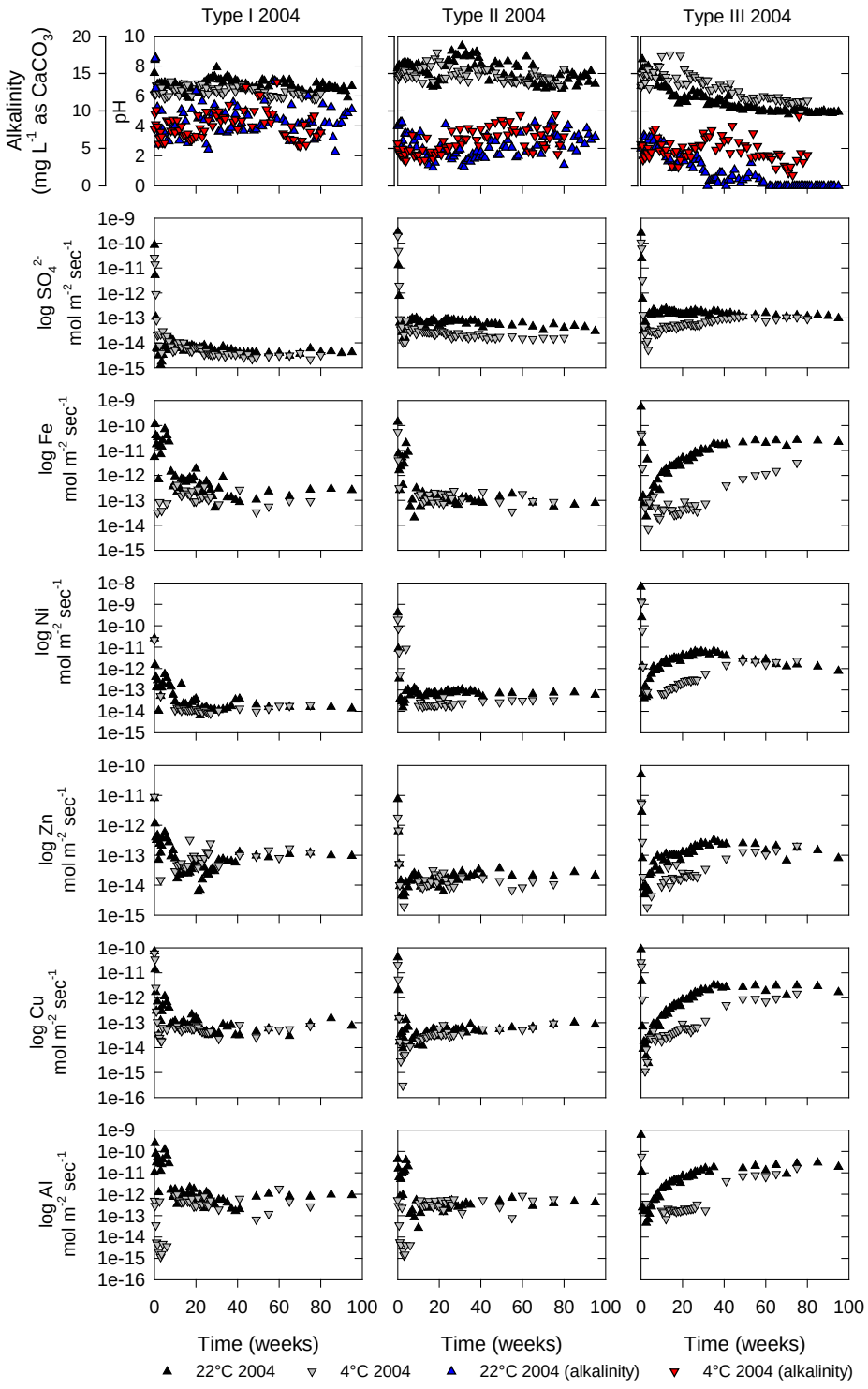

Figure 7.5 Release of SO_4^{2-}, Al, Fe, Ni, Zn, and Cu from the humidity cells normalized to the surface area of waste rock (mol m^{-2} sec^{-1}) for Type I, II, and III materials collected in 2004.

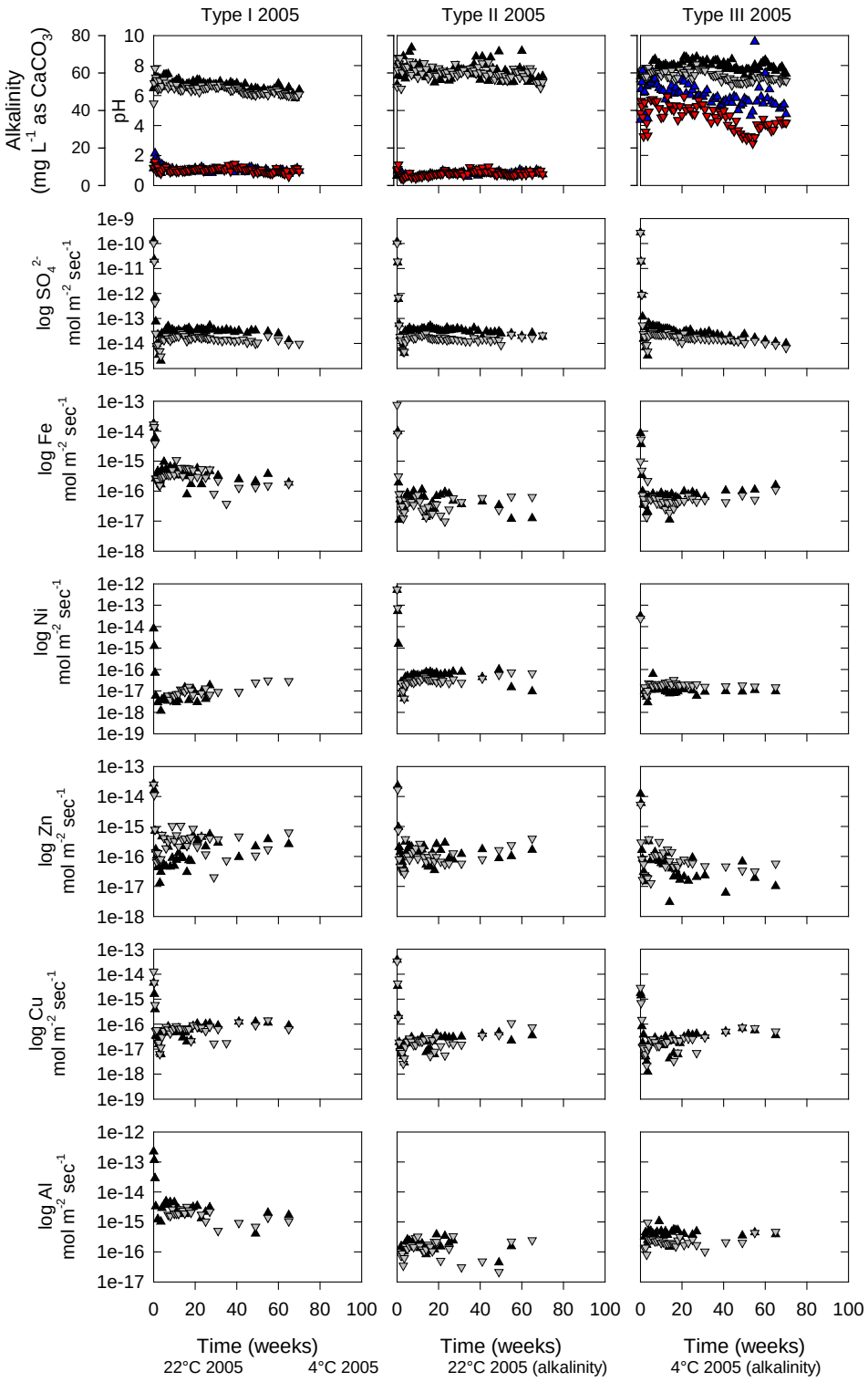

Figure 7.6 Release of SO_4^{2-}, Al, Fe, Ni, Zn, and Cu from the humidity cells normalized to the surface area of waste rock (mol m^{-2} sec^{-1}) for Type I, II, and III materials collected in 2005.

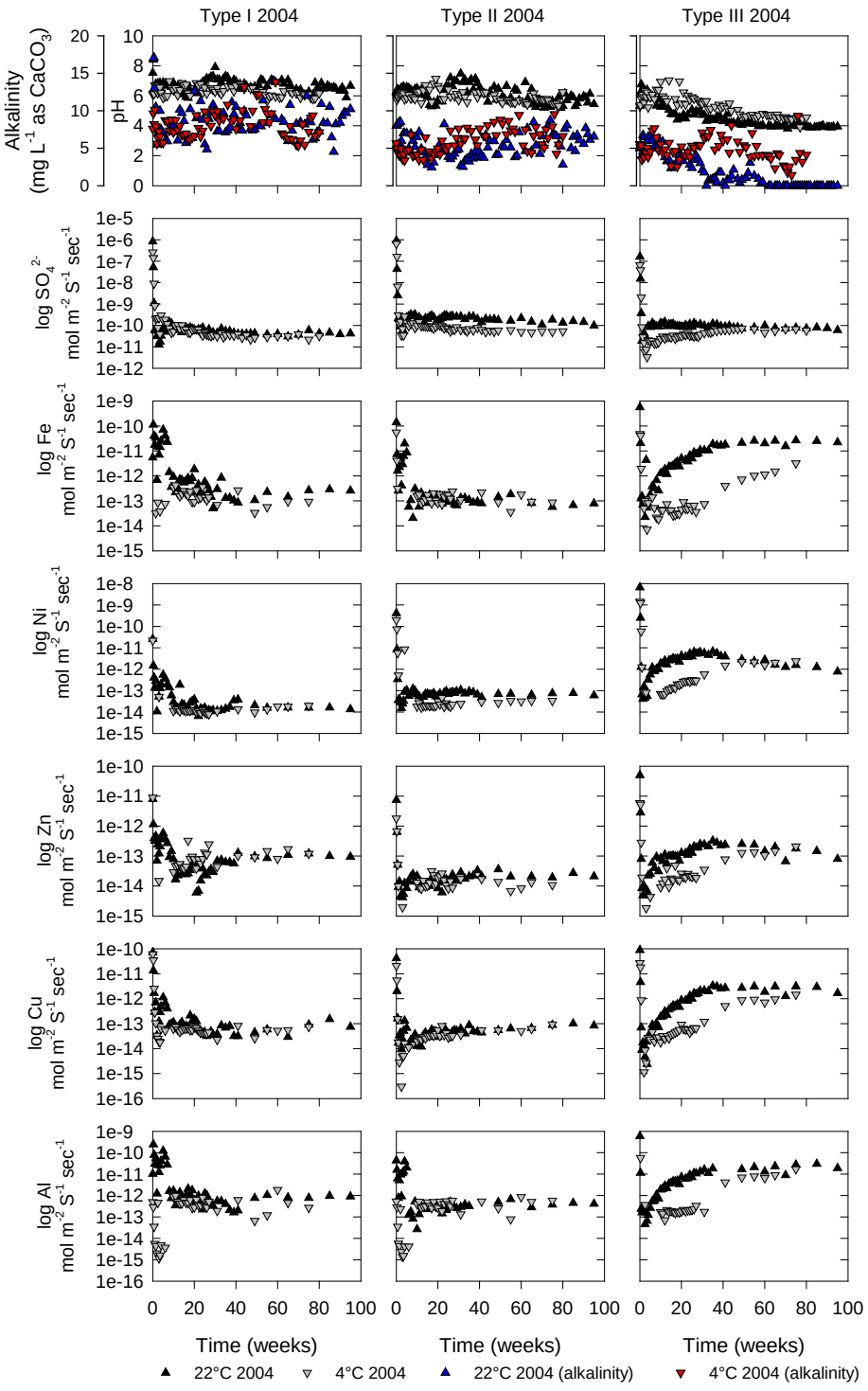

Figure 7.7 Release of SO_4^{2-}, Al, Fe, Ni, Zn, and Cu from the humidity cells normalized to the surface area of S (mol m^{-2} S^{-1} sec^{-1}) for Type I, II, and III materials collected in 2004.

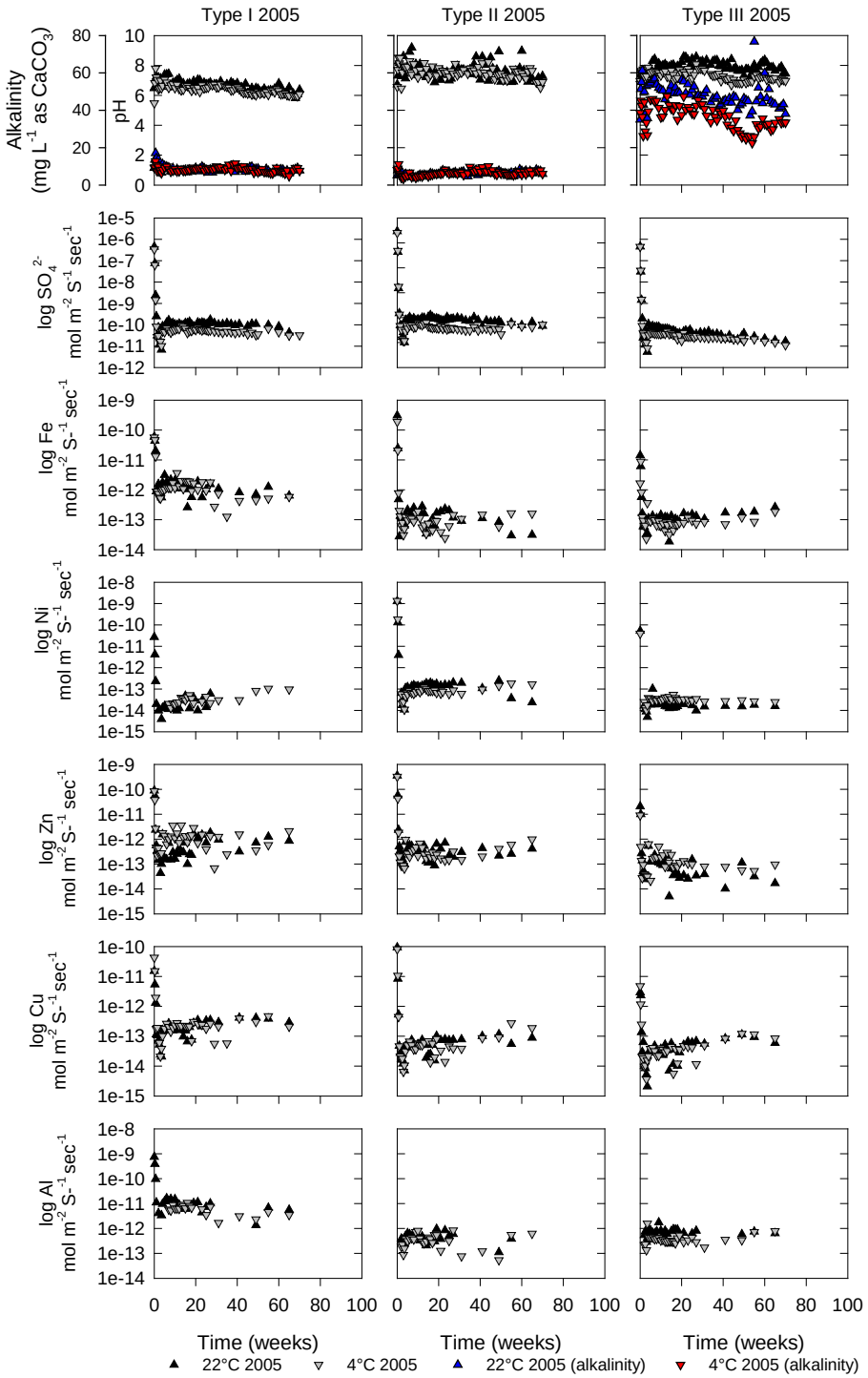

Figure 7.8 Release of SO_4^{2-}, Al, Fe, Ni, Zn, and Cu from the humidity cells normalized to the surface area of S (mol m^{-2} S^{-1} sec^{-1}) for Type I, II, and III materials collected in 2005.

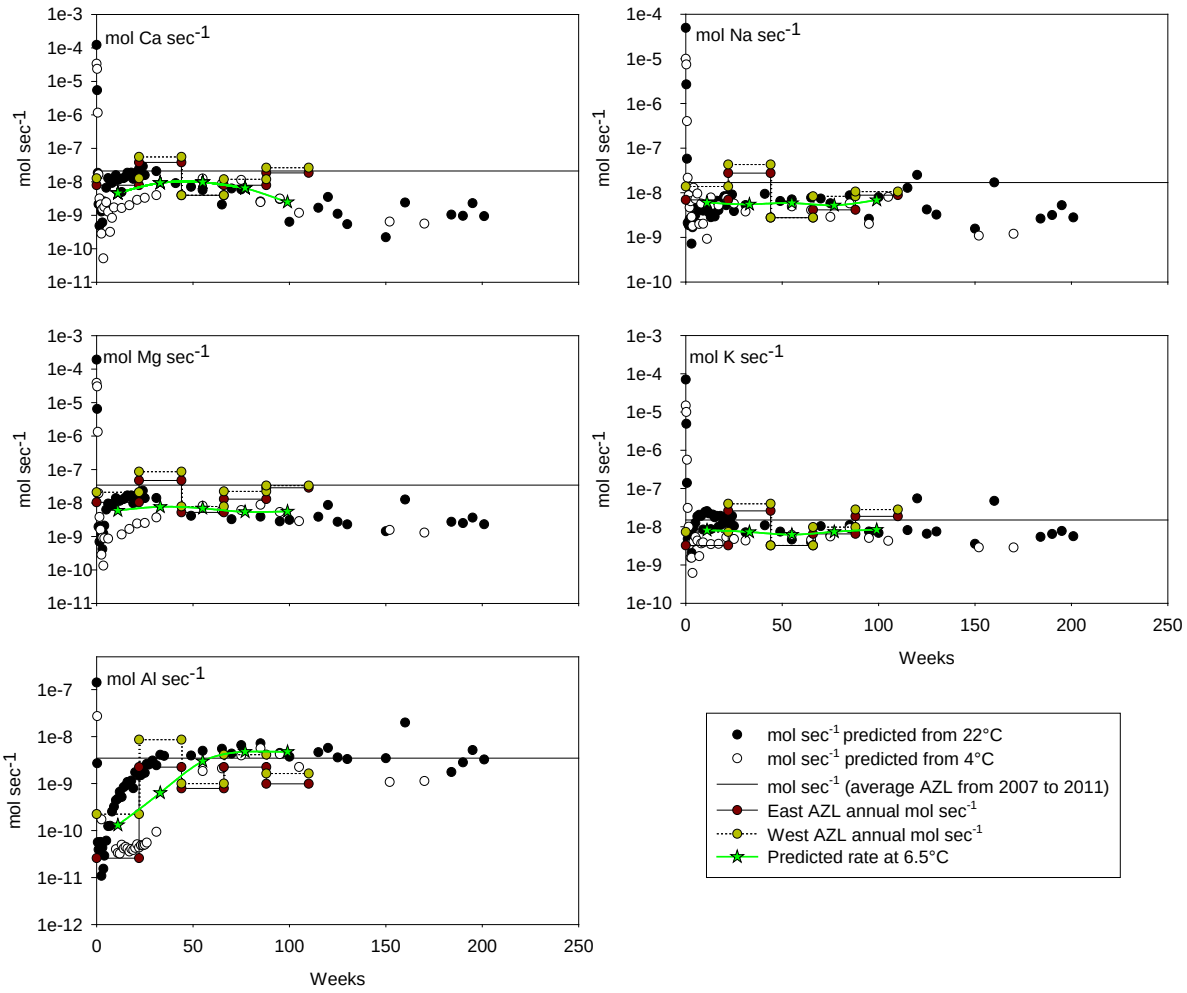

Figure 7.9 Estimated release rates of major cations from the Type III AZLs from 2007 through 2010. Each AZL year is equal to 22 weeks of the humidity-cell experiment. The solid line represents the 5 year average Type III AZL release rates.

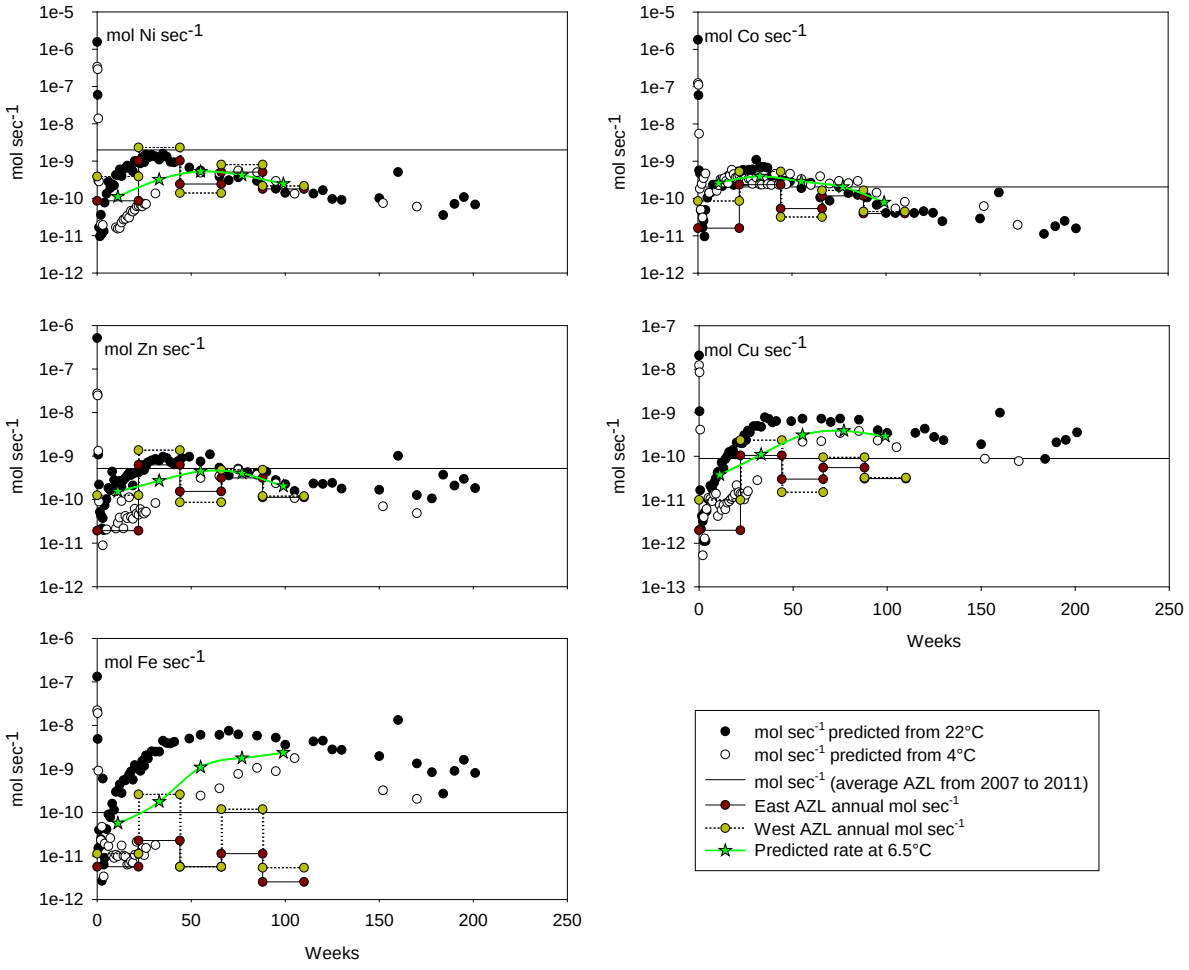

Figure 7.10 Estimated release rates of metals from the Type III AZLs from 2007 through 2010. Each AZL year is equal to 22 weeks of the humidity-cell experiment. The solid line represents the 5 year average Type III AZL release rates.

Chapter 8:

Conclusions

8.1 Summary of Findings

The focus of this research was to investigate the geochemical and microbiological characteristics of effluent and pore water from experimental waste-rock stockpiles with a low-S content (< 0.8 wt. % S), in a continuous permafrost region. Additionally, an appropriate approach for scale-up to predict effluent quality from laboratory studies to field-based studies was established. Acid generation, from sulfide-mineral oxidation, and acid-neutralization reactions are important processes controlling the effluent quality from waste-rock stockpiles. Understanding the effect of temperature on these reactions and processes is important for the management of acid mine drainage in Arctic environments. Furthermore, effluent from waste-rock stockpiles can be affected by the blasting agents used to extract waste rock to gain access to the economic grade ore, potentially releasing undetonated explosives and blasting residuals to receiving watercourses.

One of the objectives of this research was to determine the persistence of undetonated explosives and blasting residuals in experimental waste-rock test piles. Laboratory leach experiments and field studies at different scales demonstrated the mobility and depletion of NO_3^-, NO_2^-, NH_3, ClO_4^- and Cl^- from the waste rock. In the field-based 2 m by 2 m scale experiments the breakthrough of these components indicated volumes that were similar to

estimates of the matrix porosity, thereby, acting as an internal tracer (Chapter 2). The large-scale experiments (15 m in height by 50 m by 60 m at the base) had irregular concentrations and a more gradual dissipation of blasting residuals in response to changes in the ambient air temperature and the prolonged migration of wetting fronts through the test piles. These results illustrated the heterogeneity of the test piles and the temporal variations in the contributions of flow derived from different regions within the test piles. Further, during blasting some sulfide minerals near blast holes were oxidized releasing SO_4^{2-} that was also flushed during the first flush of the matrix, and was highly correlated to blasting residuals. After the dissipation of blasting residuals, additional SO_4^{2-} was derived from the *in situ* oxidation of sulfide minerals and concentrations of SO_4^{2-} were variable with ambient air temperatures. Waste rock with a higher S content released higher ratios of SO_4^{2-} to N, providing a novel approach for estimating the mass of S released during the first flush of waste rock.

The examination of effluent from the upper 2 m of Type III waste rock in the AZLs (6 t of waste rock) indicated the active freeze thaw layer underwent extensive weathering during the first 4 years of rock placement. The Type III AZLs were depleted of carbonate minerals and neutralization potential (Chapter 3) after the first field season. Whereas, the pH of the effluent from the Type I AZLs remained near-neutral, and alkalinity concentrations remained above detection, for the duration of the study. The increased mass of sulfide minerals from biotite schist in the Type III AZLs was sufficient to generate acidic drainage with high concentrations of SO_4^{2-} and dissolved metals, and to overwhelm the carbonate-mineral buffering capacity.

Waste rock in the large-scale test piles (70,000 t) was affected by the changes in season and variations in ambient air temperature that influenced sulfide-mineral oxidation rates (Chapter 4). In addition, the semi-arid climate at Diavik affected the transport of sulfide-mineral oxidation products from the top of the waste-rock test piles to the base of the waste-rock test piles. The Type III test-pile (0.053 wt. % S) effluent decreased from near-neutral pH at the beginning of each field season to acidic conditions (pH < 4.5) as the ambient air temperatures increased and the rate of sulfide-mineral oxidation exceeded the rate of acid consumption. The Type I test-pile (0.035 wt. % S) effluent maintained near-neutral pH for the duration of the study, with slight decreases at the end of each field season when the flow rate decreased. Sulfide-mineral oxidation in the Type I test pile was balanced by acid neutralization through carbonate-mineral dissolution. At the end of each field season greater portions of the test pile contributed to the outflow and higher concentrations of SO_4^{2-}, blasting residuals, and dissolved metals were observed. In addition, pore-water samples collected over 4 years showed the migration of sulfide-mineral oxidation products and blasting residuals from the top of the test piles to the base of the piles. The gradual increase in pore-water concentrations from the top of the test pile to the base of the test pile, suggests flow in the waste-rock test piles at Diavik is matrix dominated, rather than flow through the macropores or by-pass flow.

Waste rock with a low S and equally low C content in field experiments in a continuous permafrost region generated effluent with low pH and high SO_4^{2-} and dissolved metals (Chapters 3 and 4). The acid-neutralization sequence observed in the Type III AZLs and test pile was similar to other AMD studies. A series of mineral dissolution-precipitation reactions

controlled pH and metal mobility; carbonate-mineral dissolution buffered the acidity generated from sulfide-mineral oxidation at near neutral pH and the dissolution of Al and Fe (oxy)hydroxides buffered the effluent and pore water at pH < 5.0.

The results from the AZLs and test piles indicated the Type III waste rock is acid generating. At Diavik, a cover system has been approved for the closure of the Type III portion of the full-scale waste-rock stockpile. An experimental-scale test pile was constructed to evaluate the approved reclamation concept and to compare the hydrology, thermal transport, geochemistry, microbiology, and gas transport to an uncovered waste-rock test pile composed of Type III waste rock (Type III test pile). The cover system included a low permeability (1.5×10^{-10} m^2) layer of frozen till as a barrier to O_2 and water infiltration, and covered with non-reactive waste rock to act as the active freeze-thaw layer. Chapter 5 described the results from one of the first cover performance studies of this scale. The Covered test pile maintained constant internal temperatures (~2°C), due to the influence of basal lysimeter heat trace, whereas pronounced fluctuations in internal temperatures and variations in flow were observed in the Type III test pile in response to ambient temperature changes and recharge events. The till layer in the Covered test pile remained frozen, for the duration of the study, with the exception of areas directly above the basal lysimeter heat trace (Face 1 and Face 2). This lower permeability layer dampened the effects of conductive heat flow and advective gas transport compared to the Type III test pile; therefore, the Covered test pile experienced lower amplitude changes in temperature, primarily driven by conductive heat flow. As a result, the Covered test pile had a relatively steady change in flow rate, with

decreased flow from June to August, which led to a slow release of sulfide-mineral oxidation products compared to the uncovered Type III test pile.

Changes in the total bacterial biodiversity with evolving effluent geochemistry were observed in the AZLs and waste-rock test pile effluent (Chapter 6). Deep sequencing and a temporal comparison of the phylogenies were used to examine changes in the microbial community. In addition, neutrophilic and acidophilic S-oxidizers and Fe-oxidizers were enumerated using the most probable number techniques. The community profiles observed in the waste-rock test piles and AZLs suggest species typical of AMD settings were present in acidic effluent with elevated concentrations of dissolved metals, whereas microbes typical of Arctic soils were present in effluent with a near-neutral pH and lower concentrations of SO_4^{2-} and dissolved metals. The Type III test pile, Type III AZLs, and Covered test pile sustained populations of acidophilic Fe-oxidizers, whereas the Type I AZLs and Type I test pile maintained populations of neutrophilic S-oxidizers. The total bacterial biodiversity evolved with changes in the effluent quality and chemistry. For example, most locations where elevated concentrations of sulfide-mineral oxidation products were present bacterial 16s rRNA genes suggests the *Hydrogenophilaceae* family, specifically the genus *Thiobacillus,* was the dominant family. Furthermore, the abundance of N-cycling bacteria increased when concentrations of dissolved N compounds, derived from blasting residuals, increased. The results from this study provide a baseline for observing the succession of the microbial community associated with different stages of sulfide-mineral oxidation in waste-rock stockpiles in the Arctic.

The prediction, prevention and remediation of AMD are challenges for mine sites around the world. Methods have been developed to use laboratory scale experiments to predict the lag time and the longevity of poor quality effluent of AMD from full-scale waste-rock stockpiles. Humidity-cell experiments using the Diavik waste rock were completed to scale results to the AZLs then to the test piles, and ultimately, to the full scale waste-rock stockpile. In Chapter 7, the first attempt to scale the laboratory humidity-cell experiments to the field based Type III AZLs was conducted. This was achieved through the normalization of the release rates of SO_4^{2-} to the surface area of S in the waste rock to then estimate annual total mass loadings. The annual total mass loadings of SO_4^{2-}, dissolved metals, and major cations estimated for the Type III AZLs were comparable to the actual mass loadings for all years, with the exception of 2008 which had higher than predicted total mass loadings, in part due to a low precipitation year followed by a year with higher precipitation, and for Fe and Al which were over predicted. Geochemical equilibrium modeling of the estimated concentrations suggested that Fe and Al concentrations in the Type III AZLs would be controlled by the solubility and formation of secondary minerals, such as jarosite and goethite. Moreover, the results from the Type III AZLs suggest Fe and Al concentrations were controlled by secondary mineral formation, suggesting this method of prediction is promising. The results indicate annual total mass loads can be estimated in this manner if thorough characterization of the waste rock accompanies the analysis to refine the release rates.

Sapsford et a. (2009) indicate that to date there is no universally accepted technique or model for converting laboratory measured sulfide oxidation rates into predictions of the

overall rate of oxidation within waste rock materials. In addition, few studies have attempted to scale laboratory results to field based studies and in those that have, results were within order(s)-of-magnitude (Bennett *et al*., 2000; Malmstrom *et al*., 2000; Sapsford *et al*., 2009). Results obtained from the type of investigation presented in Chapter 7 could assist the mining industry and regulatory agencies improve the prediction of AMD and the management of waste rock.

8.2 Scientific Contribution

The research presented in this thesis has contributed to waste-rock characterization studies involving low-S content waste rock and blasting residuals in Arctic environments. The scientific contributions include:

- Demonstrating that undetonated explosives and blasting residuals are highly mobile and dissipate from waste-rock test piles after one flush of the matrix;
- Developing a novel approach to estimate the mass of S (due to sulfide-mineral oxidation during blasting) released in first flush of the matrix material;
- Illustrating the variations in the quality of effluent from waste-rock test-pile with ambient air temperatures in the Arctic due to changes in sulfide-mineral oxidation rates;
- Demonstrating the upper 2 m of waste rock is the most weathered region of the waste-rock test pile through the examination of 2 m by 2 m scale experiments and pore water in the waste-rock test piles;
- Illustrating the migration of solutes from the top of the test pile to the base of the test piles is through matrix dominated flow, rather than macropore or by-pass flow;
- Evaluating an approved cover system for a large-scale test pile with thermal and low permeability cover materials, and comparing the results with an uncovered pile exposed to Arctic temperature fluctuations;

- Demonstrating the first investigation of changes to the total bacterial biodiversity with evolving waste-rock effluent chemistry at an Arctic site using deep sequencing and MPN methods; and,
- Developing a novel approach to predict the water quality from field based experiments using laboratory humidity-cell experiments.

8.3 Future Research and Recommendations

The geochemical and microbiological characteristics of effluent from waste-rock test piles was examined for 4 years; however, the climatic conditions at the site limited the migration of water from the top of the test piles to the base of the test piles. The wetting front in the Type I test pile did not reach the base after 4 years. Therefore, long-term evaluation of the effluent and pore-water quality is required to provide more information on evolution of AMD in this low-S content waste rock. In addition, the large-scale test piles continue to release undetonated explosives and blasting residuals. This research would provide more information on the dissipation over time and observe the natural wetting-up phase of the test pile.

Geochemical-equilibrium modeling was used to calculate saturation indices to assess the potential for secondary-mineral formation. As part of the long-term plan for the Diavik Waste Rock Research Facility, one of the test piles will be deconstructed. Mineralogical studies of waste rock exposed to years of exposure to atmospheric oxygen and water are required to evaluate the degree of sulfide-mineral oxidation within the test piles. In addition, the investigation of secondary minerals within the AZLs and the test piles is required to confirm the presence or absence of secondary minerals potentially controlling parameters in the effluent chemistry, such as Al, Fe, and SO_4^{2-}, from waste-rock test piles.

The Covered pile basal drain heat trace was turned off in 2010. Over time it is expected that the unfrozen portion of the till layer will freeze and limit water infiltration. Long-term monitoring of this test pile should provide a more realistic evaluation of the approved cover system at Diavik under Arctic conditions.

The microbial diversity of the waste-rock effluent evolved with changes in chemistry. Long-term monitoring of the microbial community is needed to observe the succession of the population with further changes in effluent pH and dissolved metals concentrations. As the pH decreases, the population is expected to evolve and may include AMD-related species not observed to date in the test piles, such as *Acidithiobacillus* sp. and *Leptospirillum* sp. In addition, archaea were not examined in this thesis, therefore, it is recommended that deep sequencing of archaeal 16s rRNA genes be completed to determine if known S- and Fe-oxidizing archaea are present in the waste-rock effluent.

The ability to use small-scale experiments to predict the lag time and longevity of AMD from full-scale waste-rock stockpiles is beginning to receive more attention in the mining industry, with little interest in the scientific community, and a limited amount of literature is available on scaling methods. The ability to scale humidity cells to predict the effluent quality in the AZLs was met with some success. The method developed for scale-up in this thesis could potentially be improved with the examination of factors not addressed herein, such as the incorporation of flow, better estimates of residence time, and the effects of pH could potentially improve these estimates. Similarly, scaling estimates could be improved with a multi-component reactive transport model that incorporates the interactions of mass transport and geochemical reactions, including equilibrium and kinetic reactions processes,

such as MIN3P. This type of analysis may help to better understand the chemical processes within waste-rock piles and the physical transport mechanisms of sulfide-mineral oxidation products. The data obtained for this thesis can be used to improve water-quality prediction models, and be further used to estimate impacts of climate change in the Arctic.

References

Aachib, M., Mbonimpa, M., Aubertin, M., 2004. Measurement and prediction of the oxygen diffusion coefficient in unsaturated media, with applications to soil covers. Water, Air, Soil Pollut. 156, 163-193.

Acker, J.G., Bricker, O.P., 1992. The influence of pH on biotite dissolution and alteration kinetics at low temperature. Geochim. Cosmochim. Acta. 56, 3073-3092.

Adu-Wusu, C., Yanful., E.K., 1993. Performance of engineered test covers on acid generating waste rock at Whistle mine, Ontario. Can. Geotech. J. 43, 1-18.

Ahonen, L., Tuovinen, O.H., 1992. Bacterial oxidation of sulfide minerals in column leaching experiments at suboptimal temperatures. Appl. Environ. Microbiol. 58, 600-606.

Allison, J.D., Brown, D.S., Novo-Gradac, K.L., 1990. MINTEQA2/PRODEFA2, A geochemical assessment model for environmental systems, Version 3.0 User's Manual. Environmental Research Laboratory, Office of Research and Development, U.S. EPA, Athens, Ga.

Alpers, C.N., Blowes, D.W., Nordstrom, D.K., Jambor, J.L., 1994. Secondary minerals and acid mine-water chemistry. In: Jambor, J.L., Blowes, D.W. (Eds.), *Environmental Geochemistry of Sulfide Mine-Wastes*, Mineral. Assoc. Can. Short Course vol. 22. 245-270.

Altschul, S.F., Gish, W., Miller, W., Myers, E.W., Lipman, D.J., 1990. Basic local alignment search tool. J. Mol. Biol. 215, 403-410.

Amos, R.T., Blowes, D.W., Smith, L. and Sego, D.C., 2009a. Measurement of wind-induced pressure gradients in a waste rock pile. Vadose Zone J. 8, 953-962.

Amos, R. T., Smith, L., Neuner, M., Gupton, M., Blowes, D. W., Smith, L., Sego, D. C., 2009b. Diavik waste rock project: Oxygen transport in covered and uncovered piles. In: Proc. of Securing the Future and 8th International Conference on Acid Rock Drainage, Skellefteå, Sweden.

Ardau, C., Blowes, D.W., Ptacek, C.J., 2009. Comparison of laboratory testing protocols to field observations of the weathering of sulfide-bearing mine tailings. J. Geochem. Explor. 100, 182-191.

ASTM. 1998. D 5744-96, Standard test method for accelerated weathering of solid materials using a modified humidity cell. Annual book of ASTM standards. 11.04, 259-271.

Aziz, C., 2006. Alternative causes of wide-spread, low concentration perchlorate impacts to groundwater. In: Gu, B., Coates, J.D. (Eds), *Perchlorate Environmental Occurrence, Interactions and Treatment*. Springer, Boston, MA, USA, Chapter 4.

Baalsrud, K., Baalsrud, K.S., 1954. Studies on *Thiobacillus denitrificans*. Arch. Microbiol. 20, 34-62.

Bailey, B.L., Smith, L.J.D., Blowes, D.W., Ptacek, C.J., Smith, L., Sego, D., 2012. Diavik Waste Rock Project: Persistence of contaminants from blasting agents in waste rock effluent. Appl. Geochem. doi: 10.1016/j.apgeochem.2012.04.00.

Baker, B.J., Banfield, J.F., 2003. Microbial communities in acid mine drainage. FEMS Microbiol. Ecol. 44, 139-152.

Ball, J.W., Nordstrom, D.K., 1991. User's manual for WATEQF4 with revised thermal dynamic data base and test cases for calculating speciation of major, trace, and redox elements in natural waters. Open-file report, USGS. 91-183.

Banks, D., Younger, P.L., Arnesen, R.-T., Iversen, E.R., Banks, S.B., 1997. Mine-water chemistry: The good, the bad and the ugly. Environ. Geol. 32, 157-173.

Bay, D.S., 2009. Hydrological and Hydrogeochemical Characteristics of Neutral Drainage from a Waste Rock Test Pile. M.Sc. thesis. University of British Columbia, Vancouver, Canada.

Belzile, N., Maki, S., Chen, Y.-W., Goldsack, D., 1997. Inhibition of pyrite oxidation by surface treatment. Sci. Total Environ. 196, 177-186.

Benner, S.G., Gould, W.D., Blowes, D.W., 2000. Microbial populations associated with the generation and treatment of acid mine drainage. Chem. Geol. 169, 435–448.

Benzaazoua, M., Bussière, B., Dagenais, A-M., Archambault, M., 2004. Kinetic tests comparison and interpretation for prediction of the Joutel tailings acid generation potential. Environ. Geol. 46, 1086-1101.

Bierens de Haan, S., 1991. A review of the rate of pyrite oxidation in aqueous systems at low temperature. Earth-Sci. Rev. 31, 1-10.

Bigham, J.M., Nordstrom, D.K., 2000. Iron and Aluminum Hydroxysulfates from acid sulphate waters. Rev Mineral Geochem. 40, 351-403.

Blowes, D.W., Al, T., Lortie, L., Gould, W.D., Jambor, J.L., 1995. Microbiology, chemical, and mineralogical characterization of the Kidd Creek Mine tailings impoundment, Timmins Area, Ontario. Geomicrobiol. J. 13, 13-31.

Blowes, D.W., Jambor, J.L., 1990. The pore-water geochemistry and the mineralogy of the vadose zone of sulfide tailings, Waite Amulet, Quebec, Canada. Appl. Geochem. 5, 327-346.

Blowes, D.W., Jambor, J.L., Appleyard, E.C., Reardon, E.J., Cherry, J.A., 1992. Temporal observations of the geochemistry and mineralogy of a sulfide-rich mine-tailings impoundment, Heath Steele mines, New Brunswick. Explor. Min. Geol. 1, 251-264.

Blowes, D.W., Logsdon, M.J., 1998. Diavik Geochemistry baseline Report. Report to Diavik Diamond Mines Inc.

Blowes, D.W., Moncur, M.C., Smith, L., Sego, S., Bennett, J., Garvie, A., Linklater, C., Gould, D., Reinson, J., 2006. Construction of two large-scale waste rock piles in a continuous permafrost region. In: Proc. of 7th International Conference on Acid Rock Drainage, St. Louis, Mo., USA.

Blowes, D.W., Ptacek, C.J., 1994. Acid neutralization reactions in mine tailings. In: Jambor, J.L., Blowes, D.W. (Eds.), *Environmental Geochemistry of Sulfide Mine-Wastes*, Mineral. Assoc. Can. Short Course vol. 22. 271-292.

Blowes, D.W., Ptacek, C.J., Jambor, J.L., Weisner, C.G., 2004. The geochemistry of acid mine drainage. In: Holland, H.D., Turekian, K.K., Lollar, B.S. (Eds.), *Treatise on Geochemistry*, Environmental Geochemistry, vol. 9. Elsevier. 149-204.

Blowes, D.W., Ptacek, C.J., Jurjovec, J., 2003a. Mill tailings: Hydrogeology and geochemistry. In: Jambor, J.L., Blowes, D.W., Ritchie, A.I.M. (Eds.), *Environmental Aspects of Mine Wastes*, Mineral. Assoc. Can. Short Course vol. 31, 95-116.

Blowes, D.W., Reardon, E.J., Jambor, J.L., Cherry, J.A., 1991.The formation and potential importance of cemented layers in inactive sulfide mine tailings. Geochim. Cosmochim. Acta, 55, 965-978.

Blowes, D.W., Robertson, W.D., Ptacek, C.J., Merkley, C., 1994. Removal of agricultural nitrate from tile-drainage effluent water using in-line bioreactors. J. Contam. Hydrol. 15, 207-221.

Blum J. D., Gazis C. A., Jacobson A. D., Chamberlain C. P., 1998. Carbonate versus silicate weathering in the Raikhot watershed within the High Himalayan Crystalline Series. Geology 21, 411-414.

Bolhuis, H., Stal, L.J., 2011. Analysis of bacterial and archaeal diversity in coastal microbial mats using massive parallel 16S rRNA gene tag sequencing. ISME J. 5, 1701-1712.

Bond, P. L., Smriga, S. P., Banfield, J. F., 2000. Phylogeny of microorganisms populating a thick, subaerial, predominantly lithotrophic biofilm at an extreme acid mine drainage site. Appl. Environ. Microbiol. 66, 3842–3849.

Brunauer, S., Emmett, P.H., Teller, E., 1938. Adsorption of gases in multimolecular layers. J. Am. Chem. Soc. 60, 309-319.

Briggs, T.J., Kelso, I.J., 2001. Ammonium nitrate-sulfide reactivity at the Century Zn-Pb-Ag mine, northwest Queensland, Australia. Explor. Min. Geol. 10, 177-190.

Brookfield, A.E., Blowes, D.W., Mayer, K.U., 2006. Integration of field measurements and reactive transport modelling to evaluate contaminant transport to a sulfide mine tailings impoundment. J. Contam. Hydrol. 88, 1-22.

Bussière, B., Benzaazoua, M., Aubertin, M., Mbonimpa, M., 2004. A laboratory study of covers made of low-sulphide tailings to prevent acid mine drainage. Environ. Geol., 45, 609-622.

Carlsson, E., Thunberg, J., Öhlander, B., Holmström, H., 2002. Sequential extraction of sulfide-rich tailings remediated by the application of till cover, Kristineberg mine, northern Sweden. Sci. Total Environ. 299, 207-226.

Cameron, A., Corkery, D., MacDonald, G., Forsyth, B., Gong, T., 2007. An investigation of ammonium nitrate loss to mine discharge water at Diavik diamond mines. In: Proc. of EXPLO 2007 - Blasting: Techniques and Technology, Wollongong, NSW. Australasian Institute of Mining and Metallurgy Publication Series, 21-33.

Canadian Environmental Quality Guidelines (CEQG). 1999. Canadian Council of Ministers of Environment, Environment Canada, 1999, Winnipeg.

Canadian Water Quality Guidelines (CWQG), 1987. Canadian Council of Resource and Environment Ministers, Environment Canada, March 1987, Ottawa.

Chandra, A.P., Gerson, A.R., 2010. The mechanisms of pyrite oxidation and leaching: A fundamental perspective. Surface Science Reports, 65, 293-315.

Chandra, A.P., Gerson, A.R., 2011. Pyrite (FeS_2) oxidation: A sub-micron synchrotron investigation of the initial steps. Geochim. Cosmochim. Acta. 75, 6239-6254.

Chi, X., 2010. Charcterizing low-sulfide instrumented waste-rock piles: image grain-size analysis and wind-induced gas transport. MSc Thesis. University of Waterloo. Waterloo, Ontario.

Chu, H., Fierer, N., Lauber, C.L., Caporaso, J.G., Knight, R., Grogan, P., 2010. Soil bacterial diversity in the arctic is not fundamentally different from that found in other biomes. Environ. Microbiol. 12, 2998–3006.

Clark, G.B., 1981. Basic properties of ammonium nitrate fuel oil explosives (ANFO). Colorado School of Mines Quart. vol. 76 no. 1.

Clow D. W., Mast M. A., Bullen T. D., Turk J. T., 1997. Strontium 87/strontium 86 as a tracer of mineral weathering reactions and calcium sources in an alpine/subalpine watershed, Loch Vale, Colorado. Water Res. Res. 33, 1335-1351.

Cochran, W.G., 1950. Estimation of bacterial densities by means of the "most probable number". Biometrics. 6, 105-116.

Corazao Gallegos, J.C., 2007. The design, construction, instrumentation, and initial response of a field-scale waste rock test pile, M.A.Sc. thesis. University of British Columbia, Vancouver, Canada.

Cox, C., 1994. Statistical issues for animal studies of developmental neurotoxicity. In: Weiss, B., O'Donoghue, J.L. (Eds), *Neurobehavioral Toxicity: Analysis and Interpretation*. Raven Press; New York, NY, USA, 93-101.

Cravotta III, C.A. Brady, K.B.C., Rose, A.W., Douds, J.B., 1999. Frequency distribution of the pH of coal-mine drainage in Pennsylvania. In: Morganwalp, D.W., Buxton, H. (Eds.), *US Geological Survey Toxic Substances Hydrology Program – Proceedings of the Technical Meeting*, US Geological Survey Water-Resources Inv. Rep. 99-4018A, 313–324.

Dawson, R.F., Morgenstern, N.R., 1995. Static collapse of mine waste fill. In: Proceedings of the 4th International Symposium on Mine Planning and Equipment Selection, October, Calgary, Alta, 845-851.

Demers, I., Bussière, B., Aachib, M., Aubertin, M. 2011. Repeatability evaluation of instrumented column tests in cover efficiency evaluation for the prevention of acid mine drainage. Water, Air, Soil Pollut., 219, 113-128.

Diavik Diamond Mine Inc. (DDMI), 2006. Revised Ammonia Discussion Paper. Technical report submitted to Mackenzie Valley Land and Water Board May 15, 2006.

Diavik Diamond Mine Inc. (DDMI), 2011. Interim Closure and Reclamation Plan – Version 3.2 submitted to Mackenzie Valley Land and Water Board August 2011.

Diamadopoulos, E., Samaras, P., Dabou, X., Sakellaropoulos, G.P., 1997. Combined treatment of landfill leachate and domestic sewage in a sequencing batch reactor. Water Sci. Technol. 36, 61-68.

Dold, B., Fontboté, L., 2002. A mineralogical and geochemical study of element mobility in sulfide mine tailings of Fe oxide Cu - Au deposits from the Punta del Cobre belt, northern Chile. Chem. Geol. 189, 135-163.

Dowd, S.E., Sun, Y., Secor, P.R., Rhoads, D.D., Wolcott, B.M., James, G.A., Wolcott, R.D., 2008. Survey of bacterial diversity in chronic wounds using pyrosequencing, DGGE, and full ribosome shotgun sequencing. BMC Microbiol. 8, 43–58.

Drobner, E., Huber, H., Reinhard, R., Stetter, K., 1992. *Thiobacillus plumbophilus* spec. nov., a novel galena and hydrogen oxidizer. Arch. Microbiol. 157, 213-217.

Dzombak, D.A., Morel, F.M.M., 1990. *Surface Complexation Modeling: Hydrous Ferric Oxide*. John Wiley and Sons, Toronto, Canada.

Egly, R.S., Neckar, A.E., 1964. Ammonium nitrate-containing emulsion sensitizers for blasting agents, US Patent No. 3 161 551.

Elberling, B., 2005. Temperature and oxygen control on pyrite oxidation in frozen mine tailings. Cold Reg. Sci. Tech. 41, 121-133.

Elberling, B., Schippers, A., Sand, W., 2000. Bacterial and chemical oxidation of pyritic mine tailings at low temperatures. J. Contam. Hydrol. 41, 225-238.

Environment Canada, 2004. Threats to Water Availability in Canada. National Water Research Institute, Burlington, Ontario. NWRI Scientific Assessment Report Series No. 3 and ACSD Science Assessment Series No. 1.

Environment Canada, 2010. Monthly data report for Ekati A, Northwest Territories, Bulk Data 1998-2010. Accessible at: http://climate.weatheroffice.ec.gc.ca/climateData/canada_e.html

Eriksson, N., Gupta, A., Destouni, G., 1997. Comparative analysis of laboratory and field tracer tests for investigating preferential flow and transport in mining waste rock. J. Hydrol. 194, 143-163.

Evangelou V.P., Zhang Y.L., 1995. A review: pyrite oxidation mechanisms and acid mine drainage prevention. Crit. Rev. Environ. Sci. Technol. 25, 141-199.

Fala, O., Aubertin, M., Molson, J., Bussière, B., Wilson, G.W., Chapuis, R., Martin, V., 2003. Numerical modelling of unsaturated flow in uniform and heterogeneous waste rock piles. In: Proc. 6th 8th International Conference on Acid Rock Drainage, July 12–18, 2003, Cairns, Australia.

Fierer, N., Bradford, M.A., Jackson, R.B., 2007. Toward an ecological classification of soil bacteria. Ecology. 88, 1354-1364.

Fretz, N., Momeyer, S., Smith., L., Blowes, D., Sego, D., Amos, R., 2011. Diavik Waste Rock Project: Unsaturated Water Flow. In: Proc. of Tailings and Mine Waste 2011, Vancouver, BC, Canada.

Fretz, N., In preparation. M.Sc. thesis. University of British Columbia.

Frostad, S., Klein, B., Lawrence, R.W., 2005. Determining the weathering characteristics of a waste dump with field tests. IJSM. 19, 132-143.

Galan, E., Gomez-Hriza, J.L., Gonzalez, I., Fernandez-Caliani, J.C., Morales, E., Giraldez, I., 2003. Heavy metal partitioning in river sediments severely polluted by acid mine drainage in the Iberian Pyrite Belt. Appl. Geochem. 18, 409-421.

García, C., Ballester, A., González, F., Blázquez, M. L., 2005. Factors affecting the transformation of a pyritic tailing: Scaled-up column tests. J. Hazard. Mater. 118, 35-43.

Golder Associates, 2008. Report on 2007 review of baseline climate and surface water hydrology for the Diavik Diamond Mine, prepared by Golder Associates, Burnaby, BC, submitted to Diavik Diamond Mines Inc., Yellowknife, NWT, Canada.

Gunsinger, M., Ptacek, C.J., Blowes, D.W., Jambor, J.L., 2006. Evaluation of long-term sulfide oxidation processes within pyrrhotite-rich tailings, Lynn Lake, Manitoba. J. Contam. Hydrol. 83, 149-170.

Gunsinger, M., Ptacek, C.J., Blowes, D.W., Jambor, J.L., Moncur, M.C., 2006. Mechanisms controlling acid neutralization and metalmobility within a Ni-rich tailings impoundment. Appl. Geoch. 21, 1301-1321.

Hallberg, K.B., Johnson, D.B., 2003. Novel acidophiles isolated from moderately acidic mine drainage waters. Hydrometallurgy. 71, 139-148.

He, Z., Xiao, S., Xie, X., Hu, Y., 2008. Microbial diversity in acid mineral bioleaching systems of Dongxiang copper mine and Yinshan lead-zinc mine. Extremophiles. 12, 225-234.

Heikkinen, P.M., Räisänen, M.L., Johnson, R.H., 2009. Geochemical characterisation of seepage and drainage water quality from two sulphide mine tailings impoundments: Acid mine drainage versus neutral mine drainage. Mine Water Environ. 28, 30-49.

Hollings, P., Hendry, J., Nicholson, R., Kirkland, R., 2001. Quantification of oxygen consumption and sulphate release rates for waste rock piles using kinetic cells: Cluff Lake Uranium Mine, northern Saskatchewan, Canada, Appl. Geochem. 16, 1215-1230.

Huang, L.N., Zhou, W.H., Hallberg, K.B., Wan, C.-Y., Li, J., Shu, W.-S., 2011. Spatial and temporal analysis of the microbial community in the tailings of a Pb-Zn mine generating acidic drainage. Appl. Environ. Microbiol. 77, 5540-5544.

Hulshof, A.H.M., Blowes, D.W., Gould, W.D., 2006. Evaluation of *in situ* layers for treatment of acid mine drainage: A field comparison. Water Res. 40, 1816-1826.

International Commission on Large Dams (ICOLD), 1996. A Guide to Tailings Dams and Impoundments: Design, Construction, Use and Rehabilitation. ICOLD Bulletin (United Nations Environment Programme), No. 106.

Interstate Technology and Regulatory Council (ITRC), 2005. Perchlorate: Overview of Issues, Status, and Remedial Options. PERC-1. ITRC, Washington, DC. Online: http://www.itrcweb.org/Documents/PERC-1.pdf.

Jackson, W.A., Anandam, S.K., Anderson, T., Lehman, T., Rainwater, K., Rajagopalan, S., Ridley, M., Tock, R., 2005. Perchlorate occurrence in the Texas Southern High Plains aquifer system. Ground Water Monit. Remed. 25, 137-149.

Jambor, J.L., 1997. Mineralogy of the Diavik Lac de Gras kimberlites and host rocks. Report to Diavik Diamond Mines Inc.

Jambor, J.L., Ptacek, C.J., Blowes, D.W., Moncur, M.C., 2005. Acid drainage from the oxidation of iron sulfides and sphalerite in mine wastes. In: Fujisawa, T. (Ed.), Proc. Lead & Zinc ’05, vol. 1. The Mining and Materials Processing Institute of Japan. 715–737.

Janssen, P. H., 2006. Identifying the dominant soil bacterial taxa in libraries of 16S rRNA and 16S rRNA genes. Appl. Environ. Microbiol. 72, 1719–1728.

Johnson, D.B., Hallberg, K.B., 2005. Acid mine drainage remediation options: A review. Sci. Total Environ. 338, 3-14.

Johnson, D.B., Okibe, N., Hallberg, K.B., 2005. Differentiation and identification of iron-oxidizing acidophilic bacteria using cultivation techniques and amplified ribosomal DNA restriction enzyme analysis (ARDREA). J Microbiol. Methods. 60, 299–313.

Johnson, R., Blowes, D.W., Robertson, W., Jambor, J.L., 2000. The hydrogeochemistry of the Nickel Rim mine tailings impoundment, Sudbury, Ontario. J. Contam. Hydrol. 41, 49-80.

Jurjovec, J., Ptacek, C.J., Blowes, D.W., 2002. Acid neutralization mechanisms and metal release in mine tailings: A laboratory column experiments. Geochim. Cosmochim. Acta. 66, 1511-1523.

Jurjovec, J., Ptacek, C.J., Blowes, D.W., Jambor, J.L., 2003. The effect of natrojarosite addition to mine tailings. Environ. Sci. Technol. 37, 158-164.

Karlsson, S., Sandén, P., Allard, B., 1987. Environmental impacts of an old mine tailings deposit—metal adsorption by particulate matter. Nordic Hydrol. 18, 313-324

Keith, C. N., Vaughan, D. J., 2000. Mechanisms and rates of sulphide oxidation in relation to the problems of acid rock (mine) drainage. In: *Environmental Mineralogy: Microbial Interactions, Anthropogenic Influences, Contaminated Land and Waste Management*. Mineralogical Society Special Publication.

Kimball, B.A., Runkel, R.L., 2009. Spatially detailed quantification of metal loading for decision making: Metal mass loading to American fork and Mary Ellen Gulch, Utah. Mine Water Environ. 28, 274-290.

Kirby, C.S., Thomas, H.M., Southam, G., Donald, R., 1999. Relative contributions of abiotic and biological factors in Fe(II) oxidation in mine drainage. Appl. Geochem. 14, 511–530.

Koren, D.W., Gould, W.D., Bedard, P., 2000. Biological removal of ammonia and nitrate from simulated mine and mill effluents. Hydrometallurgy 56, 127-144.

Kuenen, J.G., Robertson, L.A., Tuovinen, O.H., 1992. The genera Thiobacillus, Thiomicrospira, and Thiosphaera. In: Balows, A., Trüper, H.G., Dworkin, M., Harder, W., Schleifer, K.-H. (Eds), *The Prokaryotes, vol. 3*. New York: Springer, 2638–2657.

Lapakko, K.A., White III, W.W., 2000. Modification of the ASTM 5744-96 kinetic test. In: Proc. of the 5th International Conference on Acid Rock Drainage. SME, Littleton, CO, pp. 631-639.

Leduc, L.G., Trevors, J.T., Ferroni, G.D., 1993. Thermal characterization of different isolates of Thiobacillus ferrooxidans. FEMS Microbiol. Lett. 108, 189-194.

Lee, P.K., Kang, M.J., Choi, S.H., Touray, J.C., 2005. Sulfide oxidation and the natural attenuation of arsenic and trace metals in the waste rocks of the abandoned Seobo tungsten mine, Korea. Appl. Geochem. 20, 1687-1703.

Lefebvre, R., Gélinas, P., Isabel, D., 1993. Heat transfer during acid mine drainage production in a waste rock dump, La Mine Doyon (Québec). MEND report 1.14.2c, March 1994, pp 106.

Lefebvre, R., Hockley, D., Smolensky, J., Gélinas, P., 2001. Multiphase transfer process in waste rock piles producing acid mine drainage 1: Conceptual model and system characterization. J. Contam. Hydrol. 52, 137-164.

Light, T.S., 1972. Standard solution for redox potential measurements. Anal. Chem. 44, 1038-1039.

Liljeqvist, M., Valdes, J., Holmes, D.S., Dopson, M., 2011 Draft genome of the psychrotolerant acidophile *Acidithiobacillus ferrivorans* SS3. J. Bacteriol. 16, 4304-4305.

Lindsay, M.B.J., Wakeman, K.D., Rowe, O.F., Grail, B.M., Ptacek, C.J., Blowes, D.W., Johnson, D.B., 2011. Microbiology and geochemistry of mine tailings amended with organic carbon for passive treatment of pore water. Geomicrobiol. J. 28, 229-241.

Lowson, R. T., 1982. Aqueous pyrite oxidation by molecular oxygen. Chem. Rev. 82, 461–497.

Malmström, M.E., Destouni, G., Banwart, S.A., Strömberg, B.H.E., 2000. Resolving the scale-dependence of mineral weathering rates. Environ. Sci. Technol. 34, 1375-1378.

Marcoline, J., 2008. Investigations of water and tracer movement in covered and uncovered unsaturated waste rock. Ph.D. dissertation. University of British Columbia, Vancouver, Canada.

McGregor, R.G., Blowes, D.W., 2002. The physical, chemical and mineralogical properties of three cemented layers within sulfide-bearing mine tailings. J. Geochem. Explor. 76, 195-207.

Mendez, M. O., Neilson, J. W., Maier, R. M., 2008. Characterization of a bacterial community in an abandoned semiarid lead-zinc mine tailing site. Appl. Environ. Microb. 74, 3899–3907.

Miller, S.D., Jeffery, J.J., Wong, J.W.C., 1991. Use and misuse of the acid-base account for AMD prediction. In: Proc. of Second International Conference on the Abatement of Acidic Drainage. Montreal, QC, Canada.

Mine Environment Neutral Drainage (MEND). 1995. Hydrogeology of Waste Rock Dumps. MEND Report PA-1.

Mine Environment Neutral Drainage (MEND). 1999. Assessing the subaqueous stability of oxidized waste rock. MEND Report 2.36.3

Mine Environment Neutral Drainage (MEND), 2001. MEND Manual, Volume 4 - Prevention and Control. Report 5.4.2b. Ottawa, ON, Canada.

Mine Environment Neutral Drainage (MEND). 2009. Prediction Manual for Drainage Chemistry from Sulphidic Geologic Materials. MEND Report 1.20.1.

Moncur, M.C., Ptacek, C.J., Blowes, D.W., Jambor, J.L., 2005. Release, transport and attenuation of metals from an old tailings impoundment. Appl. Geochem. 20, 639-659.

Moore, M.L., In preparation. Comparative humidity cell analysis of waste rock from the Diavik Diamond Mine, NWT, Canada. MSc Thesis. University of Waterloo.

Morin, K., 2003. Problems with acid rock drainage predications at the Ekati Diamond Mine, Northwest Territories, Canada. In: Proc. of 6th International Conference on Acid Rock Drainage. Cairns, QLD, Australia.

Morin, K.A., Cherry, J.A., Dave, N.K., Lim, T.P., Vivyurka, A.J., 1988. Migration of acidic groundwater seepage from uranium-tailings impoundments: 1. Field study and conceptual hydrogeochemical model. J. Contam. Hydrol. 2, 271–303.

Motzer, W.E., 2001. Perchlorate: Problems, detection, and solutions. Environ. Forensics. 2, 301-311.

Murr, L. E., Schlitt, W. J., Cathles, L. M., 1981. Experimental Observations of Solution Flow in the Leaching of Copper-Bearing Waste. In: Interfacing Technologies in Solution Mining: Proceedings of the 2nd SME-SPE International Solution Mining Symposium. 271-290.

National Research Council (NRC), 2005. Health Implications of Perchlorate Ingestion. The National Academy Press, Washington, DC, 3-198.

Navarro-Noya, Y.E., Jan-Roblero, J., González-Chávez, M.C., Hernández-Gama, R., Hernández-Rodríguez, C., 2010. Bacterial communities associated with the rhizosphere of pioneer plants (Bahia xylopoda and Viguiera linearis) growing on heavy metals-contaminated soils. Antonie Van Leeuwenhoek. 97, 335–349.

Neuner, M., 2009. Water flow through unsaturated mine waste rock in a permafrost region. MSc Thesis. University of British Columbia. Vancouver, BC, Canada.

Neuner, M., Smith, L., Blowes, D.W., Sego, D.C., Smith, L.J.D., Gupton, M., 2012. The Diavik Waste Rock Project: Water flow though waste rock in a permafrost terrain. Appl. Geochem. doi: 10.1016/j.apgeochem.2012.03.011

Nichol, C.F., Smith, L., Beckie, R., 2005. Field-scale experiments of unsaturated flow and solute transport in a heterogeneous porous medium. Water Resour. Res. 41, 1-11.

Nordstrom, D.K., 1977. Thermochemical redox equilibria of ZoBell's solution. Geochim. Cosmochim. Acta. 41, 1835-1841.

Nordstrom, D.K., 1982. Aqueous pyrite oxidation and the consequent formation of secondary iron minerals. In: Kittrick, J.A., Fanning, D.F., Hossner, L.R. (Eds.), *Acid Sulfate Weathering*. Soil. Sci. Soc. Spec. Publ. 10, 37-56.

Nordstrom, D.K., 2000. Advances in the hydrogeochemistry and microbiology of acid mine waters. Int. Geol. Rev., 42, 499-515.

Nordstrom, D.K., Alpers, C.N., 1999. Geochemistry of acid mine waters. In: Plumlee, G. S., Logsdon M. J. (Eds.), *The Environmental Geochemistry of Mineral Deposits*. Society of Economic Geologists Inc., Littleton, DC, vol. 6A, pp. 133-157.

Nordstrom, D.K., Southam, G., 1997. Geomicrobiology of sulfide mineral oxidation. Rev. Mineral. 35, 381-390.

Parette, R., Cannon, F.S., Weeks, K., 2005. Removing low ppb level perchlorate, RDX, and HMX from groundwater with cetyltimethylammonium chloride (CTAC) pre-loaded activated carbon. Water Resour. 39, 4683-4692.

Pham, N., Sego, D.C., Arenson, L.U., Blowes, D.W., Amos, R.T., Smith, L., 2012. The Diavik Waste Rock Project: Measurement of thermal regime in a waste rock pile under permafrost environment. Appl. Geochem. In Press.

Pham, N., Sego, D.C., Blowes, D.W., Amos, R.T., Smith, L., 2011. Diavik Waste Rock Project: Thermal transport in a covered waste rock test pile. In: Proc. of Tailings and Mine Waste 2011. Vancouver, BC, Canada.

Pham, N., In preparation. Ph.D. Thesis. University of Alberta.

Plante, B., Benzaazoua, M., Bussiere, B., 2011. Predicting geochemical behaviour of waste rock with low acid generating potential using laboratory kinetic test. Mine Water Environ. 30, 2-21.

Pommen, L.W., 1983. The effect on water quality of explosives use in surface mining. Vol. 1 Nitrogen sources, water quality, and prediction and management of impacts. British Columbia Ministry of the Environment, Victoria, British Columbia, MOE Tech. Rep. 4.

Price, W.A., 1999. Regulation as a tool for reducing the risks associated with metal leaching and acid rock drainage. Mine Reclamation Section, British Columbia Ministry of Energy and Mines.

Price, W.A., 2009. Prediction Manual of Drainage Chemistry from Sulphidic Geologic Materials. MEND Report 1.20.1.

Ribet, I., Ptacek, C.J., Blowes, D.W., Jambor, J.L., 1995. The potential for metal release by reductive dissolution of weathered mine tailings. J. Contam. Hydrol. 17, 239-273.

Rimstidt, J.D., Vaughan, D.J., 2003. Pyrite oxidation: A state-of-the-art assessment of the reaction mechanism. Geochim. Cosmochim. Acta. 67, 873-880.

Ritchie, A.I.M., 1994. The waste-rock environment. In: Jambor, J.L., Blowes, D.W. (Eds.), *Environmental Geochemistry of Sulfide Mine-Wastes*, Mineral. Assoc. Can. Short Course vol. 22. 133-161.

Ritchie, A.I.M., 2003. Oxidation and gas transport in piles of sulfidic material. In: Jambor, J.L., Blowes, D.W., Ritchie, A.I.M. (Eds.), *Environmental Aspects of Mine Wastes*, Mineral. Assoc. Can. Short Course vol. 31, 73-94.

Ritchie, A.I.M., Bennett, J.W., 2003. The Rum Jungle Mine- A Case Study. In: Jambor, J.L., Blowes, D.W., Ritchie, A.I.M. (Eds.), *Environmental Aspects of Mine Wastes*, Mineral. Assoc. Can. Short Course vol. 31, 385-406.

Robertson, W.D., Blowes, D.W., Ptacek, C.J., Cherry, J.A., 2000. Long-term performance of *in situ* reactive barriers for nitrate remediation. Ground Water. 38, 689-695.

Rohwerder, T., Gehrke, T., Kinzler, K., Sand, W., 2003. Bioleaching review part A: Progress in bioleaching: Fundamentals and mechanisms of bacterial metal sulfide oxidation. Appl. Microbiol. Biotechnol. 63, 239-248.

Salomons, W., 1995. Environmental impact of metals derived from mining activities: Processes, prediction, prevention. J. Geochem. Explor. 52, 5–23.

Sanchez, C.A., Crump, K.S, Krieger, R.I., Khandaker, N.R., Gibbs, J.P., 2005. Perchlorate and nitrate in leafy vegetables in North America. Environ. Sci. Technol. 39, 9391-9397.

Sanmugasunderam, V., Lakshmanan, V.I., Christison, J., McKim, M., 1987. Can microorganisms be used to control nitrate levels in mining process effluents? Hydrometallurgy. 18, 383-395.

Sapsford, D. J., Bowell, R. J., Dey, M., Williams, K. P., 2009. Humidity cell tests for the prediction of acid rock drainage. Miner. Eng. 22, 25-36

Sattley, W.M., Madigan, M.T., 2006. Isolation, characterization, and ecology of cold-active, chemolithotrophic, sulfur-oxidizing bacteria from perennially ice-covered Lake Fryxell, Antarctica. Appl. Environ. Microb. 72, 5562-5568.

Sawyer, C.N., McCarty, P.N., 1967. *Chemistry for Sanitary Engineers, 2nd ed*. McGraw-Hill Book Company, New York, NY, USA.

Schaefer, C.E., Fuller, M.E., Condee, C.W., Lowey, J.M., Hatzinger, P.B., 2007. Comparison of biotic and abiotic treatment approaches for co-mingled perchlorate, nitrate, and nitramine explosives in groundwater. J. Contam. Hydrol. 89, 231-250.

Schedel, M., Truper, H.G., 1980. Anaerobic oxidation of thiosulfate and elemental sulfur in *Thiobacillus denitrificans*. Arch. Microbiol. 124, 205-210.

Schoonen, M., Elsetinow, A., Borda, M., Strongin, D., 2000. Effect of temperature and illumination on pyrite oxidation between pH 2 and 6. Geochem. Trans. 1, 23-33.

Shurniak, R.E., Barbour, S.L., 2002. Modeling of water movement within reclamations covers on oilsands mining overburden piles. In: Proceedings of the 2002 National Meeting of the American Society of Mining and Reclamation, Lexington KY, June 9-13, 2002.

Singer, P.C., Stumm, W., 1970. Acid mine drainage: the rate determining step. Science. 167, 1121-1123.

Smith, L., Beckie, R., 2003. Hydrologic and geochemical transport processes in mine waste rock. In: Jambor, J.L., Blowes, D.W., Ritchie, A.I.M. (Eds.), *Environmental Aspects of Mine Wastes*, Mineral. Assoc. Can. Short Course vol. 31, 51-72.

Smith, L.J.D., Moncur, M.C., Neuner, M., Gupton, M., Blowes, D.W., Smith, L., Sego, D.C., 2012. The Diavik Waste Rock Project: Design, construction, and instrumentation of field-scale experimental waste-rock piles. Appl. Geochem. doi:10.1016/j.apgeochem.2011.12.026.

Smith, L.J.D., Blowes, D.W., Jambor, J.L., Smith, L., Sego, D.C., Neuner, M., in press. The Diavik Waste Rock Project: Particle-size distribution and sulfur characteristics of low-sulfide waste rock. Appl. Geochem.

Snyder, S.A., Vanderford, B.J., Rexing, D.J., 2005. Trace analysis of bromate, chlorate, iodate, and perchlorate in natural and bottled waters. Environ. Sci. Technol. 39, 4586-4593.

Song, Q., 2010. Physical and numerical modelling of preferential flow and oxygen diffusion in inclined multilayer soil covers over acid generating mine waste rock. PhD thesis. University of Western Ontario, London, Ontario, Canada

Sracek, O., Choquette, M., Gélinas, P., Lefebvre, R., Nicholson, R.V., 2004. Geochemical characterization of acid mine drainage from a waste rock pile, Mine Doyon, Québec, Canada. J. Contam. Hydrol., 69, 45-71.

Standard Methods for the Examination of Water and Wastewater (SMEWW), 2005. American Public Health Association, Washington, DC.

Stockwell, J., Smith, L., Jambor, J.L., Beckie, R., 2006. The relationship between fluid flow and mineral weathering in heterogeneous unsaturated porous media: A physical and geochemical characterization of a waste rock pile. Appl. Geochem. 21, 1347-1361.

Stromberg, B., Banwart, S., 1994. Kinetic modelling of geo-chemical processes at the Aitik mining waste rock site in northern Sweden. Appl. Geochem. 9, 583-595.

Stromberg, B., Banwart, S., 1999. Experimental study of acidity-consuming processes in mining waste rock: some influences of mineralogy and particle size. Appl. Geochem. 14, 1–16.

Stumm W., Morgan J. J., 1996. *Aquatic Chemistry, 3rd ed*. John Wiley, New York

Susarla, S., Collette, T.W., Garrison, A.W., Wolfe, N.L., McCutcheon, S.C., 1999. Perchlorate identification in fertilizers. Environ. Sci. Technol. 33, 3469-3472.

Tan, Y., Ritchie, A.I.M., 1997. In situ determination of thermal conductivity of waste rock dump material. Water, Air, Soil Pollut. 98, 345-359.

Taylor, A.S., Blum, J.D., Lasaga, A.C., MacInnis, I.N., 2000. Kinetics of dissolution and Sr release during biotite and phlogopite weathering. Geochim. Cosmochim. Acta. 64, 1191-1208.

Taylor, G., Spain, A., Nefiodovas, A., Timms, G., Kuznetsov, V., Bennett, J., 2003. Determination of the Reasons for Deterioration of the Rum Jungle Waste Rock Cover. Australian Centre for Mining Environmental Research; Brisbane.

Tikkanen, M.W., 2006. Development of a drinking water regulation for perchlorate in California. Anal. Chim. Acta. 567, 20-25.

Ting, D., Howd, R.A., Fan, A.M., Alexeeff, G.V., 2006. Development of a health protective drinking water level for perchlorate. Environ. Health Perspect. 114, 881-886.

U.S. Environmental Protection Agency, Office of Solid Waste, 1994. Acid Mine Drainage Prediction; Technical document prepared by the Office of Solid Waste, Washington, D.C.

Unites States Geological Survey (USGS), 2009. Minerals Yearbook, Vol. I, Metals & Minerals, 23.1-23.3.

Vlasceanu, L., Popa, R., Kinkle, B.K., 1997. Characterization of *Thiobacillus thioparus* LV43 and its distribution in a chemoautotrophically based groundwater ecosystem. Appl. Environ. Microb. 63, 3123-3127.

Wagner, K., 2004. Characterization of the geochemistry of discharge waters, pore waters, primary and secondary minerals of an experimental waste rock pile, Cluff Lake mine, Saskatchewan, Canada. M.Sc. thesis. University of British Columbia, Vancouver, Canada.

Wagner, K., Smith, L., Beckie, R., 2006. Hydrogeochemical characterization of effluent from mine waste rock, Cluff Lake, Saskatchewan. In: Proceedings of the 7th International Conference on Acid Rock Drainage, St. Louis, MO, USA.

Wang, Q., Garrity, G.M., Tiedje, J.M., Cole, J.R., 2007. Naive Bayesian classifier for rapid assignment of rRNA sequences into the new bacterial taxonomy. Appl. Environ. Microb. 73, 5261-5267.

Webster, J.G., Swedlund, P.J., Webster, K.S., 1998. Trace metal adsorption onto an acid mine drainage iron(III) oxy hydroxyl sulfate. Environ. Sci. Technol. 32, 1361-1368.

Weisskopf, L., Heller, S., Eberl, L., 2011. Burkholderia species are major inhabitants of white lupin cluster roots. Appl. Environ. Microbiol. 77, 7715-7720.

Wilkin, R.T., Fine, D.D., Burnett, N.G., 2007. Perchlorate behavior in a municipal lake following fireworks displays. Environ. Sci. Technol. 41, 3966-3971.

Williamson, M.A., Rimstidt, J.D., 1994. The kinetics and electrochemical rate-determining step of aqueous pyrite oxidation. Geochim. Cosmochim. Acta. 58, 5443-5454.

Williamson, J.M., Thurston, H.W., Heberling, M.T., 2008. Valuing acid mine drainage remediation in West Virginia: A hedonic modeling approach. Annals of Regional Science. 42, 987-999.

Xue, H.B., Jansen, S., Prasch, A., Sigg, L., 2001. Nickel speciation and complexation kinetics in freshwater by ligand exchange and DPCSV. Environ. Sci. Technol. 35, 539-546.

Yanful, E.K., Bell, A.V., Woyshner, M.R., 1993. Design of a composite soil cover for an experimental waste rock pile near Newcastle, New Brunswick, Canada. Can. Geotech. J. 30, 578-587.

Yanful, E.K., Orlandea, M.P., 2000. Controlling acid drainage in a pyritic mine waste rock. Part II: Geochemistry of drainage. Water, Air, Soil Pollut. 124, 259-284.

Zaitsev, G., Mettanen, T., Langwaldt, J., 2008. Removal of ammonium and nitrate from cold inorganic mine water by fixed-bed biofilm reactors. Min. Engin. 12, 10-15.

Appendix A
Quality Control and Quality Assurance

Quality control and quality assurance procedures were implemented to measure and control the quality of the geochemical data. Field replicate samples were collected after approximately 10 to 15 samples. At times, the flow rate at some locations was slow; therefore, replicates samples may have been collected up to 1 hour after the initial sample. This delay may have had an effect on the percent difference between replicates. A total of 59 replicate samples were submitted for ICP-MS. The average percent difference was < 20 % for Al, Ni, Zn, Mn, Si, Cd, and Co. The average percent difference was 24.0 % for Fe and 23.5 % for Cu. At times when concentrations of Fe and Cu were low (< 1.0 mg L^{-1}) there was up to 40 % difference in replicate samples. The high percent difference for Fe and Cu may have been a result of either contamination or lack of sample representativeness. A total of 67 replicate samples were submitted for IC analysis and the percent difference was < 10 % for Cl^-, NO_3^--N, and SO_4^{2-}, 17 % for Br^-, and 33 % for NO_2^--N (average concentrations in the replicates of 4.14 mg L^{-1}). A total of 72 replicate samples were submitted for ICP-OES analysis and the average percent difference was < 11 %. The charge balance error was determined for samples that had a full-suite of analysis. Data with charge balance errors greater than 5% were re-analysed, or alternatively removed from the dataset.

Quality control and quality assurance in the laboratory was assessed by measuring the concentration of several standards within the range of sample concentrations, and by the analysis of laboratory duplicates and/or blanks. In addition, the ICP-OES and ICP-MS both

have internal standards to correct for instrument drift (Sc, Y, In, Tb and Bi for ICP-MS and Y for ICP-OES). Blank samples were analyzed between sets of 7 to 8 analyses and analyte signals were corrected by blank subtraction. Percent relative standard deviations (RSD) were consistently < 2 % for IC analysis and < 3 % for both ICP-OES and ICP-MS analyses. Laboratory duplicate samples were consistently < 5 % for IC, ICP-OES and ICP-MS.

A large number of samples were collected from 2007 through 2010. Samples from each location were sent to the laboratory and analysed between March 2009 and February 2011. ICP-OES and ICP-MS analysis of the samples was analysed upon receipt to the laboratory and the detection limits for each element were calculated for each set of analysis run on any particular day. Therefore, detections limits varied over the course of the monitoring program. The detection limits for the ICP-MS were reported based on the intercept concentration of the standard curve and the range of detection limits are provided in Table A.1. The method quantification limit for ICP-OES analysis was reported based on ten times the standard deviation of 15 sample blanks and the range of detection limits are provided in Table A.2. The symbol size for individual points was generally larger than the standard deviation measurement, therefore standard deviation bars were not displayed on figures.

A total of 27 samples from 2007 were analyzed for NO_3^--N at the University of Waterloo and at an external laboratory (SGS Lakefield Research Limited, Lakefield, Ontario). The percent difference between the two facilities was < 8 %, ranging from 0.30 % to 7.23 % (Table A.3).

Table A.1 Summary of ICP-MS detection limits.

Analysis Date	Be	B	Na	Mg	Al	Si	P	K	Ca
	µg L^{-1}	µg L^{-1}	µg L^{-1}	µg L^{-1}	µg L^{-1}	µg L^{-1}	µg L^{-1}	µg L^{-1}	µg L^{-1}
18-Mar-09					0.690				
19-Mar-09					2.019				
20-Mar-09					0.163				
23-Mar-09					1.188				
1-Apr-09					0.182				
2-Apr-09					0.310				
3-Apr-09					0.115				
7-Apr-09					0.262				
8-Apr-09					0.178				
14-Apr-09					0.226				
14-Apr-09					0.226				
22-Apr-09					0.166				
27-Apr-09					0.262				
27-Apr-09					0.207				
28-Apr-09					0.828				
29-Apr-09					0.155				
29-Apr-09					0.231				
4-May-09					0.207				
5-May-09					0.522				
6-May-09					0.140				
6-May-09					0.368				
14-May-09					1.263				
23-Jul-09					0.596				
8-Oct-09					0.709	18.635			
14-Oct-09					0.527	16.095			
15-Oct-09					0.553	18.245			
29-Oct-09					1.087	20.861			
30-Oct-09					0.755	19.861			
3-Nov-09	0.025	0.851	8.817	0.531	0.682	14.934	37.348	22.937	2.024
4-Nov-09	0.041	0.708	5.015	0.583	0.711	12.273	33.457	23.759	1.930
5-Nov-09	0.031	0.602	7.661	0.840	3.044	13.137	31.070	30.193	2.595
11-Nov-09	0.004	0.726	13.872	0.391	0.898	11.214	34.216	19.804	0.350
12-Nov-09	0.018	0.622	6.481	0.452	0.708	12.829	34.145	17.021	0.714
13-Nov-09	0.028	0.625	5.301	0.346	0.478	13.208	37.406	22.240	0.728
19-Nov-09	0.043	0.739	4.798	0.770	0.958	15.548	33.043	19.436	0.871
11-Dec-09	0.007	0.901	9.194	0.784	1.109	15.661	38.018	21.231	5.782
13-Dec-09	0.010	0.943	8.435	0.892	1.746	17.617	40.764	19.147	5.818
15-Dec-09	0.009	1.147	14.245	1.221	2.167	19.666	43.060	27.200	6.918
16-Dec-09	0.010	0.759	7.830	1.201	1.874	20.182	42.182	22.418	6.242

Table A.1 Continued

Analysis Date	Be	B	Na	Mg	Al	Si	P	K	Ca
	µg L^{-1}	µg L^{-1}	µg L^{-1}	µg L^{-1}	µg L^{-1}	µg L^{-1}	µg L^{-1}	µg L^{-1}	µg L^{-1}
23-Feb-10	0.006	2.117	3.611	0.270	1.303	14.196	34.811	25.550	2.336
9-Jul-10					0.677				
28-Jul-10	0.018	0.849	0.415	0.061	0.137	2.575	12.447	16.068	1.300
9-Sep-10					3.517				
9-Sep-10					2.485				
16-Sep-10					3.657				
27-Sep-10					4.584				
30-Sep-10					5.323				
1-Oct-10					6.720				
13-Oct-10					8.717				
15-Oct-10	0.047	0.446	2.893	0.049	0.040	9.462	0.000	3.251	1.342
18-Oct-10	0.027	0.564	0.679	0.339	0.254	123.822	32.699	5.440	3.758
19-Oct-10	0.025	0.431	1.266	0.073	0.284	68.082	35.566	8.591	2.375
2-Nov-10					1.468				
24-Nov-10					1.614				
30-Nov-10	0.142	15.408	19.471	2.251	1.378	243.654	47.081	16.046	0.000
9-Feb-11					0.595				
10-Feb-11					0.442				
18-Apr-11					1.009				

Table A.1 Continued

Analysis Date	Ti	V	Cr	Mn	Fe	Co	Ni
	µg L^{-1}	µg L^{-1}	µg L^{-1}	µg L^{-1}	µg L^{-1}	µg L^{-1}	µg L^{-1}
18-Mar-09	0.003	0.005	0.005	0.004	0.434	0.008	0.043
19-Mar-09	0.003	0.002	0.004	0.005	0.441	0.007	0.068
20-Mar-09	0.014	0.001	0.002	0.005	0.433	0.009	0.013
23-Mar-09	0.010	0.002	0.003	0.007	0.422	0.009	0.006
1-Apr-09		0.004	0.005	0.005	0.420	0.001	0.018
2-Apr-09		0.003	0.005	0.003	0.412	0.007	0.022
3-Apr-09	0.021	0.002	0.005	0.003	0.474	0.004	0.011
7-Apr-09	0.031	0.001	0.004	0.004	0.366	0.006	0.010
8-Apr-09	0.009	0.003	0.003	0.004	0.382	0.004	0.016
14-Apr-09	0.013	0.003	0.002	0.005	0.329	0.010	0.017
14-Apr-09	0.013	0.003	0.002	0.005	0.329	0.010	0.017
22-Apr-09	0.005	0.003	0.004	0.008	0.299	0.014	0.003
27-Apr-09	0.011	0.008	0.003	0.010	0.308	0.013	0.009
27-Apr-09	0.008	0.001	0.004	0.090	0.419	0.022	0.082
28-Apr-09	0.009	0.001	0.004	0.024	0.445	0.015	0.017
29-Apr-09	0.016	0.003	0.007	0.009	0.308	0.010	0.015
29-Apr-09	0.011	0.004	0.004	0.008	0.354	0.006	0.008
4-May-09	0.010	0.001	0.003	0.011	0.310	0.011	0.011
5-May-09	0.016	0.005	0.013	0.018	1.483	0.022	0.012
6-May-09	0.016	0.001	0.003	0.003	0.305	0.007	0.010
6-May-09	0.006	0.003	0.002	0.008	0.306	0.010	0.022
14-May-09	0.005	0.002	0.004	0.013	0.556	0.007	0.009
23-Jul-09	0.014	-0.006	0.035	0.016	0.466	0.009	0.121
8-Oct-09	0.023	0.004	0.016	0.018	0.562	0.008	0.027
14-Oct-09	0.023	0.003	0.016	0.020	0.510	0.009	0.019
15-Oct-09	0.021	0.016	0.024	0.027	0.598	0.016	0.030
29-Oct-09	0.022	0.018	0.038	0.035	0.683	0.025	0.036
30-Oct-09	0.027	0.009	0.024	0.025	0.677	0.017	0.027
3-Nov-09	0.043	0.018	0.027	0.024	0.627	0.018	0.030
4-Nov-09	0.052	0.039	0.044	0.043	0.712	0.037	0.044
5-Nov-09	0.059	0.030	0.038	0.033	0.851	0.026	0.037
11-Nov-09	0.019	0.000	0.006	0.004	0.433	0.004	0.006
12-Nov-09	0.034	0.017	0.024	0.019	0.441	0.015	0.021
13-Nov-09	0.031	0.014	0.025	0.025	0.522	0.021	0.024
19-Nov-09	0.073	0.036	0.039	0.038	0.541	0.033	0.041
11-Dec-09	0.023	0.007	0.014	0.015	0.853	0.007	0.016
13-Dec-09	0.027	0.004	0.012	0.017	0.538	0.008	0.018
15-Dec-09	0.025	0.006	0.011	0.028	0.585	0.011	0.071
16-Dec-09	0.026	0.004	0.015	0.028	0.639	0.012	0.031

Table A.1 Continued

Analysis Date	Ti	V	Cr	Mn	Fe	Co	Ni
	µg L^{-1}	µg L^{-1}	µg L^{-1}	µg L^{-1}	µg L^{-1}	µg L^{-1}	µg L^{-1}
23-Feb-10	0.015	0.001	0.010	0.014	0.751	0.006	0.032
9-Jul-10	0.021	0.000	0.023	0.015	0.549	0.008	0.019
28-Jul-10	0.323	0.015	0.779	0.149	30.613	0.016	0.062
9-Sep-10	0.214	0.015	0.102	0.133	7.915	0.025	0.071
9-Sep-10	0.109	0.004	0.106	0.094	5.268	0.035	0.080
16-Sep-10	0.095	0.012	0.131	0.101	9.228	0.039	0.269
27-Sep-10	0.306	0.003	0.112	0.060	7.520	0.021	0.054
30-Sep-10	0.173	0.024	0.132	0.115	8.602	0.030	0.085
1-Oct-10	0.438	0.008	0.116	0.098	7.630	0.032	0.111
13-Oct-10	0.223	0.002	0.132	0.256	8.188	0.106	0.232
15-Oct-10	0.124	0.015	0.032	0.032	0.191	0.013	0.018
18-Oct-10	0.158	0.018	0.031	0.049	0.392	0.027	0.592
19-Oct-10	0.295	0.013	0.041	0.031	0.562	0.009	0.166
2-Nov-10	0.775	0.100	0.055	0.187	3.428	0.032	0.172
24-Nov-10	2.474	0.223	0.059	0.348	7.558	0.254	0.309
30-Nov-10	0.632	0.033	0.190	0.152	6.446	0.028	0.144
9-Feb-11	0.332	0.009	0.033	0.025	1.027	0.015	0.024
10-Feb-11	0.016	0.006	0.016	0.024	0.757	0.012	0.096
18-Apr-11	0.015	0.006	0.005	0.011	1.221	0.007	0.009

Table A.1 Continued

Analysis Date	Cu	Zn	As	Se	Sr	Mo	Ag	Cd
	µg L^{-1}	µg L^{-1}	µg L^{-1}	µg L^{-1}	µg L^{-1}	µg L^{-1}	µg L^{-1}	µg L^{-1}
18-Mar-09	0.014	0.124	0.043	0.172		0.002	0.007	0.001
19-Mar-09	0.022	0.238	0.062	0.210		0.0005	0.008	0.0005
20-Mar-09	0.022	0.108	0.055	0.205		0.0010	0.006	0.0004
23-Mar-09	0.023	0.176	0.065	0.231		0.0004	0.006	0.0006
1-Apr-09	0.106	0.090	0.069	0.197		0.0017	0.006	0.0002
2-Apr-09	0.016	0.106	0.011	0.218		0.0013	0.003	0.0002
3-Apr-09	0.016	0.100	0.010	0.180		0.0008	0.005	0.0004
7-Apr-09	0.024	0.123	0.050	0.116		0.0008	0.005	0.0005
8-Apr-09	0.022	0.134	0.002	0.158		0.0008	0.003	0.0003
14-Apr-09	0.030	0.077	0.068	0.178		0.0005	0.059	0.0005
14-Apr-09	0.030	0.077	0.068	0.178		0.0005	0.059	0.0005
22-Apr-09	0.017	0.246	0.074	0.179		0.0007	0.005	0.0000
27-Apr-09	0.030	0.109	0.012	0.170		0.0016	0.006	0.0007
27-Apr-09	0.026	0.085	0.016	0.189		0.0016	0.005	0.0004
28-Apr-09	0.030	0.188	0.015	0.176		0.0015	0.006	0.0003
29-Apr-09	0.017	0.097	0.032	0.196		0.0006	0.004	0.0001
29-Apr-09	0.014	0.043	0.067	0.184		0.0013	0.004	0.0002
4-May-09	0.016	0.095	0.041	0.158		0.0002	0.005	0.0000
5-May-09	0.028	0.101	0.038	0.180		0.0163	0.006	0.0001
6-May-09	0.016	0.108	0.056	0.171		0.0014	0.004	0.0003
6-May-09	0.023	0.662	0.046	0.164		0.0014	0.004	0.0002
14-May-09	0.012	0.342	0.168	0.165		0.0009	0.004	0.0001
23-Jul-09	0.240	0.684	0.018	0.143	0.005	0.0052	0.002	0.0010
8-Oct-09	0.181	0.446	0.056	0.153	0.027	0.0130	0.007	0.0072
14-Oct-09	0.117	0.303	0.009	0.160	0.016	0.0096	0.009	0.0071
15-Oct-09	0.144	0.296	0.027	0.157	0.025	0.0186	0.018	0.0145
29-Oct-09	0.196	0.456	0.097	0.143	0.037	0.0278	0.029	0.025
30-Oct-09	0.144	0.350	0.006	0.151	0.023	0.018	0.024	0.017
3-Nov-09	0.081	0.471	0.032	0.323	0.028	0.025	0.026	0.021
4-Nov-09	0.087	0.455	0.246	0.332	0.046	0.040	0.044	0.041
5-Nov-09	0.093	0.502	0.092	0.347	0.035	0.037	0.033	0.029
11-Nov-09	0.027	0.214	0.068	0.189	0.003	0.002	0.004	0.001
12-Nov-09	0.064	0.740	0.075	0.230	0.017	0.019	0.018	0.014
13-Nov-09	0.055	0.479	0.050	0.324	0.023	0.024	0.022	0.021
19-Nov-09	0.061	0.327	0.018	0.273	0.037	0.040	0.040	0.037
11-Dec-09	0.071	0.719	0.006	0.256	0.018	0.013	0.008	0.006
13-Dec-09	0.063	0.599	0.006	0.229	0.018	0.012	0.009	0.006
15-Dec-09	0.069	0.589	0.002	0.264	0.020	0.014	0.008	0.005
16-Dec-09	0.062	0.390	0.003	0.328	0.020	0.016	0.012	0.008

Table A.1 Continued

Analysis Date	Cu	Zn	As	Se	Sr	Mo	Ag	Cd
	µg L^{-1}	µg L^{-1}	µg L^{-1}	µg L^{-1}	µg L^{-1}	µg L^{-1}	µg L^{-1}	µg L^{-1}
23-Feb-10	0.089	0.121	0.019	0.270	0.011	0.008	0.010	0.002
9-Jul-10	0.053	0.201	0.020	0.269	0.013	0.011	0.066	0.008
28-Jul-10	0.134	0.175	0.015	0.396	0.027	0.053	0.024	0.009
9-Sep-10	0.705	1.955	2.448	0.350	0.035	0.147	10.171	0.007
9-Sep-10	0.232	1.435	0.037	1.807	0.046	0.644	10.541	0.014
16-Sep-10	0.639	3.089	0.005	2.604	0.074	0.075	6.077	0.018
27-Sep-10	0.400	3.138	0.146	2.195	0.041	0.053	2.754	0.006
30-Sep-10	0.551	3.309	0.210	2.351	0.109	0.109	2.415	0.011
1-Oct-10	0.544	3.782	0.031	1.863	0.109	0.180	1.911	0.008
13-Oct-10	0.407	3.258	0.145	1.879	0.142	0.300	4.501	0.074
15-Oct-10	0.046	0.120	0.015	0.443	0.007	0.028	0.017	0.006
18-Oct-10	0.087	0.299	0.020	0.378	0.027	0.035	0.052	0.014
19-Oct-10	0.084	0.334	0.021	0.345	0.015	0.044	0.099	0.005
2-Nov-10	0.776	1.407	0.091	0.848	0.038	0.047	0.893	0.028
24-Nov-10	0.085	0.369	0.155	1.854	0.010	0.007	0.028	0.001
30-Nov-10	0.062	0.257	0.015	0.645	0.019	0.033	0.045	0.007
9-Feb-11	0.045	0.200	0.011	0.380	0.020	0.044	0.352	0.011
10-Feb-11	0.032	0.147	0.033	0.380	0.012	0.032	0.036	0.006
18-Apr-11	0.046	0.790	0.029	0.337	0.006	0.007	0.090	0.041

Table A.1 Continued

Analysis Date	Sn	Sb	Ba	Hg	Tl	Pb	U
	µg L^{-1}	µg L^{-1}	µg L^{-1}	µg L^{-1}	µg L^{-1}	µg L^{-1}	µg L^{-1}
18-Mar-09	0.002	0.0009	0.117		0.001	0.001	0.0003
19-Mar-09	0.002	0.0004	0.475		0.002	0.001	0.0001
20-Mar-09	0.050	0.0007	0.018		0.003	0.001	0.0002
23-Mar-09	0.060	0.0005	0.200		0.004	0.002	0.0003
1-Apr-09	0.025	0.0007	0.003		0.003	0.001	0.0001
2-Apr-09	0.016	0.0004	0.057		0.003	0.002	0.0002
3-Apr-09	0.014	0.0003	0.001		0.002	0.002	0.0002
7-Apr-09	0.021	0.0009	0.024		0.003	0.002	0.0001
8-Apr-09	0.018	0.0005	0.004		0.004	0.002	0.0002
14-Apr-09	0.019	0.0003	0.001		0.003	0.002	0.0003
14-Apr-09	0.019	0.0003	0.001		0.003	0.002	0.0003
22-Apr-09	0.017	0.0003	0.045		0.002	0.002	0.0002
27-Apr-09	0.017	0.0005	0.025		0.002	0.002	0.0005
27-Apr-09	0.014	0.0005	0.027		0.002	0.002	0.0009
28-Apr-09	0.021	0.0004	0.080		0.002	0.002	0.0004
29-Apr-09	0.011	0.0004	0.004		0.001	0.001	0.0002
29-Apr-09	0.012	0.0004	0.013		0.001	0.001	0.0003
4-May-09	0.019	0.0002	0.006		0.002	0.003	0.0002
5-May-09	0.020	0.0003	0.018		0.001	0.003	0.0005
6-May-09	0.020	0.0003	0.004		0.002	0.002	0.0002
6-May-09	0.025	0.0004	0.016		0.001	0.004	0.0003
14-May-09	0.024	0.0037	0.073		0.001	0.174	0.0011
23-Jul-09	0.026	0.0023	0.010		0.002	0.045	0.0003
8-Oct-09	0.091	0.0312	0.067		0.006	0.024	0.0052
14-Oct-09	0.068	0.0151	0.037		0.006	0.015	0.006
15-Oct-09	0.083	0.0260	0.048		0.014	0.024	0.014
29-Oct-09	0.109	0.0307	0.099		0.021	0.034	0.022
30-Oct-09	0.086	0.0184	0.056	0.029	0.015	0.023	0.014
3-Nov-09	0.096	0.0232	0.056		0.020	0.027	0.020
4-Nov-09	0.106	0.0432	0.078		0.038	0.047	0.038
5-Nov-09	0.090	0.0350	0.124		0.026	0.035	0.027
11-Nov-09	0.043	0.000	0.004		0.001	0.003	0.002
12-Nov-09	0.060	0.017	0.027		0.015	0.018	0.015
13-Nov-09	0.060	0.021	0.028		0.020	0.022	0.021
19-Nov-09	0.078	0.036	0.051		0.033	0.036	0.034
11-Dec-09	0.054	0.007	0.097		0.006	0.015	0.006
13-Dec-09	0.057	0.006	0.116		0.006	0.016	0.006
15-Dec-09	0.055	0.005	0.144		0.004	0.016	0.007
16-Dec-09	0.061	0.009	0.125		0.008	0.018	0.010

Table A.1 Continued

Analysis Date	Sn	Sb	Ba	Hg	Tl	Pb	U
	µg L^{-1}	µg L^{-1}	µg L^{-1}	µg L^{-1}	µg L^{-1}	µg L^{-1}	µg L^{-1}
23-Feb-10	0.059	0.001	0.033		0.001	0.004	0.001
9-Jul-10	0.043	0.009	0.078		0.007	0.019	0.001
28-Jul-10	0.298	0.007	0.036	0.676	0.001	0.012	0.003
9-Sep-10	0.254	0.039	0.161		0.023	0.045	0.010
9-Sep-10	0.381	0.308	0.049		0.101	0.043	0.021
16-Sep-10	0.416	0.076	0.841		0.035	0.090	0.013
27-Sep-10	0.410	0.124	0.472		0.026	0.036	0.006
30-Sep-10	0.442	0.129	1.623		0.067	0.082	0.026
1-Oct-10	0.445	0.234	1.643		0.054	0.079	0.015
13-Oct-10	0.485	0.433	0.875		0.367	0.068	0.027
15-Oct-10	0.040	0.021	0.006	4.250	0.067	0.009	0.001
18-Oct-10	0.034	0.031	0.047	2.620	0.010	0.010	0.005
19-Oct-10	0.063	0.018	0.019	2.721	0.003	0.010	0.002
2-Nov-10	0.080	0.033	0.160		0.024	0.047	0.025
24-Nov-10	0.022	0.003	0.169		0.001	0.006	0.000
30-Nov-10	0.023	0.006	0.040	1.011	0.003	0.018	0.003
9-Feb-11	0.099	0.029	0.029		0.009	0.012	0.012
10-Feb-11	0.093	0.018	0.010		0.006	0.007	0.010
18-Apr-11	0.079	0.004	0.007		0.002	0.000	0.005

Table A.2 Summary of ICP-OES detection limits

Analysis Date	Al	As	Ca	Cd	Co	Cr	Cu	Fe
	mg L^{-1}	mg L^{-1}	mg L^{-1}	mg L^{-1}	mg L^{-1}	mg L^{-1}	mg L^{-1}	mg L^{-1}
2009-06-24	0.184	0.101	0.185		0.364	0.119		0.155
2009-06-24	0.220	0.019	0.145		0.268	0.086		0.095
2009-07-13	0.132	0.129	0.348		0.322	0.076		0.134
2009-07-14	0.226	0.144	0.313		0.350	0.123		0.145
2009-07-15	0.049	0.132	0.493		0.289	0.126		0.144
2009-07-20	0.165	0.141	0.396		0.343	0.135		0.290
2009-07-22	0.165	0.117	0.464		0.380	0.104		0.178
2009-08-07	0.173	0.060	0.430		0.175	0.057		0.233
2009-08-12	0.295	0.052	0.296		0.175	0.042		0.203
2009-08-13	0.147	0.091	0.331		0.127	0.046		0.162
2009-08-14	0.064	0.087	0.836		0.172	0.136		0.096
2009-09-10	0.100	0.077	0.796		0.163	0.058		0.220
2009-09-10	0.235	0.053	0.653		0.231	0.107		0.354
2009-09-23	0.085	0.098	0.333		0.151	0.045		0.088
2009-10-05	0.097	0.040	0.661		0.120	0.043		0.140
2009-10-06	0.181	0.037	0.635		0.145	0.045		0.070
2009-10-07	0.233	0.036	0.543		0.175	0.039		0.107
2009-10-15	0.227	0.041	1.472		0.181	0.080		0.180
2009-10-16	0.177	0.061	0.779		0.191	0.079		0.278
2009-10-26	0.250	0.027	0.494		0.173	0.097		0.290
2009-10-28	0.183	0.034	1.214		0.254	0.162		0.319
2009-10-30	0.234	0.102	0.901		0.226	0.102		0.106
2009-11-04	0.264	0.220	0.519		0.184	0.062		0.297
2009-11-05	0.249	0.097	0.738		0.189	0.043		0.054
2009-11-06	0.228	0.074	0.812		0.178	0.067		0.309
2009-11-11	0.278	0.045	0.634		0.172	0.054		0.176
2009-11-18	0.209	0.017	0.833		0.206	0.073		0.180
2010-07-08	0.500	1.000	0.500	0.300	0.300	0.400	0.500	0.500
2010-07-09	0.210	0.174	0.093	0.068	0.099	0.101	0.140	0.113
2010-07-15	0.217	0.201	0.047	0.090	0.069	0.062	0.064	0.052
2010-07-28	0.411	0.094	0.102	0.126	0.062	0.102	0.074	0.091
2010-08-31	0.247	0.251	0.148	0.127	0.121	0.130	0.154	0.122
2010-09-03	0.072	0.221	0.037	0.079	0.176	0.035	0.085	0.062
2010-09-09	0.371	0.774	0.247		0.287	0.097		0.206

Table A.2 Continued

Analysis Date	Al	As	Ca	Cd	Co	Cr	Cu	Fe
	mg L^{-1}	mg L^{-1}	mg L^{-1}	mg L^{-1}	mg L^{-1}	mg L^{-1}	mg L^{-1}	mg L^{-1}
2010-09-23	0.590	0.704	0.313		0.241	0.263		0.313
2010-09-29	0.086	0.174	0.142	0.095	0.076	0.078	0.114	0.100
2010-10-01	0.153	0.186	0.229		0.138	0.138		0.112
2010-10-05	0.302	0.785	0.153		0.218	0.072		0.119
2010-10-18	0.632	0.715	1.005	0.197	0.190	0.216	0.374	0.202
2010-10-21	0.103	0.109	0.062	0.209	0.042	0.051	0.064	0.036
2010-10-29	0.089	0.224	0.215	0.079	0.072	0.060	0.080	0.043
2010-11-24	0.798	0.377	0.709		0.186	0.259		0.246
2011-01-27	0.509	0.490	0.206		0.257	0.207		0.217
2011-02-08	0.879	0.513	0.196		0.231	0.204		0.266
2011-02-08	0.896	0.489	0.285		0.273	0.141		0.185

Table A.2 Continued

Analysis Date	K	Mg	Mn	Na	Ni	Pb	S
	mg L^{-1}	mg L^{-1}	mg L^{-1}	mg L^{-1}	mg L^{-1}	mg L^{-1}	mg L^{-1}
2009-06-24	0.248	0.108		0.104	0.105	0.084	
2009-06-24	0.053	0.096		0.074	0.019	0.099	
2009-07-13	0.071	0.049		0.088	0.097	0.085	
2009-07-14	0.267	0.054		0.256	0.117	0.073	
2009-07-15	0.263	0.090		0.616	0.167	0.065	
2009-07-20	0.152	0.213		0.135	0.124	0.082	
2009-07-22	0.398	0.273		0.172	0.201	0.084	
2009-08-07	0.667	0.499		0.330	0.164	0.185	
2009-08-12	0.355	0.379		0.188	0.120	0.170	
2009-08-13	0.162	0.338		0.191	0.189	0.092	
2009-08-14	0.411	0.702		0.713	0.235	0.151	
2009-09-10	0.612	0.589		0.393	0.063	0.095	
2009-09-10	0.826	0.811		0.424	0.293	0.213	
2009-09-23	0.222	0.358		0.232	0.181	0.081	
2009-10-05	0.861	0.925		0.763	0.332	0.204	
2009-10-06	0.274	0.304		0.383	0.130	0.237	
2009-10-07	0.375	0.356		0.221	0.071	0.217	
2009-10-15	1.060	1.412		0.691	0.199	0.208	
2009-10-16	0.364	0.912		0.293	0.138	0.205	
2009-10-26	0.519	0.564		0.313	0.235	0.180	
2009-10-28	0.974	1.155		1.728	0.206	0.256	
2009-10-30	0.736	0.519		1.429	0.203	0.265	
2009-11-04	0.585	0.527		0.639	0.286	0.234	
2009-11-05	0.597	0.661		0.468	0.137	0.156	
2009-11-06	0.615	1.031		0.361	0.138	0.180	
2009-11-11	0.103	0.412		0.292	0.227	0.202	
2009-11-18	0.434	0.532		0.801	0.151	0.236	
2010-07-08	0.600	0.300	0.600	0.300	0.500	0.500	
2010-07-09	0.128	0.091	0.076	0.086	0.089	0.071	0.207
2010-07-15	0.050	0.036	0.112	0.013	0.061	0.071	0.248
2010-07-28	0.055	0.092	0.086	0.110	0.132	0.078	0.110
2010-08-31	0.438	0.114	0.152	0.125	0.126	0.134	0.744
2010-09-03	0.218	0.048	0.126	0.053	0.252	0.118	0.259
2010-09-09	0.346	0.187		0.276	0.196	0.296	

Table A.2 Continued

Analysis Date	K	Mg	Mn	Na	Ni	Pb	S
	mg L^{-1}	mg L^{-1}	mg L^{-1}	mg L^{-1}	mg L^{-1}	mg L^{-1}	mg L^{-1}
2010-09-23	0.671	0.272		0.343	0.223	0.289	
2010-09-29	0.231	0.152	0.088	0.185	0.076	0.280	0.274
2010-10-01	0.047	0.224		0.231	0.174	0.115	
2010-10-05	0.587	0.149		0.345	0.229	0.318	
2010-10-18	0.084	0.996	0.347	0.880	0.113	0.251	0.863
2010-10-21	0.111	0.069	0.112	0.037	0.059	0.108	0.166
2010-10-29	0.021	0.241	0.111	0.242	0.099	0.094	0.279
2010-11-24	0.261	0.702		0.078	0.069	0.104	
2011-01-27	0.688	0.250		0.335	0.138	0.547	
2011-02-08	0.678	0.348		0.415	0.172	0.574	
2011-02-08	1.695	0.357		0.404	0.162	0.632	

Table A.2 Continued

Analysis Date	Sb	Se	Si	Sr	Tl	Zn
	mg L^{-1}	mg L^{-1}	mg L^{-1}	mg L^{-1}	mg L^{-1}	mg L^{-1}
2009-06-24		0.052		0.135		0.227
2009-06-24		0.056		0.151		0.019
2009-07-13		0.093		0.078		0.027
2009-07-14		0.106		0.132		0.031
2009-07-15		0.070		0.084		0.028
2009-07-20		0.063		0.117		0.033
2009-07-22		0.055		0.099		0.069
2009-08-07		0.050		0.423		0.143
2009-08-12		0.057		0.452		0.092
2009-08-13		0.047		0.341		0.025
2009-08-14		0.073		0.629		0.091
2009-09-10		0.035		0.444		0.219
2009-09-10		0.040		0.649		0.170
2009-09-23		0.076		0.435		0.122
2009-10-05		0.078	0.104	0.252		0.157
2009-10-06		0.069	0.108	0.362		0.129
2009-10-07		0.089	0.116	0.334		0.168
2009-10-15		0.112	0.244	0.477		0.144
2009-10-16		0.087	0.328	0.515		0.166
2009-10-26		0.042	0.320	0.629		0.161
2009-10-28		0.101	0.265	0.574		0.093
2009-10-30		0.182	0.465	0.422		0.176
2009-11-04		0.177	0.520	0.578		0.836
2009-11-05		0.128	0.387	0.466		0.054
2009-11-06		0.145	0.233	0.575		0.114
2009-11-11		0.059	0.207	0.404		0.052
2009-11-18		0.099	0.364	0.541		0.084
2010-07-08	0.900	0.700	0.200	0.060	0.240	0.250
2010-07-09	0.096	0.112	0.062	0.095	0.097	0.046
2010-07-15	0.062	0.118	0.034	0.083	0.058	0.065
2010-07-28	0.072	0.068	0.000	0.046	0.086	0.144
2010-08-31	0.140	0.166	0.065	0.092	0.107	0.120
2010-09-03	0.188	0.175	0.107	0.016	0.157	0.088
2010-09-09	0	0.563	0.136	0.156		0.047

Table A.2 Continued

Analysis Date	Sb	Se	Si	Sr	Tl	Zn
	mg L^{-1}	mg L^{-1}	mg L^{-1}	mg L^{-1}	mg L^{-1}	mg L^{-1}
2010-09-23		0.456	0.239	0.132		0.215
2010-09-29	0.102	0.118	0.085	0.077	0.100	0.084
2010-10-01		0.164	0.052	0.048		0.084
2010-10-05		0.591	0.059	0.013		0.220
2010-10-18	0.038	0.529	0.108	0.349	0.155	0.142
2010-10-21	0.022	0.084	0.028	0.122	0.017	0.144
2010-10-29	0.059	0.132	0.089	0.133	0.069	0.078
2010-11-24		0.183	0.150	0.124		0.272
2011-01-27		0.143	0.206	0.171		0.143
2011-02-08		0.331	0.118	0.193		0.244
2011-02-08		0.292	0.090	0.168		0.328

Table A.3 Analysis completed at the University of Waterloo compared to analysis at SGS Lakefield Research Limited, Lakefield, Ontario

		UW	SGS	
Name	**Date**	NO_3^--N mg L^{-1}	NO_3^--N mg L^{-1}	% difference
C3w2swsX	11-Aug-07	2090	2120	1.42
C3w2swsY	11-Aug-07	1512	1580	4.43
C3w2swsZ	11-Aug-07	946	988	4.39
33S2sws05	02-Aug-07	826	836	1.18
32S2sws01	02-Aug-07	469	490	4.35
32S2sws03	02-Aug-07	1649	1640	0.56
32S2sws07	02-Aug-07	1455	1480	1.67
32N2tenXX	31-Jul-07	1116	1200	7.23
33N2sws05	02-Aug-07	575	600	4.21
32N2sws03	20-Aug-07	1549	1490	3.91
32N2sws05	20-Aug-07	1926	1920	0.31
31S2sws02	03-Aug-07	3820	3680	3.73
C2E2sws09	11-Aug-07	469	483	2.92
3UWxlys02	26-Aug-07	599	626	4.48
C3W2sws"X"	30-Aug-07	2166	2020	6.97
C3W2sws"Y"	30-Aug-07	1633	1610	1.42
3UWxlys02	28-Aug-07	531	542	2.01
3UWxlys02	02-Sep-07	522	535	2.41
32N2sws03	01-Sep-07	1359	1350	0.67
32N2sws05	01-Sep-07	3380	3190	5.78
32N2ten05	01-Sep-07	1649	1630	1.14
C2E2sws09	30-Aug-07	501	497	0.79
C2E2sws05	30-Aug-07	831	829	0.30
C3W2sws"Z"	30-Aug-07	1163	1160	0.30
31S2sws02	01-Sep-07	2726	2600	4.72
33N2sws05	01-Sep-07	1062	1080	1.65
33S2sws05	01-Sep-07	1476	1430	3.18